

**Micro-Scale Bio-Inspired Structured Polymer Surfaces for
Tissue Adhesion**

Ashley Marie Bell

Submitted in accordance with the requirements for the degree of
Doctor of Philosophy

The University of Leeds

School of Mechanical Engineering

September 2015

The candidate confirms that the work submitted is his/her own and that appropriate credit has been given where reference has been made to the work of others.

This copy has been supplied on the understanding that it is copyright material and that no quotation from the thesis may be published without proper acknowledgement.

The right of Ashley Marie Bell to be identified as Author of this work has been asserted by her in accordance with the Copyright, Designs and Patents Act 1988.

© 2015 The University of Leeds and Ashley Marie Bell

Acknowledgements

Firstly, I would like to extend my greatest gratitude to Professor Anne Neville, for her continuous support, knowledge, and guidance throughout the duration of this work. Your patience, advice, and enthusiasm have made this whole process enjoyable and a pleasure from start to finish, and for that I am forever grateful. Also I would like to thank Professor Phillip Gaskell, for co-supervising the project, providing knowledgeable insights and for all of your support throughout this project.

I would like to acknowledge the iFS staff for their help and support throughout the past four years, without their technical support and help this thesis would not have been possible. I would also like to extend this thanks to Jackie, Fiona and Alice, who have helped with so many issues over these four years.

I would also like to show appreciation to the cleanroom and CBS staff. Specifically Dr Li Chen, your valuable knowledge and expertise in micro-fabrication techniques have been invaluable. I would also like to thank Dr Chris Russell, for his help and support with everything cleanroom related from day one, and also Adrian Eagles for guidance with white light interferometry.

I would like to thank the surgical technologies research group, in particular Adrian and Jen for helping with *in-vivo* testing and tissue knowledge, and William for your LabVIEW and Matlab help.

I would like to thank all of my friends and colleagues; it has been a pleasure to work with such a lovely group of people, particularly office 247 for the tea breaks, lunches and cakes. I couldn't have asked for a better group of people to work with. And to everyone in office 132 who have put up with me during the write up, listened to my moaning and ranting and supported me throughout the last stages

of this work. And also to Louise, thank you for being a brilliant friend and keeping me sane from day one, it would not have been the same without you.

I would also like to thank my close friends and family, especially to Chris, for motivating me and being so understanding throughout this write up.

Finally, to my Mam, Dad and Matthew, for the endless encouragement, support, patience and believing in me during not only this thesis but in everything, for this I am forever thankful.

Abstract

There are many cases when it would be beneficial to provide reliable, reversible adhesion at a tissue-device interface. There are currently many adhesion mechanisms used during surgical procedures such as graspers, vacuum cups and hooks. However, these are known to cause some scale of tissue trauma. This thesis investigates the viability of using a bio-inspired, structured polymer surfaces to provide wet adhesion forces through the formation of liquid bridges on the tip of discrete pillars. The mechanism described involves a contribution from both Stefan forces and capillary forces to provide the total adhesion force.

A main factor to this work is the ability to successfully, repeatedly and reliably fabricate polymer surfaces at a micron scale with varying geometry, specifically in terms of pillar spacing. The substrate should be flexible and have the ability to tune the wettability. A number of lithography techniques have been explored for a range of polymers, finally settling on a nano-imprint lithography technique with Poly (dimethylsiloxane) (PDMS) as the polymer.

Experimental adhesion tests have been performed and it has been found, that for such an adhesion mechanism to be successful, an optimal contact angle must be reached. If the contact angle is too high, repulsive forces in convex menisci will form and the adhesion will be low as a result. If the contact angle is too low, the capillary length : pillar height ratio results in the surface acting super-hydrophobic and completely wetting the pillars, preventing the formation of liquid bridges, and again resulting in low adhesion, it is proposed that such a mechanism would occur at contact angles lower than 50° . A mathematical model has been investigated, encompassing both the Stefan and adhesion forces and the limitations of this have been discussed in relation to the complexity of this system.

Table of Contents

Acknowledgements.....	ii
Abstract.....	iv
Table of Contents.....	v
List of Tables.....	xi
List of Figures	xii
Publication List and Conference Proceedings	xxv
Chapter 1. Introduction	1
1.1 Background	1
1.2 Motivation	2
1.3 Aims and Objectives	4
1.4 Contributions and Novelty.....	4
1.5 Thesis Outline.....	5
Chapter 2. Literature Review	7
2.1 Introduction.....	7
2.2 The Effect of Technology on Laparoscopic Surgery	8
2.2.1 Background	8
2.2.2 Development of Laparoscopic Surgery	9
2.2.3 Single Incision Surgery and NOTES	10
2.2.4 Robotics in Surgery	11
2.2.5 Section Summary	15
2.3 Mechanisms of Adhesion.....	16

2.3.1	Mechanical Interactions.....	18
2.3.2	Chemical Interactions.....	18
2.3.3	Magnetic Attachment Systems.....	18
2.3.4	Passive Adhesion.....	20
2.3.5	Wet Adhesion.....	21
2.3.5.1	Capillary Adhesion	21
2.3.5.2	Surface Wettability	22
2.3.6	Biomimetic Wet Adhesion	24
2.3.7	Biomimetic Dry Adhesion	27
2.4	Fabrication Techniques and Surface Optimisation	29
2.4.1	Introduction	29
2.4.2	Surface Optimisation.....	29
2.4.2.1	Surface Geometry	30
2.4.3	Photolithography	34
2.4.3.1	Soft Lithography	37
2.4.3.2	Nano-Imprint Lithography.....	38
2.4.4	Surface Chemistry.....	40
2.4.4.1	Polyurethane (PU).....	40
2.4.4.2	Polymethylmethacrylate (PMMA)	41
2.4.4.3	Polydimethylsiloxane (PDMS)	41
2.4.4.4	SU8	43
2.4.5	Summary.....	44

Chapter 3. Experimental Procedures and Methodology	46
3.1 Introduction.....	46
3.2 Experimental Conditions.....	46
3.3 Biological Specimens.....	47
3.4 Surface Preparation Equipment.....	47
3.4.1 Wafer Saw.....	47
3.4.2 Reactive Ion Etcher	48
3.4.3 Plasma Prep 2 - Plasma Chamber	50
3.5 Surface Analysis Equipment.....	50
3.5.1 Nano-Indentation.....	50
3.5.2 Scanning Electron Microscope (SEM).....	51
3.5.3 White Light Interferometry - Bruker Npflex™	54
3.5.4 Contact Angle Goniometry - FTA4000™	55
3.6 Adhesion Test Equipment.....	56
3.6.1 Modular Universal Surface Test (MUST) Instrument.....	56
3.6.2 Tissue Adhesion Testing Rig.....	61
3.6.3 Modular Mechanical Characterisation (MMC) Rig.....	63
3.7 Summary	65
Chapter 4. Polymer Selection and Fabrication Techniques	66
4.1 Introduction.....	66
4.2 Polymer Selection.....	67
4.2.1 Polyurethane Acrylate (PU).....	68

4.2.2	Poly (Methyl Methacrylate) (PMMA)	69
4.2.3	SU8	70
4.2.4	Poly (dimethylsiloxane) (PDMS)	72
4.2.5	Silicon Template	75
4.3	Polymer Fabrication Techniques	79
4.3.1	Autotex [®]	79
4.3.1.1	Method 1: Autotex [®]	79
4.3.2	SU8	82
4.3.2.1	Method 2: SU8 2002 as a Base for Autotex [®]	82
4.3.2.3	Method 4: SU8 2010 as a Mould for PDMS	86
4.3.3	Poly (Dimethylsiloxane) (PDMS)	89
4.3.3.1	Method 5: Direct Patterning of PDMS	89
4.4	Summary	94
Chapter 5.	Experimental Results	96
5.1	Introduction	96
5.2	Sample Preparation	96
5.2.1	Polymer Properties	96
5.2.1.1	Mechanical Properties	97
5.2.1.2	Wettability	101
5.2.2	Fluid Characterisation	107
5.3	Adhesion Results	109
5.3.1	Effect of Polymer Selection	110

5.3.2	Effect of Geometry on Hydrophobic PDMS Samples	113
5.3.3	Effect of Fluid Viscosity on Hydrophobic PDMS Samples	116
5.3.4	Hydrophilic Adhesion against Water.....	118
5.3.4.1	Effect of Wettability on PDMS Samples	118
5.3.4.2	Effect of Surface Geometry on PDMS Samples	121
5.3.5	Adhesion against Glycerol - Water Mix	123
5.3.5.1	Effect of Wettability on PDMS Samples	123
5.3.5.2	Effect of Surface Geometry on PDMS Samples	125
5.4	Adhesion against Tissue.....	127
5.4.1.1	Effect of Wettability on PDMS Samples	128
5.4.1.2	Effect of Surface Geometry on PDMS Samples	129
5.4.2	Effect of Fluid Properties on Adhesion	131
5.4.2.1	Initial Traction Testing	135
5.5	Summary	137
Chapter 6.	Results - Mathematical Wet Adhesion Model.....	139
6.1	Introduction.....	139
6.2	Capillarity.....	141
6.3	Tissue Characterisation	144
6.4	Proposed Mechanism	148
6.5	Theoretical Results.....	153
6.5.1	Effect of Separation on the Adhesion Mechanism Occurring	154
6.5.2	Effect of Surface Wettability (Pillared Polymer Surface).....	157

6.5.3	Effect of Micro-Pillared Geometry (Spacing)	161
6.6	Summary	166
Chapter 7.	Discussion.....	167
7.1	Introduction.....	167
7.2	Uniqueness of This System	168
7.3	Discussion of Experimental Results.....	171
7.4	Work of Adhesion	177
7.5	Mathematical Model Discussion	178
7.6	Summary	183
7.7	Practical Applications.....	184
7.7.1	Colon Tissue as a Comparison to Peritoneal Tissue.....	186
7.7.2	CoDir Applications.....	186
7.7.3	Surgical Graspers.....	187
Chapter 8.	Conclusions and Recommendations for Future Work.....	188
8.1	Recommendations for Future Work.....	193

List of Tables

Table 2.1 - Summary of miniature robotic devices and how an adhesive surface can aid functionality.	16
Table 5.1 - Table of viscosities for the fluids used during testing.	108
Table 5.2 - Table containing the film thickness of fluids used during adhesion tests	109
Table 5.3 - Constant values [21, 148, 150, 151]	110
Table 5.4 - Values for surface tension, measured using krüss k100 tensiometer	117
Table 6.1 - Comparison of elastic modulus of common materials [148, 156, 157]	140
Table 7.1 - Table of literature comparisons of wet adhesion mechanisms with various micro-structured surfaces.	169
Table 7.2 - Theoretical number of pillars on the surface of each wafer.....	180

List of Figures

Figure 1.1 - (a) Intra-corporeal robot [7], where the highlighted areas indicate the location of the pads (b) Laparoscopic Grasper	2
Figure 1.2 - Simplified diagram of the location of the peritoneum.	3
Figure 2.1 - Laparoscopic surgery set-up, showing the laparoscopes with different functionalities entering the abdominal cavity through small access ports [18]. ...	9
Figure 2.2 - Transgastric, transvaginal and transrectal notes procedures [24] .	10
Figure 2.3 - Components of the da-Vinci surgical system, a) the surgeon's console, b) the patient side cart, c) the endowrist instruments and d) the vision system [27].....	12
Figure 2.4 - Image of the PillCam device, which has been designed to provide visualisation through the digestive tract [33].	14
Figure 2.5 - The HeartLander device, which uses suction to traverse the surface of the heart in an inch-worm like motion [8]	14
Figure 2.6 - The mobile Nebraska robotic device, which uses metallic wheels to traverse abdominal organs [37].....	15
Figure 2.7 - Injection of ferromagnetic fluid into a porcine stomach, an external permanent magnet can be seen to retract the tissue [45].	19
Figure 2.8 - Schematic of the cohesion of water molecules via hydrogen bonds (dashed lines).	21
Figure 2.9 - Young's model of a liquid droplet on a solid surface.....	23
Figure 2.10 - Results by Hanna <i>et al.</i> [65], where a horizontal force was applied in a forward direction, mimicking the forces that would be applied to the toe pads of a frog tending to slide backwards down a vertical slope. The graph shows that	

resistive forces of single toe pads to movement in the shear plane are dependent on the velocity of the applied movement.....	25
Figure 2.11 - The structure of a tree frog's foot pad, on both the micro and nanoscale, followed by polymer bio-inspired micro-structured surfaces mimicking it [21].	26
Figure 2.12 - The toe pad of a frog in contact with a glass surface with an attractive concave meniscus formed [73].	27
Figure 2.13 - Structural hierarchy of the gecko adhesive system. (A) Gecko. (B) Macrostructure. (C) Meso-structure: view of the foot with adhesive lamellae. (D) micro-structure: portion of a single lamella, setae array visible. (E) Nano-structure: single seta with branched structure terminating in hundreds of spatula tips [78].	28
Figure 2.14 - Formation of liquid bridges from a continuous fluid film on the tip of micro-pillars.....	30
Figure 2.15 - Results by Roshan <i>et al.</i> [21] showing the maximum adhesion force as a function of area for flat and micro-structured surfaces adhering to a wet surface. It can be seen there is an optimum contact surface area at 113mm^2 , areas larger than this have a detrimental effect on the adhesion forces produced.	31
Figure 2.16 - Variables of capillary forces.....	33
Figure 2.17 - Wafer Geometries, (a) Wafer 1, Pillar Spacing = $1.5\ \mu\text{m}$, (b) Wafer 2, Pillar Spacing = $4.5\ \mu\text{m}$, (c) Wafer 3, Pillar Spacing = $6\ \mu\text{m}$	34

Figure 2.18 - Positive and negative photoresists. The positive resist replicates the mask structure through polymer chain scission. The negative resist replicates the inverse of the mask structure through polymer chain bonding.	36
Figure 2.19 - Wall profiles caused by different etching techniques. Wet etching commonly produces an isotropic wall profile, where as a dry etch will provide a straight anisotropic profile.	37
Figure 2.20 - Process of a novel nano-imprinting technique.	39
Figure 2.21 - PU structure.....	40
Figure 2.22 - PMMA structure	41
Figure 2.23 - PDMS structure	42
Figure 2.24 - (a) PDMS microfluidic chip [107] (b.1.) - Schematic of a pressure sensing organic transistor, which makes use of a micro-structured PDMS film. (b.2.) Flexible electronic device [110].....	43
Figure 2.25 - SU8 structure, detailing the presence of eight epoxy groups (average per molecule) which cross link as a result of UV exposure	44
Figure 3.1 - Microace 66, Loadpoint Ltd. Precision wafer saw for the dicing of silicon wafers [111]	48
Figure 3.2 - Schematic of the Oxford Instruments Plasma Pro reactive ion etcher [112].....	49
Figure 3.3 - The Gala Instrumente Plasma Prep II plasma chamber [113]	50
Figure 3.4 - Example of the data read out from nano-indentation tests. Data is provided in a load vs depth curve, allowing the mechanical properties to be calculated.....	51
Figure 3.5 - Carl Zeiss EVO SEM with oxford instruments EDX system [117]. .	53

Figure 3.6 - White light interferometry, Bruker Npflex™[118].....	54
Figure 3.7 - Example of liquid droplet formed by FTA4000 on a hydrophobic surface of volume 0.497 μl	55
Figure 3.8 - FTA 4000 [119].....	56
Figure 3.9 - Cantilever set up, showing the parallel arrangement of the cantilevers, mirror positioning and stud positioning for sample mounting.	57
Figure 3.10 - Set-up used for the calibration of the cantilever. Mass is added, and the resultant displacement of the cantilever pair is recorded. From this it is possible to calculate the spring constant	58
Figure 3.11 - Calibration curve with gradient of 0.6 $\text{mN}/\mu\text{m}$	59
Figure 3.12 - MUST rig set-up. The optical sensor detects displacement as the mirror moves. The spring constant is known and therefore allows the displacement to be translated into a force.	59
Figure 3.13 - Typical force displacement curve. The test starts at point A. At point B an attractive force to build up across the interface pulling the surfaces together and they contact at point C. A predetermined maximum force is reached by point D, at this point separation begins. The maximum adhesion force occurs at point E.	61
Figure 3.14 - Tissue adhesion testing rig. Image shows the apparatus at an inclination to the horizontal [21].....	62
Figure 3.15 - S100 - thin film load cell (1N) [120].....	63
Figure 3.16 - Modular mechanical characterisation (MMC) rig set up, with an indenter in contact with a tissue sample	64
Figure 3.17 - S100 calibration curve.	65

Figure 4.1 - Schematic of the liquid bridge and encapsulating meniscus formed on the tip of a single micro-pillar adjacent to an idealised rigid surface.	67
Figure 4.2 - PU chemical structure.....	68
Figure 4.3 - SEM images of polyurethane fibres showing (a) spatula tips, (b) spherical tips, (c) suction-cup like tips and (b) large diameter tips. [99]	69
Figure 4.4 - PMMA structure	70
Figure 4.5 - SEM image of PMMA micro-pillars of height 24.02 μm , fabricated using a nano-imprint Process [139].....	70
Figure 4.6 - SU8 structure.....	71
Figure 4.7 - Patterned SU8 surfaces with vertical sidewalls [140]	71
Figure 4.8 - Data to show the effect of spin speed on thickness of SU8 2000 series [32]	72
Figure 4.9 - PDMS structure	73
Figure 4.10 - SEM image of a high density PDMS micro pillar array to be used as a cellular force transducer [141].....	73
Figure 4.11 - Results by Jiang <i>et al.</i> [142] showing the water droplet contact angle on a flat PDMS surface as a function of atmospheric air plasma treatment time [143].....	74
Figure 4.12 - Etching profiles obtained during (a) isotropic wet etching and (b) anisotropic dry etching [86]	77
Figure 4.13 - Photolithography method used to pattern the silicon master mould (not to scale)	78

Figure 4.14 - Optical microscope image of a successfully fabricated silicon master mould, showing a regular array of micro-pillars.....	79
Figure 4.15 - Simplified schematic for Autotex [®] fabrication technique (not to scale)	81
Figure 4.16 - Scanning electron microscope image of Autotex [®] pillars at a 75 degree tilt angle	82
Figure 4.17 - Simplified diagram using SU8 2002 as a base for Autotex [®] to test the surface chemistry (not to scale).	83
Figure 4.18 - Fabrication technique for the direct patterning of micro-pillars in SU8 2010 (not to scale)	84
Figure 4.19 - Microscope image of directly patterned SU8. Showing an edge bead formed due to the viscous nature of the polymer, resulting in an uneven contact to the photo mask	85
Figure 4.20 - SEM image showing fallen and absent SU8 pillars, due to a combination of high aspect ratio and weak adhesion between SU8 and pet substrate	86
Figure 4.21 - Fabrication technique for the use of SU8 as a mould for PDMS (not to scale)	87
Figure 4.22 - Movement of a liquid developer around the extruded pillar features, allowing all exposed areas to be reached.	88
Figure 4.23 - Movement of a liquid developer in and around the in recessed features, showing the fluidic eddy currents which will form preventing the fabrication of cylindrical holes.	88

Figure 4.24 - White light interferometry image of the PDMS hole mould (Geometry one - 1.5 μm spacing)	90
Figure 4.25 - PDMS fabrication technique (not to scale).....	91
Figure 4.26 - White light interferometry image of micro-structured PDMS surface (geometry one - 1.5 μm spacing)	92
Figure 4.27 - White light interferometry image of micro-structured PDMS surface (Geometry two - 4.5 μm spacing).....	92
Figure 4.28 - White light interferometry image of micro-structured PDMS surface (Geometry three - 6 μm spacing)	92
Figure 4.29 - Contact angle of a flat PDMS sample as a result of exposure to atmospheric air plasma. Data has been collected using a contact angle goniometer.....	93
Figure 5.1 - Indentation pattern of 35 localised indentation points over a single PDMS sample over time.	98
Figure 5.2 - Nano-indentation data for the change in mechanical properties of a PDMS sample over specific time periods. The data is the average curves for five data sets taken in one time frame.	98
Figure 5.3 - Oliver-Pharr method of analysis used to calculate the elastic modulus and hardness of a substrate using nano-indentation.	99
Figure 5.4 - Exploded view of the thermal drift correction, as consequence of a change in dimension of the indenter, sample, or instrument as a result of a temperature change during the test.	100

Figure 5.5 - Changes in elastic modulus and hardness for a typical PDMS sample over time. Average errors: hardness = 0.01 MPa, elastic modulus = 0.02 MPa. 101

Figure 5.6 - Contact angle as a function of air plasma exposure time for a flat PDMS sample of mix ratio 10:1, this data is a modification to the data in Figure 4.29, showing specifically the contact angles investigated for the pillared samples. 102

Figure 5.7 - The effect of plasma exposure time on the pillar diameter. 103

Figure 5.8 - The effect of plasma exposure time on the pillar height..... 104

Figure 5.9 - The effect on the pillar profile as a result of exposure to atmospheric air plasma for (a) 0 seconds, (b) 40 seconds, (c) 80 seconds and (d) 120 seconds. 104

Figure 5.10 - White light interferometry images of (a) an unexposed PDMS sample and (b) a sample after 120 seconds of exposure. The area highlighted shows where etching has occurred around the base of the pillar..... 105

Figure 5.11 - Contact angle as a function of air plasma exposure time for three pillared PDMS samples; see section 4.3.3.1 for wafer specification 106

Figure 5.12 - Adhesion results for the original Autotex[®] sample compared to the PDMS sample of the same geometry – against glass coated in water. * signifies statistical significance within the difference in data where $p \leq \alpha$ 111

Figure 5.13 - Theoretical results for both Autotex[®] and PDMS in the same geometry, against a glass slide coated in water..... 112

Figure 5.14 - Theoretical results for both Autotex [®] and PDMS in the same geometry, against a glass slide coated in water with the same surface contact angle.	113
Figure 5.15 - The effect of pillar spacing on adhesion. * signifies statistical significance within the difference in data where $p \leq \alpha$	114
Figure 5.16 - Theoretical effect of pillar spacing on adhesion.	115
Figure 5.17- Theoretical effect of pillar spacing on adhesion, with relation to the number of pillars on the surface.	115
Figure 5.18 - The effect of fluid viscosity on adhesion of a hydrophobic PDMS sample against glass coated in a film of water, * signifies statistical significance within the difference in data where $p \leq \alpha$	116
Figure 5.19 - Theoretical effect of fluid viscosity on adhesion of a hydrophobic PDMS sample against wet glass.	117
Figure 5.20 - Theoretical effect of fluid surface tension on adhesion of a hydrophobic PDMS sample.	118
Figure 5.21 - The effect of wettability on adhesion - against a glass slide and water. * signifies statistical significance within the difference in data where $p \leq \alpha$	119
Figure 5.22 - Theoretical effect of wettability on adhesion for hydrophilic samples - against a glass slide and water.	120
Figure 5.23 - The effect of surface geometry on adhesion – against a glass slide and water * signifies statistical significance within the difference in data where $p \leq \alpha$	121

Figure 5.24 - Theoretical effect of surface geometry on adhesion for hydrophilic samples - against a glass slide and water	122
Figure 5.25 - The effect of wettability on adhesion - against a glass slide and glycerol * signifies statistical significance within the difference in data where $p \leq \alpha$	124
Figure 5.26 - Theoretical effect of wettability on adhesion for hydrophilic - against a glass slide and glycerol	125
Figure 5.27 - The effect of surface geometry on adhesion - against a glass slide and glycerol * signifies statistical significance within the difference in data where $p \leq \alpha$	126
Figure 5.28 - Theoretical effect of surface geometry on adhesion for hydrophilic samples - against a glass slide and glycerol	127
Figure 5.29 - The effect of wettability on adhesion - against tissue.....	128
Figure 5.30 - Theoretical effect of wettability on adhesion for hydrophilic samples - against tissue, where the value for surface tension of tissue has been taken as the average of blood [152], urine [153] and bovine serum [17] (5.53×10^{-2} N/m).	129
Figure 5.31 - The effect of surface geometry on adhesion - against tissue * signifies statistical significance within the difference in data where $p \leq \alpha$	130
Figure 5.32 - Theoretical effect of surface geometry on adhesion for hydrophilic samples - against tissue	131
Figure 5.33 - The effect of fluid viscosity on adhesion force for hydrophilic samples * signifies statistical significance within the difference in data where $p \leq \alpha$	133

Figure 5.34 - Theoretical effect of fluid properties on adhesion force	134
Figure 5.35 - Rendered CAD drawing of the traction rig.	135
Figure 5.36 - Initial data for work into the viability of micro-structured surfaces in the colon to produce traction on a miniature robotic device.	136
Figure 6.1 - Variables involved in wet adhesion mathematical model. Where: θ_1 = contact angle at the tissue surface, θ_2 = the contact angle at the pillar, r_m = radius of the meniscus and h = separation of the two surfaces over the given time, t . R = pillar radius and s = spacing between pillars.	142
Figure 6.2 - Example of a force-displacement curve highlighting the contact mechanism - snap on point, contact propagation and the variable point.	144
Figure 6.3 - Schematic of a phospholipid bilayer, consisting of a hydrophilic head group and hydrophobic tail, allowing phospholipids to be easily absorbed onto the outer surface of the cell membrane.....	146
Figure 6.4 - Schematic to show the formation of discrete liquid bridges on the tip of each individual pillar when in contact with a wet interface. It is the sum of these which give rise to the total adhesive force.	149
Figure 6.5 - The effect on the formation of liquid bridges, due to surface roughness at the base of the pillars and contact with a conformable surface.	152
Figure 6.6 - The effect of separation on the percentage contribution of each adhesion component for varying viscosity fluids: (a) water, (b) ex-vivo and (c) in-vivo.	155
Figure 6.7 - Effect of fluid viscosity on the separation point at which capillary action dominates rather than Stefan forces.	156

Figure 6.8 - The effect of surface wettability in different environments, (a) wet glass, (b) <i>ex-vivo</i> tissue and (c) <i>in-vivo</i> for the three geometries.	158
Figure 6.9 - The effect of wettability on the adhesion. (a) wafer 1, (b) wafer 2 and (c) wafer 3.	160
Figure 6.10 - The effect of pillar spacing in each environment, (a) water, (b) <i>ex-vivo</i> and (c) <i>in-vivo</i> - whilst adhesion is due to capillary forces.	162
Figure 6.11 - Summary - The effect of pillar spacing in each environment.	163
Figure 6.12 - The effect of pillar spacing in each environment, (a) water, (b) <i>ex-vivo</i> and (c) <i>in-vivo</i> - whilst adhesion is due to stefan forces.	164
Figure 6.13 - Summary of the effect of pillar spacing in each environment.	165
Figure 7.1 - Adhesion results from literature compared to the maximum adhesion force acquired with PDMS and Autotex [®] through this thesis. Results are also related to pillar height.	170
Figure 7.2 - The effect of having any form to the base on which the pillars have been fabricated, where the maximum separation at which bridges can form is dependent on the fluid film thickness.	172
Figure 7.3 - Modified schematic diagram from Cai <i>et al.</i> showing the separation of two smooth surfaces – hydrophilic forming concave menisci and hydrophobic forming convex [61].	173
Figure 7.4 - The effect of contact angle, pillar height on meniscus formation. If the contact angle is less than 50° it is proposed that the surface will act super hydrophilic, and the surface will completely flood, resulting in no liquid bridge formation and therefore minimal adhesion forces.	174

Figure 7.5 - The effect of pillars on the adhesion forces provided, for hydrophobic and a hydrophilic PDMS samples. 176

Figure 7.6 - Liquid bridge formation on individual hydrophobic pillar tips and a flat hydrophobic surface..... 176

Figure 7.7 - Image to show the work of adhesion from a force-displacement curve. 177

Figure 7.8 - Work of adhesion as a function of contact angle. All three wafers are averaged to remove the effect of surface geometry..... 177

Figure 7.9 - The effect of pillar height on the adhesive forces produced. This data incorporates wet adhesion results from Cheung et al. [95] He *et al.* [173] Kovalev *et al.* [174]. 182

Publication List and Conference Proceedings

- Charpentier TVJ; Neville A; Baudin S; Smith MJ; Euvrard M; **Bell A**; Wang C; Barker R
Liquid infused porous surfaces for mineral fouling mitigation. Journal of Colloid and Interface Science, vol. 444, pp.81-86. 2015.
- Physics in Healthcare (2012) – London, UK (Poster Presentation)
“Micro-Scale biomimetic Structured Polymer Surfaces for Tissue Adhesion”
A. Bell, P. H. Gaskell, D. G. Jayne, A. Neville, R. Roshan.
- European Association of Endoscopic Surgery (2013) – Vienna, Austria (Oral presentation)
“Micro-Scale Bio-Inspired Structured Polymer Surfaces for Tissue Adhesion, Traction and Friction”
A. Bell, A. Hood, J. Barrie, G. Taylor, D. G. Jayne, A. Neville, P. H. Gaskell
- Gordon Conference of Adhesion (2013) – Boston, USA (Poster Presentation and Biomimetics Session Chair)
“Micro-Scale Bio-Inspired Structured Surfaces for Tissue Adhesion”
A. Bell, P. H. Gaskell, D. G. Jayne, A. Neville, R. Roshan
- Adhesion Society Annual Conference (2014) – San Diego, USA (Oral Presentation)
“A Bio-Inspired Wet Adhesion Mechanism for Surgical Devices”
A. Bell, P.H. Gaskell, A. Neville

Chapter 1. Introduction

1.1 Background

Despite minimally invasive surgery (MIS) becoming the practice of choice for many abdominal surgical procedures, there are limitations with this technique, specifically regarding the ability to provide reliable, repeatable adhesion at a tissue-device interface. The importance of providing and ensuring minimal damage, improved cosmesis, and a reduced risk of infection is essential in revolutionising abdominal surgical techniques. First introduced into abdominal surgery in the 1980's [1], minimally invasive laparoscopic techniques allow the surgeon to perform, what once was an open procedure, through a small incision. Laparoscopes are used to provide a light source into the abdominal cavity and to hold a camera, relaying images to a monitor inside the operating theatre.

However, there are limitations with this current technique; specifically involving constricted access, restricted visualisation and poor ergonomics. Technological advances to make laparoscopic surgery easier are being sought and the research area of surgical technologies has been growing over the last two decades. If it were possible to provide atraumatic reversible, reliable adhesion against gravity, an intra-corporeal robot, weighing 20g, as shown in Figure 1.1a, would be able to traverse the insufflated peritoneum enabling intraoperative vision. An alternative application is laparoscopic graspers, Figure 1.1b. The metal fenestrations on a laparoscopic grasper are known to cause unnecessary and sometimes irreversible tissue damage [2-6]. If it were possible to create adhesive forces by utilising the tissue fluid, whilst maintaining functionality, this damage could be prevented.

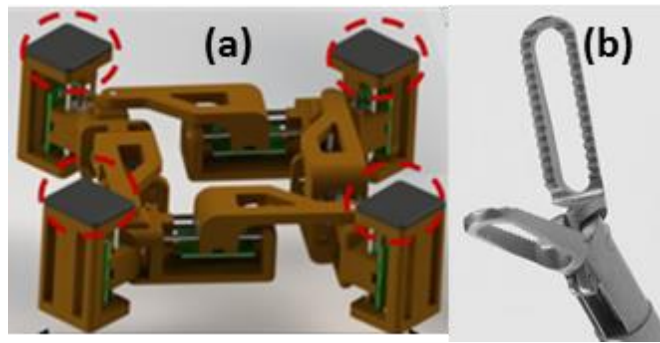


Figure 1.1 - (a) Intra-corporeal robot [7], where the highlighted areas indicate the location of the pads (b) Laparoscopic Grasper

1.2 Motivation

As described in the following literature review (Chapter 2), there are many adhesive systems including graspers, hooks and vacuum cups [8-12], which are capable of providing adhesive forces during surgery. However, many provide trauma to the tissue. In order to have a device to successfully adhere to the peritoneum, it is vital that the mechanism used can produce large enough forces to provide functionality, whilst also successfully allowing repeatable, atraumatic removal. The ability to do so, would not only aid minimally invasive abdominal surgery, but also have a role to play in any medical situation when an adhesive force is required at a tissue-device interface.

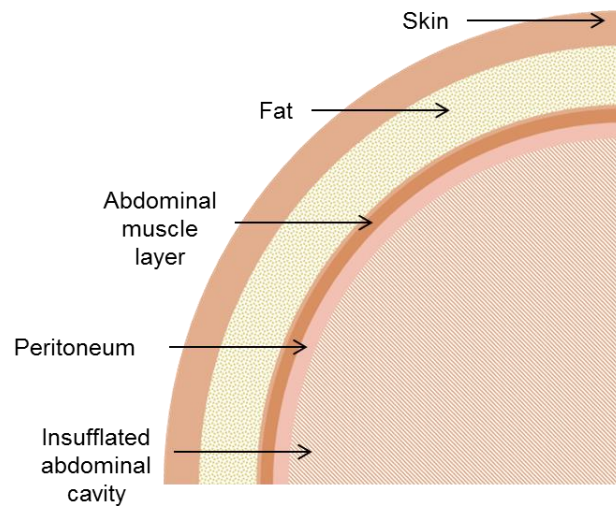


Figure 1.2 - Simplified diagram of the location of the peritoneum.

The peritoneum is a relatively flat, compliant thin layer of tissue, which provides protection to the abdominal organs, the diaphragm and the abdominal wall. Its basic structure is composed of a sheet of supportive collagen fibres, elastic elastin fibres, blood vessels and lymphatic channels all covered by a mesothelial layer [13-16]. This layer has a phospholipid bilayer membrane which surrounds the cell cytoplasm giving the layer viscoelastic properties. Despite the peritoneum surface being predominantly hydrophilic [17], the mesothelial layer secretes a fluid comprised of phospholipids similar to those in the bilayer [15, 16]. This fluid aids lubrication and increases the contact angle of the tissue in certain areas to become hydrophobic, and therefore, optimising adhesion through the formation of liquid bridges in the hydrophilic regions. Taking this into consideration it is possible to develop a mathematical model, combining the effects of capillary and Stefan forces to provide an overall wet adhesion mechanism. This model utilises the tissue fluid available on the tissue surface and provides the adhesive forces necessary for a removable, atraumatic, repeatable and reliable attachment mechanism.

1.3 Aims and Objectives

This thesis aims to provide an understanding of a reversible, reliable and repeatable wet adhesion mechanism. Specifically the focus is on how variation in the surface geometry and surface chemistry of bio-inspired structured polymers affect adhesive forces. The effect of the interacting fluid properties on adhesion will also be investigated. The combination will allow the optimisation of the adhesion system for surgical devices at a tissue device interface, whilst providing minimal trauma.

The objectives of this thesis are:

- To optimise existing lithography methods for the fabrication of micro-structured polymer surfaces with varying surface geometry
- To investigate an optimal wettability of polymer surfaces, specifically how exposure to a plasma treatment affects adhesion without altering the surface geometry.
- To investigate a wet adhesion mathematical model, encompassing both capillary and Stefan adhesive forces
- To investigate the viability of such surfaces in a surgical environment, in the simplest case docking a camera, and in the most complex case surgical tools.

1.4 Contributions and Novelty

This section outlines the areas of novelty found in this thesis along with the contributions this work has made to current literature.

- Micro-structure geometry

When comparing the adhesion mechanism in this thesis to that in literature, it can be seen that the scale of the micro-structures investigated

is as low as one tenth of that in literature. This not only affects the adhesion regime, specifically in terms of reaching a point of super-hydrophilicity, but also highlights issues with fabrication.

- Biological tissue

The main aim of this work is to produce a micro-structured surface capable of providing adhesion forces large enough to hold a device to the peritoneum, during surgical procedures. This raised many uncertainties in this work, specifically due to compliance, varying fluid properties, as well as the potential that the PDMS polymer surface may be adsorbing proteins - the effect of which is unknown.

Potential applications have also been highlighted, specifically other surgical devices which would benefit from having a method of reversible, repeatable and reliable adhesion and traction. The main focus being the use of such surfaces on a miniature robotic system, to provide traction through an inflated colon; as well as mention of their use on surgical graspers.

1.5 Thesis Outline

The chapter which follows will detail an extensive literature review (Chapter 2) covering the topics of technologies involvement in laparoscopic surgery, mechanisms of adhesion - encompassing both current surgical adhesives and alternative methods, and finally fabrication techniques.

Chapter 3 will detail the experimental techniques utilised throughout this thesis, including surface fabrication using cleanroom facilities, surface analysis techniques and the adhesion testing equipment.

Following this is the initial results chapter - Chapter 4, where polymer selections will be described and fabrication techniques will be explored, including

lithography procedures. This chapter outlines a range of fabrication procedures for a number of polymers, which are tried and tested before the final methodology is reached.

Chapter 5 will display the adhesion results for a varying wettability, surface geometry and fluid properties for testing against both wet glass and tissue.

Subsequently, a mathematical model will be discussed in Chapter 6 incorporating both capillary and Stefan adhesion mechanisms. A number of variables will be investigated in order to identify a theoretical optimum system.

Chapter 7 will discuss both the experimental and mathematical model results comparing the two and discussing the adhesion mechanism which is taking place. Potential surgical applications, including the design and development of a traction rig, and plans to utilise micro-structures onto a laparoscopic grasper will also be discussed.

Finally, Chapter 8 will conclude this thesis with recommendations for future work.

Chapter 2. Literature Review

2.1 Introduction

What follows is a review of the current relevant literature, the objective being to assess the viability of using a bio-inspired micro-structured polymer surfaces to adhere to the peritoneum during laparoscopic abdominal surgical procedures. Such a surface will allow a device, such as a camera or light, to be docked against the peritoneum enhancing intra-operative vision and aiding the surgeon.

First, minimally invasive surgery (MIS) is reviewed, including a brief history of how surgical procedures have evolved as a result of technological advances. Also included is an evaluation of the current uses of attachment mechanisms involved in robotic, natural orifice transluminal endoscopic (NOTES) techniques and single-port laparoscopy (SILS) procedures.

Next, a variety of adhesion mechanisms are reviewed in order to identify an optimal system which can provide reversible, reliable adhesion at a tissue-device interface without causing any unnecessary trauma to the patient. Bio-inspired systems are also assessed in this section.

Finally, a range of polymers are discussed with the aim of determining a suitable bio-compatible material which can be modified in terms of surface chemistry and geometry, in order to optimise adhesion. Micro-fabrication techniques are also discussed to define a suitable methodology to enable polymer micro-structured features to be produced reliably and repeatedly. The key points and findings are summarised at the end.

2.2 The Effect of Technology on Laparoscopic Surgery

It is essential to identify a clinical need for such a surface as that proposed here and to provide justification that there will be significant benefits to not only the patient but also the clinician. Surgical techniques have come a long way in the last two decades with technological advances, specifically in terms of access and visualisation. Below the advances in surgery, from open procedures to single access techniques are explored, the remaining issues are discussed; the possibility of a micro-structured surface to be used in collaboration with current and future surgical devices is then outlined.

2.2.1 Background

In recent years the field of medicine has experienced major changes, especially in terms of how surgical procedures are performed. It is no longer necessary for the surgeon to make large incisions to access the abdominal cavity and the organs contained therein. First introduced into abdominal surgery in the 1980's [1], minimally invasive laparoscopic techniques allow the surgeon to perform, what once was an open procedure, through a small incision or natural orifices which provide access for the surgical tools. Intraoperative vision is provided using endoscopic tools carrying a camera and providing a light source inside the cavity. Detailed images can then be relayed to an externally located monitor within the operating theatre. The abdominal cavity is usually insufflated with carbon dioxide, to elevate the abdominal wall above the internal organs allowing a sufficiently large working area and viewing space, as shown in Figure 2.1.

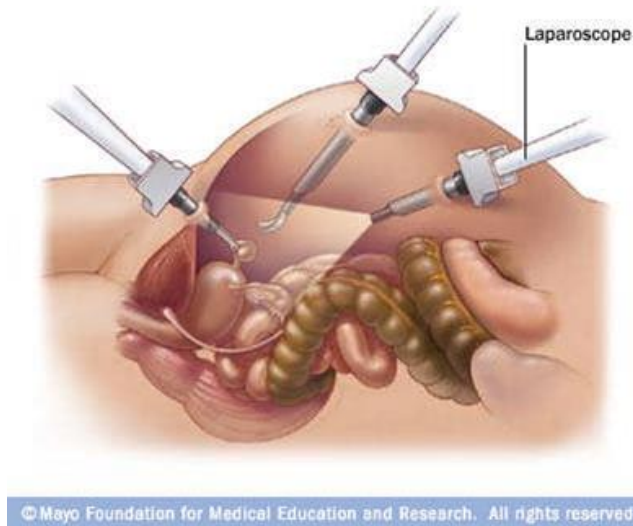


Figure 2.1 - Laparoscopic surgery set-up, showing the laparoscopes with different functionalities entering the abdominal cavity through small access ports [18].

2.2.2 Development of Laparoscopic Surgery

Over the past two decades in particular, surgical procedures have developed rapidly due to technological advances. It is shown, that using minimally invasive laparoscopic surgery, patients receive less scarring, achieve a faster recovery time and experience less post-operative pain [19]. These advances have allowed what were once complex procedures to be performed safely and efficiently. However, the benefits of laparoscopic surgery are still to be proven for many abdominal procedures involving more than one quadrant of the abdomen [20, 21], mainly due to not all patients being suitable for the procedure, cumbersome non-ergonomic equipment, leading to exaggeration of hand tremors [22], loss of dexterity and inadequate vision and tactile feedback [19, 20]. It is this reasoning that is propelling the technological advance in order to improve surgical procedures for use by surgeons [20].

2.2.3 Single Incision Surgery and NOTES

A current field of active research in minimally invasive surgery is natural orifice transluminal endoscopic surgery (NOTES). By entering through a natural orifice, as shown in Figure 2.2, NOTES is a technique which offers the opportunity of scar less surgery, resulting in even faster recovery times, limited pain and reduced risk of infection. Much of the work in this area has focused in the main on access to the abdominal cavity; however, due to technical difficulties in transluminal access, the only NOTES procedures reported with regard to humans is a hybrid procedure in which the natural orifice approach is used for purely visualisation, access and extraction purposes [23].

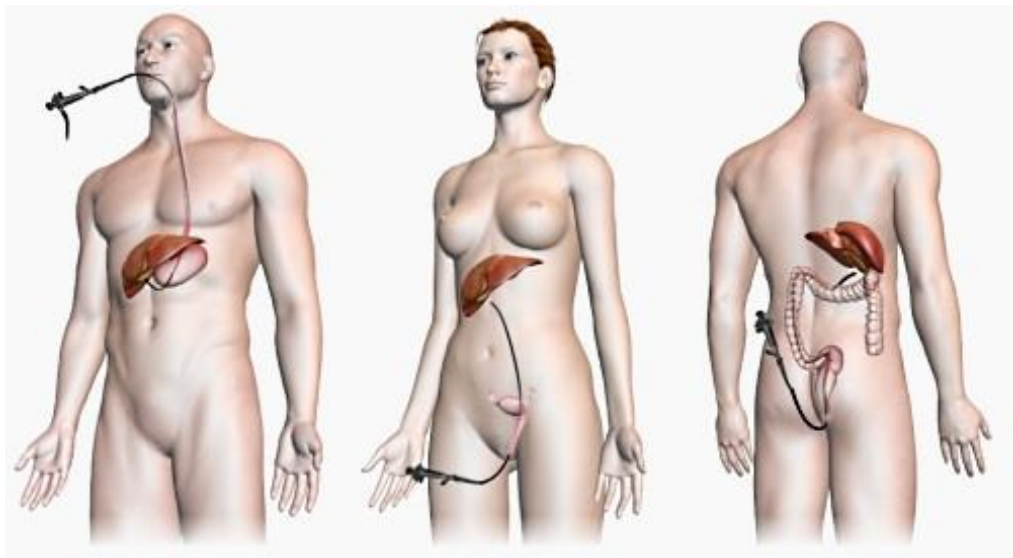


Figure 2.2 - Transgastric, transvaginal and transrectal notes procedures

[24]

True NOTES is a large area of interest due to the ability to potentially minimise access during intra-abdominal surgery, as well as the possibility of providing a gateway to many capabilities in endoscopic techniques. However, many of the barriers preventing widespread uptake are related to the limited instrumentation available. Specifically, current endoscopes are maximised for use within lumens

but will fail when utilised in open cavities such as the abdomen. This is due to their incapability to twist and turn, resulting in spatial issues for the user [25].

2.2.4 Robotics in Surgery

In the early 1990's a team at the National Air and Space Administration (NASA) proposed the concept of using master-slave based surgery, in which a virtual image of the abdominal cavity is sent to a remote site, where the surgeon performs the procedure without having actual contact with the patient [22]. A system has been developed which can give the surgeon a sense of operating directly on the patient whilst on the other side of the operating theatre, known as da-Vinci. The da-Vinci system consists of three separate parts: the surgeon's console, a video unit and robotic arms. The console is a non-sterile area which allows the surgeon to control the robotic arms (one for the camera and one for the instruments), these are shown in Figure 2.3, and are placed over the operating table. Both the console and the arms are connected to the video unit. The da-Vinci system provides intuitive instrument control, enhanced dexterity, an improved image and a depth to the field of view [26]; however, the machines used are large and not very agile thus making the working space in the theatre cramped, which could potentially lead to ergonomic problems during surgery. It is possible that many of the complications present in the master slave robots and other minimally invasive techniques could be overcome by using a miniature intra-corporeal robotic device which, using controlled wet adhesion from a bio-inspired surface, can be inserted into the patient during surgery.



Figure 2.3 - Components of the da-Vinci surgical system, a) the surgeon's console, b) the patient side cart, c) the endowrist instruments and d) the vision system [27]

The goal of such a miniature robotic device is not to replace the surgeon in the operating theatre but to provide the surgeon with a new set of versatile tools extending their ability to treat patients [28]. For example, Harrell and Heniford [26] describe how robotic devices may improve the visual feedback to a surgeon, more specifically an improved stability, focus and tilt. Li *et al* [29], also show that a robotic device would be able to follow the surgeon's line of sight and improve the awkward ergonomics by removing the constraint on the degrees of freedom, as well as being capable of adjusting for patient movement.

Moving on from this, the next obvious step in surgical technologies is arguably to move to an internal miniature device, which is free to manoeuvre throughout the cavity in to which it is inserted. This would allow the optimisation of single incision surgery and NOTES, by providing greater visualisation and would provide the potential to deliver surgical tools to a required site without the need for an extra port.

The design of a miniature internal device is dependent on the environment in which it is required to traverse and the interactions required at the tissue-device interface. For example devices which are required to function in a luminal

environment such as the colon [14, 30-32], will have their locomotion facilitated by the shape and functionality of the organ, having one main direction. However, negotiating intricate bends and obtaining traction may be a major issue. On the other hand, it will be a different locomotion method that is required when working in a non-tubular environment such as an insufflated abdomen which has been created specifically for the surgical procedure.

Recent advances in micro-manufacturing, specifically 3D printing, have allowed the development of miniature components such as motors, actuators and sensors, which will allow for a range of miniature robots to be developed for a range of surgical applications. There are already such devices available, as discussed below, however these have limitations specifically in terms of adhering to biological tissue atraumatically whilst traversing and providing traction.

A PillCam¹, Figure 2.4, has been developed, measuring 11 mm x 26 mm and weighing less than 4 g [33], which can be swallowed to provide visualisation of the oesophagus or the entire small bowel. Despite being a novel device for imaging, one limitation of the PillCam is its inability to control its positioning as it passes through the alimentary canal [23]. This could be optimised by using a bio-inspired structured surface to form reliable adhesion to tissue, allowing the PillCam to adhere to and detach from a desirable site atraumatically. There are developments underway to modify this device to include legs to enable manoeuvrability within the bowel [9]. These legs rely on providing a tension across the small bowel lumen to gain purchase. This is something which may prove problematic in certain disease situations where there is a dilation of the lumen or a thinning of the wall [17].

¹ Given Imaging, Yoqneam, Israel



Figure 2.4 - Image of the PillCam device, which has been designed to provide visualisation through the digestive tract [33].

There is currently a device under development which is both mobile and independently adherent to an internal body surface - HeartLander, Figure 2.5 [8]. HeartLander immobilizes the heart surface to fix it in a fixed frame of reference of the beating heart, without deflation of a lung. HeartLander enters the body through a minimally invasive port and attaches itself to the surface of the heart, travels to the desired location, using power on-board and establishes a stable platform for surgery to take place [8]. It makes use of suction cups at a safe vacuum pressure, supplied by an external pump to adhere to the heart tissue and makes inch-worm like movements across the surface of the heart at a crawling speed of approximately 0.5 mms^{-1} [8].

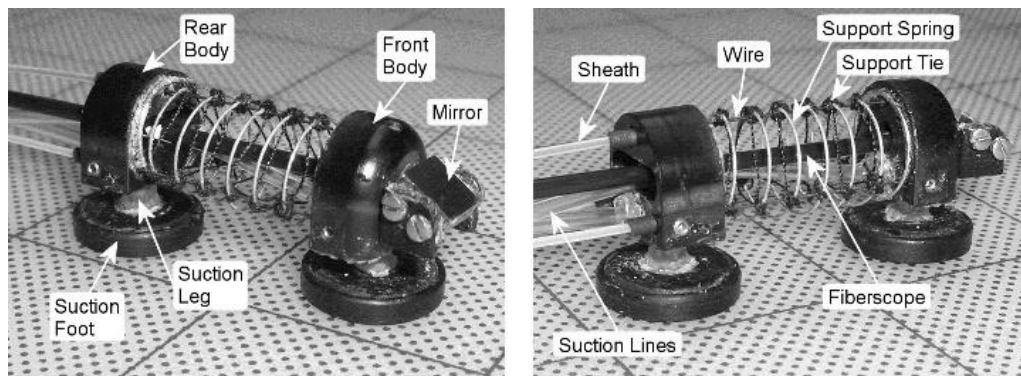


Figure 2.5 - The HeartLander device, which uses suction to traverse the surface of the heart in an inch-worm like motion [8]

The Nebraska device, Figure 2.6, is designed to move around the abdominal organs with two metallic wheels driven by two independent motors [34], carrying a camera and biopsy tweezers [35, 36]. The wheel profile of the device was investigated using bovine liver, and it was found that a helical structure on aluminium wheels provided optimum adhesion and traction on viscoelastic tissue; however it was unable to attach to and climb an organ surface.



Figure 2.6 - The mobile Nebraska robotic device, which uses metallic wheels to traverse abdominal organs [37].

2.2.5 Section Summary

Technological developments have enabled abdominal surgical procedures to enhance dramatically. What was once an open procedure with high mortality rates, an increased risk of infection and longer hospital stay can now be performed through a minimal number of ports or even through a natural orifice, enabling reduced scarring, higher survival rates and shorter hospital stays. The development of intra-body devices proves the potential to carry out exploration and procedures from inside of the body, with designs specific to the requirements for the areas in which they will be operating and traversing, manoeuvring intricate bends and specialist terrains. As shown in Table 2.1, it is therefore vital in order for these systems to evolve, to be able to provide a system with a reliable adhesion to and locomotion mechanism over the surface of tissue, whilst

ensuring minimal trauma. The mechanisms of adhesion with reference to this thesis are described in the following section.

Table 2.1 - Summary of miniature robotic devices and how an adhesive surface can aid functionality.

Miniature robotic surgical device	Current performance limitations which could be overcome through the use of an adhesive surface
PillCam	Inability to control its positioning as it passes through the alimentary canal [23].
HeartLander	Works well on a small surface area such as the Heart. However, suction cups covering a large surface area, can cause irreversible tissue damage [8].
Nebraska	Unable to attach to and climb an organ surface [37].

2.3 Mechanisms of Adhesion

Attaining reliable adhesion to the surface of tissue is an important component of the research presented in this thesis. In order to achieve this it is important to understand the basic principles of adhesion, which will later be necessary to enable an understanding of adhesion at a complex interface such as tissue. It is predicted that the chosen adhesion mechanism would be required to hold a payload of around 50 g, including a light source, camera, electronics and motors.

Adhesion is the interaction which occurs between molecules, resulting in attractive forces large enough to hold the molecules together. There are a range

of intermolecular mechanisms by which adhesion can occur, with a variation in the length scale of the forces and the strength of the resultant bonds [38]. The main mechanisms are as follows:

- Mechanical interaction
 - Interlocking joints
 - Graspers
 - Vacuum
- Chemical interactions
 - Covalent bonds
 - Ionic bonds
 - Interaction between polar molecules
- Locally induced electrostatic charge
 - Polarisation of molecules
- Quantum mechanical forces
 - Van der Waals
 - Magnetics
- Hydrogen bonds
- Capillarity
- Hydrophobic interactions.

There are currently a range of permanent surgical adhesives which can be used in many different surgical situations, for example BioGlue² [39] and Surgical sealant film - TissuePatch³ [40]. However as these provide only permanent adhesion, it is necessary to develop a structure which can allow reliable adhesion whilst also being reversible.

² CryoLife, Georgia, USA

³ Tissuemed Ltd, Leeds, UK

2.3.1 Mechanical Interactions

There are many other varied mechanical methods of attachment, the most common arguably being that of the application bio-inspiration in the form of burdock seeds in [41]. Other simple mechanical attachment mechanisms include graspers [11], micro hooks [9, 11] and vacuum cups [12]; however, despite providing reliable adhesion, such methods lead to differing degrees of tissue damage [17]. The damage to human tissue caused by a single journey to a specific location by a miniature device may be acceptable due to the regenerating effects of tissue. However, for a surgical device, minimal trauma is an essential requirement since, during healing, tissue is prone to bands of scar tissue forming between adjacent areas. This is a significant problem which can lead to long term complications [42-44].

2.3.2 Chemical Interactions

It is possible to attach a device to tissue using chemical interactions, but it is likely this method will lead to irreversible adhesion. It is also possible that chemical interactions to tissue could disturb the electrolyte concentration or cause changes to the pH of the tissue, which is reliant on the transfer of ions and active proteins at the cell membrane; therefore any disruptions would have major consequences for the patient [17].

2.3.3 Magnetic Attachment Systems

The use of magnetic attachment systems have also been widely investigated as they cause no chemical or traumatic damage to tissue, providing the compression and friction forces are small enough so as not to disturb the mesothelium surface of the tissue [17]. Mechanisms involving magnets have been successfully trialled in animal models as shown in Zhigang *et al.* [45], which investigates the injection

of a magnetic fluid into a porcine stomach, with an external permanent magnet used to retract the ferromagnetic induced tissue as shown in Figure 2.7.



Figure 2.7 - Injection of ferromagnetic fluid into a porcine stomach, an external permanent magnet can be seen to retract the tissue [45].

The experimental data recorded in Zhigang *et al.* [45] shows that magnetic retraction can be used to retract tissue for dissection, cutting and resection. The use of ferromagnetic fluids for tissue retraction during minimally invasive surgery has also been investigated by Lin [46]. Where 0.3 ml of ferromagnetic fluids was injected into the small bowel and a 0.6 T magnetic field was applied. In this work, a vertical retraction of 80 mm was possible.

The mechanism of using magnetic adhesion has also been investigated in conjunction with natural orifice transluminal endoscopic surgery (NOTES) – Section 2.2.3 The advantage of using a magnetic device along with the NOTES technology is that it provides successful anchorage as shown by Scott *et al* [47]. The purpose of their research was to perform a transvaginal cholecystectomy using instruments which incorporate magnetic anchoring and guidance systems. It can be seen from their data that this collaboration of systems is advantageous

in providing a stable surgical platform. However, the porcine abdominal wall thickness used was a maximum of 2.5 cm and it can be seen that the magnetic attraction forces diminish exponentially over this distance; therefore in human samples - where the abdominal tissue is thicker - a larger magnetic force would be needed. There are distinct disadvantages; as extra power and equipment would be required to establish a large enough magnetic field, the procedure becomes more complex and more expensive with limited precision [17].

2.3.4 Passive Adhesion

The mechanisms described above require active manipulation to gain any adhesive forces. This delivers a multitude of disadvantages with the possible disturbance of the tissue structure, a requirement for additional moving parts, external equipment and power. Therefore it would be more beneficial to adopt a passive form of adhesion which can utilise the properties normally present at tissue interfaces [17]. There is a range of attractive forces present on surfaces under normal circumstances, the main examples are van der Waals interactions and the interactions related to hydrogen bonding of water that is capillary effects as explained in section 2.3.5.1. The main disadvantage of intermolecular forces is that they are very weak forces and act over a very small length scale; therefore their use for macroscopic adhesion is reliant on an increase in contact area to increase the adhesive forces. Recent progress in understanding adhesion mechanisms has led to the mimicking of the adhesive abilities of insects and other creatures for engineering applications [21]. It is clear that the most interest has been directed at surfaces inspired by the gecko's foot pad [48-59].

2.3.5 Wet Adhesion

While most interest in bio-inspired adhesion has arguably come from the gecko, it is widely known that other species use a similar adhesive mechanism which may be easier to replicate. Van der Waals forces alone cannot be responsible for adhesion in these systems, as at molecular levels the compliance is no longer available [17]. Instead these species must utilise liquid from the local environment to produce capillary forces to generate wet adhesion.

2.3.5.1 Capillary Adhesion

Capillary adhesion initially arises from the structure and arrangements of water molecules.

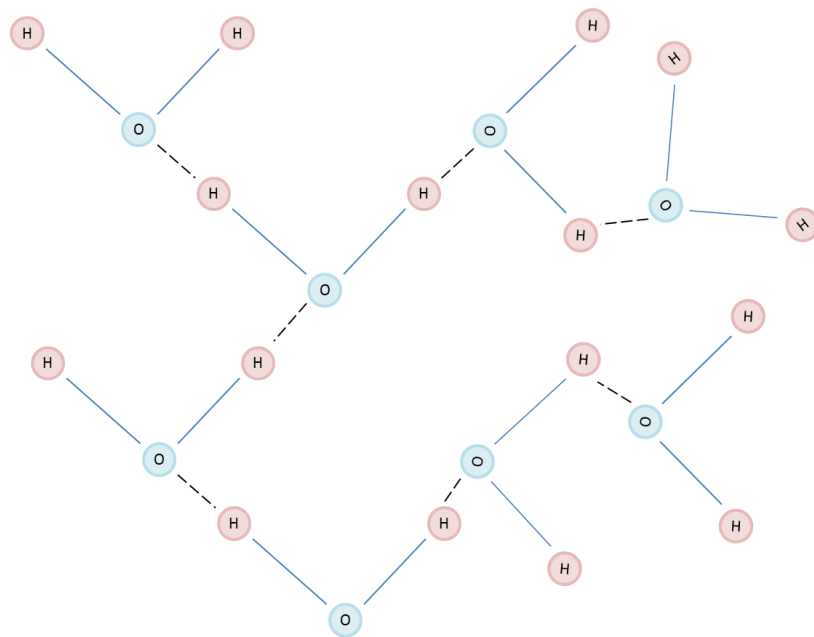


Figure 2.8 - Schematic of the cohesion of water molecules via hydrogen bonds (dashed lines).

Hydrogen bonds are formed between hydrogen and oxygen atoms on neighbouring water molecules, as shown in Figure 2.8. These attractive forces are dipole-dipole interactions, due to the polar nature of water. This cohesion of

water molecules gives rise to a surface tension and contact angle, as well as resulting in the hydrophobic and hydrophilic effects of any material surface which may come into contact with it. These are all interrelated and create a capillary force when water is present on a surface. When dealing with water and its interactions, there is a difference in energy at the solid-air interface and the water-air interface. It is these differences which lead to differing capillary effects and give rise to hydrophobicity and hydrophilicity.

2.3.5.2 Surface Wettability

When a surface contains a negative charge, the positively polarised hydrogen atoms are able to form a weak interaction, lowering the interfacial energy and making the surface more compatible with water, this is referred to being a hydrophilic surface. On the other hand, if the surface is inert and has no electronegative molecules to interact with the positive hydrogen, the interfacial energy remains high, allowing the water molecules to then form hydrogen bonds between themselves to increase the stability, such a surface is hydrophobic. The cohesive force in this state is stronger than the adhesive force [17]. The hydrophobic and hydrophilic nature of a surface is best described by the contact angle; the angle subtended by water droplets on a solid surface in air. If the contact angle is greater than 90 degrees, the surface is hydrophobic. It follows therefore that if the contact angle is less than 90 degrees the surface is hydrophilic.

If a surface is wetted by a liquid at an angle $\theta_E < 90^\circ$ a droplet will remain as shown in Figure 2.9, and will form a capillary bridge, with radius R and surface area πR^2 allowing two surfaces to stick together with great strength [60].

$$\cos \theta_E = \frac{\gamma_{SV} - \gamma_{SL}}{\gamma_{LV}} \quad (2.1)$$

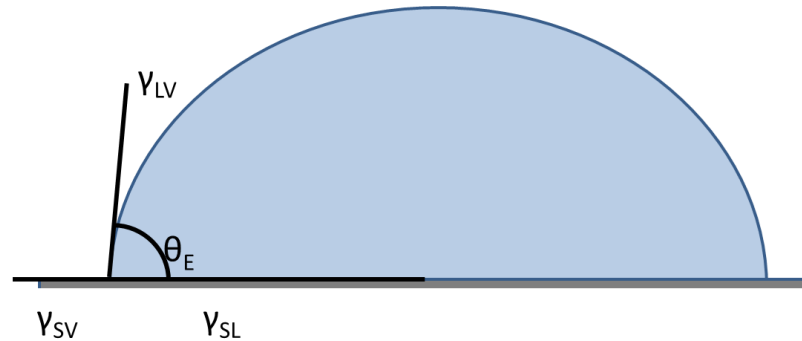


Figure 2.9 - Young's model of a liquid droplet on a solid surface

Where: γ_{lv} = surface tension at the liquid/vapour interface,

γ_{sv} = surface tension at the solid/vapour interface,

γ_{sl} = surface tension at the liquid/solid interface,

θ_E = Contact angle

Once the contact angle of water is linked to the work of adhesion in removing it, the presence of water between two surfaces affects the adhesion between them. For a hydrophobic surface a convex meniscus is formed, and the work of adhesion is therefore negative, and the two surfaces are not held together, but as the surfaces separate there is a slight attractive force at the end stage of separation [61]. However for a hydrophilic surface, a concave meniscus is formed which provides an adhesive force as the liquid attempts to wet each surface and water can be seen to move between the surfaces as it spreads. This can be seen in a capillary tube, where the closer the surfaces of the tube are in proximity to one another, i.e. the smaller the radius, the further the liquid will spread (rise). If

the two surfaces are to be pulled apart a certain distance, the separating force must overcome the adhesive force of the liquid.

2.3.6 Biomimetic Wet Adhesion

In order for a structure to adhere to a wet surface such as tissue, it is useful to understand the mechanisms of wet adhesion employed by various creatures in nature, such as the tree frog. The pads on a tree frog's foot consist of an hierarchical array of peg studded hexagonal cells, approximately 10 μ m in diameter [21], with deep channels 1 μ m wide running between them [62], covered in a dense array of hexagonal micro-structures. These footpads are able to deform at the micro-scale to gain a large enough surface area of contact. As the end units in the footpads are held very closely together the channels between them are very narrow, and so capillary forces within the channels can manipulate the amount of fluid flowing in and out of the spaces [63]. The micro-structured surfaces fabricated in this thesis, although are modelled on the footpads of the tree frog, have some major differences in that in order to provide adhesion to a wet surface, the tree frogs pads are permanently wetted by mucous glands which open onto the surface allowing the mucus to spread over the pad through the hexagonal channels, it is also believed that these channels may also serve to remove any excess fluid which might be encountered by the frogs during rain fall [64]. It was first believed that this mucous layer had a glue like function, however experimental studies have shown that the tree frog is able to stick to a surface by using the combined forces of surface tension and viscosity generated by a fluid filled joint between the pad and the substrate [62, 65-69]. This is shown in a number of cases. Firstly, a visible meniscus around the area of contact between the substrate and toe pad can be seen [62]; secondly, shear forces of the toe pads were found to be velocity dependant (Figure 2.10) [62, 65], and finally due

to the sticking ability becoming reduced when the toe pads were fully immersed in water [62, 70]. Therefore by mimicking the shape of the tree frog along a fluid filled joint can form between the wet surface and the structured polymer and provide the adhesive forces necessary.

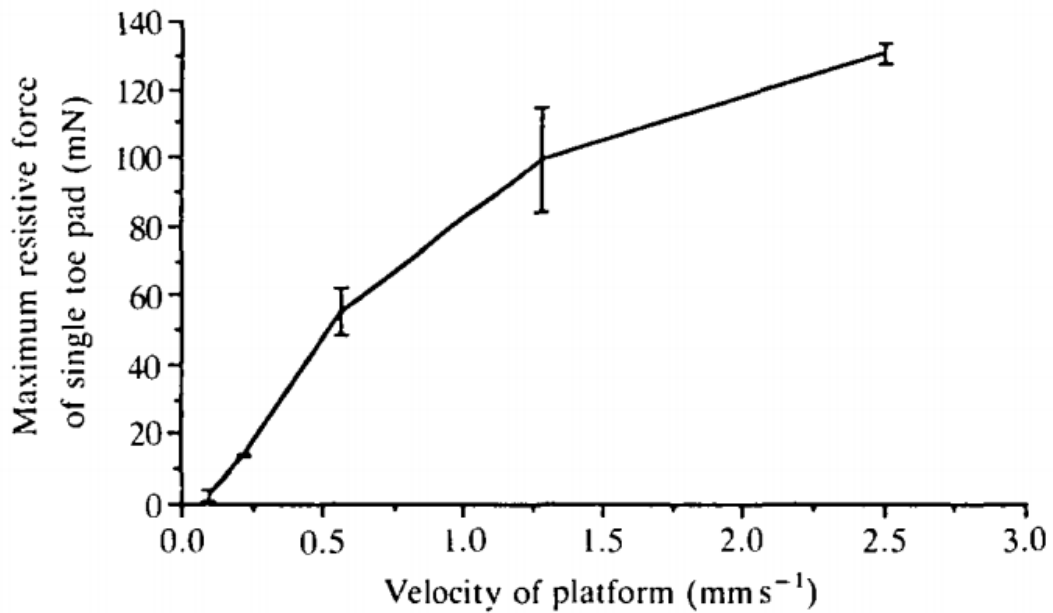


Figure 2.10 - Results by Hanna *et al.* [65], where a horizontal force was applied in a forward direction, mimicking the forces that would be applied to the toe pads of a frog tending to slide backwards down a vertical slope. The graph shows that resistive forces of single toe pads to movement in the shear plane are dependent on the velocity of the applied movement.

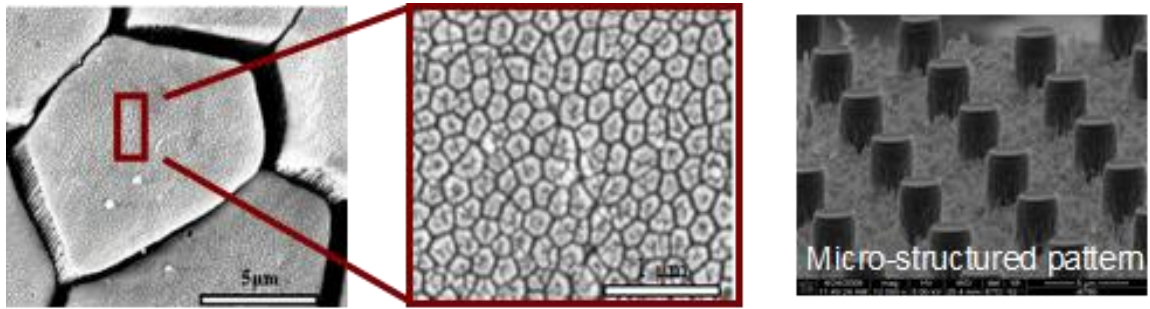


Figure 2.11 - The structure of a tree frog's foot pad, on both the micro and nanoscale, followed by polymer bio-inspired micro-structured surfaces mimicking it [21].

In order for a structured surface to adhere to a wet surface such as tissue, it is necessary to utilise the tissue fluid in the form of Stefan adhesion and capillary forces [71], where the Stefan adhesion is a consequence of the viscosity of the fluid, and capillary forces are as a result of surface tension and surface wettability. The adhesion mechanism is discussed further in Chapter 6. As these mechanisms of passive adhesion require intimate contacts between molecules as the forces only act over a short length scale, it is required for there to be an increase in the total contact surface area. However, mimicking the toe pad of a tree frog will result in a microscopic roughness on the surface, preventing an intermediate contact across a large area, therefore the contact area needs to be enhanced [17] - this can be achieved using surface wetting.. When microstructures become wetted a meniscus is formed around the area of contact showing that the pad and surface are connected by a fluid filled joint [72]. The shape of the meniscus formed is determined by the equilibrium between capillary forces and gravity. Figure 2.12 shows the formation of a concave meniscus (highlighted by arrows) formed around the toe pad of a frog in contact with a glass surface.



Figure 2.12 - The toe pad of a frog in contact with a glass surface with an attractive concave meniscus formed [73].

2.3.7 Biomimetic Dry Adhesion

Inspection of a gecko's toe pads suggests a hierarchical structure of 5 toes, each with transversely arranged lamella. The lamella is made up of keratinous structures, setae, of which there are approximately 500,000 per gecko foot. Each of these structures is then sub-divided further into spatulae, which are as small as 200 nm in diameter [74], as shown in Figure 2.13. It is this hierarchical structure which allows the gecko to gain intimate contact with a surface across a large surface area [23]. Autumn *et al.* [75] have investigated two competing hypotheses of the adhesion mechanisms in the tiny foot-hairs of the gecko (setae): firstly the use of capillary forces and mechanisms relying on hydrophobicity, and secondly the use of van der Waals forces [75]. It can be seen in Autumn *et al.* [76] that the proposed mechanism for dry adhesion occurring in the case of the gecko, is that of van der Waals forces as adhesion is not dependent on the hydrophilicity of substrates [76].

Van der Waals interactions are generated by small differences in charge, as clouds of electrons move around their distinct orbits. At a specific separation the

net charge can be either attractive or repulsive, but it is strongly attractive between molecules containing atoms whose electron orbits can be induced to shift by an external charge or force [17, 76, 77]. These interactions are small when alone, but when they are multiplied over the contact area from the spatulae, a large enough adhesive force is generated to support the weight of the gecko [23].

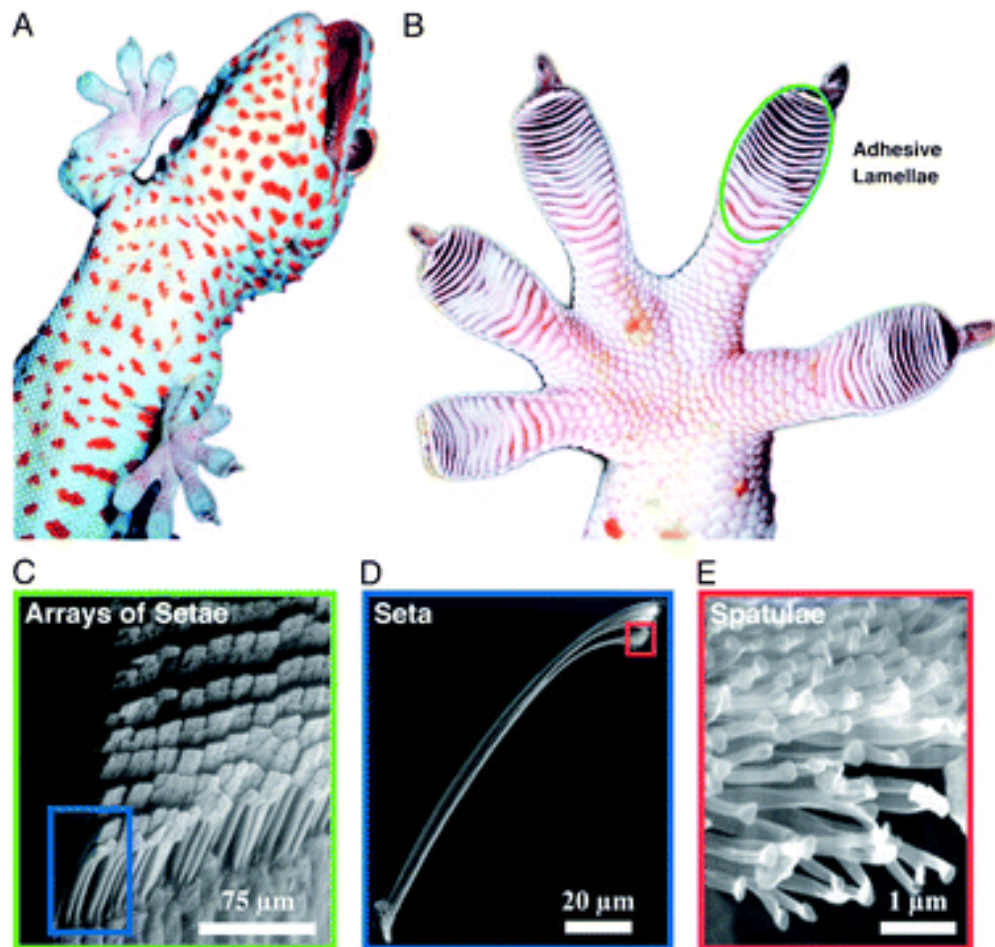


Figure 2.13 - Structural hierarchy of the gecko adhesive system. (A) Gecko. (B) Macrostructure. (C) Meso-structure: view of the foot with adhesive lamellae. (D) micro-structure: portion of a single lamella, setae array visible. (E) Nano-structure: single seta with branched structure terminating in hundreds of spatula tips [78].

2.4 Fabrication Techniques and Surface Optimisation

2.4.1 Introduction

The viability of a number of fabrication techniques, which can be exploited to create a regular array of micro-structures on a flexible polymer substrate, is now explored. Micro-fabrication techniques are commonplace for many applications, specifically in the field of micro-electronics. Arguably the most common technique is that of lithography. Lithography, encompassing the processes of photolithography, soft lithography and nano-imprint lithography together with the ability to fabricate varying surface geometries is discussed, with the aim of highlighting the techniques which will be carried forward during this work. As well as exploring fabrication techniques, a range of polymers is considered in terms of which are viable for this research, specifically in terms of bio-compatibility, flexibility and also the ability to be fabricated into a micro-pillared array. The possibility of altering the surface chemistry, in terms of wettability is also discussed.

2.4.2 Surface Optimisation

As an aim of this thesis is to repeatedly and reliably fabricate flexible, structured surfaces to be used in a surgical environment, it is important to have a background understanding of the polymers available. It is also necessary to consider polymers in terms of which can be fabricated into the micro structured surfaces using a suitable technique, and also allowing for controlled wettability. This next section will discuss the fabrication techniques available as well as the suitable polymers whilst also discussing possible contact shapes, concluding with an awareness of the best polymer and geometry shape possible with the fabrication techniques available.

2.4.2.1 Surface Geometry

It is necessary to ensure the surface geometry is one which can utilise contact mechanics and provide the greatest adhesion force possible. The ideal adhesion mechanism to enable this uses attractive interfacial forces, specifically Stefan forces and Capillary forces. At a small contact distance it will be Stefan forces which dominate; as this distance increases it is then capillarity which is the governing force. This will occur through the formation of liquid bridges on the tip of each pillar, and cohesive forces occurring at the interface (Figure 2.14). It is therefore necessary to evaluate what geometry will aid this action, specifically in terms of pillar size and spacing to allow the formation of liquid bridges and contact surface area by applying a structured roughness to the surface.

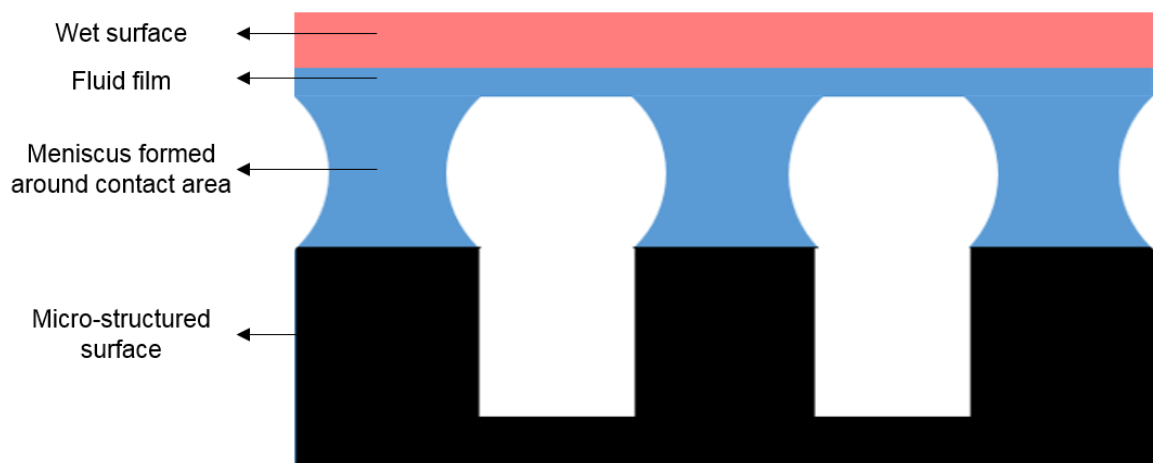


Figure 2.14 - Formation of liquid bridges from a continuous fluid film on the tip of micro-pillars

It has been shown that the division of a contact area into small discrete points is beneficial to increasing adhesion forces [21, 51, 79], as shown in Figure 2.15, where flat surfaces and micro-structured surfaces were compared for varying contact areas. It can be seen that the adhesion force is enhanced through the presence of the micro-structures. This is something which is seen vastly in nature from the tree frog [72] to insects [80]. This therefore supports the initial proposal

to use a pillared array will in fact aid adhesion. However, the next issue is that of size.

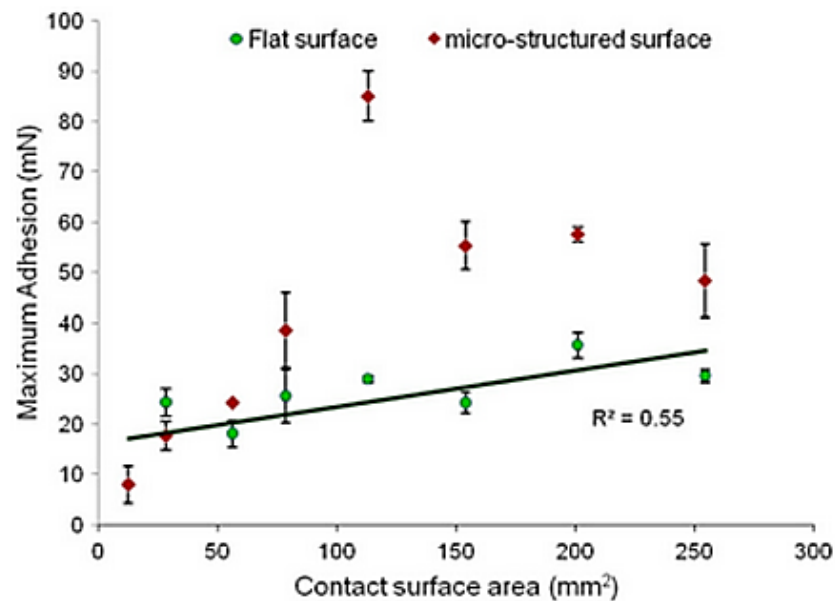


Figure 2.15 - Results by Roshan *et al.* [21] showing the maximum adhesion force as a function of area for flat and micro-structured surfaces adhering to a wet surface. It can be seen there is an optimum contact surface area at 113mm², areas larger than this have a detrimental effect on the adhesion forces produced.

Nano-pillars will increase the contact surface area due to their low contact distance and as previously mentioned this will result in Stefan forces being the driving force in the mechanism. However in this case there will be a high surface roughness, which would hinder and capillarity mechanism as the distance increases, as it would only take a small fluid volume to completely flood the surface. It may also be the case that the presence of nano-pillars will render the surface hydrophobic. Although this is detrimental to the adhesion forces, according to the model presented, it may be the case that at the end stage of separation there may be a slightly attractive adhesion force. [61]

It is also shown in [63, 79] that the capillary forces are reliant on the diameter of the asperities, as well as their height, and the spacing between them; if they are too small this will decrease the meniscus size and therefore be prone to instability. For capillary bridges this occurs at diameters around $1\mu\text{m}$ - therefore it is necessary to have a pillar of diameter larger than this, as pillar height is not expected to be as important a factor for adhesion as the diameter, the aspect ratio for these surfaces will remain 1:1.

It is also important to discuss the wettability of the surface, as when a hydrophobic surface has an increased roughness the surfaces' affinity to water will alter. The contact angle increases with surface roughness, and therefore the surface will not be wetted and as a result no capillary bridges will form and capillary rise will not be possible in the spaces, this can be shown in (2.2), where if both surfaces are hydrophilic i.e. θ_1 and θ_2 both are less than 90° , the adhesive force will be positive (attractive).

$$F_{\text{cap}} = 2\pi r_m \gamma (\cos\theta_1 + \cos\theta_2) \quad (2.2)$$

Where, r_m is the radius of the meniscus, γ is the surface tension, θ_1 , is the contact angle at the wet surface and θ_2 , is the contact angle at the micro-pillared surface as shown in Figure 2.16.

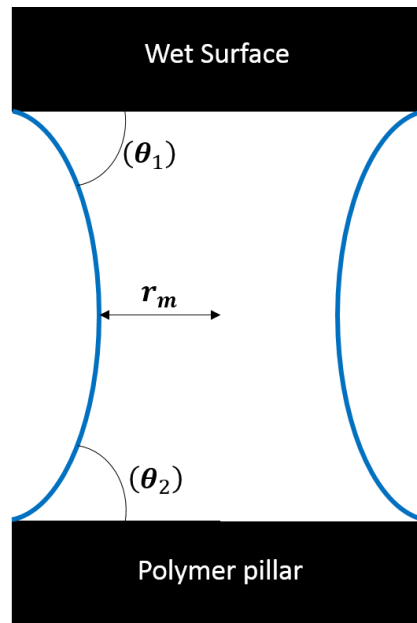


Figure 2.16 - Variables of capillary forces.

Despite this however, De Souza *et al.* [81] have shown that there is an optimal contact angle (70°) to provide maximum adhesion through the mechanism of discrete liquid bridges. It has also been shown by the same group that it is also possible for this mechanism to be successful with one hydrophobic surface, as long as the other is significantly hydrophilic, ensuring that $\cos \theta_1 + \cos \theta_2$ is positive [82]. The effect of altering the contact angle experimentally is shown in Chapter 5.

With this in mind, it has been decided to use an initial design specification, following the work of Roshan *et al* [21], to have an array of micro-pillars, $3 \mu\text{m}$ in diameter, with a $3 \mu\text{m}$ spacing and of $3 \mu\text{m}$ in height. The effect of the pillar spacing has been investigated and the results are shown in Chapter 5, where a pillar spacing of 1.5, 4.5 and $6 \mu\text{m}$ (Figure 2.17) have been tested individually against a wet surface in order to optimise the adhesion. It is important that these pillars are fabricated accurately, as a large variation in pillar size and shape across the surface will result in a large change in the adhesive forces recorded,

as according to the mathematical model, the geometry of the pillars is one of the main factors at influencing the adhesive force as shown in Chapter 6.

It is vital when fabricating the pillars that their walls are as close to being perpendicular to the base as possible, in order to ensure that the capillary rise effect can occur successfully.

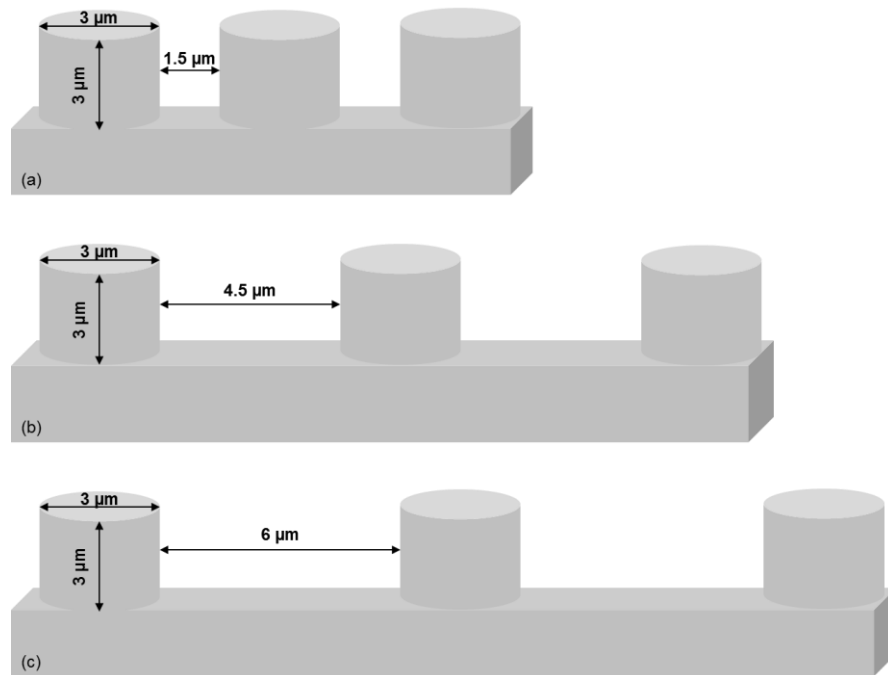


Figure 2.17 - Wafer Geometries, (a) Wafer 1, Pillar Spacing = $1.5\ \mu\text{m}$, (b) Wafer 2, Pillar Spacing = $4.5\ \mu\text{m}$, (c) Wafer 3, Pillar Spacing = $6\ \mu\text{m}$.

2.4.3 Photolithography

Photolithography is defined as the modification of a surface by illumination through a photo mask [83], and is widely used in biological applications and tissue engineering to pattern substrates with biological functionalities [83]. This method provides straight forward scaling and uses a broad basis of equipment and expertise [84]. Using photolithography also provides the scope to alter the surface wettability as shown by Deval *et al.* [85].

Ultraclean conditions must be maintained whilst carrying out photolithography as any dust particles which may fall onto the substrate during processing will result in pattern defects in the final surface [86]. Therefore it is important that photolithography is performed in a cleanroom which has a filtration system to remove particles from the air. The main photolithography steps are detailed below, but the technique can be specifically tuned depending on the resist and the features required.

There are two main specific photolithographic techniques available, both of which result in a micro-patterned surface; additive and subtractive. In additive and subtractive lithography, the resist is structured first using irradiation and development. During these first steps the resist film is partially removed allowing, during further processing, materials to either be deposited or removed from the bare areas of the substrate [87]. Additive photolithography involves a lift-off process, in which the photoresist is used as a contact mask [84], deposited straight onto the substrate, exposed and developed to leave parts of the substrate bare. The film to be patterned is then deposited, coating both the bare parts of the substrate and the surface of the resist. The remaining photoresist is then dissolved, removing the film which had been deposited on it [84]. In subtractive photolithography, the film which is to be patterned is coated with a polymeric photoresist using spin coating. The resist is then exposed to a UV source through a photo-mask containing the pattern to be transferred onto the film.

The photoresists involved in photolithography are described as either positive or negative toned depending on the polymer crosslinking mechanism. Resists with a tendency to chain scission are positive tones, replicating the photo mask structure, whilst those which bond their chains are negative, and replicate the inverse of the photo mask as shown in Figure 2.18 [88]. The remaining

photoresist on the surface, is then used as a mask and an etching step is employed to finally transfer the pattern to the base film [84]. The photoresist can then be stripped of by a suitable solvent.

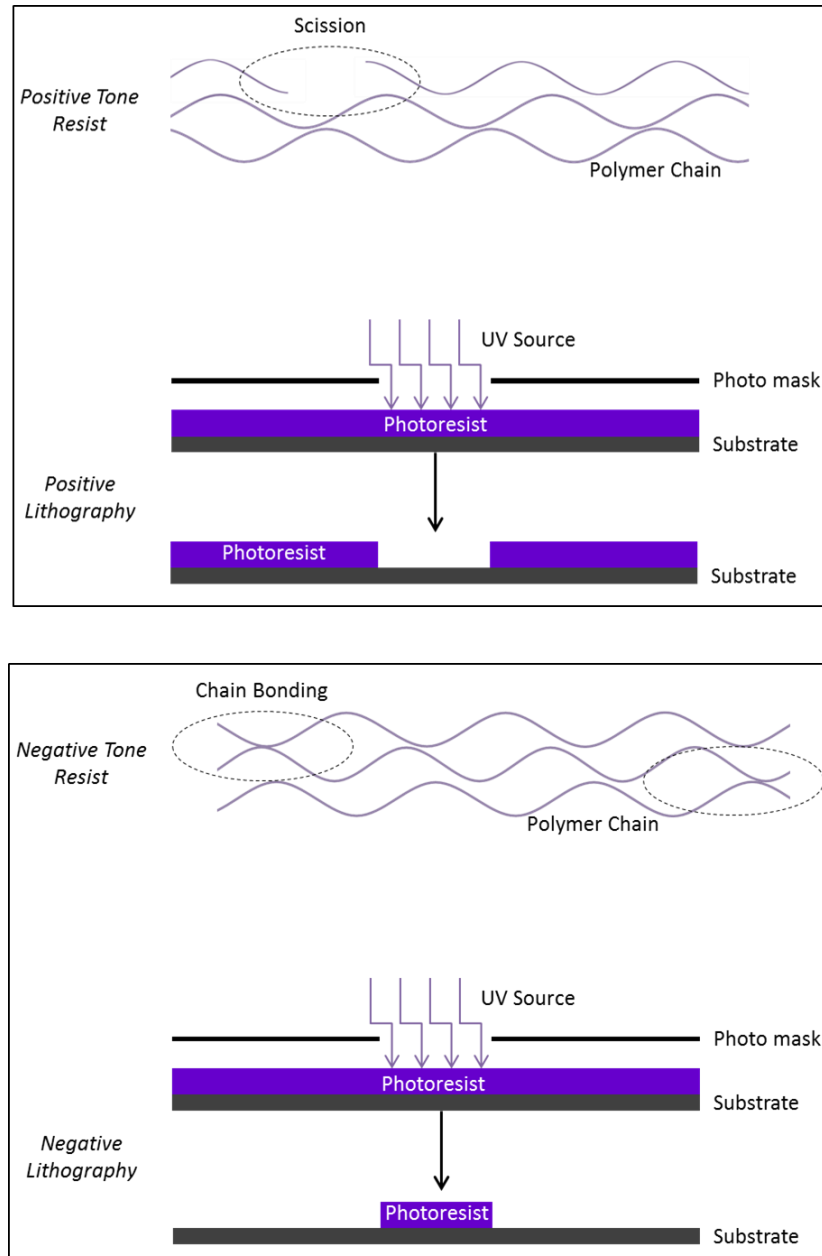


Figure 2.18 - Positive and negative photoresists. The positive resist replicates the mask structure through polymer chain scission. The negative resist replicates the inverse of the mask structure through polymer chain bonding.

Depending on the final etching technique used, it is possible to determine varying wall profiles; specifically isotropic or anisotropic (Figure 2.19). Wet etching commonly produces an isotropic profile, due to the etch occurring at the same velocity laterally as vertically. However, it is also possible to dry etch using plasma. This will result in an anisotropic profile [88], which is desirable for the production of the necessary micro-structured surface.



Figure 2.19 - Wall profiles caused by different etching techniques. Wet etching commonly produces an isotropic wall profile, whereas a dry etch will provide a straight anisotropic profile.

Whilst photolithography is a successful and well established technique, many of the processes are optimised for hard materials, such as silicon, which are beneficial to microelectromechanical systems (MEMS). Therefore alternative methods are considered and discussed for the production of the final polymer surface, whilst photolithography will be used for the production of the silicon master mould.

2.4.3.1 Soft Lithography

Soft lithography provides a simple, inexpensive and reliable option for producing structured surfaces. It represents a collection of techniques based on printing, moulding and embossing with an elastomeric stamp [89], creating surface structures with well-defined geometries [90]. Unlike photolithography, which transfers a pattern using optical techniques [91], soft lithography is a direct printing method.

Soft lithography techniques can also be used to produce complex hierarchical arrangements which does not seem to positively influence the force of adhesion of structured surfaces to a wet counterpart, but may be relevant when rough substrates are used due to their ability to aid adhesion within surface conformities [50].

2.4.3.2 Nano-Imprint Lithography

Nano-imprinting lithography is a very common technique which can simultaneously improve pattern resolution and reduce complexity [91]. It is based on the use of a rigid template containing a structured pattern on to which a photoresist is spun, soft baked, causing the resist to harden and improve adhesion, and then flood exposed to a UV source, to crosslink the polymer as in photolithography. It is then baked further before development and hard baked to strengthen the resist structure [92, 93] and allow the pattern to remain in the photoresist when peeled away.

This nano-imprinting technique, has been furthered to provide a large scale, low cost roll-to-roll processing method based on the concept of a disposable master [94] (Figure 2.20). This novel technique involves, spin coating a pre-fabricated surface with a photoresist, baking and imprinting the pattern onto a film using a hand held roller [94]. The sample is then exposed to a UV source and baked, before peeling apart, leaving a negative replica of the original template [94].

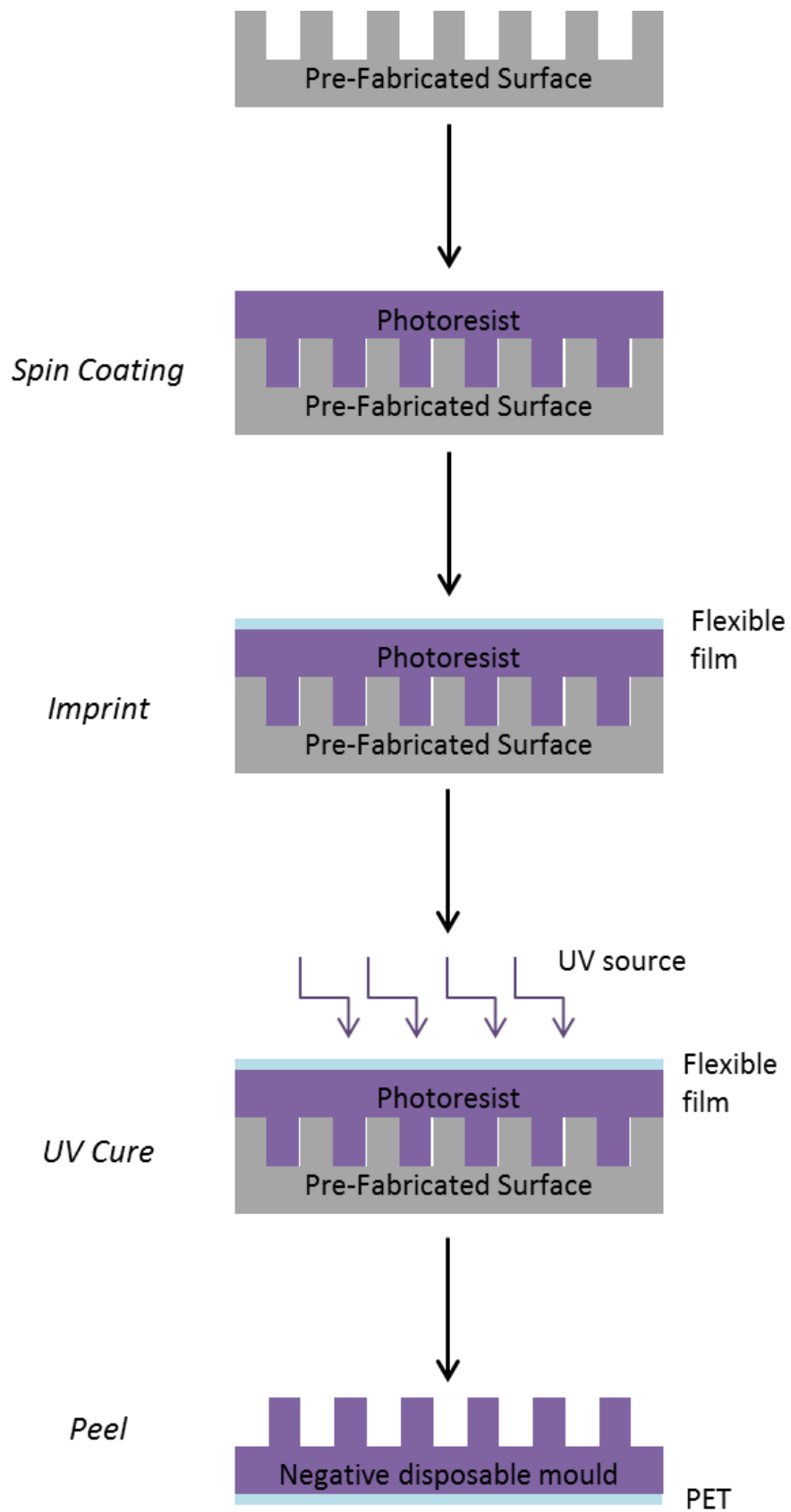


Figure 2.20 - Process of a novel nano-imprinting technique.

2.4.4 Surface Chemistry

The surfaces once fabricated are to be used in a clinical environment; therefore polymer selection is a vital process, in order to, not only ensure that fabrication can occur successfully, but also to ensure that the surface is bio-compatible, water resistant and flexible. This section will discuss a variety of polymers which may be possible for this application.

2.4.4.1 Polyurethane (PU)

Polyurethane (Figure 2.21) is used in many micro-fabrication techniques to produce micro-fibre and nano-pillar arrays [95-103], for a range of applications. However, due to its high stiffness polyurethane structures are prone to lateral collapse. The structure of polyurethane allows surface modification, specifically in terms of wettability, while it is also possible to alter the chemical structure to attach biologically active species on to the surface. It is these properties which enable the wide use of this polymer in many biological systems from catheters [27] to artificial organs [20, 37], as well as mediating the acceptance and healing of an implant or device [24].

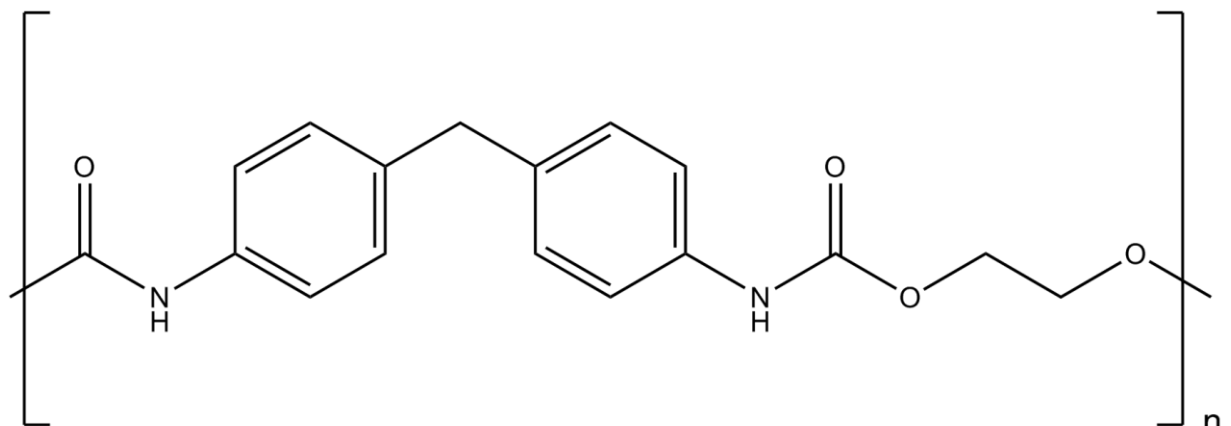


Figure 2.21 - PU structure

2.4.4.2 Polymethylmethacrylate (PMMA)

PMMA (Figure 2.22) is strong lightweight thermo-softening polymer. It is particularly versatile in terms of fabrication methods, with the ability to be injection moulded and hot embossed, as well as undergoing laser ablation and lithographic techniques [14, 30, 32, 35, 104]. PMMA is used in a variety of microfluidic devices [30, 31, 36], including high aspect ratio microstructures [14], blood filtration [32] and micro-reactors [30]. It is compatible with human tissue, making it highly common in a range of biomedical situations such as Intraocular lenses [105], and being one of the most enduring materials in orthopaedic surgery [106] by being utilised to affix implants and the remodelling of lost bone. However, at room and body temperature PMMA is rigid, which is undesirable for use in a surgical environment, as in order to conform to a flexible substrate such as the peritoneum during surgery, the polymer surface is required to be flexible.

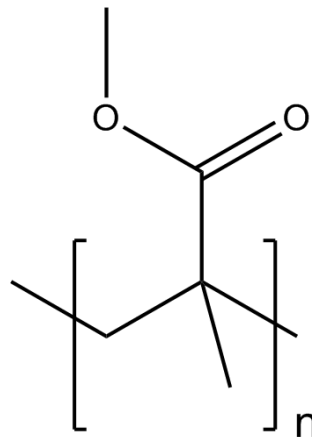


Figure 2.22 - PMMA structure

2.4.4.3 Polydimethylsiloxane (PDMS)

PDMS (Figure 2.23) is a silicon based, organic polymer, which is viscoelastic and non-toxic.

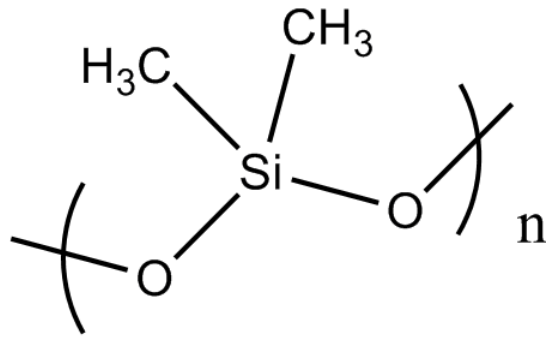


Figure 2.23 - PDMS structure

The polymer is prepared by combining an elastomer base and curing agent at a specific ratio. The ratio is dependent on the mechanical properties required for a specific application, the higher the ratio, the stiffer the material. After the crosslinking process the solid PDMS sample has a hydrophobic surface, however atmospheric air plasma adds a silanol functional group to the surface, resulting in a reduction in contact angle by switching the wettability to hydrophilic. The recovery of hydrophobicity will occur in 30 minutes in air, however this can be delayed further by storing the samples in de-ionised water [24]. PDMS is commonly used in a range of applications, specifically antifoaming agents, and a range of medical and cosmetic applications such as over the counter drugs, skin protection moisturisers, shampoos and conditioners [20, 27, 30, 37]. Structures are commonly produced in PDMS using nano-imprint lithography as described above, where the features give rise to many more applications such as microfluidic chips [107], biomedical microelectromechanical systems (Bio-MEMS) [108, 109], and flexible electronics [110] as shown in Figure 2.24.

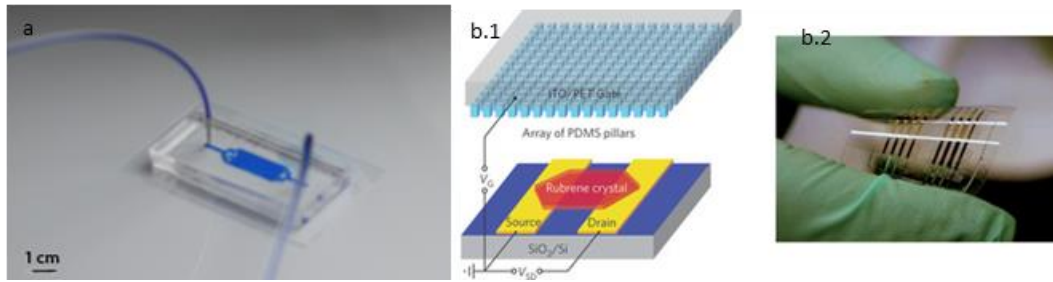


Figure 2.24 - (a) PDMS microfluidic chip [107] (b.1.) - Schematic of a pressure sensing organic transistor, which makes use of a micro-structured PDMS film. (b.2.) Flexible electronic device [110].

PDMS is also being used to mimic Gecko adhesion for dry adhesive materials as previously discussed in section 2.3.7.

2.4.4.4 SU8

SU8 (Figure 2.25) is a negative tone, epoxy based photoresist, which is commonly used for permanent structures. In this work it the SU8 2000 series in particular which has been explored, due to its ability to produce vertical sidewalls and high resolution [14]. When SU8 photoresist undergoes ultra-violet exposure cross-linking occurs in two steps. Firstly, a strong acid is formed during the exposure, followed by an acid-catalysed thermally driven crosslinking during baking [14]. There are six viscosities available in the SU8 2000 series. However it is only SU8 2002 (7.5 CSt) and SU8 2010 (380 CSt) [14] which have been used throughout this work, due to their theoretical ability to produce the resolution required for the pillars; according to the product data sheet where a correlation is described between the spin speed, spin time and thickness. The spin speed and spin time for each viscosity determines the film thickness produced - a higher spin speed for a longer time will produce a thinner film. Often a two-step spin process is used; the first spin recipe is to coat the surface uniformly, whilst the second determines the thickness.

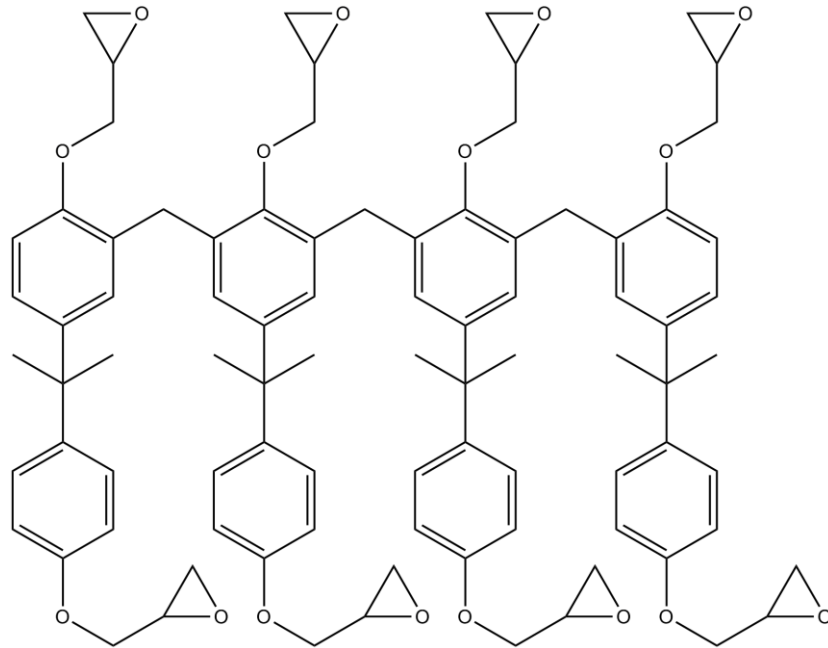


Figure 2.25 - SU8 structure, detailing the presence of eight epoxy groups (average per molecule) which cross link as a result of UV exposure

It is clear from the above that photolithography is an ideal candidate for the silicon master mould to then be used in conjunction with a nano-imprint procedure. In terms of polymer selection, a range of polymers have been identified which may be suitable for this specific application. However, an ethyl acrylate based polymer, SU8 and PDMS will be carried forward due to their ability to be fabricated into the patterns required and their ease of use.

2.4.5 Summary

The literature review covers the fields of minimally invasive surgery, the mechanisms of adhesion and fabrication techniques, revealing a number of limitations and knowledge within current methodology.

The mechanisms of adhesion have also been investigated. It can be seen that there are many varied mechanical methods of attachment, including graspers, micro-hooks and vacuum cups which, despite providing adhesion, cause some degree of tissue damage. It is also shown that adhesion can be produced using

a chemical interaction; however this mechanism of adhesion is likely to prove irreversible. The use of magnetic attachment systems have also been widely investigated as they cause no chemical disturbances or traumatic damage to tissue. However, in areas where tissue is thicker a larger magnetic force is required - leading to a need for extra power and resulting in a complex, expensive procedure, with limited precision. Therefore as these mechanisms require active manipulation to gain an adhesive force, it would appear more beneficial to utilise the properties present at the tissue interface in the form of van der Waals interactions and the interactions related to hydrogen bonds. As these forces are weak it is important to increase the contact area, in order to maximise adhesion. Recent progress in this mainly involves mimicking the adhesion mechanisms used by creatures and insects in nature, for example the tree frog. The focus, therefore, has been the fabrication of a bio-inspired micro-structured surface which will provide an adhesive force by utilising the fluid present in tissue, in the form of Stefan adhesion and capillary forces. As the liquid wets the surface a meniscus will form around the micro-pillars in contact with the surface. These micro-structures can be successfully fabricated onto a polymer surface using a nano imprinting technique.

Chapter 3. Experimental Procedures and Methodology

3.1 Introduction

In order to successfully fabricate and analyse micro-structured surfaces, a range of specialist test equipment has been used. This chapter describes the sample preparation equipment utilised, including wafer saw and reactive ion etcher. Post-fabrication, the structured surfaces were analysed visually enabling the micro-pillared geometry to be measured and inspected. Initially Scanning Electron Microscopy (SEM) was employed; however, as a conductive coating is required, altering the surface chemistry, White Light Interferometry and Optical Microscopy was found to provide a more efficient visual analysis technique. Details of the three inspection techniques together with the experimental techniques used to evaluate the adhesion properties of the fabricated surfaces, including a modular universal surface tester and a bespoke tissue adhesion testing rig are given. Combining these rigs allow the effect of pre-load, speed of approach and tilt angle, on the adhesive forces produced, to be observed. This chapter does not include the details of the micro-structured surface fabrication as this is presented as a substantial part of the results chapters to come.

3.2 Experimental Conditions

Sample preparation and micro-fabrication techniques were undertaken in a class 100 nanotechnology cleanroom, designed to never allow more than 100 particles, 0.5 microns or larger, per cubic foot of air⁴ to be present, Further sample preparation was performed in a class 1000 clean room⁵. Each adhesion

⁴ School of Electrical and Electronic Engineering, University of Leeds

⁵ School of Engineering and Computing Sciences, University of Durham

experimental procedure has been conducted three times to allow statistical analysis to be conducted on the data sets.

3.3 Biological Specimens

A representative tissue surface was required for adhesion studies. Fresh rat peritoneal tissue was obtained from the University of Leeds, Central Biomedical Services. The handling and culling of the animals was performed by licensed technicians in accordance with Home Office regulations. The tissue was dissected immediately after death to ensure freshness. The skin layer was removed prior to the removal of the abdominal wall, encompassing both the fascial and muscular layers. The internal surface, with the peritoneum attached was placed immediately in phosphate buffer solution (PBS) to ensure the cell structure is maintained and the sample remains hydrated. If the samples are allowed to dry this would dramatically alter the fluid viscosity and therefore any results would not be representative of an *in-vivo* model. It was also ensured that all testing was carried out within eight hours of dissection; samples were transported between labs, handled and disposed of in accordance to the health and safety tissue protocol present in the laboratory.

3.4 Surface Preparation Equipment

3.4.1 Wafer Saw

A precision wafer saw (Microace 66, Loadpoint Ltd), as shown in Figure 3.1, was used for dicing 3 inch front polished silicon wafers of orientation $\langle 100 \rangle$, purchased from Si-Mat, Kaufering, into 2 x 2 cm² chips.

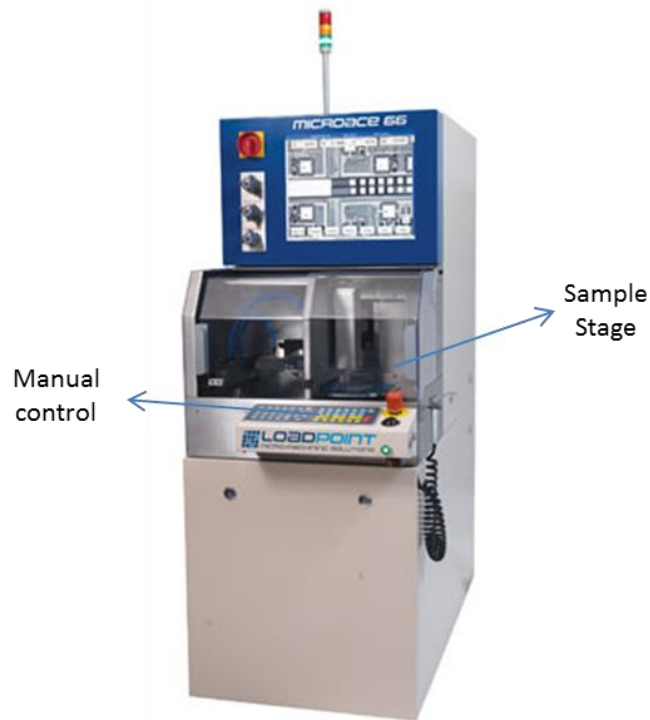


Figure 3.1 - Microace 66, Loadpoint Ltd. Precision wafer saw for the dicing of silicon wafers [111]

Post dicing, the chips were prepared by cleaning them in acetone, isopropanol and de-ionised water. They were then dried with nitrogen. This process was performed in the cleanroom to allow optimum removal of any contaminants before the photolithography patterning took place. The photolithography method is described in Chapter 4.

3.4.2 Reactive Ion Etcher

Reactive Ion Etching (RIE) uses chemically reactive plasma to remove a deposited layer of material on a wafer; this method was used in the fabrication of a silicon master mould, to dry etch the substrate. RIE can also be used to coat a polymer with a functional layer, using a low power and shorter time, rather than etch away at the surface.

The RIE is a parallel plate system with gas inlet at the top of a cylindrical vacuum chamber and an exit through a vacuum pump housed near the wafer platter at the bottom of the chamber; a schematic diagram of the process is provided in Figure 3.2. The chamber is pumped to vacuum (approx. 19 mTorr), before the gas is allowed to fill the chamber. Once the gas flow is set, plasma is initiated by applying a radio frequency (RF) electromagnetic field. This oscillating electromagnetic field ionises gas molecules by stripping them of their electrons. As the electrons oscillate, they bombard the parallel plates causing a build-up of charge on the bottom plate due to its DC isolation. This build up results in a large negative voltage, as the plasma consists of a higher concentration of positive ions than free electrons; the ions drift towards the sample, colliding with the surface. If the kinetic energy is large enough, these collisions result in etching of the sample.

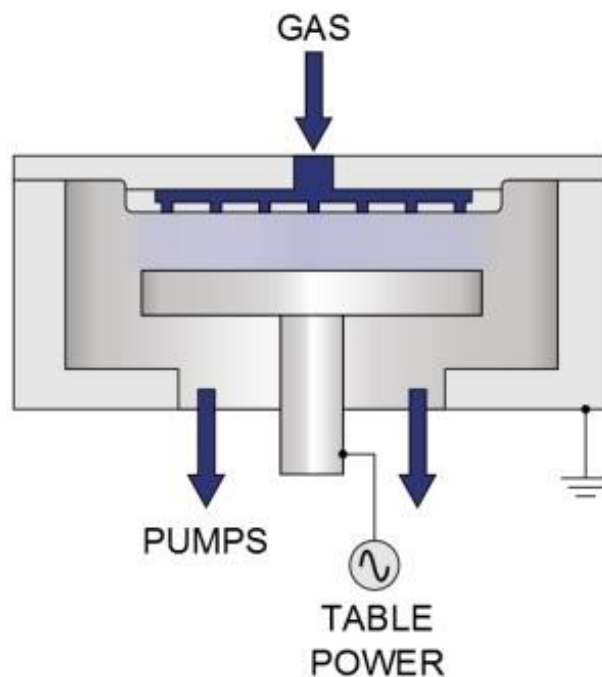


Figure 3.2 - Schematic of the Oxford Instruments Plasma Pro reactive ion etcher [112]

3.4.3 Plasma Prep 2 - Plasma Chamber

A Gala Instrumente Plasma Prep 2 chamber see Figure 3.3 were used to vary the wettability of the polymer surface. As Polydimethylsiloxane (PDMS) is naturally hydrophobic, by exposing the surface to atmospheric air plasma, it is possible to vary the surface wettability and optimise the adhesion. This process is discussed further in section 5.2.1.2.



Figure 3.3 - The Gala Instrumente Plasma Prep II plasma chamber [113]

3.5 Surface Analysis Equipment

3.5.1 Nano-Indentation

A Micro-Metrics NanoTest was employed to perform nano-indentation of the polymer surfaces to calculate the modulus of the material. The NanoTest uses electromagnetic force application and depth measurement to determine the elastic and plastic properties of materials at the nano-scale [114]. The data is presented in the form of a loading and unloading curve as shown in Figure 3.4.

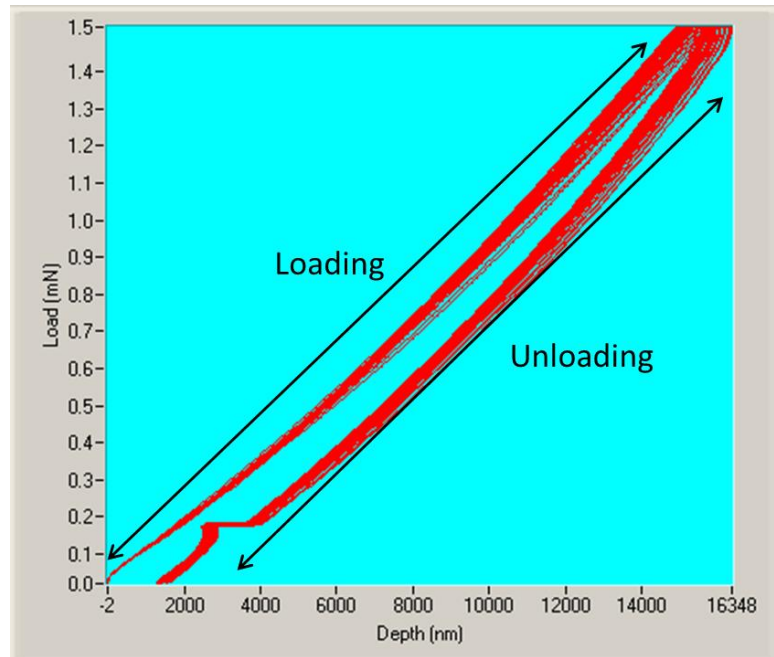


Figure 3.4 - Example of the data read out from nano-indentation tests.

Data is provided in a load vs depth curve, allowing the mechanical properties to be calculated.

The equipment starts with the indenter tip in contact with the sample. The load is then increased, increasing the depth of the tip into the surface, once the pre-determined load is reached, the tip is reversed. This test allows the stability of the modulus and hardness of the polymer to be calculated as a function of time, using the data collected from the gradient of the tangent to the unloading curve using Oliver-Pharr data analysis technique [115] as outlined in section 5.2.1.1. As both the hardness and modulus affect the adhesion of a surface it is particularly important to only test once the surface is stable.

3.5.2 Scanning Electron Microscope (SEM)

Scanning electron microscopes (SEMs) are used widely in the study of polymers, due to their ease of operation and the interpretation of images [116]. However, there are limitations to this technique; specifically due to the requirement of a

conductive coating and the impinging high energy electron beam causing structural damage to the substrate [116].

Scanning electron microscopes are designed around the interaction between a beam of high energy electrons and a solid interface. The electron beam is accelerated through a vacuum by a potential difference between the filament and the anode. The beam passes through a hole in the anode and is focused via a lens onto the surface to be analysed. As the beam interacts with the surface, with various detectors positioned around the target, the resultant signal is received.

There are two types of interactions which take place as the electron beam impinges onto the substrate. Some electrons are 'backscattered' due to electrostatic attractions between the free electron within the incident beam, and the positive nucleus within the surface [116]. This Rutherford scattering is an elastic process and so these backscattered electrons can change direction without loss of kinetic energy. If they are turned through a large enough angle they may escape, allowing them to be detected and measured [116].

Some of the beam electrons may also interact directly with electrons in the atoms of the substrate, causing them to be knocked free and become 'secondary' electrons [116]. A proportion of secondary electrons escape and are detected and measured. Once these have been removed from an inner shell, it is then possible for an electron in a less tightly bound state to fall into an inner shell, emitting energy in the form of a photon in the x-ray range of the electromagnetic spectrum. Each x-ray photon produced has an energy characteristic of the electron transition specific to the element in which it has been produced. Therefore, by measuring the wavelength or energy of this photon it is possible to determine the elements at the surface.

These measured signals, which change simultaneously with the changing characteristics of the surface, are amplified to control the brightness of a spot on a cathode ray tube (CRT). The CRT scan is controlled by the same generator which controls the beam position allowing a spatial correspondence to be maintained.

The scanning electron microscope used was a Carl Zeiss EVO MA15⁶, as shown below in Figure 3.5.



Figure 3.5 - Carl Zeiss EVO SEM with oxford instruments EDX system [117].

In order to analyse a polymer surface, the sample is mounted on a conductive plate, and outlined with conductive carbon gel. To allow image production in the SEM, the sample must be electrically conductive; therefore the polymer is treated with a low vacuum, gold sputter coating.

⁶ Leeds Electron Microscopy and Spectroscopy Centre (LEMAS) in the School of Chemical and Process Engineering (SCAPE).

3.5.3 White Light Interferometry - Bruker Npflex™

Surface profile measurements were performed using white light interferometry (Bruker NPFLEX™ - Figure 3.6), an advanced surface metrology system which allows three-dimensional, non-contact analysis of samples providing a true topographical representation of the polymer surface without damaging it.

White light interferometry relies on the principle of wave superposition to extract information of surface topography from instantaneous wave fronts. Reflected light from light beams is captured and recombined allowing a CCD camera to process the image. To ensure any surface measurements were not affected by the surface form such as the presence of the pillars, post processing was carried out on the data using Bruker's Vision Software.

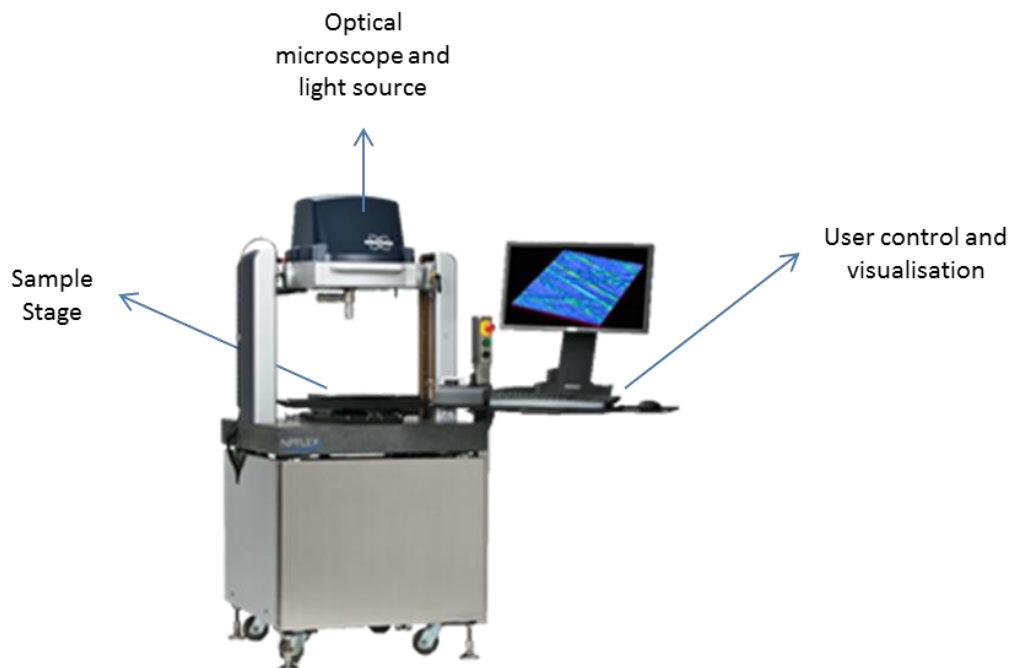


Figure 3.6 - White light interferometry, Bruker Npflex™[118]

3.5.4 Contact Angle Goniometry - FTA4000™

The FTA4000⁷, see Figure 3.8, is an analysis system optimised for small liquid droplets created by a nano-dispense pump which allows the production of drop volumes down to 10 Pico-litres [119]; an example of such a drop can be seen in Figure 3.7. During each measurement it was ensured that the droplet had reached a steady state before the data was collected – 10 seconds from initial contact.

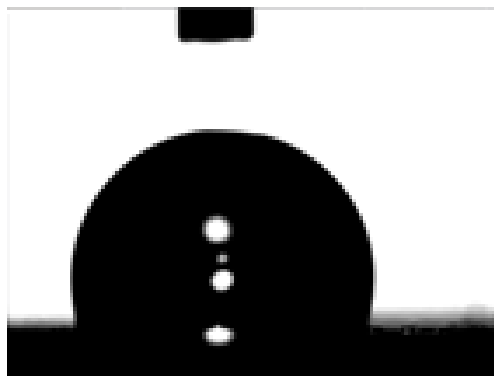


Figure 3.7 - Example of liquid droplet formed by FTA4000 on a hydrophobic surface of volume 0.497 μl .

The equipment is fitted with two microscopes, one to image the droplet shape and the other to provide a top down view of the specimen. Image capture allows an accurate contact angle to be measured.

⁷ School of Physics and Astronomy, University of Leeds



Figure 3.8 - FTA 4000 [119]

3.6 Adhesion Test Equipment

3.6.1 Modular Universal Surface Test (MUST) Instrument

In order to quantify the adhesive forces produced by the polymer surfaces, indentation tests are required. These were carried out using a Modular Universal Surface Test (MUST) instrument. The MUST consists of a force transducer and a sliding sample stage. The transducer is made up of a cantilever with a parallel spring arrangement. The micro-structured surfaces are mounted onto the contact side of the cantilever. A micro-mirror is attached to the other side of the cantilever, allowing it to reflect light back to a fibre optic sensor. This set up is shown in Figure 3.9.

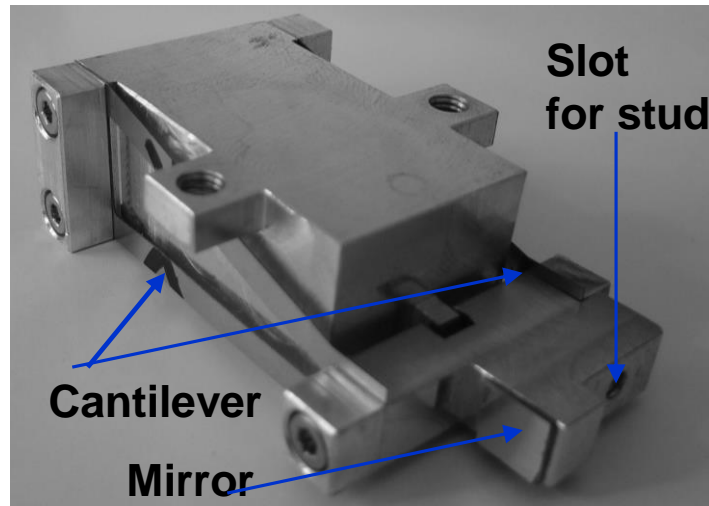


Figure 3.9 - Cantilever set up, showing the parallel arrangement of the cantilevers, mirror positioning and stud positioning for sample mounting.

The deflection of the cantilever is multiplied by the known spring constant to calculate the displacement force. The force transducer is calibrated by positioning the fibre optic sensor close to the mirror allowing the feedback voltage to be set as close to the maximum possible, giving the largest possible range for the cantilever spring. A parallel spring with spring constant $0.6 \text{ mN}/\mu\text{m}$ was chosen to measure forces in the range 0-100 mN without reaching maximum deflection.

Each cantilever is calibrated by rotating the cantilever mount 90 degrees allowing masses to be hung from the cantilever and the displacement as a function of force to be measured. The set-up used to find the spring constant is shown in Figure 3.10.

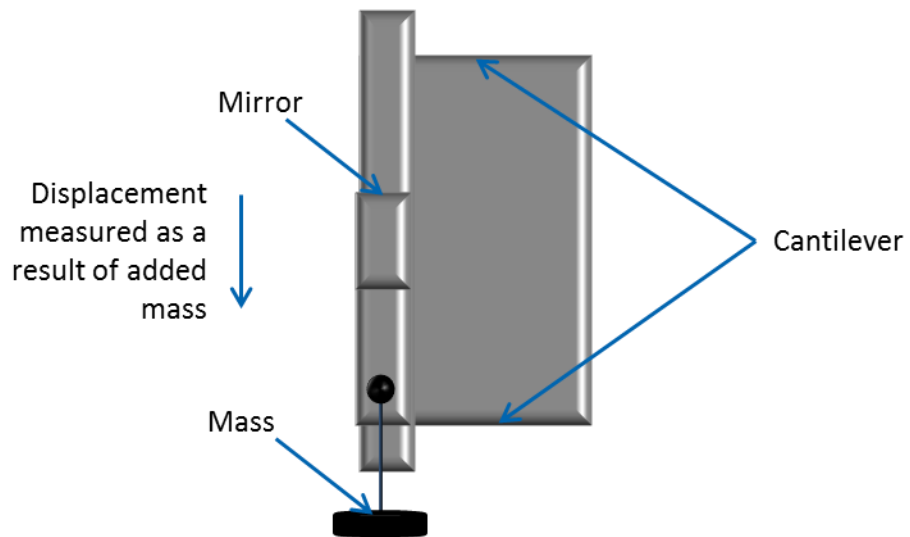


Figure 3.10 - Set-up used for the calibration of the cantilever. Mass is added, and the resultant displacement of the cantilever pair is recorded.

From this it is possible to calculate the spring constant

Whereas the force is calculated from the mass added, the extension is measured from the cantilever displacement; plotting force against extension gives the spring constant, via Hooke's Law:

$$F = k * e \quad (3.1)$$

The result of the cantilever calibration is shown below in Figure 3.11. It is shown that the force is proportional to the extension of the spring, giving a gradient and therefore spring constant of 0.6 mN/μm.

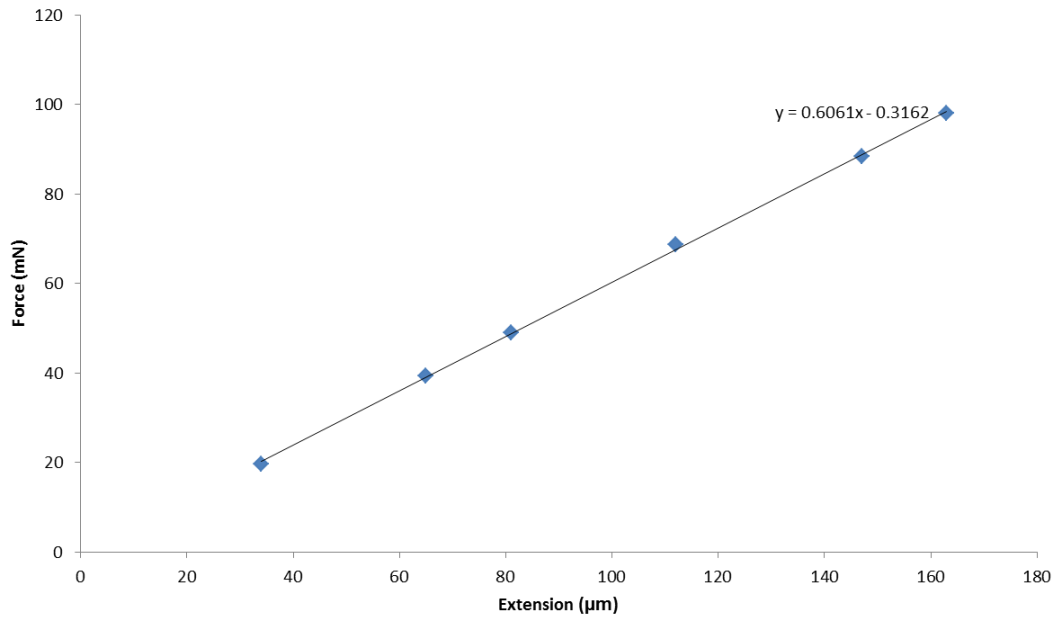


Figure 3.11 - Calibration curve with gradient of 0.6 mN/µm

For the adhesion tests, perpendicular contact with the wet surface and polymer samples is required. Therefore the wet sample was mounted perpendicular to the travelling direction of the sliding stage.

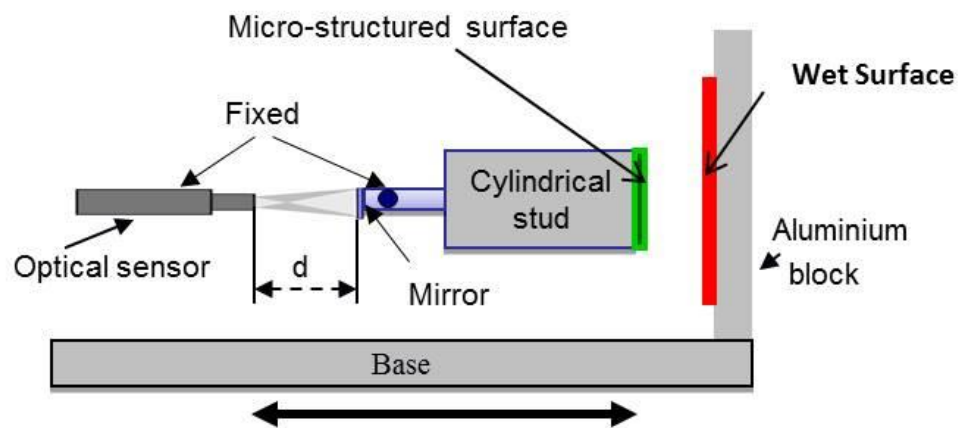


Figure 3.12 - MUST rig set-up. The optical sensor detects displacement as the mirror moves. The spring constant is known and therefore allows the displacement to be translated into a force.

The built in software performs the calculation of the displacement forces. The output from the equipment is in the form of force-displacement data, this is then plotted as a force-displacement curve; Figure 3.13 is a typical example output.

With regards to Figure 3.13, the test starts at point A, where the sliding platform moves the wet sample towards the micro-structured surface. At point B the distance between the two samples is small enough to allow an attractive force to build up across the interface. This force pulls the surfaces together and they contact at point C. This effect has a value equal to the gradient of the line BC. The equipment continues to push the surfaces together until a predetermined maximum force is reached by point D. The slope CD therefore represents the deformation of the spring in the direction of the applied force. The gradient is therefore dependent on the spring constant. The variations in the gradient show there are further deformations occurring in the system, potentially due to the test surface. When testing against biological tissue, which is a soft viscoelastic material, it is reasonable to assume any deformation will occur on the tissue side [17].

At D the sliding platform begins to reverse and separate the two surfaces. The surfaces remain in contact even when the applied force reduces beyond zero to have a negative value. The maximum adhesion force of the cycle is equal to the value of the recorded negative value at point E. At this point the adhesion force is overcome and the surfaces begin to separate. As this is a force-displacement curve, the area under the curve lying below zero is the work of adhesion.

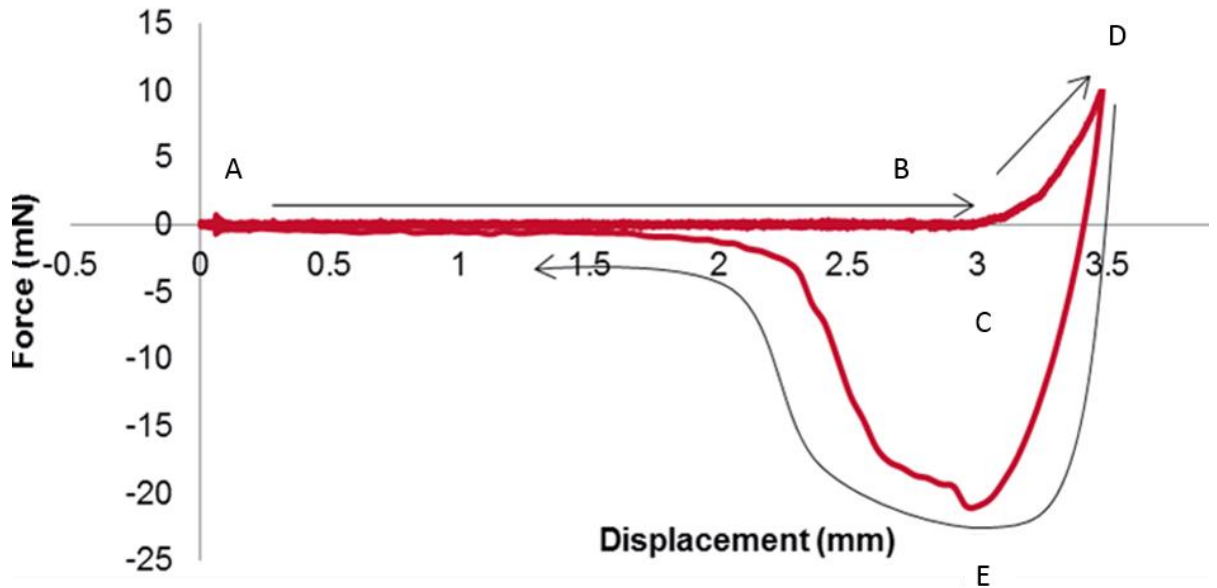


Figure 3.13 - Typical force displacement curve. The test starts at point A. At point B an attractive force to build up across the interface pulling the surfaces together and they contact at point C. A predetermined maximum force is reached by point D, at this point separation begins. The maximum adhesion force occurs at point E.

As the pre-load forces are small, the equipment is prone to overshooting this force. This will affect the adhesion forces. Therefore, in order to prevent this overshoot 100 cycles were performed on both steel - glass indentations and flat PDMS - glass indentations. This allowed calibration of the force sensor and ensured that the pre-load force is accurate.

3.6.2 Tissue Adhesion Testing Rig

Although as previously discussed, the Modular Universal Surface Test (MUST) instrument can perform indentation tests as a function of distance and time, with a given pre-load. However, as the end goal of this work is to investigate the viability of surfaces to be used against gravity in a surgical environment, tests in the vertical plane are required. A Tissue Adhesion Testing rig (TAT), Figure 3.14,

was designed and built in the School of Mechanical Engineering, University of Leeds, to allow adhesion tests to be performed against the action of gravity. This provides a maximum load/adhesion force to be determined and mimic the surgical procedure more precisely than the MUST rig, in that the adhesion force is in a vertical plane as opposed to the horizontal plane. The rig consists of a tissue mount attached to a horizontal bar and an adjustable joint allowing the re-positioning of the tissue at a predefined height. A single acting pin cylinder linear pneumatic actuator was used to attach the micro-structured surface with a weight to the tissue sample [21].

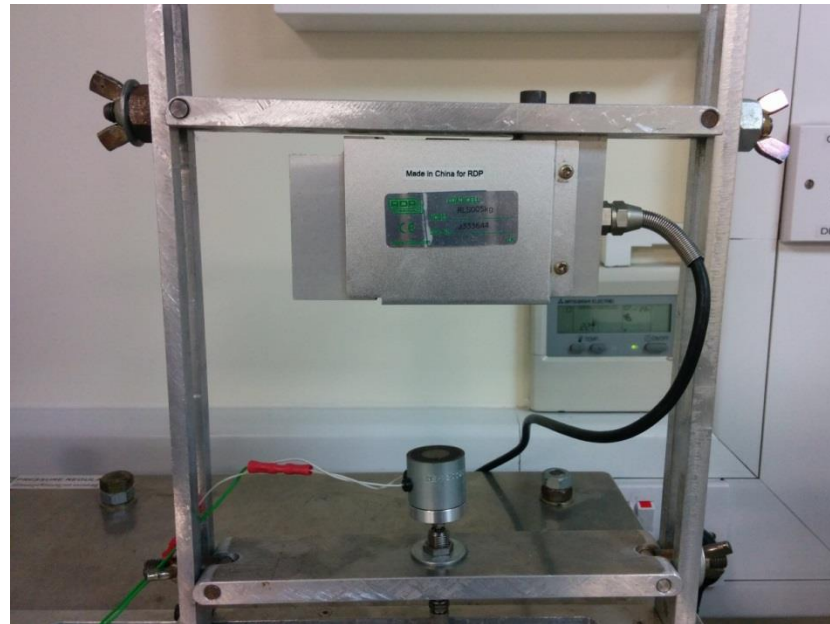


Figure 3.14 - Tissue adhesion testing rig. Image shows the apparatus at an inclination to the horizontal [21].

The combination of adhesion results from the MUST instrument and the TAT rig, provides enough data to compare adhesion results in two planes, the MUST giving quantitative data of adhesion and the TAT rig providing visualisation of the weight that can be held by the contacting surfaces.

However, due to equipment failure, a third rig has been employed, the Modular Mechanical Characterisation rig (MMC), to replace the MUST rig. To ensure consistency in results all experimental parameters are kept constant throughout the testing.

3.6.3 Modular Mechanical Characterisation (MMC) Rig

The Modular Mechanical Characterisation (MMC) rig has been designed and built⁸ as a bespoke piece of test equipment; where, a 1 N thin film load cell⁹ (Figure 3.15) is mounted between a sample holder and a linear stage actuator¹⁰ with a step resolution of 1 nm.



Figure 3.15 - S100 - thin film load cell (1N) [120]

The actuator is fixed vertically to a Rexroth aluminium frame to allow indentations to be performed in the x-y direction. An amplifier has been used to amplify the voltage obtained from the load cell and a National Instrument data acquisition card myDAQ is used at the interface of the amplifier and the PC. The control and data acquisition have been programmed using LabVIEW, allowing force and

⁸ Ms Zahra Ehteshami, School of Mechanical Engineering, University of Leeds, Leeds, UK

⁹ Strain Measurement Devices (S100), Suffolk, UK

¹⁰ VT-80 motor and controller, Physik Instrumente, Germany

displacement data to be recorded at 60 Hz for subsequent analysis. All the experimental data were exported in form of time-displacement-force for analysis, in the same process as with the data from the MUST rig. An image of the experimental set up is shown below in Figure 3.16. This test rig allowed more accurate, reliable data to be gathered after equipment failure with the MUST rig.

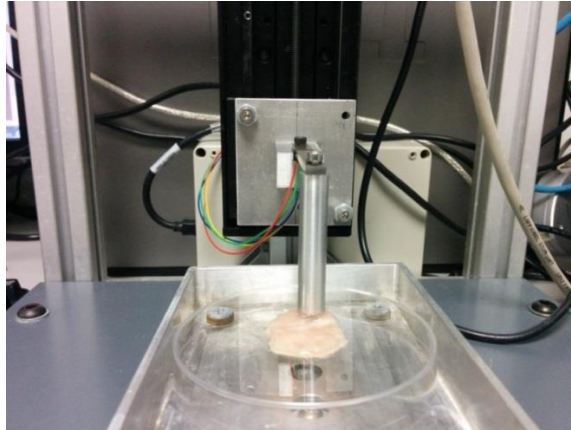


Figure 3.16 - Modular mechanical characterisation (MMC) rig set up, with an indenter in contact with a tissue sample

Before testing the load cell was calibrated by applying a weight to the tip and recording the corresponding voltage output, the calibration is shown in (Figure 3.17). The equation of the line could then be inputted into the LabVIEW programme with a component of gravity to give force readout.

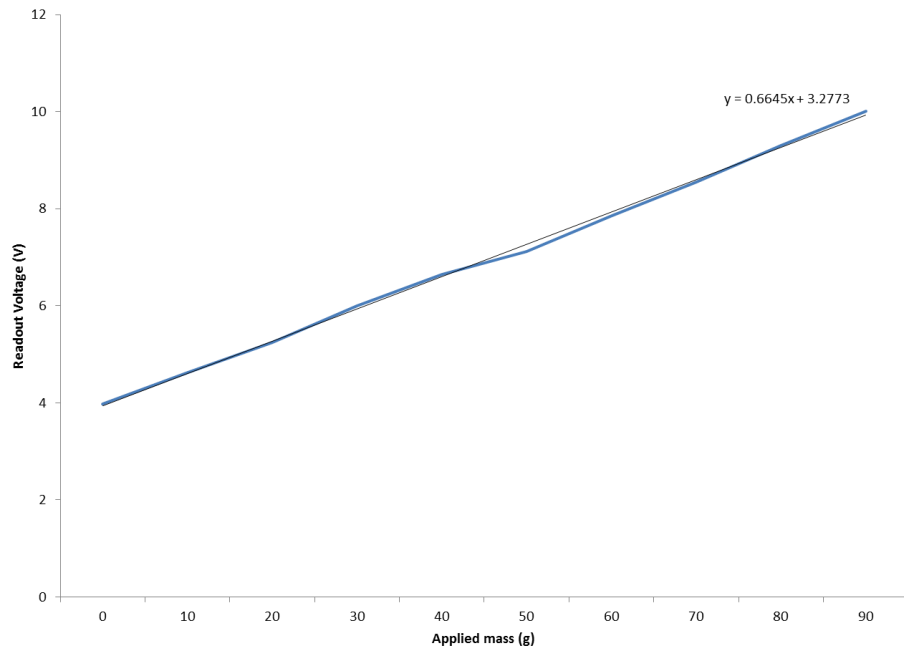


Figure 3.17 - S100 calibration curve.

3.7 Summary

This chapter has highlighted a range of specialist test equipment, specifically sample preparation equipment which has been utilised, alongside analytical equipment which has allowed the visualisation of the micro-pillared surfaces. Details of the three inspection techniques together with the experimental techniques used to evaluate the adhesion properties of the fabricated surfaces, have been given. The following chapter includes the details of the micro-structured surface fabrication.

Chapter 4. Polymer Selection and Fabrication Techniques

4.1 Introduction

This chapter is concerned with the methodology required to create a micro-scale topographically patterned functional polymer surface to achieve maximum adhesion between the latter and tissue. The choice of polymer to successfully fabricate flexible, bio-inspired, micro-structured surfaces is important in order to provide repeatable fabrication, the maximum wet adhesive forces available, and also ensure safety in a surgical environment.

Initially the focus was on the use of a commercial ethyl acrylate polymer, more specifically, Autotex[®] (MacDermid Autotype) motivated by previous work by Roshan *et al* [21]. They showed that a micro-pillared flexible array can be fabricated with a specific geometry. However, due to limitations such as protected chemical structure and availability associated with working with a bespoke industrial product, other polymers were investigated. The viability of the epoxy based photoresist - SU8 - was explored due to its extensive use in micro fabrication in the cleanroom facility used, and literature has shown that successful, repeatable fabrication of micro-pillars is possible using this photoresist [121-123]. Poly (dimethylsiloxane) (PDMS) is also been investigated, due to its wide use and ease of use whilst fabricating micro-structures on varying scales and geometries for micro-fluidics and flexible electronics [124-129]. Although PDMS is naturally hydrophobic, it is sensitive to plasma treatment and by exposing the sample to air plasma it is possible to vary the wettability and as a result tune the contact angle in order to optimise the adhesion, as discussed in Chapter 5.

4.2 Polymer Selection

Ideally it is beneficial to employ a polymer which can be fabricated repeatedly to form a flexible micro-structured pillar array, for which it is possible to tune the surface wettability. Whilst the fabrication of polymer, micro-pillared arrays is common place [48, 130-134], as is the wettability of polymer surfaces [135-137], it is the combination of these, and the small feature sizes which provide novelty.

As discussed in Chapter 6, surface wettability is a major factor in wet adhesion, where it is found that when the contact angle is too high (super hydrophobic), there is a reduced adhesion force; equally when the contact angle is too low (super hydrophilic) the surface will flood and there will be a thin liquid film which inhibits the formation of numerous individual liquid bridges, and therefore prevent an adhesive force - see Figure 4.1. The ability to modify the contact angle is vital in order to arrive at the optimum contact angle for a specific polymer to produce the maximum adhesive forces.

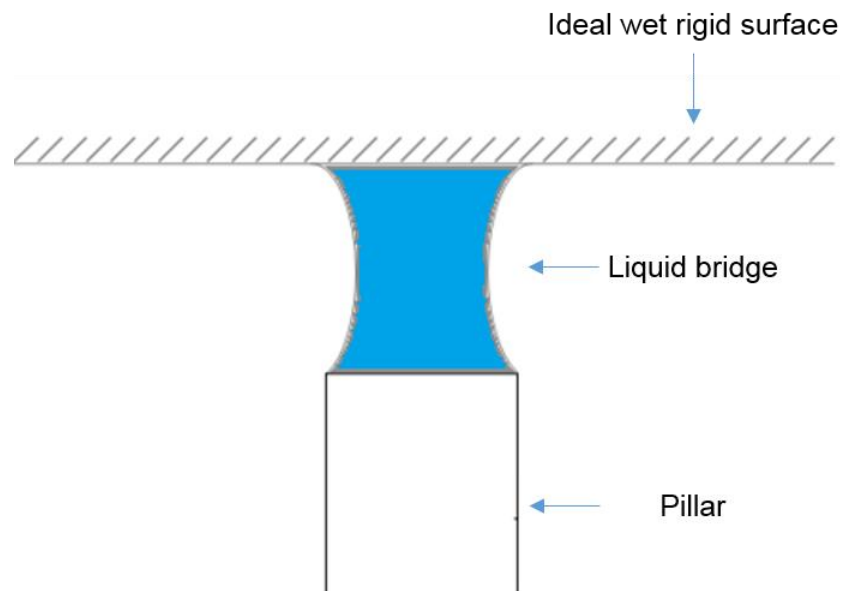


Figure 4.1 - Schematic of the liquid bridge and encapsulating meniscus formed on the tip of a single micro-pillar adjacent to an idealised rigid surface.

The surfaces generated are to be used in surgical applications so it is also essential that they are biocompatible, water resistant and inert. As tissue is significantly deformable, it is also desirable for such manmade surfaces to be flexible, to ensure optimum contact at the pillar tips. However, the polymer counterparts will never be flexible when compared to tissue, but any flexibility is desired as it would allow the surfaces to be mounted onto a range of devices, if employed in surgical procedures.

There is a vast range of polymers available, which would be suitable for a surgical environment. These are discussed below.

4.2.1 Polyurethane Acrylate (PU)

Polyurethane (Figure 4.2) is used in many micro-fabrication techniques to produce micro-fibre and nano-pillar arrays as shown in Figure 4.3, [95-103] for a range of applications, using mainly a soft lithography technique [138].

The structure of polyurethane allows surface modification, specifically in terms of wettability and functionalising the surface with biologically active species. It is these properties which facilitates the wide use of this polymer in many biological systems [20, 24, 27, 37].

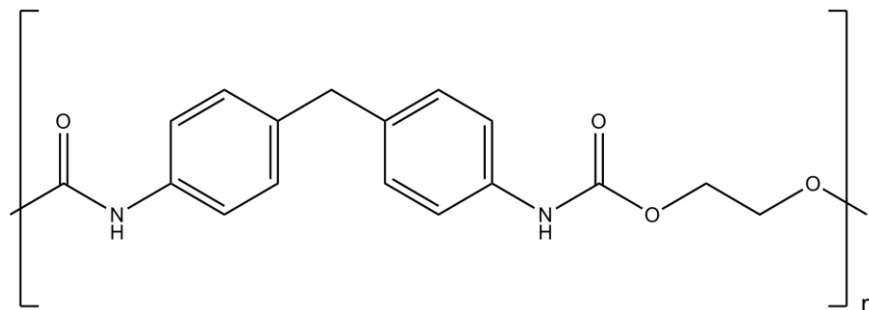


Figure 4.2 - PU chemical structure

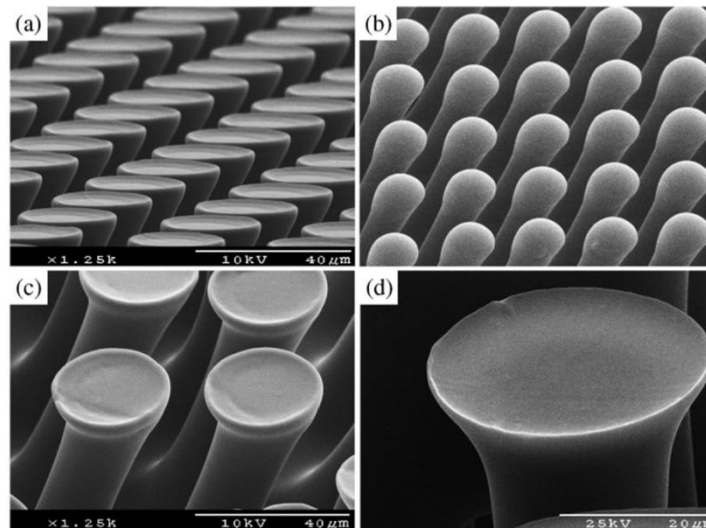


Figure 4.3 - SEM images of polyurethane fibres showing (a) spatula tips, (b) spherical tips, (c) suction-cup like tips and (b) large diameter tips. [99]

4.2.2 Poly (Methyl Methacrylate) (PMMA)

PMMA (Figure 2.22) is strong lightweight thermo-softening polymer which is particularly versatile in terms of fabrication methods [14, 30, 32, 35, 104] and is currently used in a variety of applications [14, 30-32, 36, 105, 106]. However, due to the glass transition temperature of this polymer (105°C), at room/body temperature PMMA is rigid. This is undesirable for this work, due to the need for these surfaces to conform to a flexible substrate such as tissue. An SEM image of PMMA microstructures is given below; see Figure 4.5, showing the capability of such a polymer if the rigidity were not an issue for this work.

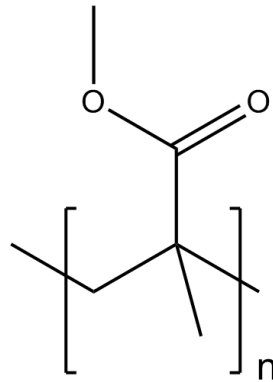


Figure 4.4 - PMMA structure

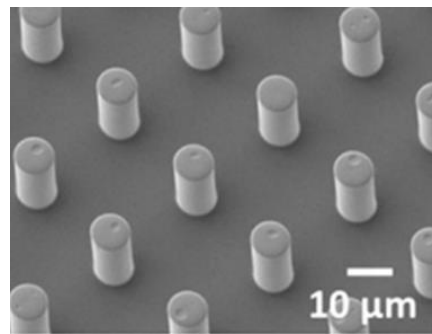


Figure 4.5 - SEM image of PMMA micro-pillars of height 24.02 μm, fabricated using a nano-imprint Process [139].

4.2.3 SU8

SU8 (Figure 2.25) is a negative tone, epoxy based photoresist, which is commonly used for permanent structures. In this work it is specifically the SU8 2000 series which has been explored, due to its ability to facilitate the production of pillar structures with vertical sidewalls, as shown in Figure 4.7, and high resolution [14].

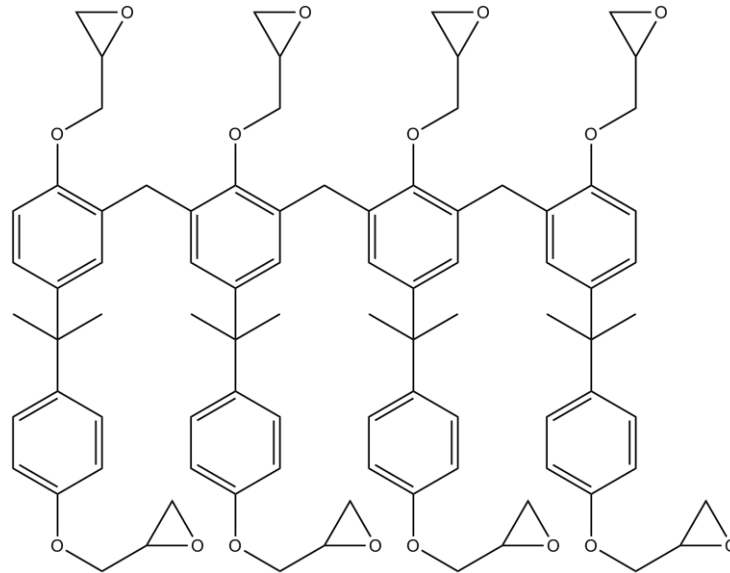


Figure 4.6 - SU8 structure

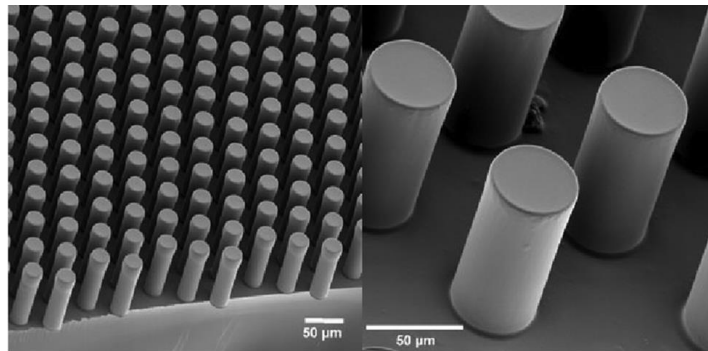


Figure 4.7 - Patterned SU8 surfaces with vertical sidewalls [140]

When SU8 photoresist undergoes ultra-violet exposure cross-linking occurs in two steps. Firstly, a strong acid is formed during the exposure, followed by an acid-catalysed thermally driven crosslinking during baking [14]. There are six viscosities available in the SU8 2000 series. However, it is only SU8 2002 (7.5 CSt) and SU8 2010 (380 CSt) [14] which have been used throughout this work, due to chemical availability and the ease of use to produce structures on the required scale. The spin speed for each determines the uniformity and the film thickness produced, as shown in Figure 4.8, as well as the spin time.

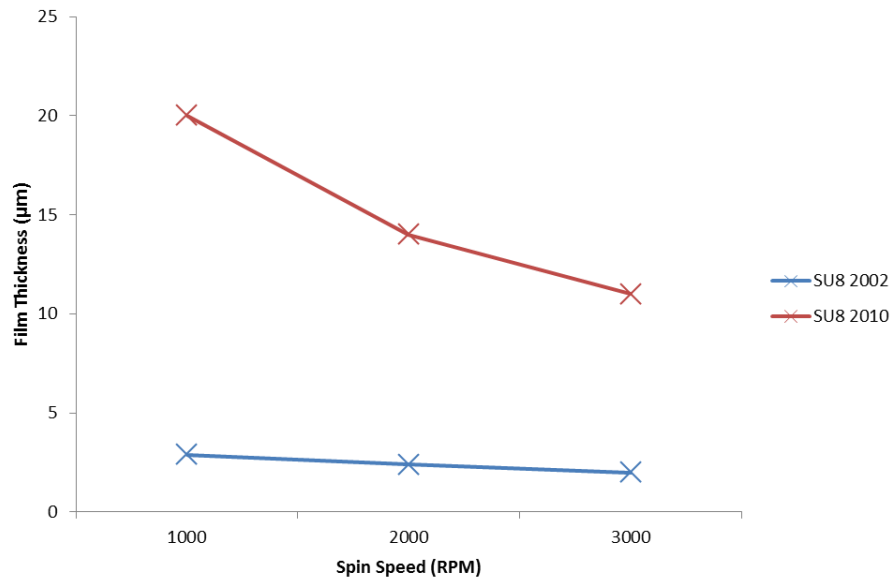


Figure 4.8 - Data to show the effect of spin speed on thickness of SU8 2000 series [32]

The fabrication of SU8 on a flexible substrate can prove problematic as standard process are optimised for rigid surfaces used mainly in microelectromechanical (MEMS) systems, such as silicon. Delamination and cracking may occur during the heating process due to different thermal expansion coefficients [34].

4.2.4 Poly (dimethylsiloxane) (PDMS)

PDMS (Figure 2.23) is a silicon-based, organic polymer, which is viscoelastic and non-toxic; as a result is used in a range of applications [20, 27, 30, 37]. PDMS is widely used as part of nano-imprint lithography processes, either to produce the final patterned surface or to be used as a mould.

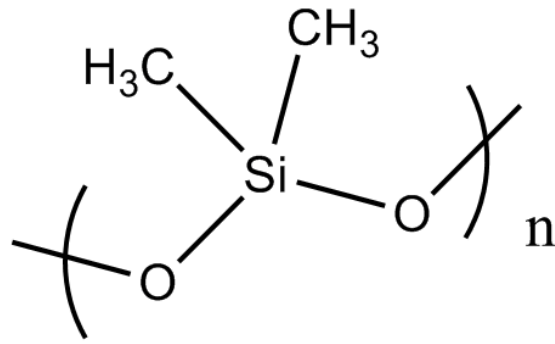


Figure 4.9 - PDMS structure

An example PDMS surface is shown below (Figure 4.10).

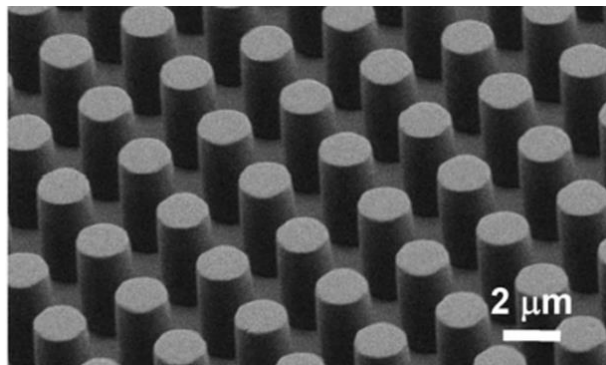


Figure 4.10 - SEM image of a high density PDMS micro pillar array to be used as a cellular force transducer [141].

A solid PDMS sample has a hydrophobic surface. The surface wettability can be changed by appropriate surface treatments. Atmospheric air plasma adds a silanol functional group to the surface, resulting in a reduction in contact angle therefore a hydrophilic surface.

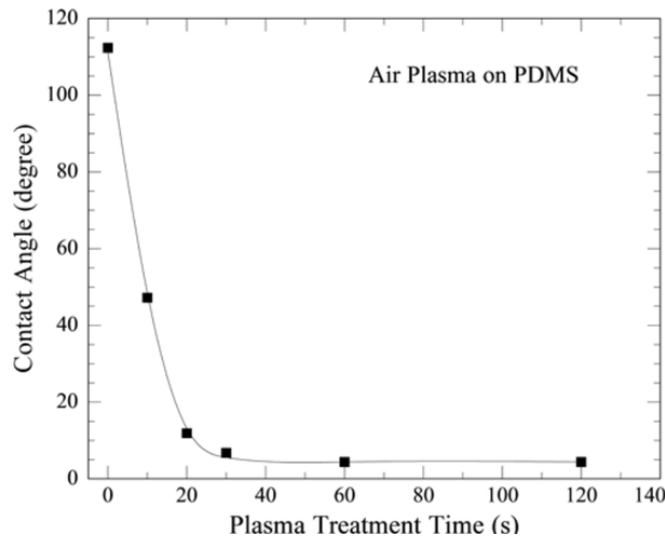


Figure 4.11 - Results by Jiang *et al.* [142] showing the water droplet contact angle on a flat PDMS surface as a function of atmospheric air plasma treatment time [143].

There is a vast range of fabrication techniques suitable for producing micro-structured polymer surfaces; the most commonly used involve the processes of lithography. There are three main lithography methods: photolithography; (additive and subtractive), soft and imprint [50, 83-85, 87, 89-94]. A nano-imprinting lithographic technique was chosen for this application. Unlike traditional lithography techniques, which rely on the use of photons or electrons to modify the chemical and physical characteristics to achieve a pattern, a nano-imprint technique allows direct mechanical deformation of the material, leading to resolutions which are not limited by light diffraction or scattering [91, 144]. The fabrication of such structured surfaces was carried out in a nano-technology clean room¹¹. Once a master mould has been defined, the repeatability of this process is high, as well as requiring fewer infrastructures, such as UV-sources and photo mask aligners, making it attractive for out of cleanroom applications.

¹¹ School of Electronic and Electrical Engineering at the University of Leeds

Medical grade PDMS is also available, however due to the nature of testing in this thesis it was deemed unnecessary for it to be evaluated as part of this work.

4.2.5 Silicon Template

For the fabrication of the micro-pillars, a pre-made silicon master was fabricated using lithography¹² as illustrated in Figure 4.13. The fabrication of the wafers involved the dicing of a 3" single side polished silicon wafer, purchased from Si-Mat, Kaufering, into 2 x 2 cm² substrates, using a precision wafer saw (Microace 66, Loadpoint Ltd).

Ultraclean conditions were required throughout, as any particles which land onto the surface during the process may result in defects. Before the process begins, the wafer is cleaned chemically in acetone in an ultrasonic bath for 5 minutes to remove any organic contamination on the surface, followed by immersion in isopropanol in an ultrasonic bath for 5 minutes, and finally de-ionised water is used to rinse it to remove any impurities, debris and solvents on the surface. Inspection under an optical microscope is carried out to ensure the cleaning process is successful.

A thin layer of a silicon dioxide barrier layer is then deposited onto the surface using PECVD, followed by spin coating onto the surface a light sensitive, positive tone photo-resist, S1813.

In order to achieve good adhesion of the resist to the wafer, it is essential that the freshly oxidised wafer is dry. The thickness of the resist layer is dependent mainly on the spin speed. To improve the adhesion further and to reduce the remaining solvent concentration in the photoresist, the sample is then soft-baked. Following

¹² Silicon Fabrication performed by Dr Li Chen, Cleanroom Technician (University of Leeds)

this, the sample is exposed to ultra-violet light through a patterned photo mask specially designed with dot arrays using a mask aligner.

As the resist is a positive tone, the mask contains a direct copy of the pattern which is required on the surface. The exposure to UV changes the molecular structure of the resist, making it more soluble in the developer MF319; meaning the exposed areas, where the silicon dioxide is to be removed, will be washed away. During this process it is crucial to ensure that the mask is fully aligned and in contact with the photoresist surface.

Following exposure, the sample is developed fully in developer MF319, and then rinsed in de-ionised water. Nitrogen is used to blow dry the surface, completing the lithography process. The samples are soft baked, in order to remove water from substrate surface and improve the resist adhesion to the substrate. The samples are then loaded into a thermal evaporator where a thin film (300 nm) of chromium is evaporated on to the substrate under vacuum, to act as a barrier material to protect the wafer. After removing the samples from the evaporator chamber, they are immersed in acetone solution for lift-off process; the process in which any deposited material on top of the photoresist will be removed along with the photoresist, leaving only the patterned material [86]. The samples are dried with nitrogen and ready for the next process.

The samples have chromium dot arrays on top of a silicon dioxide film. There are commonly two techniques which can be adopted to etch silicon dioxide; wet chemical etching and dry etching. With a wet chemical etch; samples are immersed in a hydrofluoric acid solution. Due to the nature of the acid the exposed area will be attacked in all directions, resulting in an isotropic silicon dioxide sidewall as shown in Figure 4.12.

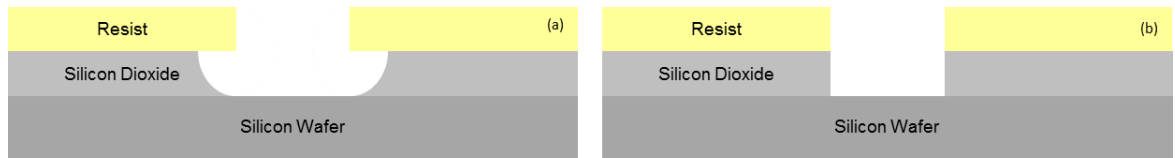


Figure 4.12 - Etching profiles obtained during (a) isotropic wet etching and (b) anisotropic dry etching [86]

Dry etching is used in the present work in order to avoid an isotropic pillar profile and ensure the previously mentioned straight sidewalls. Dry etching processes use Reactive Ion Etching (RIE), in which a plasma system ionises reactive gases. They are then accelerated to bombard the silicon wafer surface, causing etching through a mixture of chemical reactions and a momentum transfer from the etching species [86]. Initially, the silicon dioxide layer is etched to the silicon interface using trifluoromethane (CHF_3) and argon (Ar). Following this, the gases are changed and the silicon dioxide acts as an etching mask facilitating the etching of the silicon wafer into pillars using sulphur hexafluoride (SF_6) and oxygen (O_2). After the silicon pillars have been formed, the remaining layers are removed using a chemical clean in a buffered HF solution. The final mould is shown in Figure 4.14.

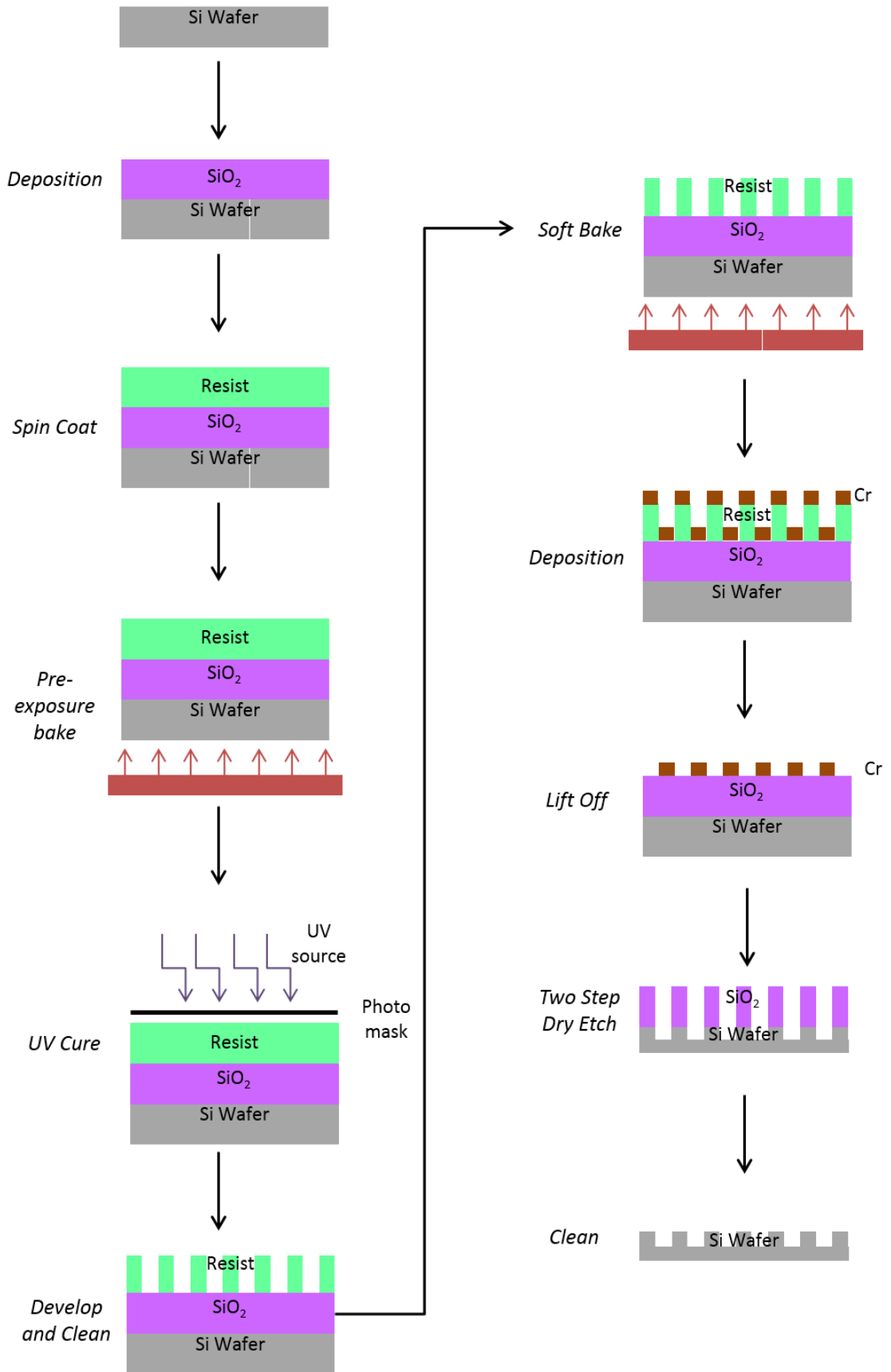


Figure 4.13 - Photolithography method used to pattern the silicon master mould (not to scale)

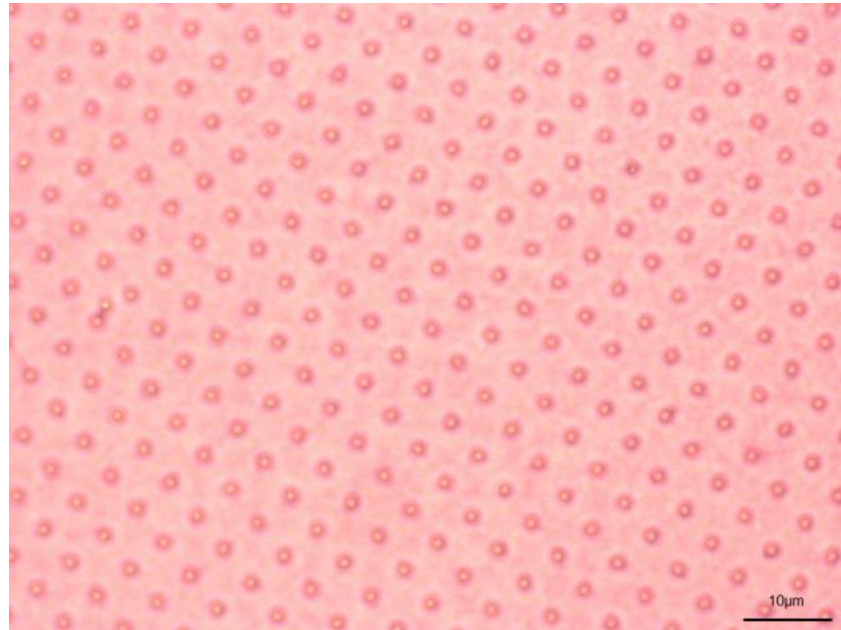


Figure 4.14 - Optical microscope image of a successfully fabricated silicon master mould, showing a regular array of micro-pillars

4.3 Polymer Fabrication Techniques

4.3.1 Autotex[®]

The previous work by Roshan *et al* [21], reported the successful fabrication of a micro-structured pillared surface employing a nano-imprinting technique using an ethyl acrylate based polymer, Autotex[®]. Therefore, an initial investigation was performed using this polymer, but with the aim of maximising the adhesive forces by varying the geometry and surface chemistry, specifically in terms of wettability.

4.3.1.1 Method 1: Autotex[®]

This method was replicated by spin coating the silicon template of 25 x 25 mm², composed of pillars in the geometry, diameter = 3 μm, separation = 6 μm and pillar height = 3 μm, at 2000 rpm for 60 seconds, to provide a film thickness capable of producing the pillar height required. The pattern was then transferred to a polyethylene terephthalate (PET) sheet using a hand held roller; this was

then exposed to an ultra violet source¹³ for 2 minutes to cure. The PET is then peeled away leaving a negative master mould (holes). The process was then repeated using the negative mould, spin coating the Autotex[®] at 4000 rpm for 40 seconds and rolling another PET backing. This sample was then cured under the ultra violet source for 3 minutes to produce the final positive mould. This method is summarised in Figure 4.15.

This process lead to a successful surface for this specific geometry (diameter = 3 μm , spacing = 6 μm , height = 3 μm) as shown in Figure 4.16. The full and comprehensive optimization of this polymer in terms of wettability and geometric parameters was not possible due to it being a made-to-order product. Due to copyright protection of the chemical structure for this polymer, material parameters such as Young's modulus and hardness, to name a few, are not readily available, further obstructing any possibility of a full and systematic theoretical and experimental comparison with other materials. Additionally, the limited volume of the polymer which was made available for this project and cannot be replenished was not sufficient for the amount of testing which would be required to obtain any substantial conclusions. Therefore, other polymers were investigated; however, the imprint lithography technique used in this process proved to be successful and therefore alternative polymer studies were based on this technique.

¹³ The mask aligner used throughout this work has an energy of 7.3 mW/cm².

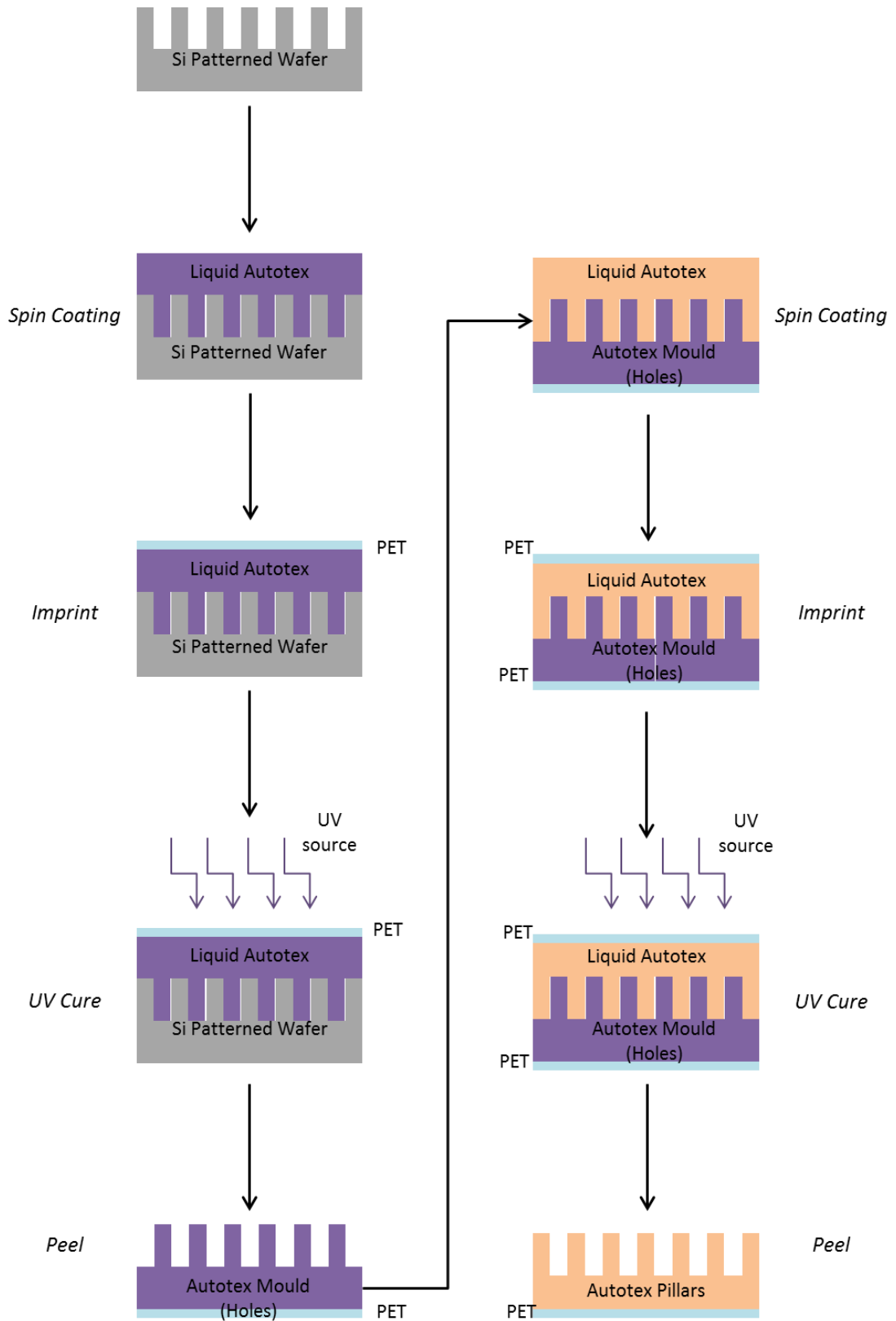


Figure 4.15 - Simplified schematic for Autotex[®] fabrication technique (not to scale)

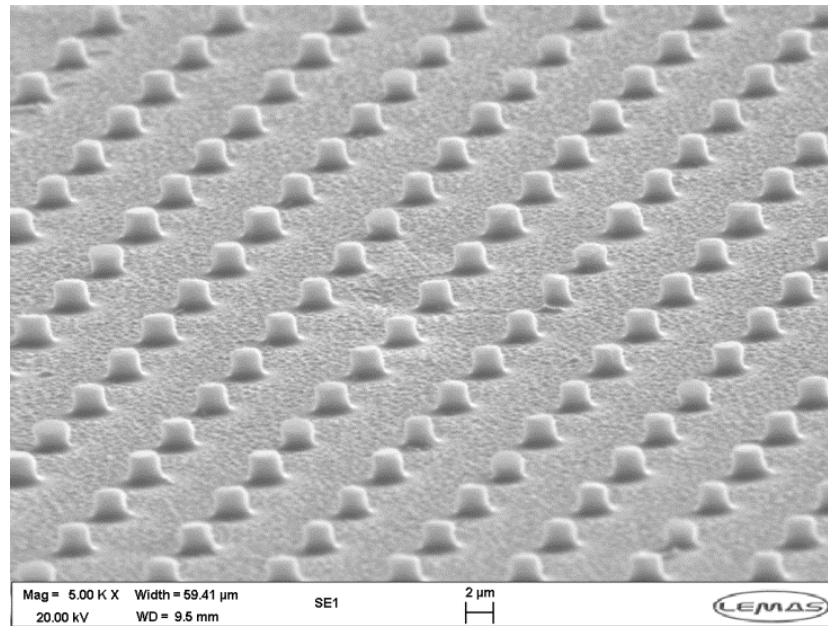


Figure 4.16 - Scanning electron microscope image of Autotex[®] pillars at a 75 degree tilt angle

4.3.2 SU8

The second polymer investigated was SU8, a negative tone, epoxy-based photoresist, which is commonly used in micro-electronics, micro-fluidics and bio-MEMS [145] due to its ability to provide a high-resolution mask for lithography methods.

4.3.2.1 Method 2: SU8 2002 as a Base for Autotex[®]

SU8 is an epoxy-based, viscous polymer which, when exposed to a ultra-violet source, solidifies due to long chain cross linking [32]. SU8 was firstly investigated in conjunction with Autotex[®], in which the SU8 2002 was spun on to a PET sheet with a two-step spin to ensure uniform coverage before determining the film thickness, (1000 rpm for 10 seconds and again at 2500 rpm for 30 seconds). Following this the sample underwent a pre-exposure bake at 95 degrees for 1 minute. The sample was then cured under a ultra-violet source, and then post exposure baked at 95 degrees for 10 minutes and finally developed in EC Solvent

and cleaned using isopropanol. Autotex[®] was then spun onto the SU8 for 10 seconds at 1000 rpm and again at 2500 rpm for 30 seconds a second PET sheet was hand rolled over the surface and ultra-violet cured (Figure 4.17). The first technique involving SU8 2002 required using the photoresist to fabricate a mask for the Autotex[®]. However, during fabrication, it was found not to be possible to peel the Autotex[®] from the SU8 2002 mask. As the chemistry of the bespoke Autotex[®] is not known this problem could not be investigated further, and therefore different fabrication techniques were explored with SU8 without Autotex[®].

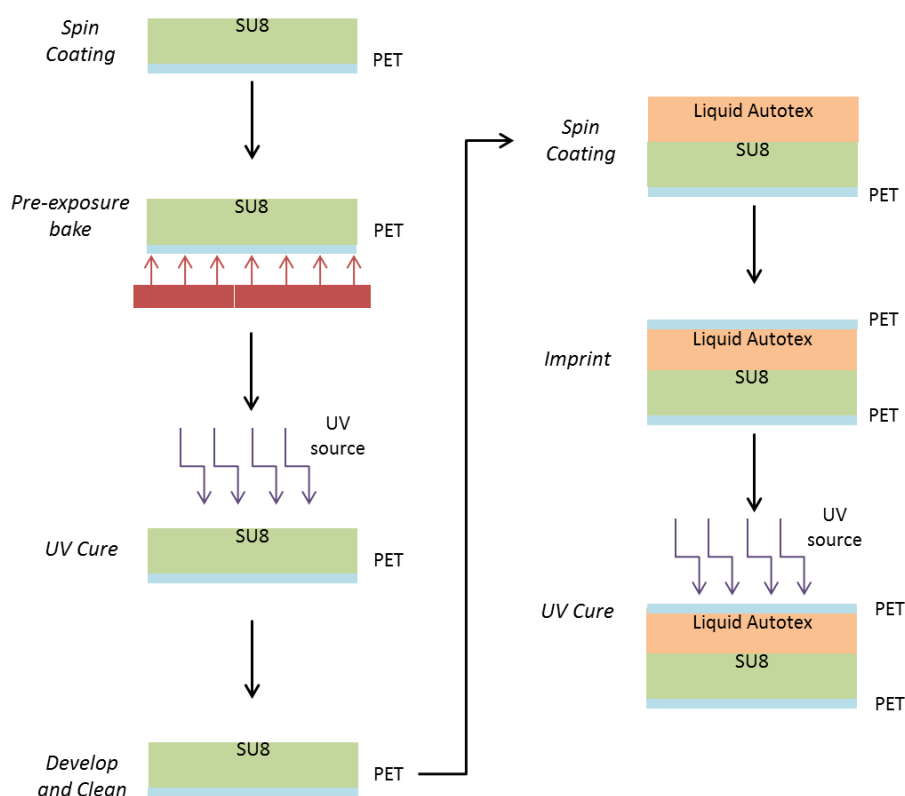


Figure 4.17 - Simplified diagram using SU8 2002 as a base for Autotex[®] to test the surface chemistry (not to scale).

4.3.2.2 Method 3: Direct patterning of SU8 2010

As SU8 is mainly used to fabricate high-resolution masks, the viability of patterning the photo-resist directly was considered [32].

This process involved spin coating SU8 2010 onto a PET film at 1000 rpm for 10 seconds and again at 3000 rpm for 60 seconds giving a surface thickness of approximately 12 μm . The sample was then baked at 95 degrees for 90 seconds and placed under a ultra-violet source in the presence of a photo mask containing the micro-structured pattern (Figure 4.18). The sample was then baked for 2 minutes at 95 degrees and developed in EC solvent, before a final hard bake for 10 minutes at 95 degrees.

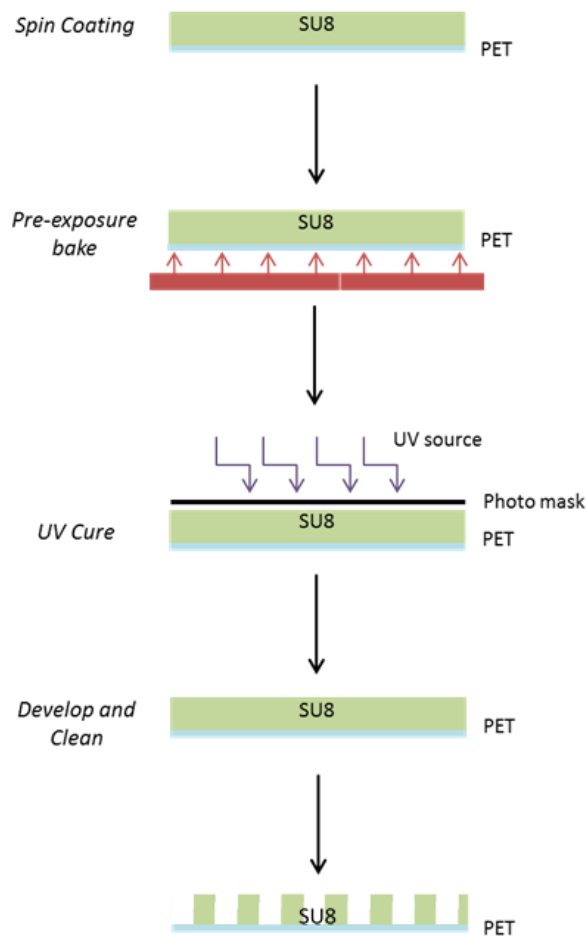


Figure 4.18 - Fabrication technique for the direct patterning of micro-pillars in SU8 2010 (not to scale)

Due to the highly viscous nature of the polymer (380 CSt), when it was spun onto the PET film there was an edge bead effect, resulting in clear features only being present towards the edge of the surface due to there being better contact between this thick edge bead and the photo-mask there, resulting in an uneven exposure across the surface. This effect can be seen in Figure 4.19.

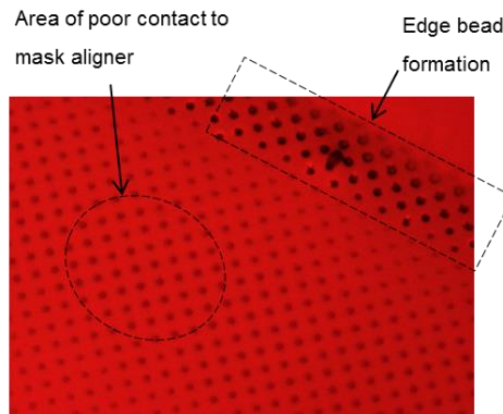


Figure 4.19 - Microscope image of directly patterned SU8. Showing an edge bead formed due to the viscous nature of the polymer, resulting in an uneven contact to the photo mask

Further testing was performed with this technique with the edge bead removed using dry cotton buds after the pre-exposure bake. This enabled pillars to be formed on the surface; however, due to the viscous nature of the photoresist the aspect ratio of the resulting pillars was high (10:1). Figure 4.20 shows that some pillars are formed, others have fallen over and yet others are completely absent. The latter effect is due to a weak adhesion force between the SU8 and the PET resulting in removal of the pillars from the base due to shrinkage during the SU8 cross-linking as a result of the different thermal expansion coefficients and shear forces existing at the PET-SU8 interface [34].

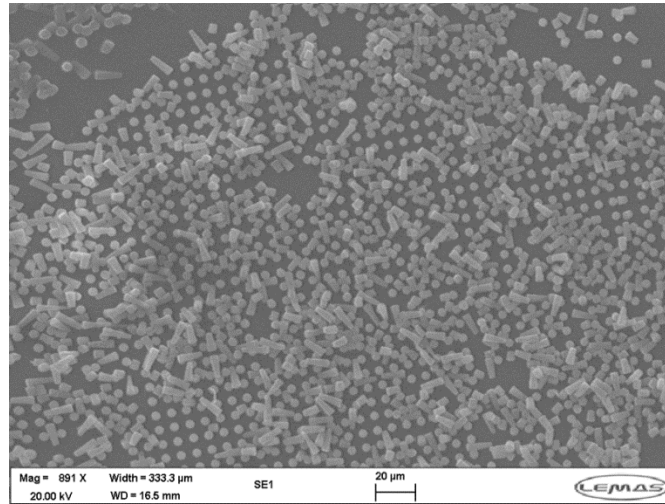


Figure 4.20 - SEM image showing fallen and absent SU8 pillars, due to a combination of high aspect ratio and weak adhesion between SU8 and pet substrate

To improve this poor adhesion at the SU8-PET interface, an adhesion promoter hexamethyldisilzane (HMDS) was used to create a bond between the resist and substrate, by spinning the HMDS onto the surface before applying the SU8. However, as there is no hydrated layer at the surface, this approach proved unsuccessful and resulted in de-lamination of the pillars.

4.3.2.3 Method 4: SU8 2010 as a Mould for PDMS¹⁴

SU8 2010 has also been investigated for use as a mould for PDMS (Figure 4.21). This method varied from the use of the SU8 mould with Autotex[®], in that this technique required holes in the master mould as opposed to pillars. In this process a silicon wafer was cleaned using acetone in an ultra-sonic bath, isopropanol and de-ionised water. After dehydration bake (10 minutes at 95 degrees), the SU8 photoresist was then spun onto the silicon at 500 rpm for 10 seconds and then again at 3000 rpm for 60 seconds, giving a thickness of

¹⁴ Sylgard 184, Dow Corning.

approximately 12 μm . The edge bead was removed using a dry cotton bud to optimise the contact between the surface and the photo mask, ensuring equal ultra-violet exposure over the full surface. The substrate was baked for 2 minutes at 95 $^{\circ}\text{C}$ before ultra-violet exposure through a negative photo mask to produce holes on the substrate. The surface was then post-exposure baked for 3 minutes at 95 $^{\circ}\text{C}$, developed in EC solvent for 2 minutes and cleaned in isopropanol.

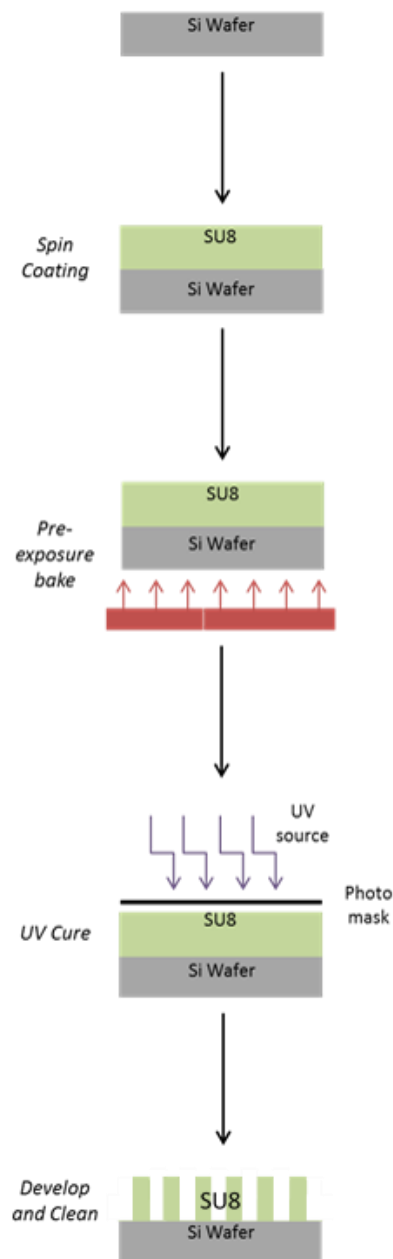


Figure 4.21 - Fabrication technique for the use of SU8 as a mould for PDMS (not to scale)

Once again this mechanism proved unsuccessful as it was not possible to expose the feature size required due to issues with development; specifically, when developing extruded features, the developer is able to target all exposed areas as shown in Figure 4.22.

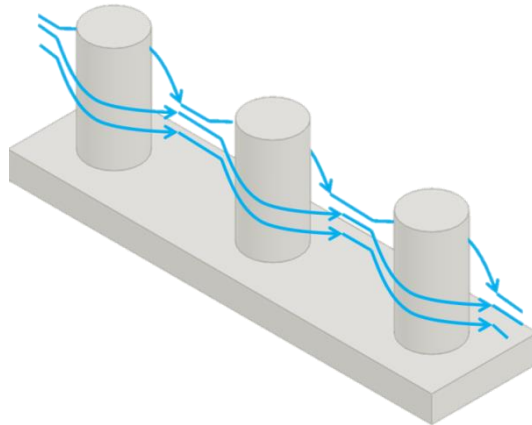


Figure 4.22 - Movement of a liquid developer around the extruded pillar features, allowing all exposed areas to be reached.

However, when developing recessed features, such as holes, the liquid developer becomes exhausted in the top section of the feature. This means that it is not possible to develop the full depth of the holes, resulting in narrow round bottomed dimples as opposed to deep cylindrical holes. This is shown in Figure 4.23.

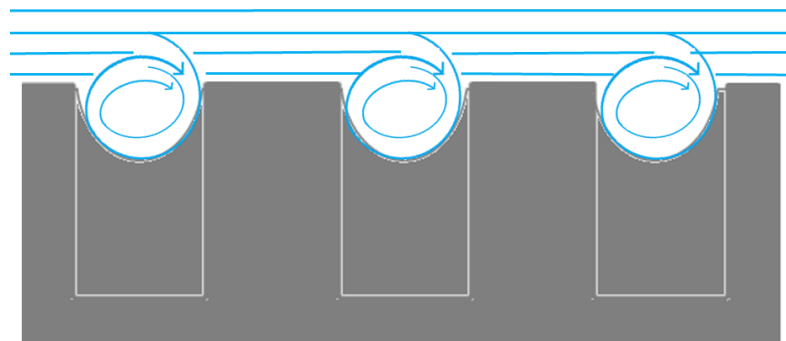


Figure 4.23 - Movement of a liquid developer in and around the in recessed features, showing the fluidic eddy currents which will form preventing the fabrication of cylindrical holes.

4.3.3 Poly (Dimethylsiloxane) (PDMS)

Following the unsuccessful outcomes with existing polymers, the final fabrication technique explored involved the Poly (dimethylsiloxane) (PDMS) alone. PDMS is a silicon based organic polymer, used in a wide range of applications such as medical devices, lubricants and shampoos [20, 30, 31]. It is commonly employed in micro-fabrication techniques specifically for use in micro-fluidics due to advantages in fabrication ease, physical properties and its relatively low cost. PDMS is a two part mixture allowing varying ratios of base to curing agent to be produced, allowing the mechanical properties of the polymer to be controlled. PDMS was not initially chosen due to the restrictions with using the polymer in the cleanroom. Therefore, when fabricating the micro-structured surfaces, it is possible that deformities will be present on the surfaces, due to dust and contamination associated with working in a conventional laboratory environment.

4.3.3.1 Method 5: Direct Patterning of PDMS

A pre-made silicon template, as previously described in 4.2.5, containing the micro-structures is coated with a ratio of 5:1 base/curing agent mix and cured for 6 hours at 50°C on a hot plate then at room temperature for a further 18 hours. The sample is peeled away leaving holes in the PDMS (Figure 4.24).

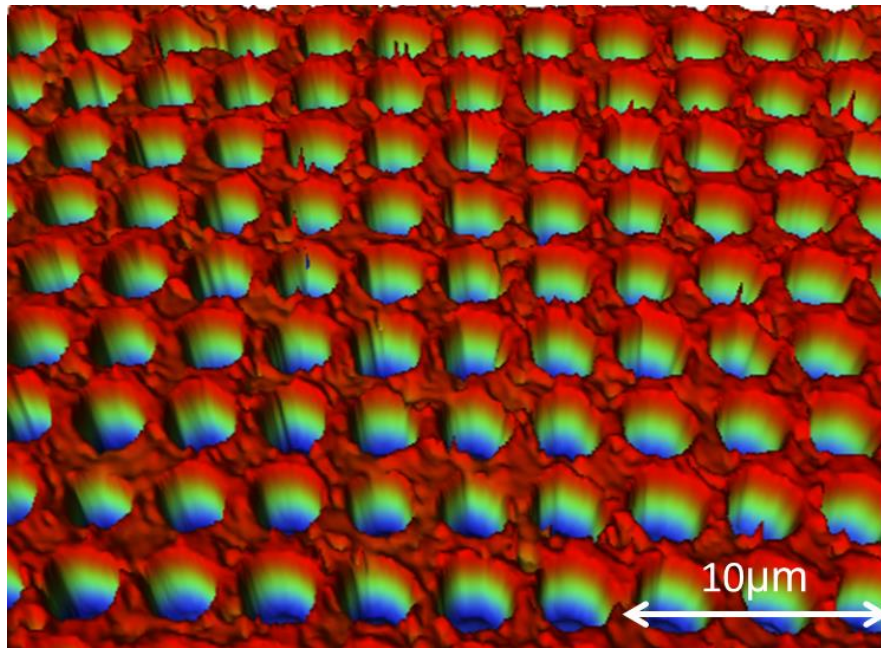


**Figure 4.24 - White light interferometry image of the PDMS hole mould
(Geometry one - 1.5 μm spacing)**

This surface is then placed in a Reactive Ion Etcher (RIE) and exposed to 25 sccm trifluoromethane (CHF_3) at 45 W for 1 minute, at a pressure of 19 millitorr, to provide a super-hydrophobic coating, without etching the substrate, resulting in a successful peel off when a layer of 10:1 PDMS mix is cured in the holes using the same procedure as that for the 5:1 ratio, as illustrated in Figure 4.25. This difference in base/curing agent ratio also provides successful peel off.

This mechanism was found to lead to a reliable and repeatable mechanism for producing polymer micro-structures, as shown in Figure 4.26, and able to do so for a range of geometries (Figure 4.27 & Figure 4.28).

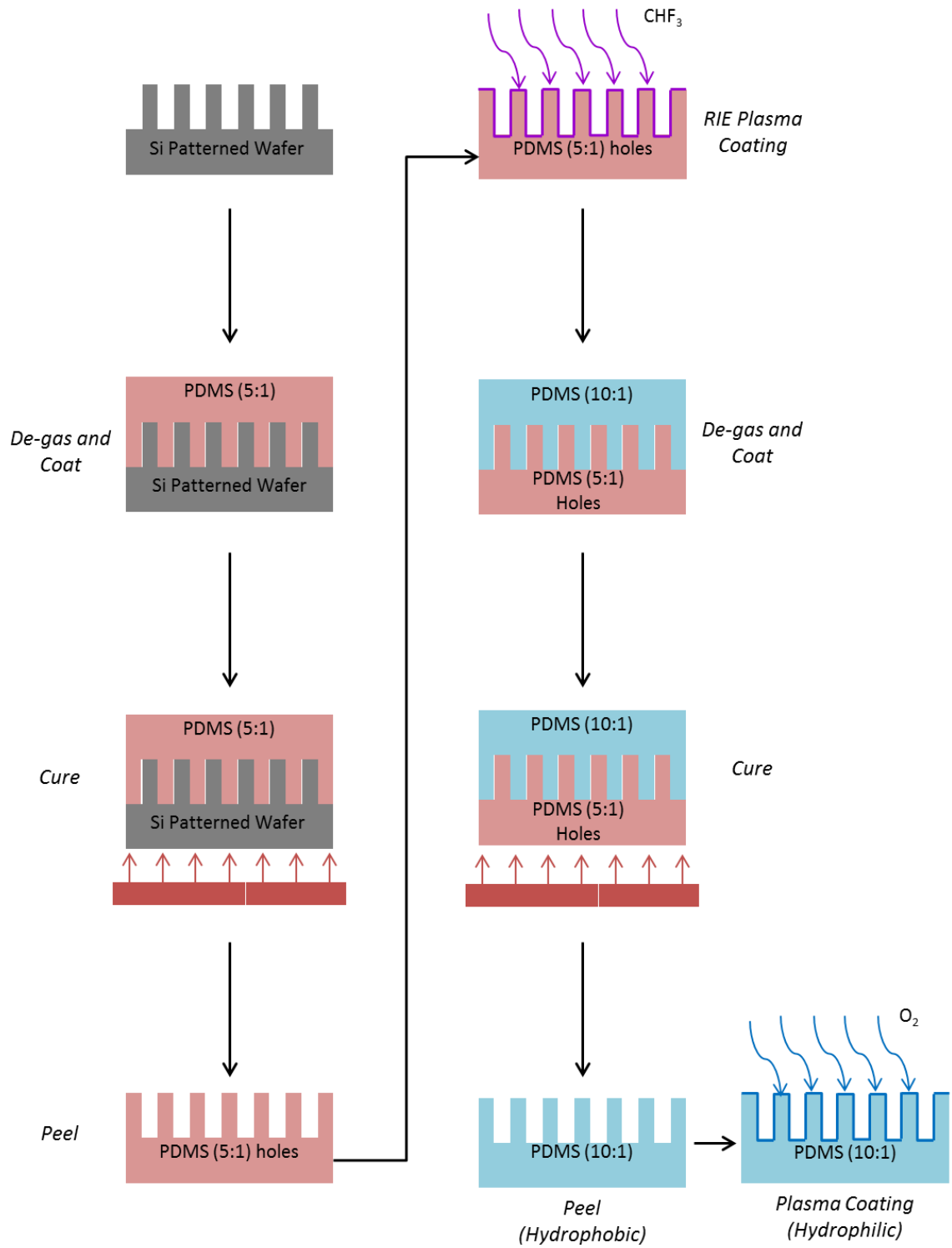


Figure 4.25 - PDMS fabrication technique (not to scale)

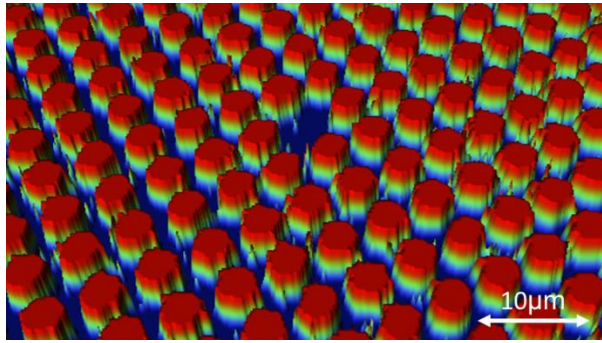


Figure 4.26 - White light interferometry image of micro-structured PDMS surface (geometry one - 1.5 μm spacing)

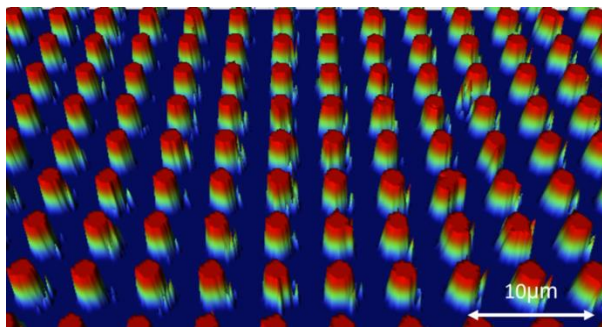


Figure 4.27 - White light interferometry image of micro-structured PDMS surface (Geometry two - 4.5 μm spacing)

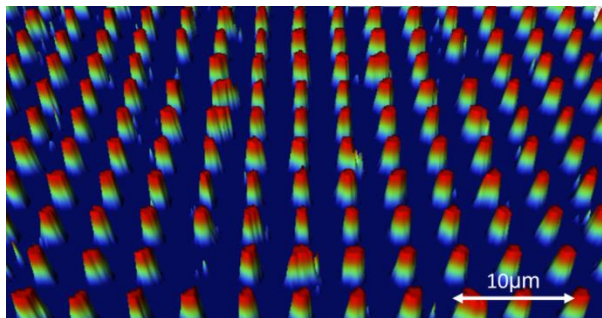


Figure 4.28 - White light interferometry image of micro-structured PDMS surface (Geometry three - 6 μm spacing)

It can be seen that on these sections of the micro pillared surfaces there are missing pillars, and have irregularities, such as irregular deformed features and extra, small dimples on the surface between pillars, compared to the regular array of micro-pillars formed in Autotex[®]. This is due to defects from the fabrication

process. As the PDMS processing was not carried out in a clean room, there may be contamination from dust, and particles in the air. Air bubbles may also be present in the polymer due to unsuccessful degassing. However, as there is a larger area of successful lithography this is deemed to be acceptable, although, this may result in a lower force of adhesion. It can also be seen however that the wall profile of that on the PDMS surfaces is more anisotropic than those on the Autotex[®] surface. This is due to the fabrication technique used.

As PDMS is hydrophobic in nature the samples can be exposed to atmospheric air plasma to decrease the surface contact angle, and as a result optimise adhesion. Exposing the sample to plasma, adds a silanol group which switches the wettability as shown in Figure 4.29. Where individual flat PDMS samples were exposed for varying time periods to the plasma and the contact angle measured using contact angle goniometry as described in 3.5.4.

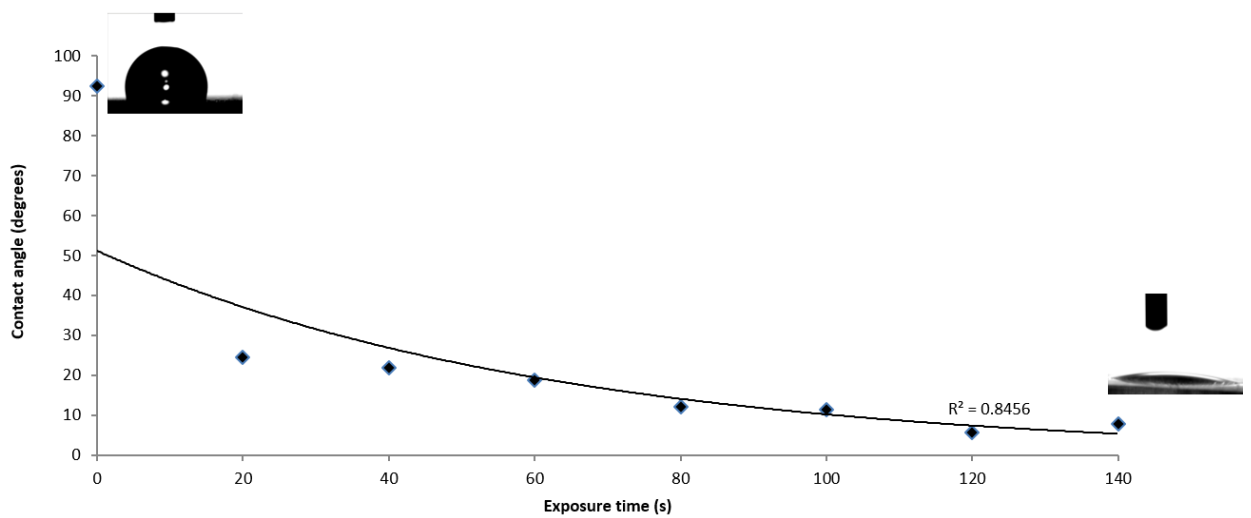


Figure 4.29 - Contact angle of a flat PDMS sample as a result of exposure to atmospheric air plasma. Data has been collected using a contact angle goniometer¹⁵.

¹⁵ Molecular and Nanoscale Physics facilities, Faculty of Mathematics and Physical Sciences, University of Leeds, UK

Figure 4.29 shows that as the flat PDMS samples are exposed to plasma treatment the contact angle drops dramatically, before reaching a minimum angle at 120 s, this is then maintained. Despite this however, the maximum exposure time during experimental adhesion testing will be 80 s as longer exposure results in etching of the surface rather than coating. This would be detrimental to the polymer pillars where it is important for the comparison of geometry this is described further in Chapter 5.

4.4 Summary

A range of fabrication techniques and polymers have been investigated in order to arrive at a means of successfully fabricating flexible bio-inspired, micro-structured surfaces. Following the techniques described, it is found that:

1. Autotex[®] can be used to successfully produce a repeatable micro-structured surface for one specific geometry. However, the full and comprehensive optimization of this polymer in terms of wettability and geometric parameters was not possible due to it being a made-to-order product. Additionally, the limited volume of the polymer which was made available for this project and cannot be replenished was not sufficient for the amount of testing which would be required to obtain any substantial conclusions.
2. SU8 is not capable of producing a micro-pillared array on a flexible substrate. Shrinkages occurred in the cross linking process as a result of the large differences in glass transition temperatures (SU8 = 210°C; PET = 76°C) and therefore causing delamination of the pillars from the PET sheet.
3. SU8 could not be used as a mask/mould for any of the other candidate polymers, due to the resolution of the mask and the unknown chemical interaction which occurred at the SU8-Autotex[®] interface.

4. Poly (dimethylsiloxane) leads to successfully fabricated repeatable micro-structured surfaces for varying geometries as discussed above (4.3.3.1), and as it is possible to tune the surface's affinity to fluids, it is this process which was adapted and carried forward throughout this work.

In conclusion, a range of polymers and fabrication techniques, which are most commonly used for microelectromechanical systems (MEMS), have been investigated in order to successfully fabricate a bio-inspired, micro-structured polymer surface on a flexible substrate.

This chapter has shown that using an imprint lithography method is a viable option to create a regular array of pillars on the micro-scale. PDMS has proven to be the most effective polymer, allowing successful repeatable fabrication in a range of geometries, and also has the ability to functionalise the surface to provide optimum repeatable, reliable adhesion to a wet surface, by tuning the wettability through exposure to atmospheric air plasma, dramatically decreasing the contact angle. Due to the low glass transition temperature of PDMS (-125°C), PDMS is also flexible at room temperature, a desirable quality for this work.

Chapter 5. Experimental Results

5.1 Introduction

This chapter incorporates aspects of sample preparation to ensure repeatable, good quality pillared surfaces are able to be routinely produced. Results from a parametric study of adhesion measurements are then presented; these form a basis for comparison with the modelling work presented in the next chapter.

5.2 Sample Preparation

Once the micro-pillared surfaces have been fabricated successfully, it was necessary to characterise the surface to ensure repeatability; specifically in terms of mechanical properties and wettability. It is also necessary to characterise the fluids to be used during the testing, as these will have a direct impact on the adhesion. All work reported in this chapter has been performed using PDMS with a mix ratio of 10:1 - the same ratio as used in the final PDMS pillar samples.

5.2.1 Polymer Properties

As described in section 2.4, initial testing was performed using a made-to-order product - Autotex[®]. However, the full and comprehensive optimization of this polymer in terms of wettability and geometric parameters was not possible due to copyright protection associated with the chemical structure; the material parameters are also not readily available, further obstructing any possibility of a full and systematic theoretical and experimental comparison with other materials. Accordingly, other polymers were investigated, specifically Poly (dimethylsiloxane) (PDMS). To ensure the PDMS is stable before testing its mechanical properties were investigated over a seven-day period (section 5.2.1.1). PDMS is a naturally hydrophobic silicon based polymer which, when

subjected to air plasma, transforms to being hydrophilic due to the addition of silanol (SiOH) groups to the surface. Section 5.2.1.2 outlines the result of plasma exposure as a function of time on the associated polymer contact angle.

5.2.1.1 Mechanical Properties

As both the hardness and modulus of the polymer affect the adhesion of a surface it is particularly important to only perform adhesion tests once the surface is stable. Therefore nano-indentation was performed in order to determine the stability.

These tests were carried out on PDMS fabricated in a 10:1 base/curing agent ratio, which was cured on a hotplate for 6 hours at 50°C and then left at room temperature for 24 hours. The surface was then mounted into the nano-indenter and aligned with a 100 µm diamond spherical tip. The tests were performed out of normal laboratory hours to ensure minimal vibrations and a constant room temperature. An array of test areas across the PDMS samples were identified from which readings have been taken to ensure the uniformity of the PDMS samples, a diagram of the array is provided in Figure 5.1. The results of this test are presented in Figure 5.2, where the load-displacement curves for each of five indentations made after each 24 hour period have been averaged and plotted, to show only the average load-displacement data for the sample at that time frame.

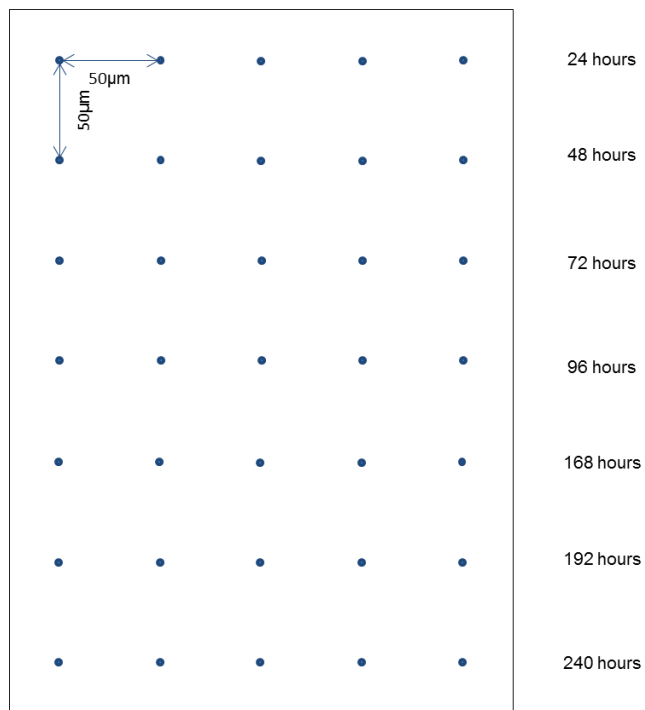


Figure 5.1 - Indentation pattern of 35 localised indentation points over a single PDMS sample over time.

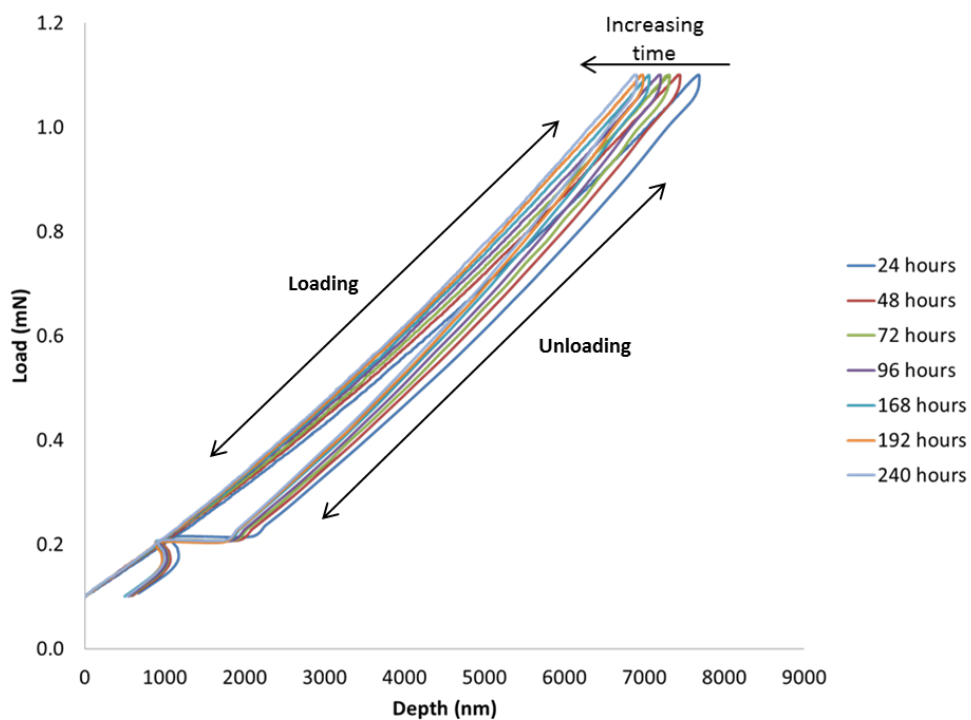


Figure 5.2 - Nano-indentation data for the change in mechanical properties of a PDMS sample over specific time periods. The data is the average curves for five data sets taken in one time frame.

It can be seen that the hysteresis curves are shifted slightly as a function of time. The values for elastic modulus and hardness have been extracted using an Oliver-Pharr analysis technique [115], in which the gradient of the tangent to the unloading curve is calculated between 20% and 80% of the data, as shown in Figure 5.3.

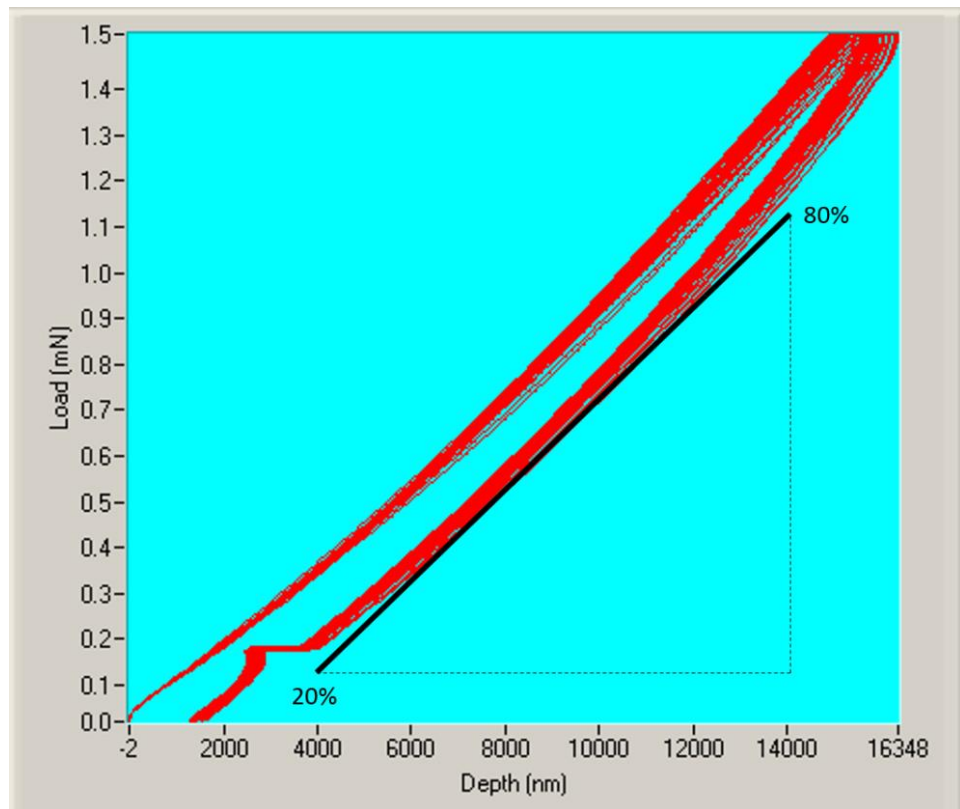


Figure 5.3 - Oliver-Pharr method of analysis used to calculate the elastic modulus and hardness of a substrate using nano-indentation.

It is worth noting that there is a glitch in the data in each hysteresis curve. This is due to a thermal drift correction, as shown in more detail in Figure 5.4.

Thermal drift is a change in dimension of the indenter, sample, or instrument as a result of a temperature change during the test. However as this happens within the bottom 20% it will not affect the resultant data due to the analysis technique used.

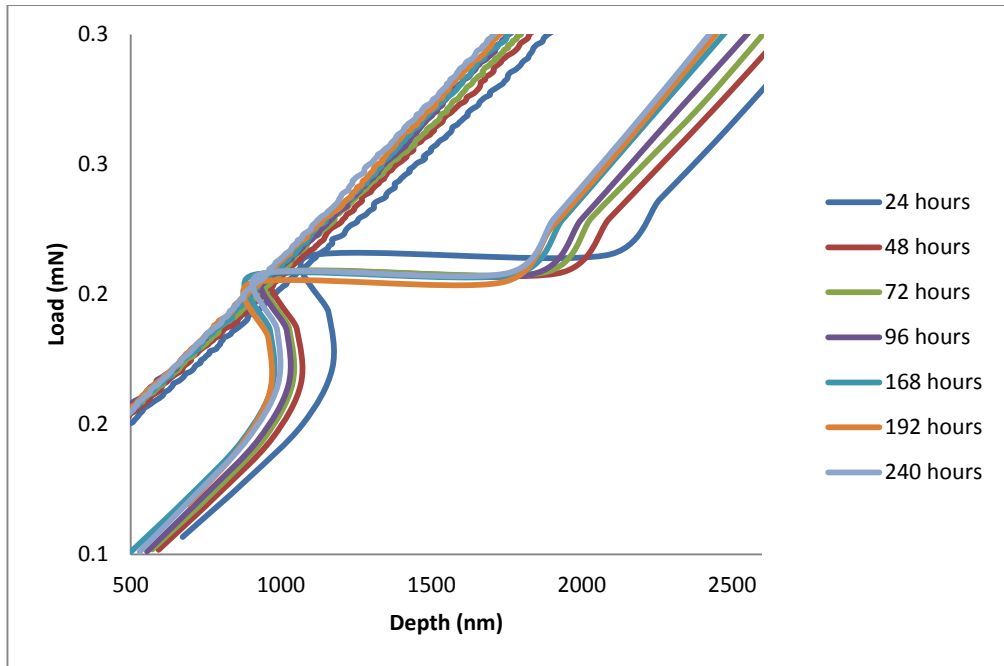


Figure 5.4 - Exploded view of the thermal drift correction, as consequence of a change in dimension of the indenter, sample, or instrument as a result of a temperature change during the test.

The creep in data as a function of time is shown in Figure 5.5, where the average values for hardness and elastic modulus have been calculated for each time frame. It can be seen that the surface remains stable over a 240 hour period with change in hardness and elastic modulus of 12% and 17%, respectively, with the highest percentage change occurring within the first 48 hours. Therefore it was concluded that there would be negligible variation in adhesion tests due to the time period over which PDMS samples were fabricated.

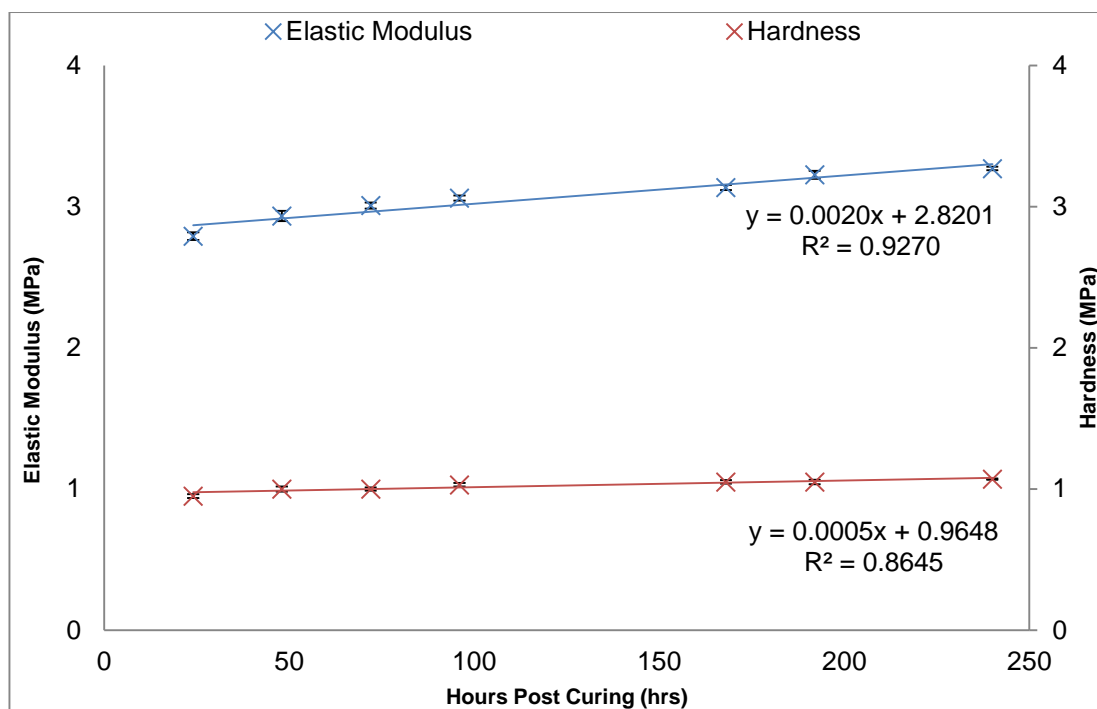


Figure 5.5 - Changes in elastic modulus and hardness for a typical PDMS sample over time. Average errors: hardness = 0.01 MPa, elastic modulus = 0.02 MPa.

As this work looks at the use of a polymer substrate in a wet environment, it is necessary to evaluate the effects of water on the mechanical properties. Hydrolysis can lead to chain scission, and as a result, decreasing the molecular weight and therefore altering the mechanical properties [146]. However, all polymer samples are exposed to the fluid equally, any change in mechanical properties is consistent across all samples. Mata *et al.* have also found that when immersed in water, there is no change to the geometry of PDMS micro-structures [109].

5.2.1.2 Wettability

The effect of wettability on the wet adhesion force was a parameter that was indicated in the experimental matrix and has been investigated. In order to characterise the surface, small PDMS samples were mounted into the Plasma

Prep II chamber for varying times at a power of 100 W and pressure of approximately 0.01 mbar [113] and the contact angle was measured using Contact Angle Goniometry¹⁶. Firstly, flat samples were treated and tested at varying times in the range of 0 - 140 seconds. The results are shown in Figure 5.6.

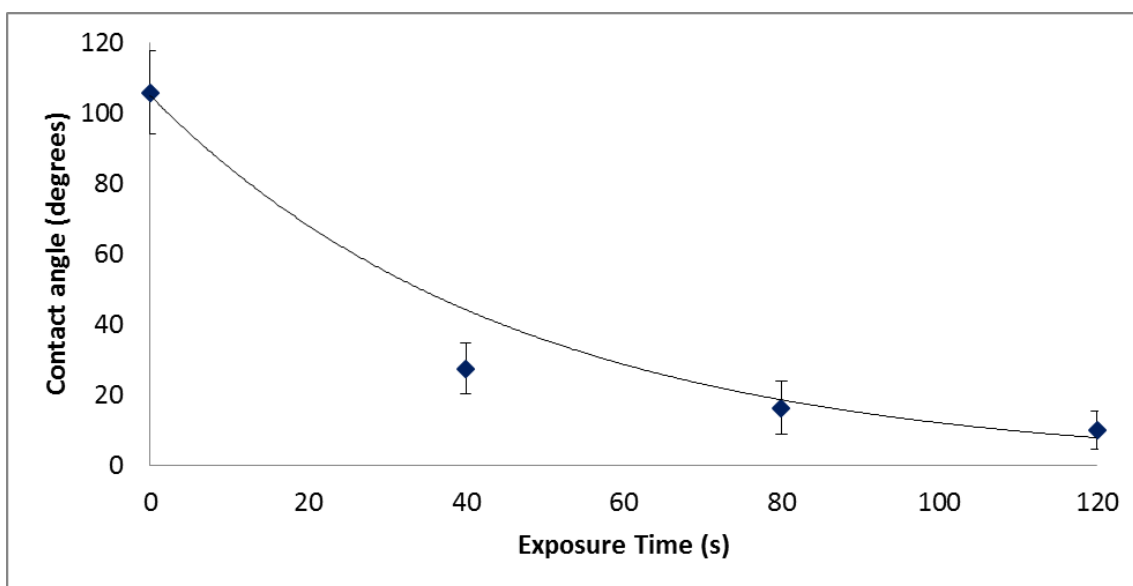


Figure 5.6 - Contact angle as a function of air plasma exposure time for a flat PDMS sample of mix ratio 10:1, this data is a modification to the data in Figure 4.29, showing specifically the contact angles investigated for the pillared samples.

It can be seen that the contact angle of the PDMS does decrease from hydrophobic 105.8° to a hydrophilic 27.5° within 40 seconds of exposure as expected, due to the addition of a silanol group onto the surface. Although initially this would suggest that the longer the exposure time, the greater the adhesion force due to the decrease in contact angle, practically this would not be the case. Firstly, if the contact angle is too low, the surface will act super-hydrophilic and flood. Secondly, an extended plasma exposure would result in the etching of the

¹⁶ School of Physics and Astronomy, University of Leeds

polymer. This would be detrimental to this work as it is vital to ensure that the micro-pillared geometry remains consistent.

Pillared surfaces were exposed for the same durations; however before the contact angle was measured, they were investigated using white light interferometry to determine whether the longer exposure times were etching the structures or just applying the silanol group to the surface. It is apparent that after 40 seconds the polymer begins to undergo an etching process rather than a chemical treatment. As this is dry etching from a plasma chamber, an isotropic etching will be taking place resulting in not only the top surface being etched, but also the sidewalls. The results are shown in Figure 5.7 and Figure 5.8.

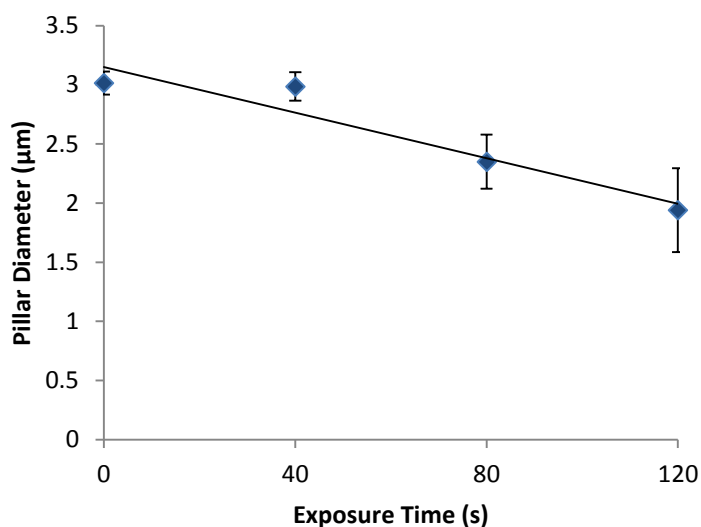


Figure 5.7 - The effect of plasma exposure time on the pillar diameter.

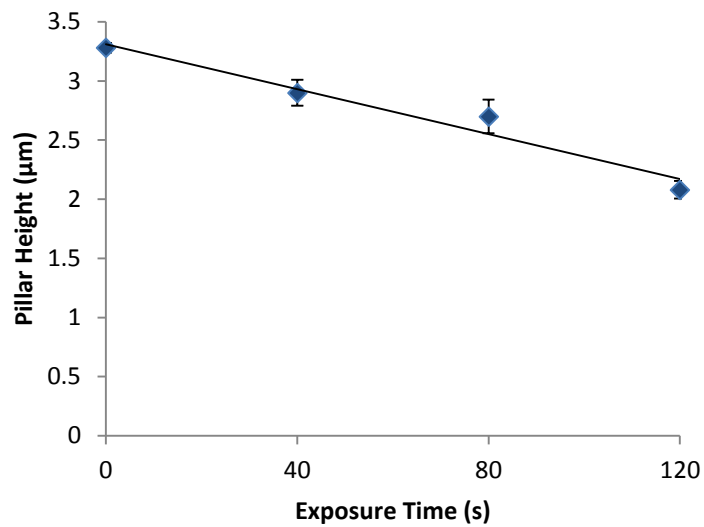


Figure 5.8 - The effect of plasma exposure time on the pillar height.

It can also be seen that the pillar profile is also changed as a result of the plasma treatment, as shown in Figure 5.9.

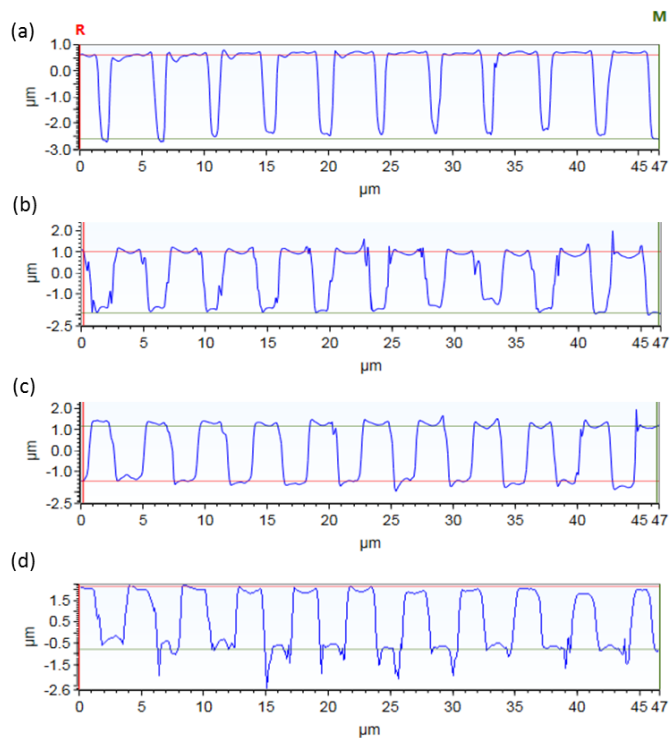


Figure 5.9 - The effect on the pillar profile as a result of exposure to atmospheric air plasma for (a) 0 seconds, (b) 40 seconds, (c) 80 seconds and (d) 120 seconds.

A dimple-like feature appears to form on top of the surface of the pillar after a short exposure, it is also clear that there is increased roughness around the pillar due to etching occurring at the base of the pillar as the exposure time increases to 120 seconds. This is shown more clearly in a 3D plot, when comparing the unexposed surface and that of the sample exposed for 120 seconds (Figure 5.10).

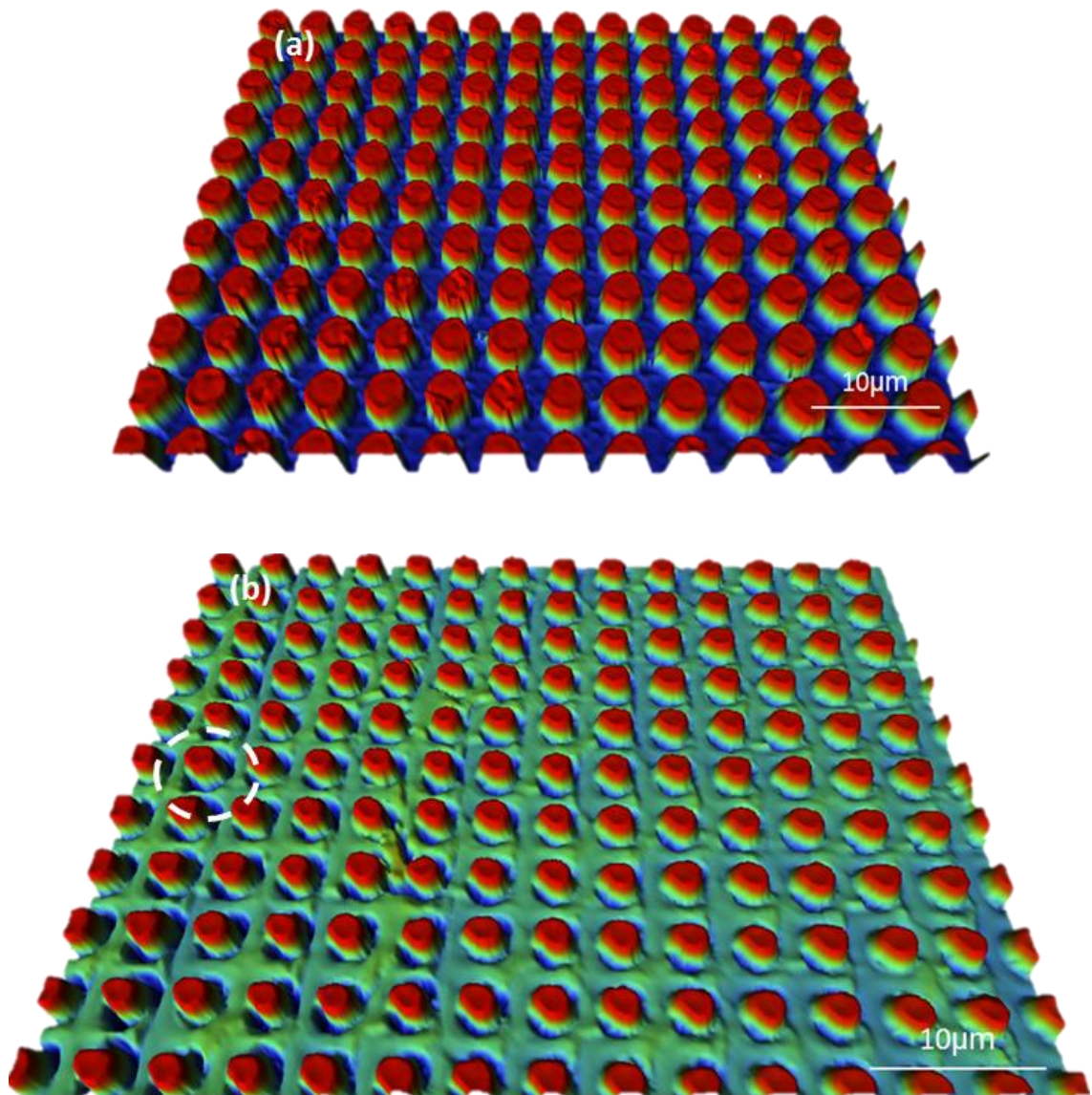


Figure 5.10 - White light interferometry images of (a) an unexposed PDMS sample and (b) a sample after 120 seconds of exposure. The area highlighted shows where etching has occurred around the base of the pillar.

If samples were to be tested in a wet environment with such etching profiles around the pillars, this would affect the adhesion mechanism as it is possible these features could act as a reservoir for the liquid. Due to this, only the shorter exposure times could be explored for the pillared surface. It was therefore decided to use 0 seconds, 20 seconds and 40 seconds exposures. The corresponding contact angle results are shown in Figure 5.11, revealing that the contact angle is larger on the pillared surfaces than that of the unstructured sample (Figure 5.6) due to the added roughness on the surface.

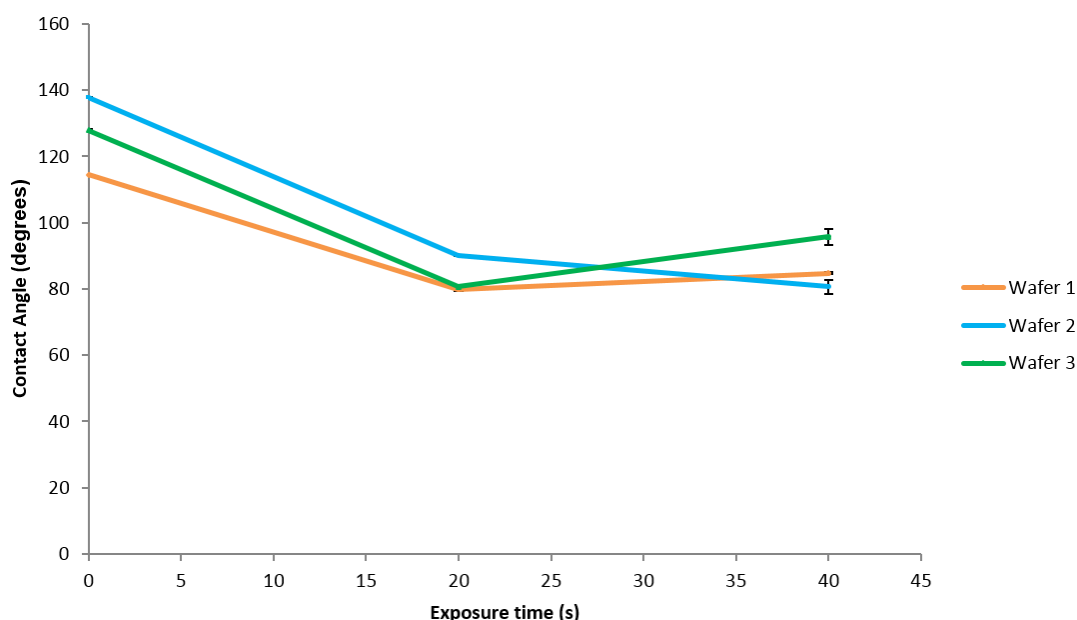


Figure 5.11 - Contact angle as a function of air plasma exposure time for three pillared PDMS samples; see section 4.3.3.1 for wafer specification

Figure 5.11, shows that there is a decrease in the contact angle with exposure time of the samples to air plasma; however, it is not as large a change as with the flat sample. This is due to the pillared surface having a roughness value, as shown by Quéré *et al.* [60], as the surface roughness increases so does the apparent contact angle, with the exception of a super hydrophilic surface.

$$\cos\theta^* = r \cos\theta \quad (5.1) [147]$$

Where θ^* is the apparent rough contact angle; r is the roughness ratio (defined as 1 for a smooth surface) and θ is the contact angle on an ideal flat surface, as described above in section 6.5.2.

When comparing the surface wettability for the adhesion results it will be the values for flat samples which will be used. This is due to the model assuming a single liquid bridge forming on the tip of each individual pillar. Therefore, an average contact angle over a number of pillars is not an accurate representation of the wettability of a single pillar tip.

5.2.2 Fluid Characterisation

As the fluid viscosity is expected to have a major impact on the adhesion values and mechanism, this has been varied during adhesion testing. Tests have been performed with two different liquids, de-ionised water alone and a water-glycerol mix, on a glass slide and rat peritoneal fluid on *ex-vivo* tissue. Only one mixture of water and glycerol was used as a too high glycerol percentage would result in an uneven coverage of the glass slide, and too low a percentage of glycerol would not give a significant difference to that of water.

All tests were performed at room temperature. The values for the viscosities are given in Table 5.1.

Table 5.1 - Table of viscosities for the fluids used during testing.

Fluid	Viscosity (Ns/m ²) at 25°C
Water	1 x 10 ⁻³
Water - Glycerol mix	630 x 10 ⁻³
Peritoneal fluid	151 x 10 ⁻³

These values were measured using a Kinexus rheometer¹⁷. Ott *et al.* [148] observed changes in the viscosity of peritoneal fluid during exposure to CO₂, during laparoscopic surgery, their values, before the addition of CO₂, have been extracted for the value for the *ex-vivo* peritoneal tissue [148]. This value was converted to a dynamic viscosity by multiplying their value by the specific gravity of blood (1.06) [149].

For the fluid tests, glass slides have been coated with a small volume of fluid to form a thin film across its surface. The film thickness is calculated by measuring the mass of the fluid, to allow a volume to be calculated according to equation (5.2), and the film thickness according to (5.3).

$$V = m/\rho \quad (5.2)$$

$$H = V/A \quad (5.3)$$

Where, V is the volume of liquid, m is the mass, ρ is the density, H is the fluid height and the area (A) is taken to be the area of the glass surface. The values for film thickness are given in Table 5.2.

¹⁷ Malvern Instruments, UK - measured at a 0.1 s⁻¹ shear rate.

Table 5.2 - Table containing the film thickness of fluids used during adhesion tests

Material	Film Thickness (μm)
Water	70
Glycerol - Water mix	200

Despite there being a difference in the fluid film thickness for the water and water - glycerol mix, this should not affect the adhesion mechanism, as both are large enough to flood the surface as would happen against the compliant *ex-vivo* peritoneal samples.

5.3 Adhesion Results

Wet adhesion tests of the micro-structured surfaces (figures 5.12 - 5.18) were performed initially using the Modular Universal Surface Test rig, as described in section 3.6.1. However, final tests were carried out on the Modular Mechanical Characterisation rig, as described in section 3.6.3 due to issues which arose with the MUST rig - specifically regarding the pre-load. The pre-load could not be controlled due to mechanical issues which arose part way through testing with the equipment. This resulted in a non-consistent overshoot even at low approach velocities. As the adhesion force is dependent on the pre-load applied, it is critical to ensure this value is the same for each test. Despite the change in test equipment, all conditions; pre-load, approach velocity and indenter size remained the same throughout all of the tests. The surface area of the pillars also has been kept constant with relation to the work by Roshan *et al.* [21] where it was found that having a surface area of 113 mm^2 provided the greatest adhesion. The adhesion at areas larger than this then became much less consistent, and no

benefit was gained by increasing further. [21]. As the surface area of the samples has remained constant throughout these tests, the adhesion force results are presented in mN. Results in this chapter have analysed using both standard deviation and ANOVA analysis, where a significance level, α , of 0.05 has been used.

This chapter also compares the experimental results to those which have been calculated using the mathematical model given in Chapter 6. The variables for this model are given in Table 5.3

Table 5.3 - Constant values [21, 148, 150, 151]

Constant	Value
Pillar Radius, R	1.5×10^{-6} m
Bridge Height, H	5.4×10^{-7} m
Surface Tension, γ	0.073 N/m
Time, t	2.85 s
Viscosity - Water, η	1 cP
Viscosity - <i>Ex-Vivo</i> , η	1.425 cP
Viscosity - <i>In-Vivo</i> , η	73.5 cP
Contact Angle - Wet Glass, θ_1	14°
Contact Angle - Tissue, θ_1	40.5°

5.3.1 Effect of Polymer Selection

As both Autotex[®] and PDMS produced surfaces containing a reliable, array of pillars, it is these that are compared. Autotex[®] could be fabricated for one specific geometry only, with the largest pillar spacing - 6 μ m. As the pillar spacing

decreased and the density of pillars increased, peel-off from the silicon master mould became unsuccessful. Therefore this geometry alone has been tested against a glass substrate coated with water, and compared to the same geometry in PDMS.

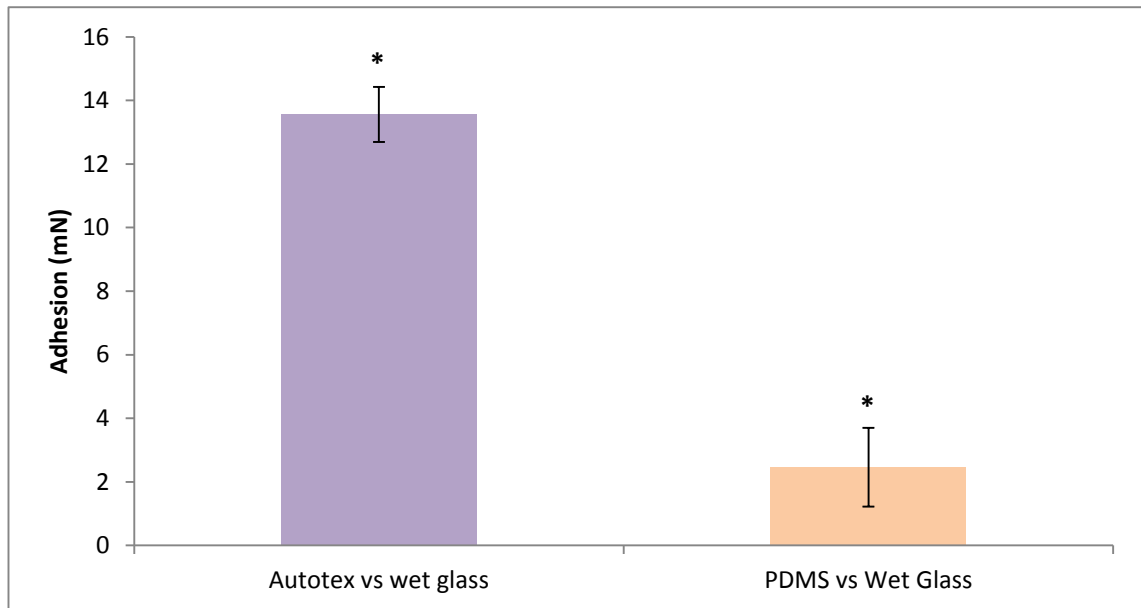


Figure 5.12 - Adhesion results for the original Autotex[®] sample compared to the PDMS sample of the same geometry – against glass coated in water. * signifies statistical significance within the difference in data where $p \leq \alpha$.

5.12 compares adhesion results for the original Autotex[®] sample and a hydrophobic PDMS sample (105.8°) in wafer 3 geometry - 6 μm spacing, against glass coated in water. It can be seen that the Autotex[®] sample provides 5.5 times greater adhesion than the PDMS sample. As the surfaces have the same geometry and the same fluid interacting with the surface, this result can only be due to the difference in contact angle and surface energies of the different polymers. Taylor measured the Autotex[®] contact angle to be 67.5° [17] using the FTA 4000 described in section 3.5.4. This contact angle is the average contact

angle over a number of pillars depending on the droplet size; therefore it can be assumed that the contact angle on a flat surface would be lower due to the lack of surface roughness resulted from the pillars, however it could not be measured due to the limited volume of the material which could not be replenished. Despite this, the Autotex[®] sample is still more hydrophilic than the PDMS. This, as described earlier, is beneficial in aiding adhesion. This is something which is discussed in Chapter 7.

The mathematical model is described in detail in the following chapter, encompassing both Stefan adhesion and capillary forces. However, shown below are the theoretical adhesion results for the two polymers. It can be seen that the adhesion is double that of the PDMS sample for the Autotex[®] sample, when all variables are the same except the contact angle.

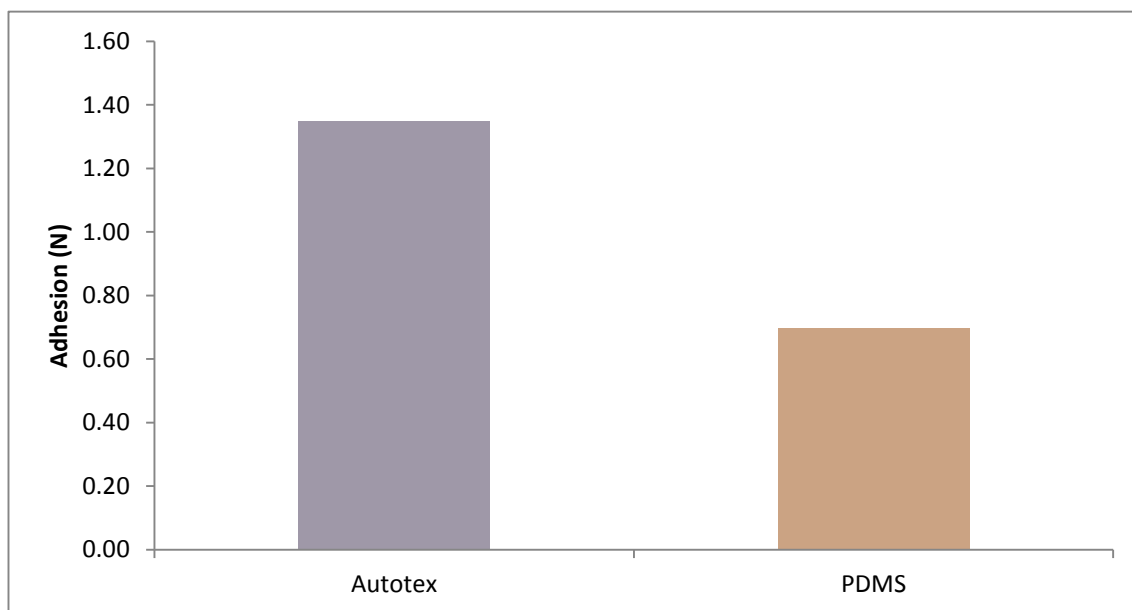


Figure 5.13 - Theoretical results for both Autotex[®] and PDMS in the same geometry, against a glass slide coated in water.

It should be noted that the adhesion is substantially larger (100 times) in the theoretical model. This is discussed further in Chapter 7. Here it can also be seen that there is a larger difference between the two polymers in the experimental

setup than that in the theoretical. It is proposed that this is due to the lack of compliance term in the model in addition to the different contact angles between the polymers. This model has been repeated for a PDMS sample with the same surface area as that of the Autotex[®]. This is shown in Figure 5.14, where it can be seen that the adhesion forces are now equal.

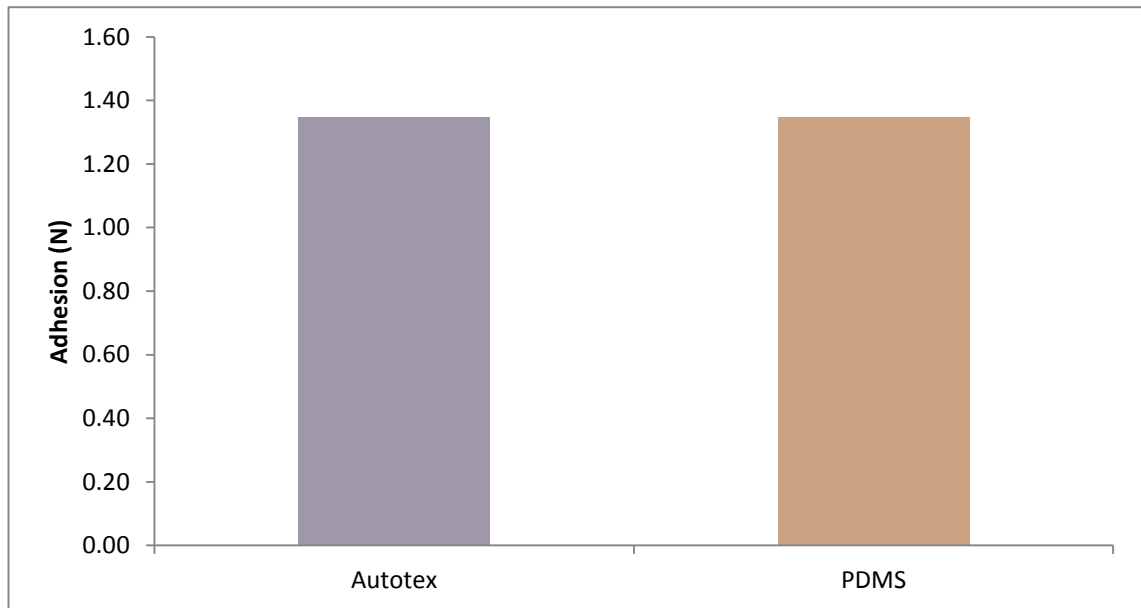


Figure 5.14 - Theoretical results for both Autotex[®] and PDMS in the same geometry, against a glass slide coated in water with the same surface contact angle.

5.3.2 Effect of Geometry on Hydrophobic PDMS Samples

This section investigates the effect of geometry on hydrophobic PDMS samples.

The effects of varying contact angles are discussed from section 5.3.4.

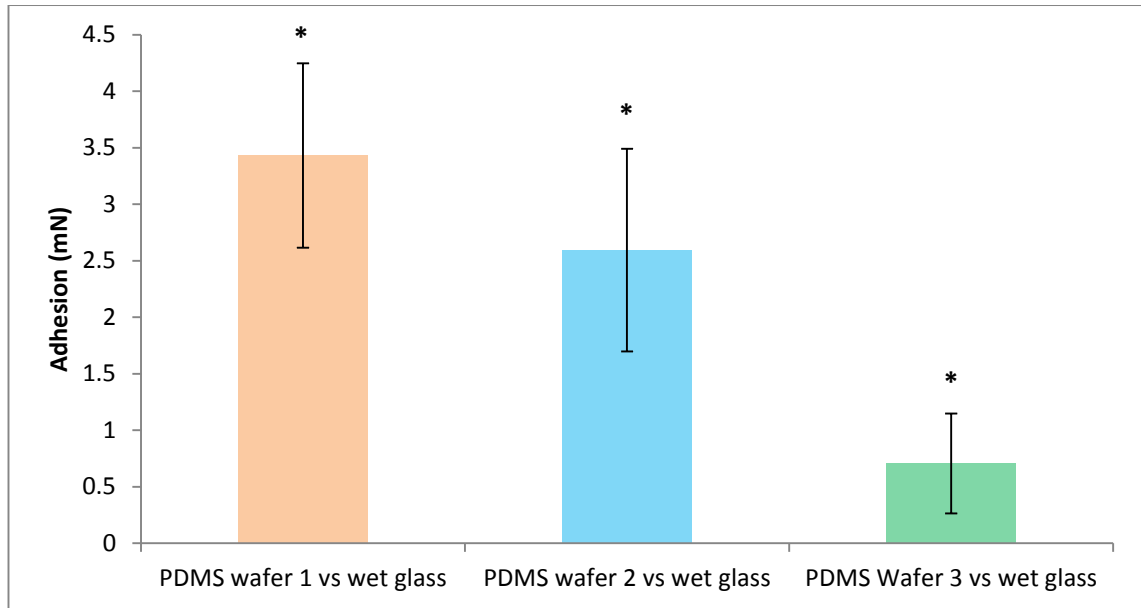


Figure 5.15 - The effect of pillar spacing on adhesion. * signifies statistical significance within the difference in data where $p \leq \alpha$.

Figure 5.15 compares the effect of geometry on adhesion. These samples are hydrophobic, with a contact angle of 105.8° ; therefore it is only the effect of pillar spacing on adhesion which is affecting the results. This data shows that, as expected, as the pillar spacing increases, the adhesion decreases. This is due to fewer pillars on the surface and therefore fewer liquid bridges contributing to the adhesive force, as predicted in the mathematical model as shown in Figure 5.16.

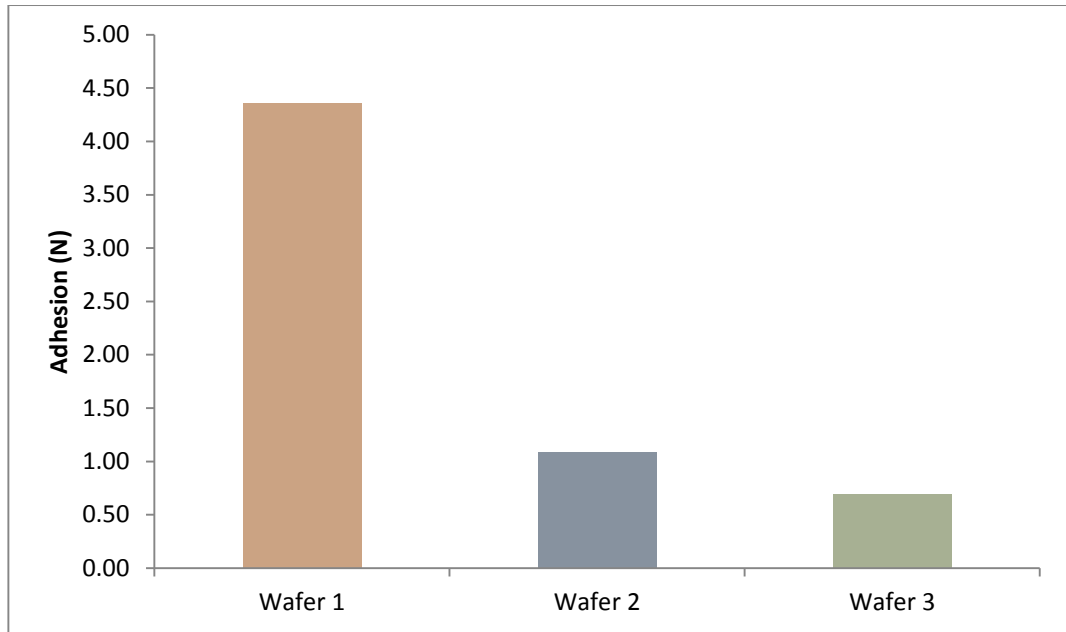


Figure 5.16 - Theoretical effect of pillar spacing on adhesion.

As in Figure 5.13, the adhesion results are predicted to be 100 times larger than the experimental results show. Again this is discussed in detail in Chapter 7. Figure 5.17 shows the effect of the pillar spacing on adhesion in terms of the number of pillars on the surface, where it can be seen that the adhesion force decrease is directly proportional to the number of pillars on each surface.

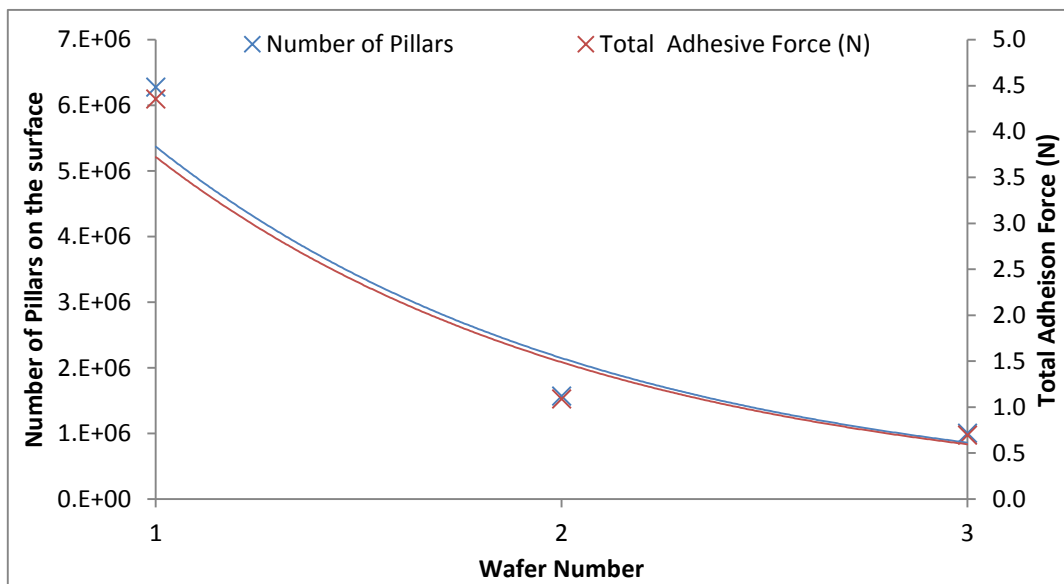


Figure 5.17- Theoretical effect of pillar spacing on adhesion, with relation to the number of pillars on the surface

5.3.3 Effect of Fluid Viscosity on Hydrophobic PDMS Samples

This section investigates the effect of fluid viscosity on hydrophobic PDMS samples, the effects of varying contact angles, is discussed from section 5.3.4.

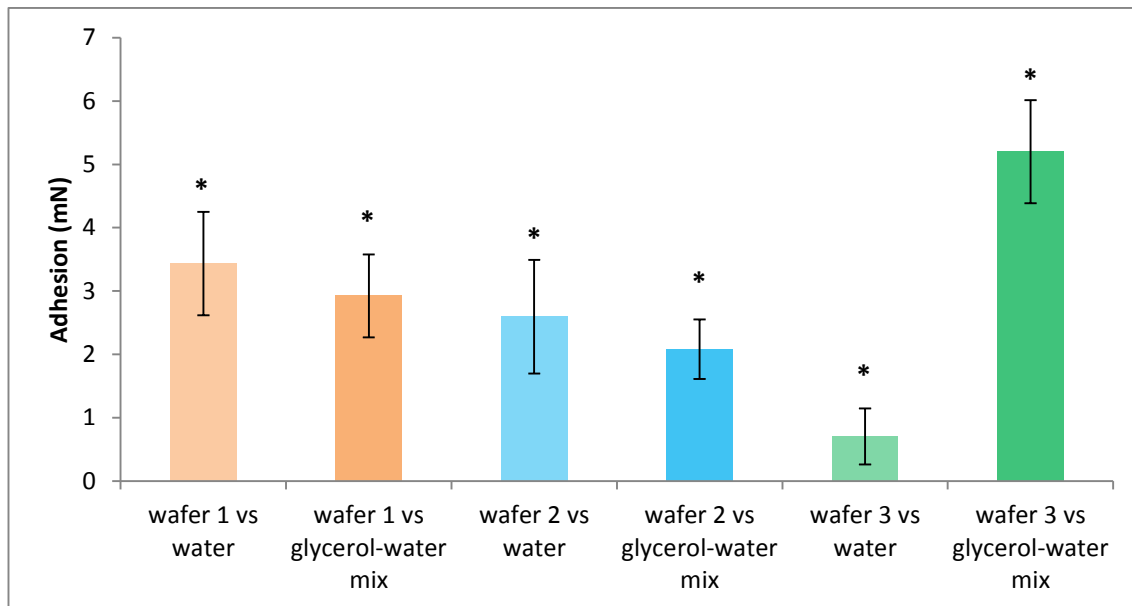


Figure 5.18 - The effect of fluid viscosity on adhesion of a hydrophobic PDMS sample against glass coated in a film of water, * signifies statistical significance within the difference in data where $p \leq \alpha$

Figure 5.18 illustrates the effect of increasing the fluid viscosity on adhesion. It can be seen that as the viscosity increases, the adhesion decreases for wafers 1 and 2. This contradicts the model in terms of Stefan adhesion; there the viscosity is directly proportional to the Stefan adhesion force. However, when considering the whole adhesion model, the Stefan component is negligible, and it is the factors which govern the capillary force which dominate. This is discussed further in Chapter 6. Figure 5.19, shows that actually, these results are affected only by the pillar spacing rather than the viscosity. This therefore suggests that the result for wafer 3 vs glycerol-water mix is an error in measurements, as it would be suggested from the model that this adhesion force should be lower than or equal to that of water. With this in mind, it can be seen that it is more beneficial to

discuss the fluid properties in terms of surface tension as opposed to viscosity as surface tension is a component of dominant capillary adhesion the theoretical results for the effect of surface tension on adhesion for these samples is shown in Figure 5.20, with the values used for surface tension given in Table 5.4.

Table 5.4 - Values for surface tension, measured using krüss k100 tensiometer¹⁸

Material	Surface Tension (N/m)
Water	7.30×10^{-2}
Glycerol - Water mix	6.51×10^{-2}

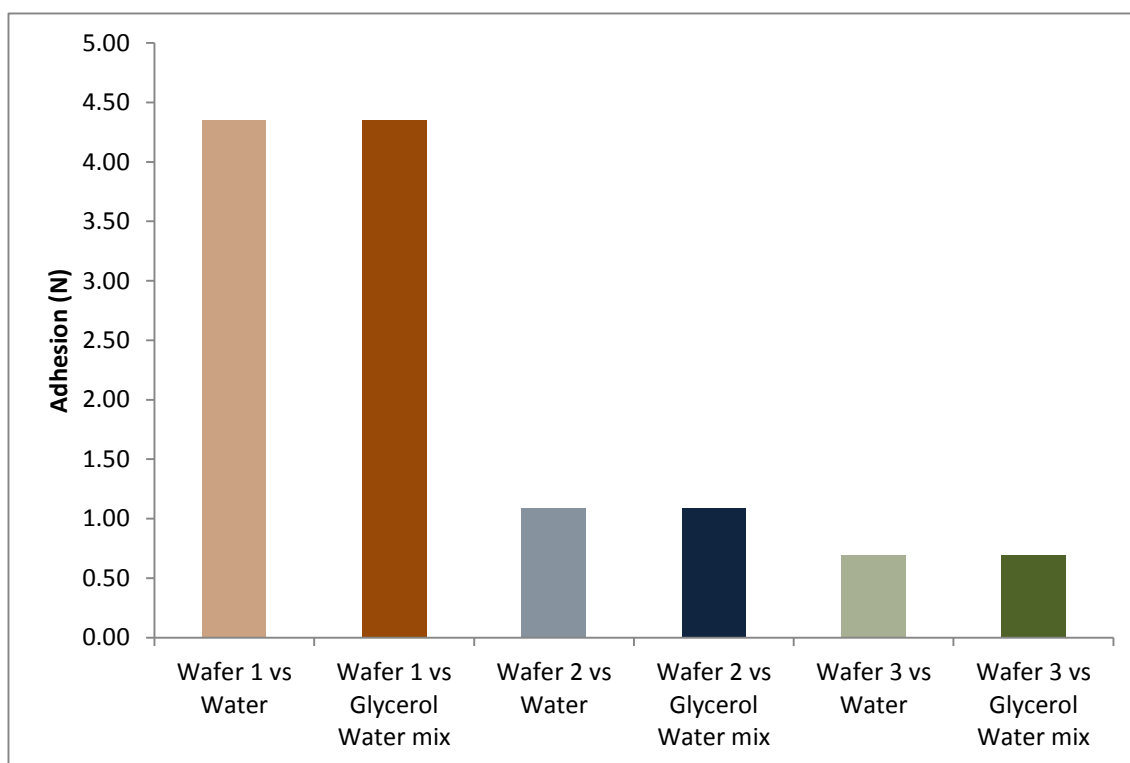


Figure 5.19 - Theoretical effect of fluid viscosity on adhesion of a hydrophobic PDMS sample against wet glass.

¹⁸ Nanowovens Innovation & Research institute (NIRI), c/o Centre for Technical Textiles, University of Leeds, Leeds, UK

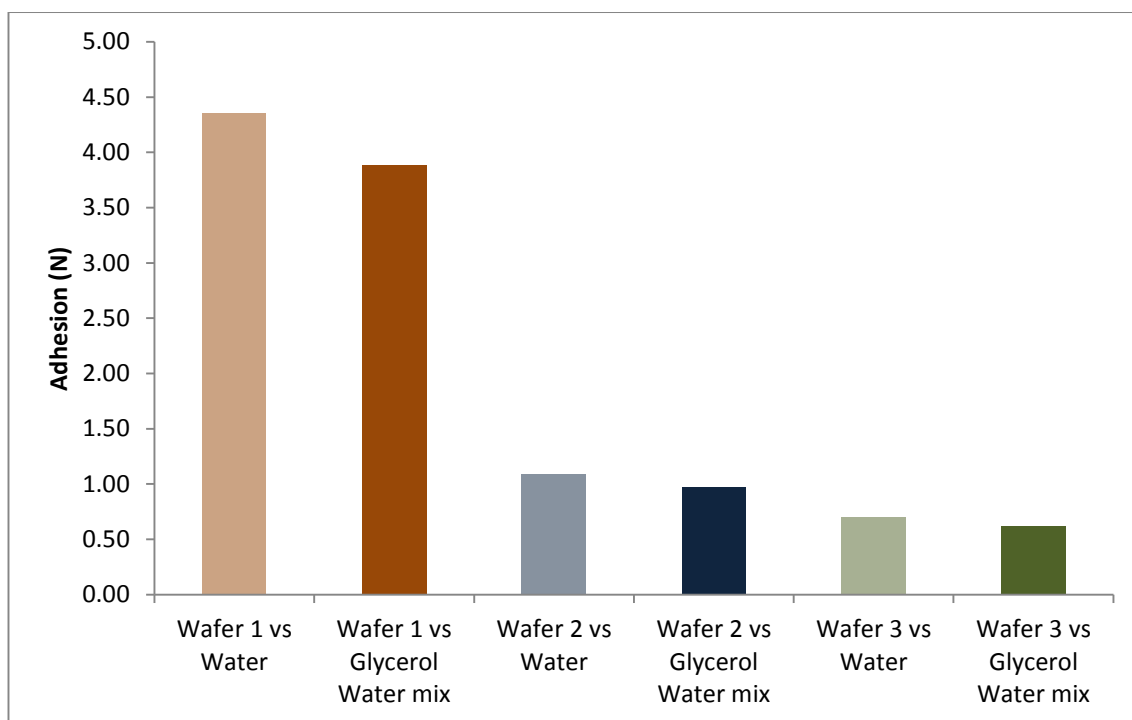


Figure 5.20 - Theoretical effect of fluid surface tension on adhesion of a hydrophobic PDMS sample.

Once again, the adhesion results are predicted to be 100 times larger than the experimental results show. This will be discussed in detail in Chapter 7.

5.3.4 Hydrophilic Adhesion against Water

This section looks at the effect of varying parameters on adhesion to a glass slide coated in water, for samples which have been plasma treated. Throughout these hydrophilic adhesion tests, the results are ten times smaller than the hydrophobic testing, this is due to a proposed wetting regime occurring, this is discussed further in Chapter 7.

5.3.4.1 Effect of Wettability on PDMS Samples

Figure 5.21 shows the effect of wettability on adhesion when in contact with a glass slide for each of the wafers independently.

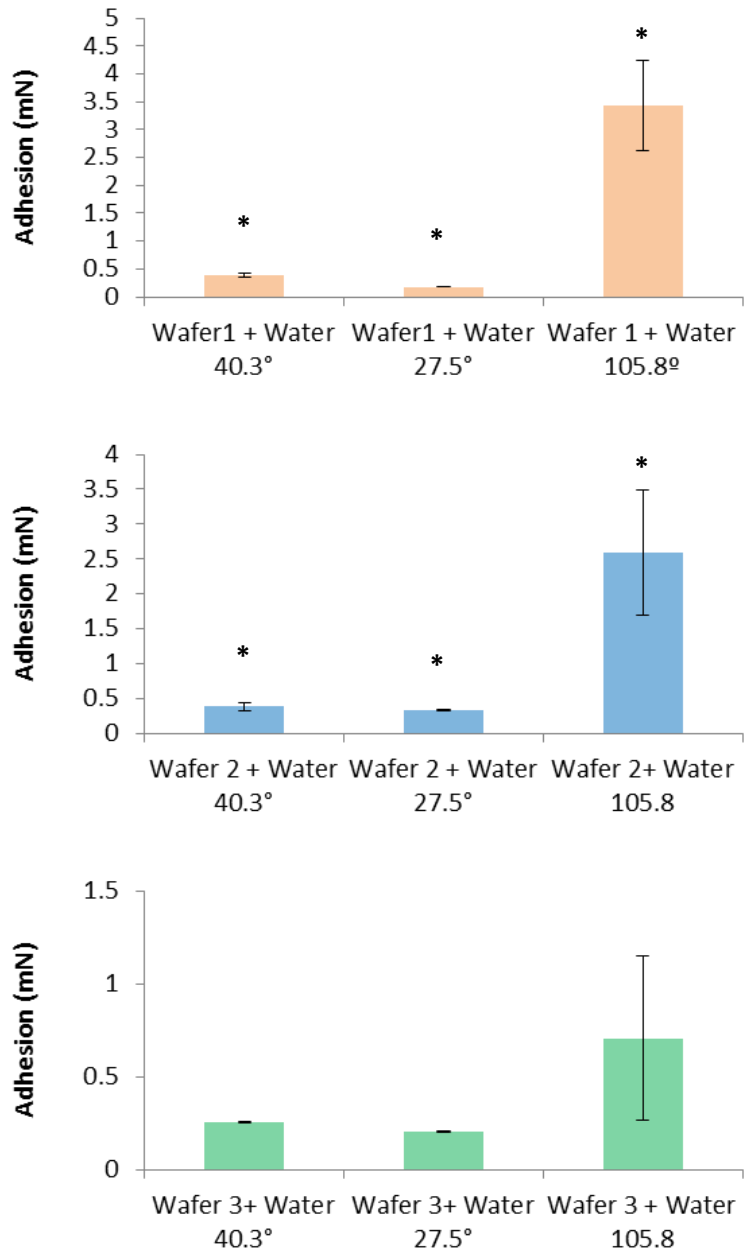


Figure 5.21 - The effect of wettability on adhesion - against a glass slide and water. * signifies statistical significance within the difference in data where $p \leq \alpha$.

For all of the samples it can be seen that as the contact angle decreases, so does the adhesion; comparing these results to those of hydrophobic surfaces it can be seen that the adhesion force is 10 times lower. This contradicts the model, which states that the more hydrophilic the surface, the higher the predicted adhesion (Figure 5.22). These results are discussed in more detail in Chapter 7, where it

is suggested that there is a point at which a surface will no longer act hydrophilic, but act super hydrophilic, flooding the surface having a detrimental effect on the resultant adhesion force. As all of the tests have been performed at a constant temperature above the glass transition temperature of PDMS (-125°C) this will not have had an effect on the adhesion forces produced.

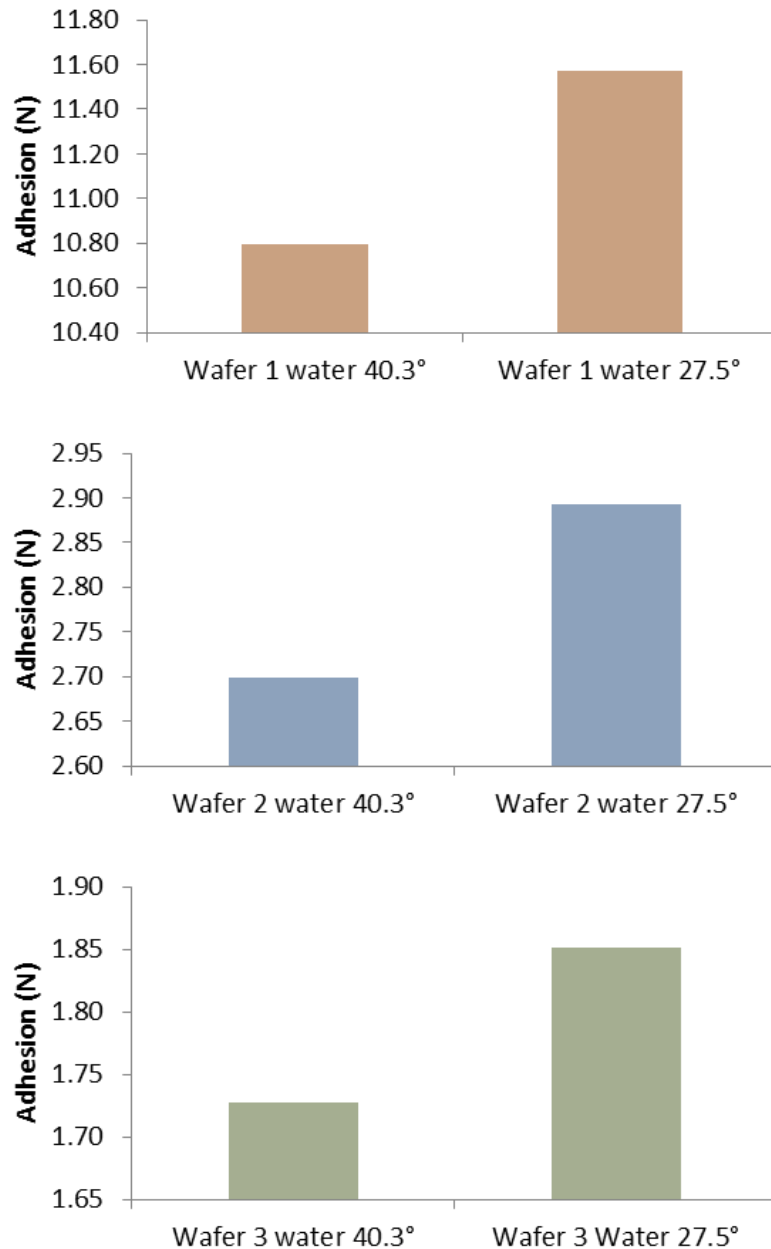


Figure 5.22 - Theoretical effect of wettability on adhesion for hydrophilic samples - against a glass slide and water

5.3.4.2 Effect of Surface Geometry on PDMS Samples

Figure 5.23 shows the effect of the surface geometry on adhesion when the surfaces are brought in contact with glass coated with water.

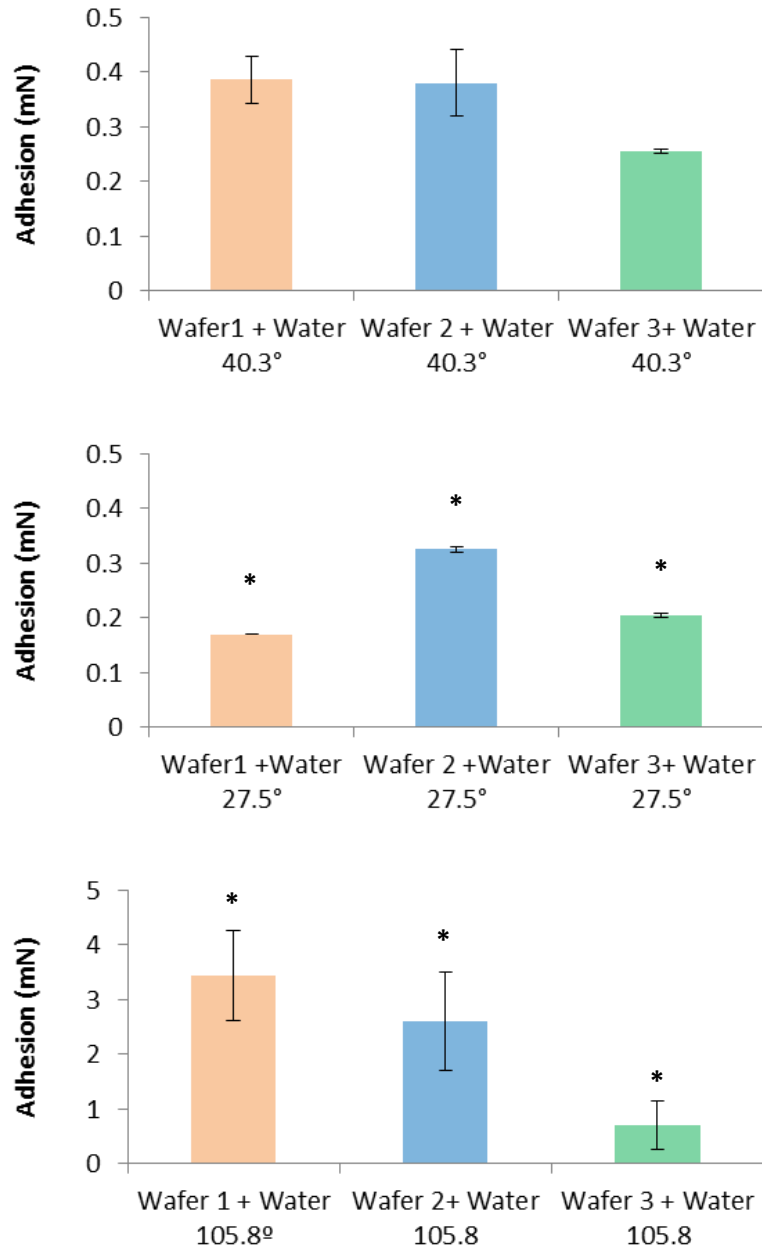


Figure 5.23 - The effect of surface geometry on adhesion – against a glass slide and water * signifies statistical significance within the difference in data where $p \leq \alpha$

It can be seen that for the higher contact angle the results are as expected - as the pillar spacing increases, the number of pillars on the surface decreases and the adhesion falls as a result. The expected results are shown in Figure 5.24. However, the lower contact angle shows a different trend, in that wafer 1, the sample with the smallest pillar spacing, shows the lowest adhesion force. This is explored in more detail in Chapter 7, where it is suggested that due to the lower contact angle the surface is totally flooding. In this situation the number of pillars on the surface would be irrelevant as no liquid bridges are able to form.

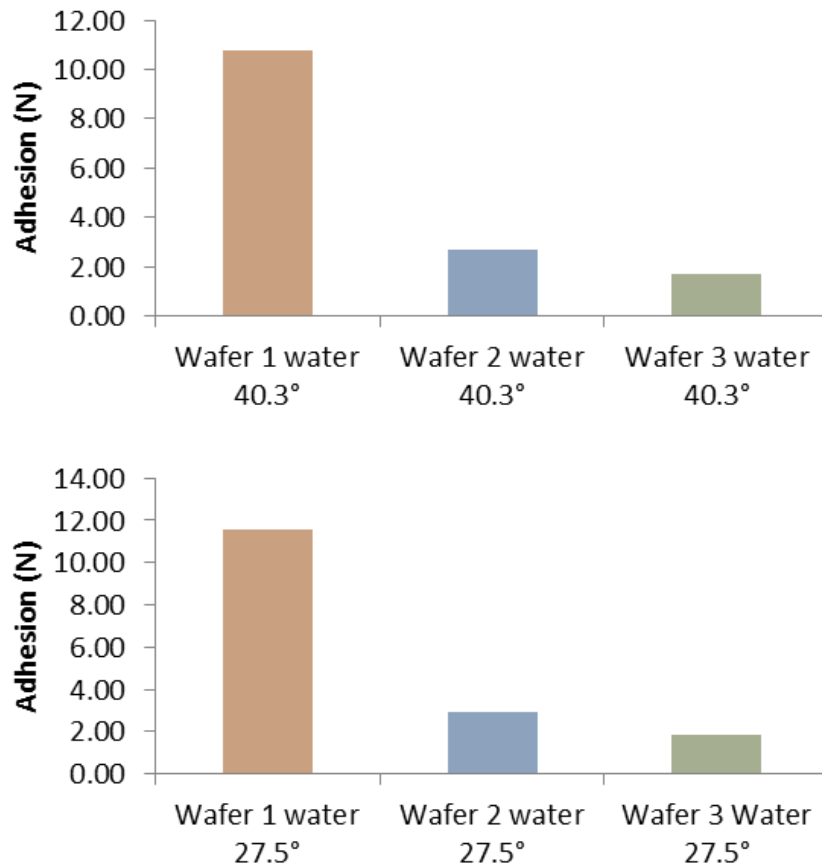


Figure 5.24 - Theoretical effect of surface geometry on adhesion for hydrophilic samples - against a glass slide and water

5.3.5 Adhesion against Glycerol - Water Mix

This section looks at the effect of varying parameters on adhesion to a glass slide coated in a glycerol-water mix, for samples which have been plasma treated.

5.3.5.1 Effect of Wettability on PDMS Samples

Figure 5.25 shows the effect of wettability on adhesion when in contact with a glass slide coated in a water-glycerol mix for each of the wafers independently. For these samples it can be seen that for wafers 1 and 2, as the contact angle decreases the adhesion increases, as expected from the mathematical model (Figure 5.26). However, this is not shown as expected for wafer 3, where the adhesion decreases.

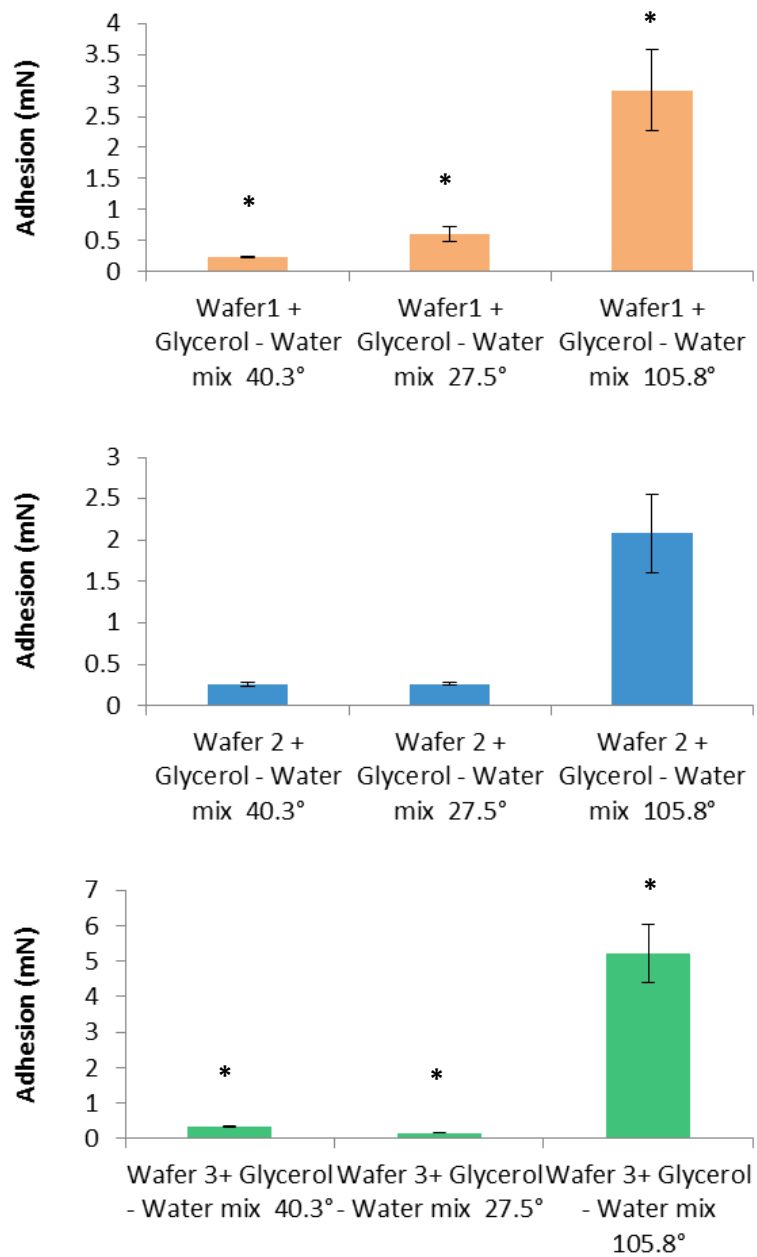


Figure 5.25 - The effect of wettability on adhesion - against a glass slide and glycerol * signifies statistical significance within the difference in data where $p \leq \alpha$

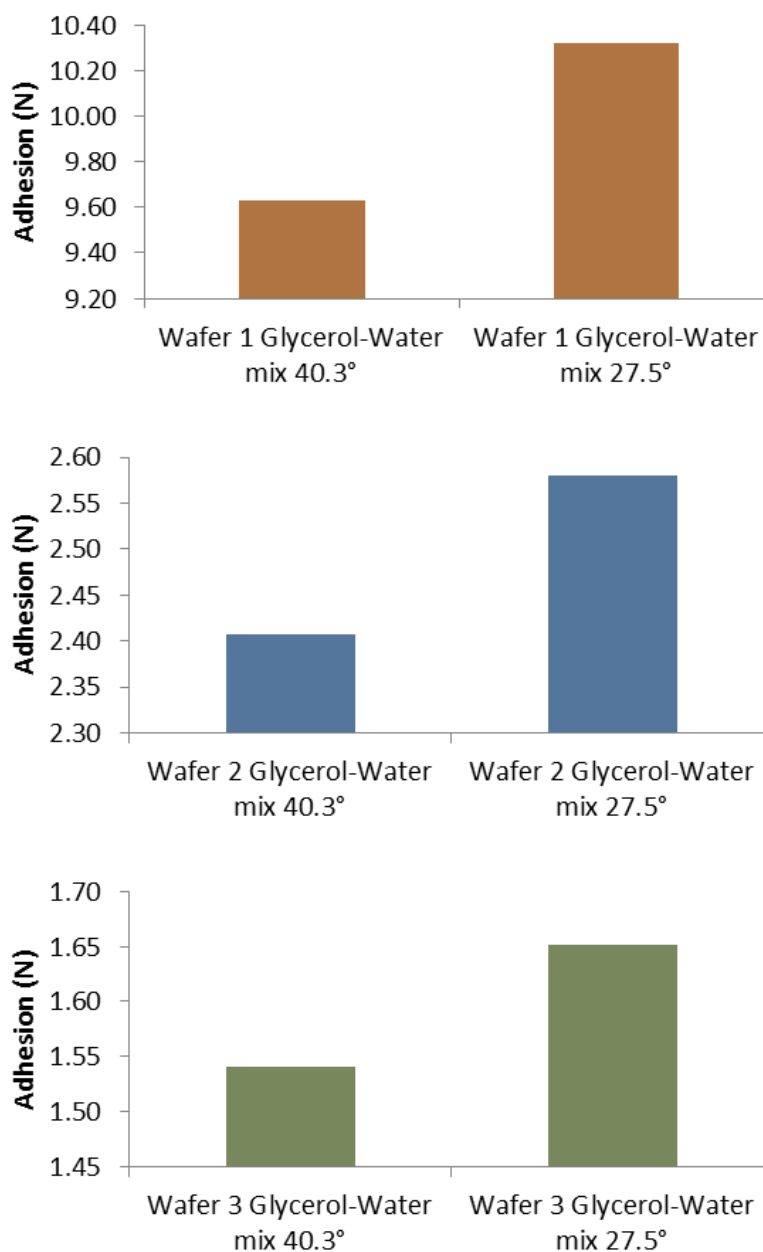


Figure 5.26 - Theoretical effect of wettability on adhesion for hydrophilic - against a glass slide and glycerol

5.3.5.2 Effect of Surface Geometry on PDMS Samples

Figure 5.27 shows the effect of the surface geometry on adhesion when the surfaces are brought in contact with glass coated in glycerol. It can be seen that for the higher contact angle the results are not as expected, in that wafer 1, the sample with the smallest pillar spacing, showed the lowest adhesion force. The

expected results, given by the model, are shown in Figure 5.28. However, the lower contact angle shows a different trend, as expected, as the pillar spacing increases, the number of pillars on the surface decreases and the adhesion falls as a result.

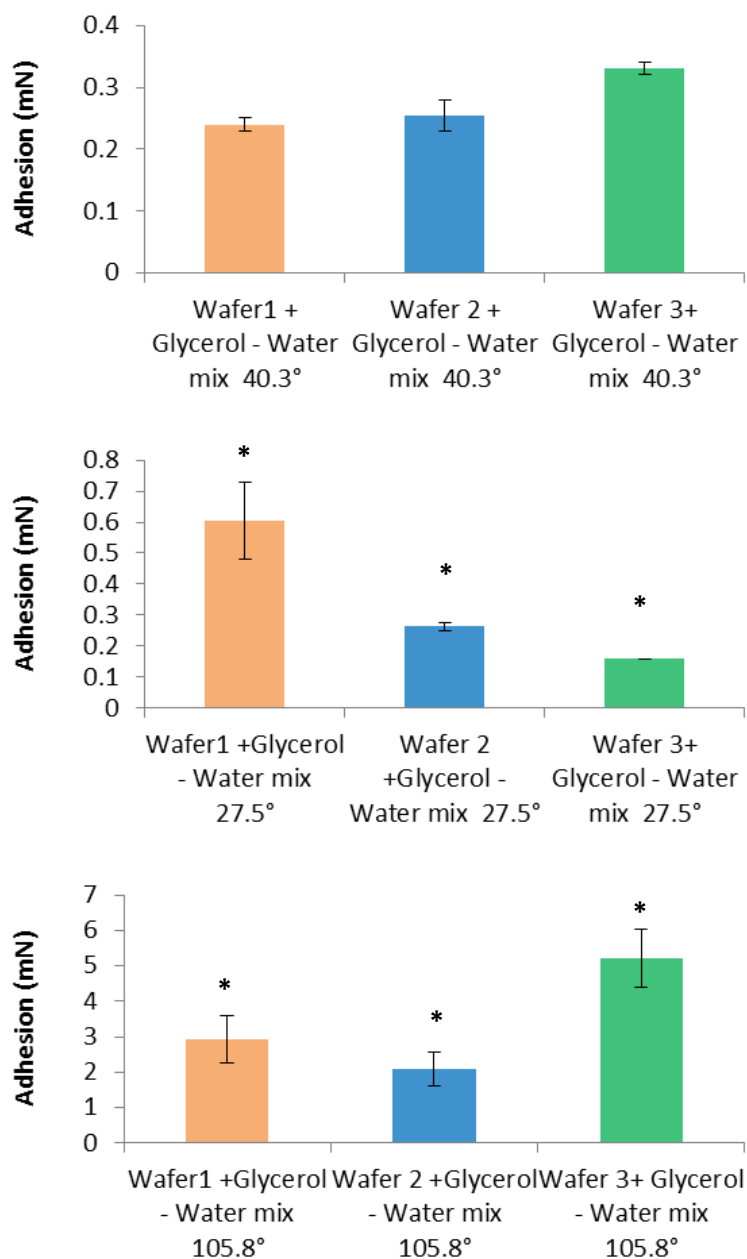


Figure 5.27 - The effect of surface geometry on adhesion - against a glass slide and glycerol * signifies statistical significance within the difference

in data where $p \leq \alpha$

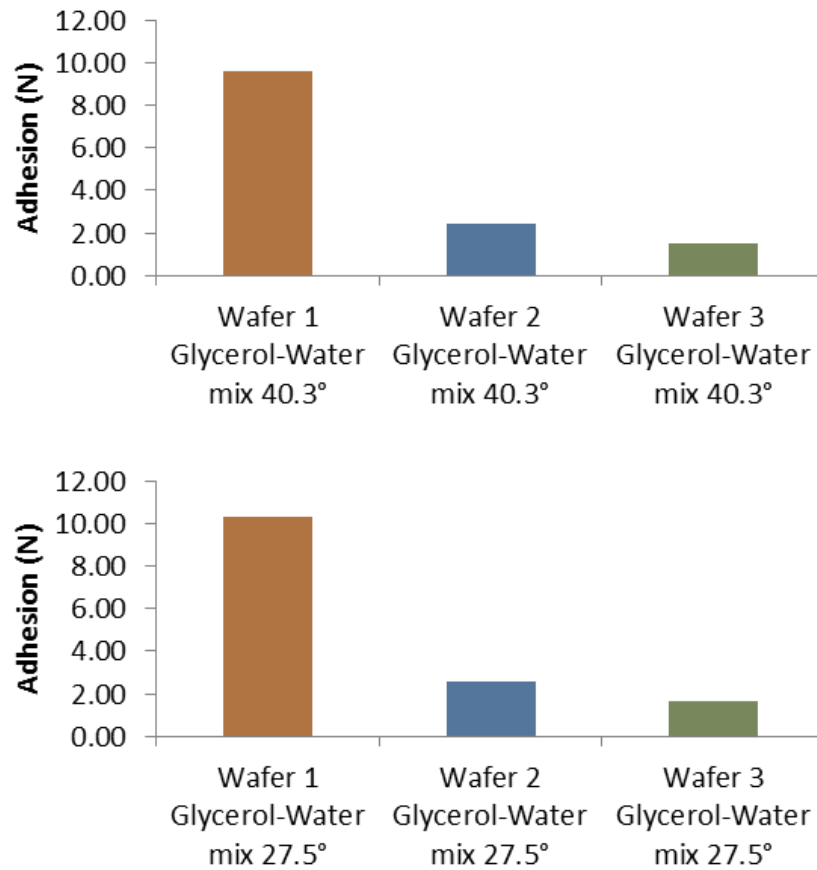


Figure 5.28 - Theoretical effect of surface geometry on adhesion for hydrophilic samples - against a glass slide and glycerol

5.4 Adhesion against Tissue

In the previous section the adhesion of the pillared surfaces against glass has been measured; in this section the counter surface is tissue which brings a whole new complexity to the interface. The system is now a pillared (relatively soft) substrate versus a wet but ultra-soft tissue counter face. This section summarises how the adhesion is affected by all the previous factors (pillar spacing/geometry and surface wettability) against the new counter face.

This section looks at the effect of varying parameters on adhesion to an *ex-vivo* peritoneal tissue, for the samples which have been plasma treated.

5.4.1.1 Effect of Wettability on PDMS Samples

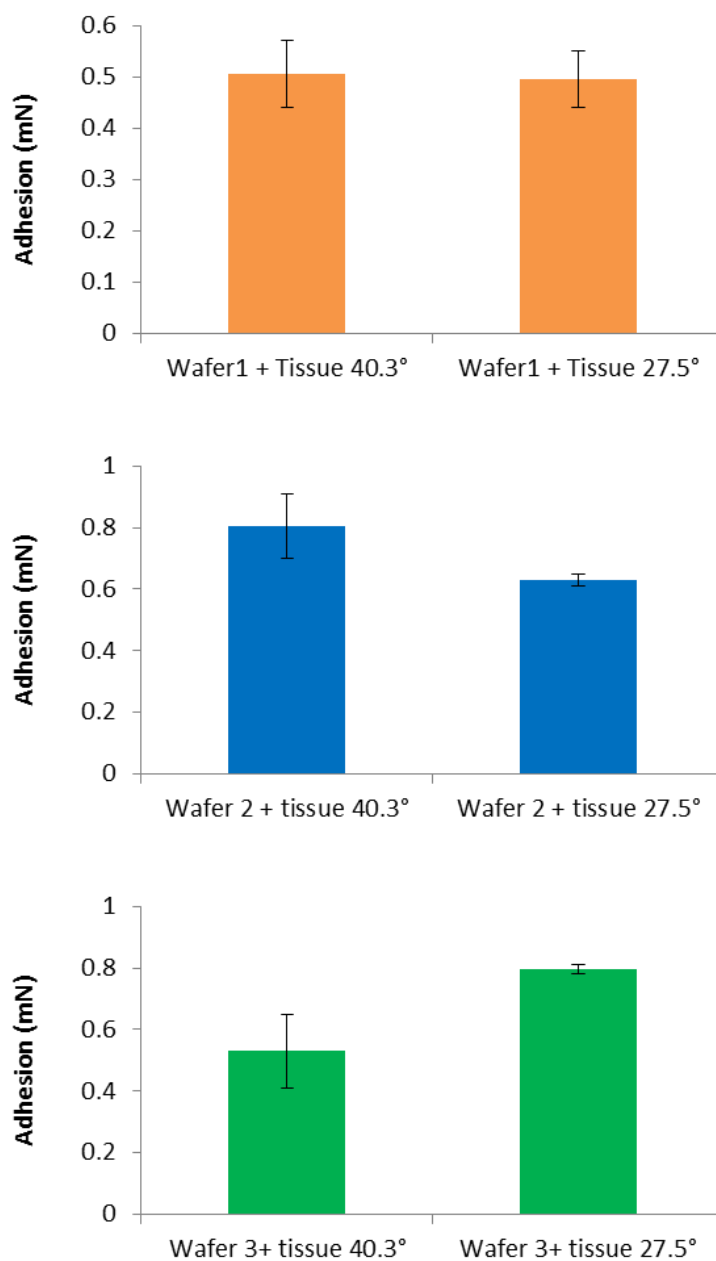


Figure 5.29 - The effect of wettability on adhesion - against tissue

Figure 5.29, shows the effect of wettability on adhesion when the surfaces are brought into contact with tissue. It can be seen that for wafers 1 and 2, as the contact angle is decreased the adhesion increases as expected from the model (Figure 5.30), however for wafer 3 when the contact angle is decreased the adhesion also decreases.

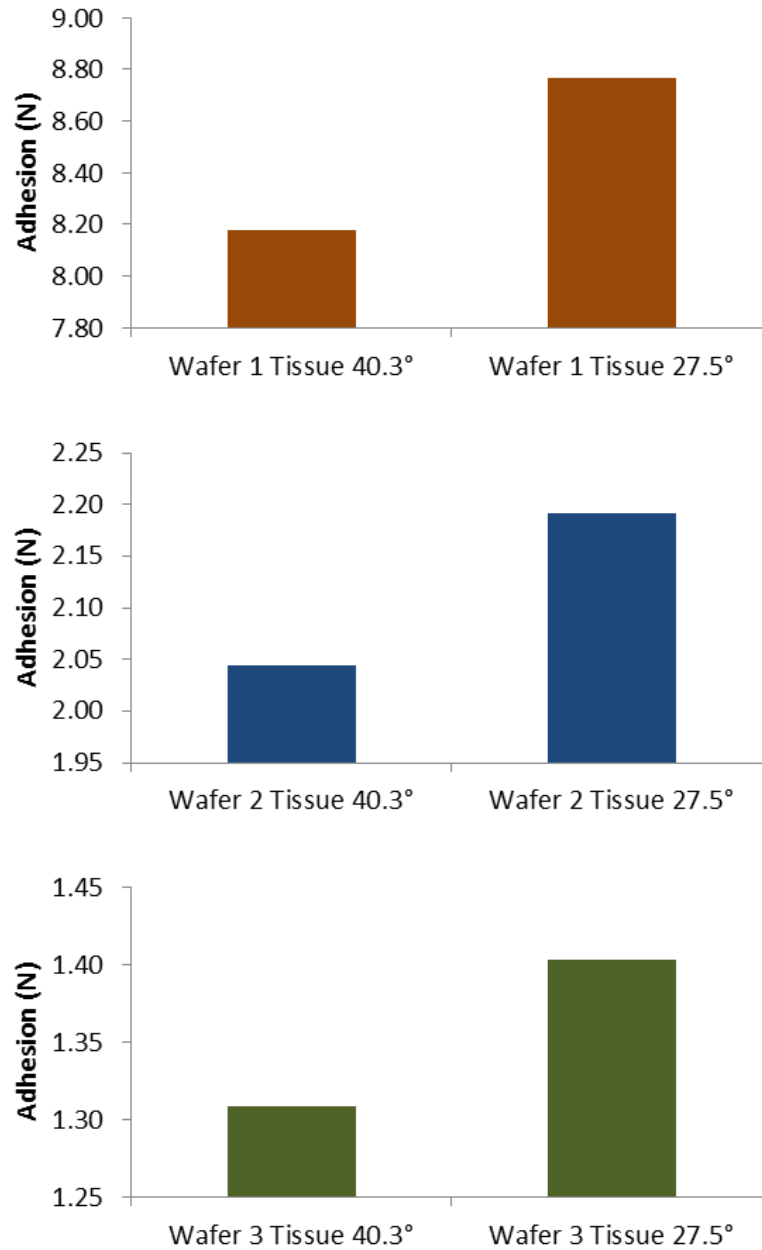


Figure 5.30 - Theoretical effect of wettability on adhesion for hydrophilic samples - against tissue, where the value for surface tension of tissue has been taken as the average of blood [152], urine [153] and bovine serum [17] ($5.53 \times 10^{-2} \text{ N/m}$).

5.4.1.2 Effect of Surface Geometry on PDMS Samples

Figure 5.31, shows the effect of surface geometry when in contact with tissue. It can be seen that for the higher contact angle that there is a peak for wafer 2; this

is not what would be expected when considering the capillary versus Stefan adhesion forces. Similarly, the lower contact angle samples show the same trend as previous plots, indicating that as the pillar spacing increases, and there are less pillars on the surface, the adhesion increases. The expected theoretical results are shown in (Figure 5.32).

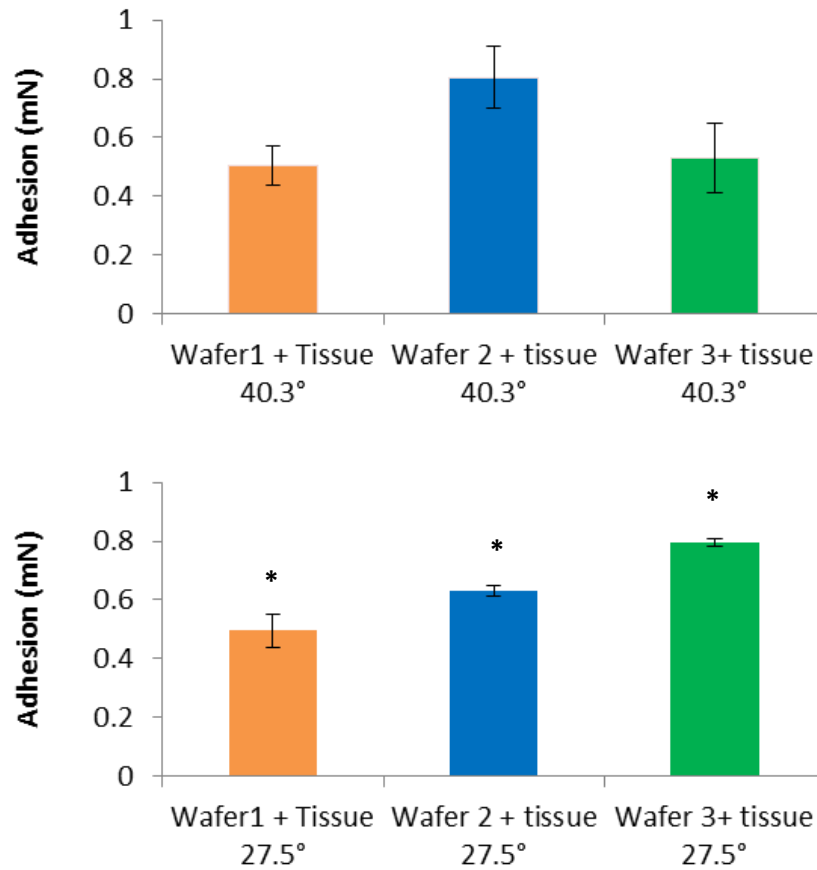


Figure 5.31 - The effect of surface geometry on adhesion - against tissue *
signifies statistical significance within the difference in data where $p \leq \alpha$.

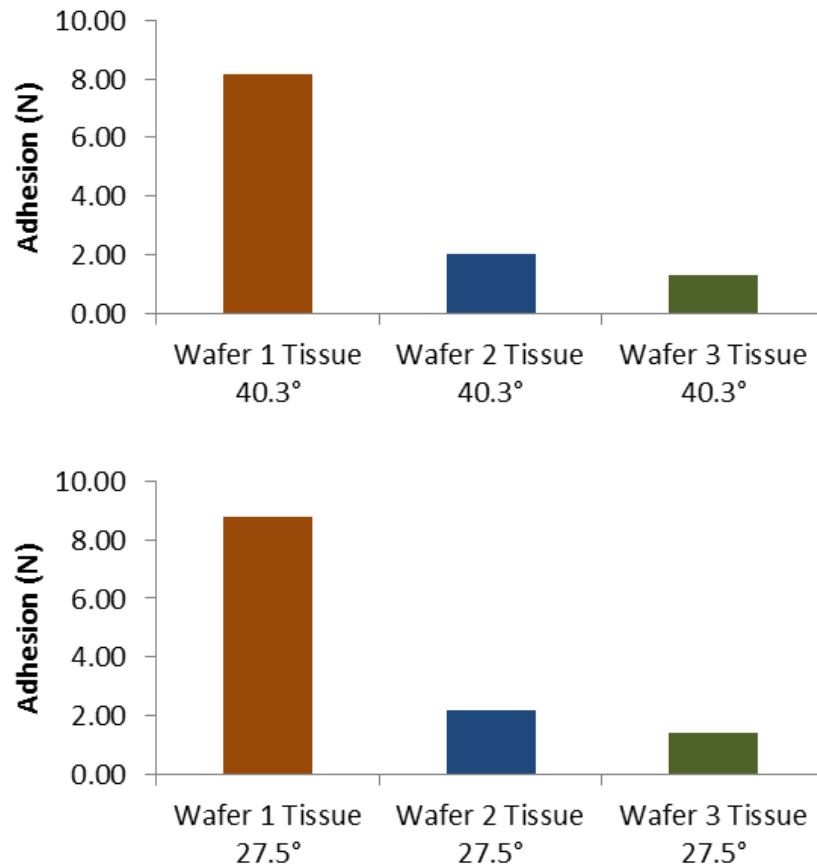


Figure 5.32 - Theoretical effect of surface geometry on adhesion for hydrophilic samples - against tissue

5.4.2 Effect of Fluid Properties on Adhesion

Figure 5.33 shows the effect of fluid viscosity on adhesion, the fluid viscosities are given in Table 5.1, where water was the lowest, and the glycerol-water mix the highest. Therefore, it would be expected that the adhesion would be greater for the glycerol-water mix tests and lowest for water. However, this data shows that for all tests, except wafer 1 with the lowest contact angle, all samples performed better against tissue. This could be due to as shown by the mathematical model used in section 6.5.1, the viscous force, is only dominant over a small separation distance. Therefore, when working with a compliant surface such as tissue, the separation remains at a minimum for longer, meaning

the adhesion mechanisms remains in the viscous dominant regime for a longer time frame and aiding the adhesion. However it is not possible to describe this effect with the discussed mathematical model as there is no impact if the material compliance discussed. The effects of the samples in contact with a water only film and a water-glycerol film are interchangeable. This again is due to the fact that the viscous term is only dominant over a very small separation distance, therefore when working with a rigid surface, such as glass, the effects of viscosity are negligible.

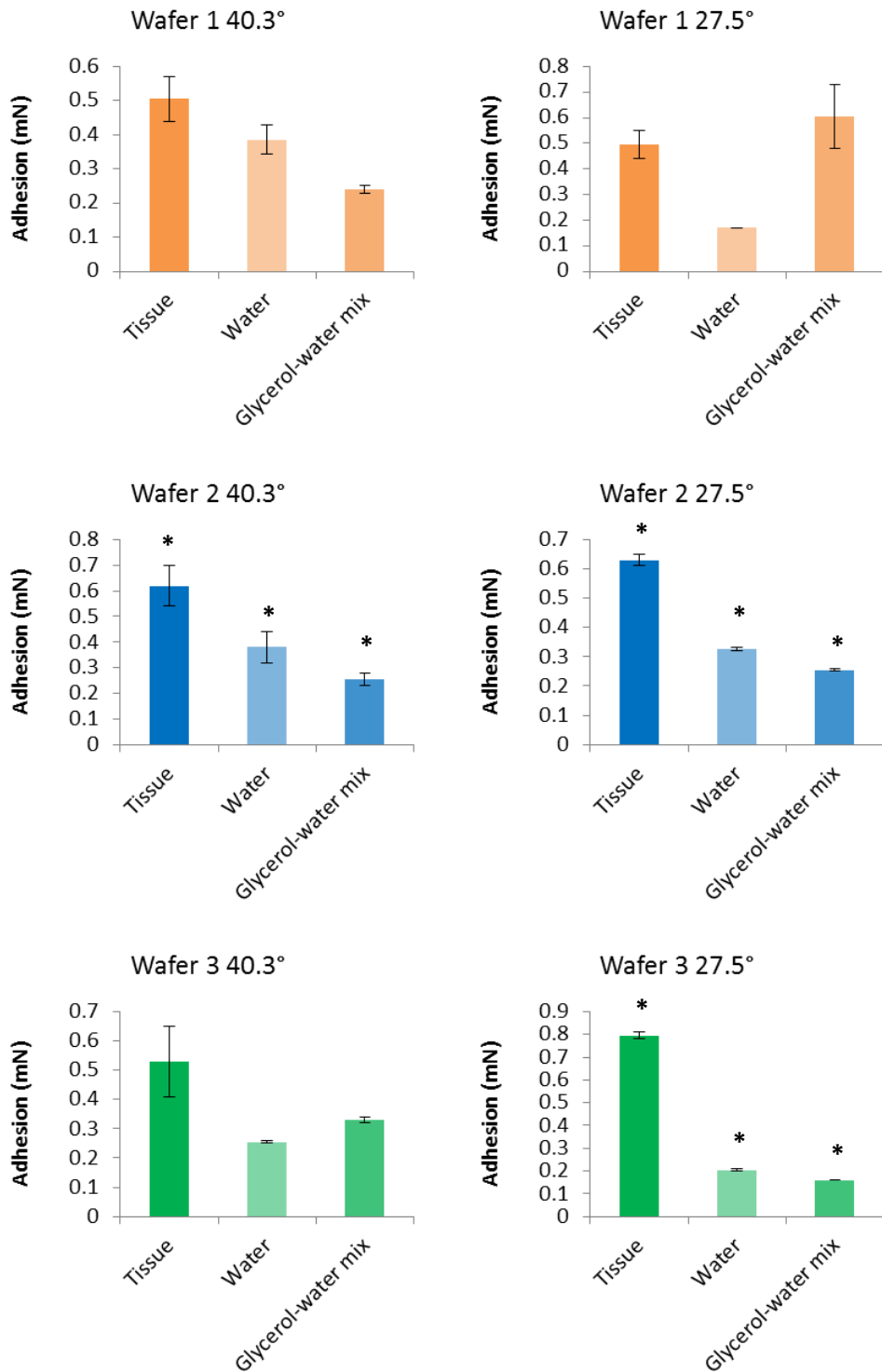


Figure 5.33 - The effect of fluid viscosity on adhesion force for hydrophilic samples * signifies statistical significance within the difference in data where $p \leq \alpha$

However, as discussed in section 5.3.3, as the viscosity term is negligible in this system, it is more accurate to describe the effects in terms of varying surface

tension as opposed to fluid viscosity, due to the dominance of the capillary term.

Figure 5.34 shows the theoretical effects for the change in fluid properties.

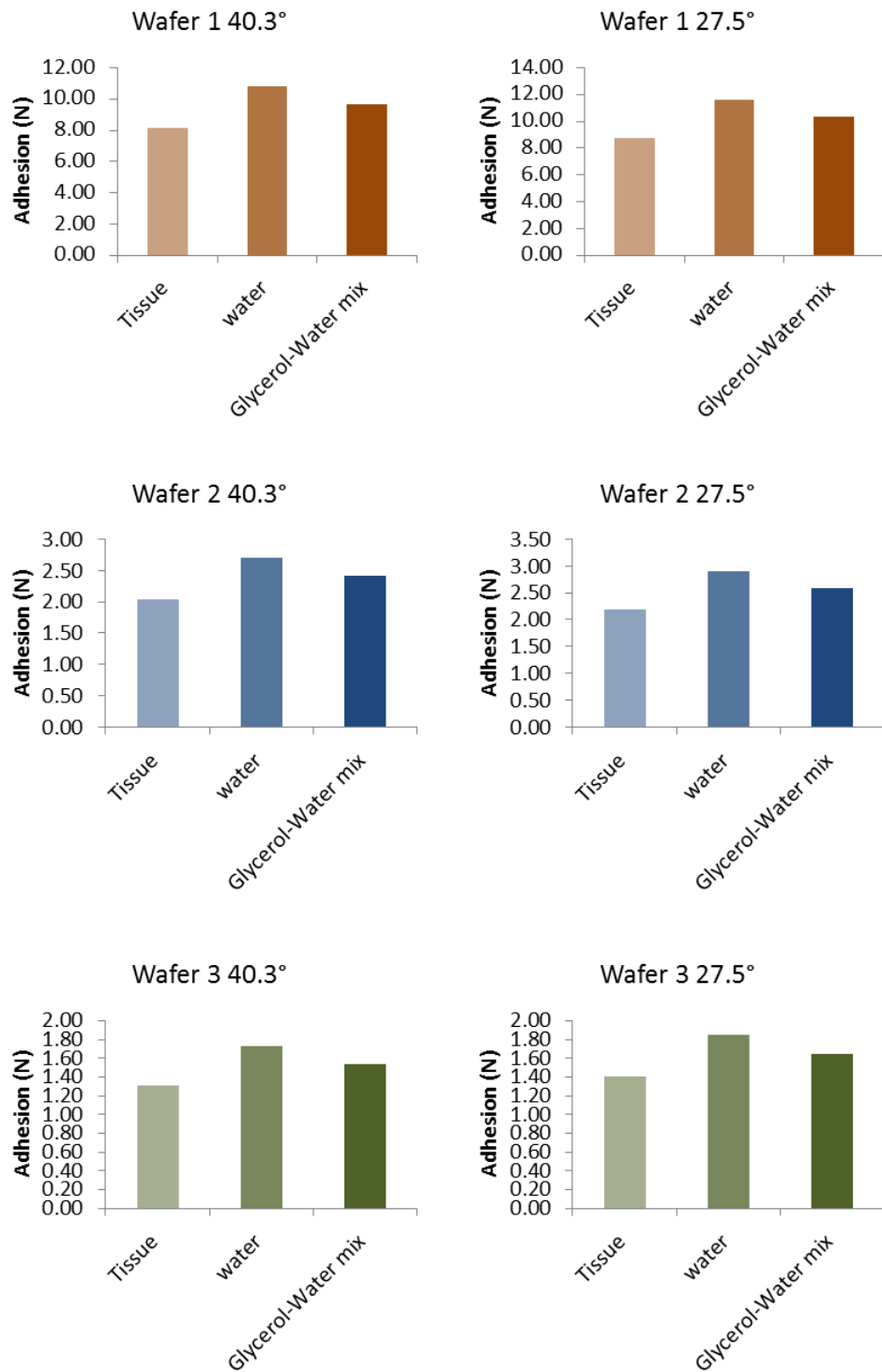


Figure 5.34 - Theoretical effect of fluid properties on adhesion force

5.4.2.1 Initial Traction Testing

The ability to have a miniature robotic device perform a surgical procedure opposed to a standard colonoscopy method would enable an on-board camera and biopsy tool to identify any suspicious tissues and perform the biopsy in one procedure. This will not only be beneficial to the patient but will also reduce costs by minimising the amount of time a patient has to spend with a specialist. Such a device would be required to be amphibious to enable it to swim through the full colon, but also to allow docking. Providing adhesion and traction in a flooded system was briefly investigated, using a bespoke traction rig¹⁹, built using a SMAC actuator, force sensors and programmed in LabVIEW. This test rig allowed the micro-structured surfaces to be mounted on an indenter and placed on firstly a wet glass slide, and then rat peritoneum, followed by porcine colon. The actuator ramps up the force of the test bed recording the displacement of the bed. The LabVIEW programme records both the force and displacement allowing a graph to be plotted and identify the force at which slip occurs. A diagram of the test set-up can be seen in Figure 5.35.

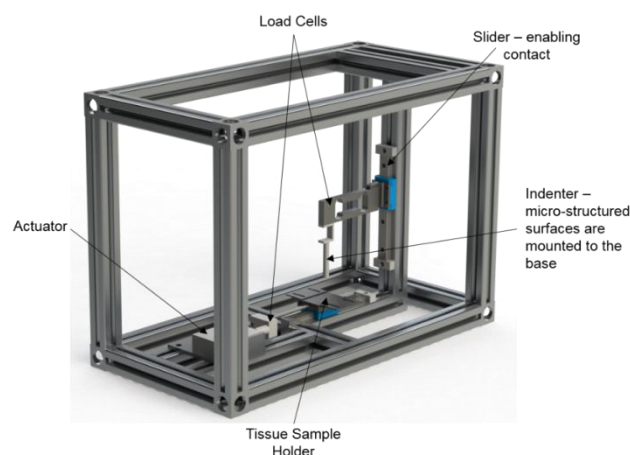


Figure 5.35 - Rendered CAD drawing of the traction rig.

¹⁹ Traction rig developed alongside Mr William Mayfield, University of Leeds, UK

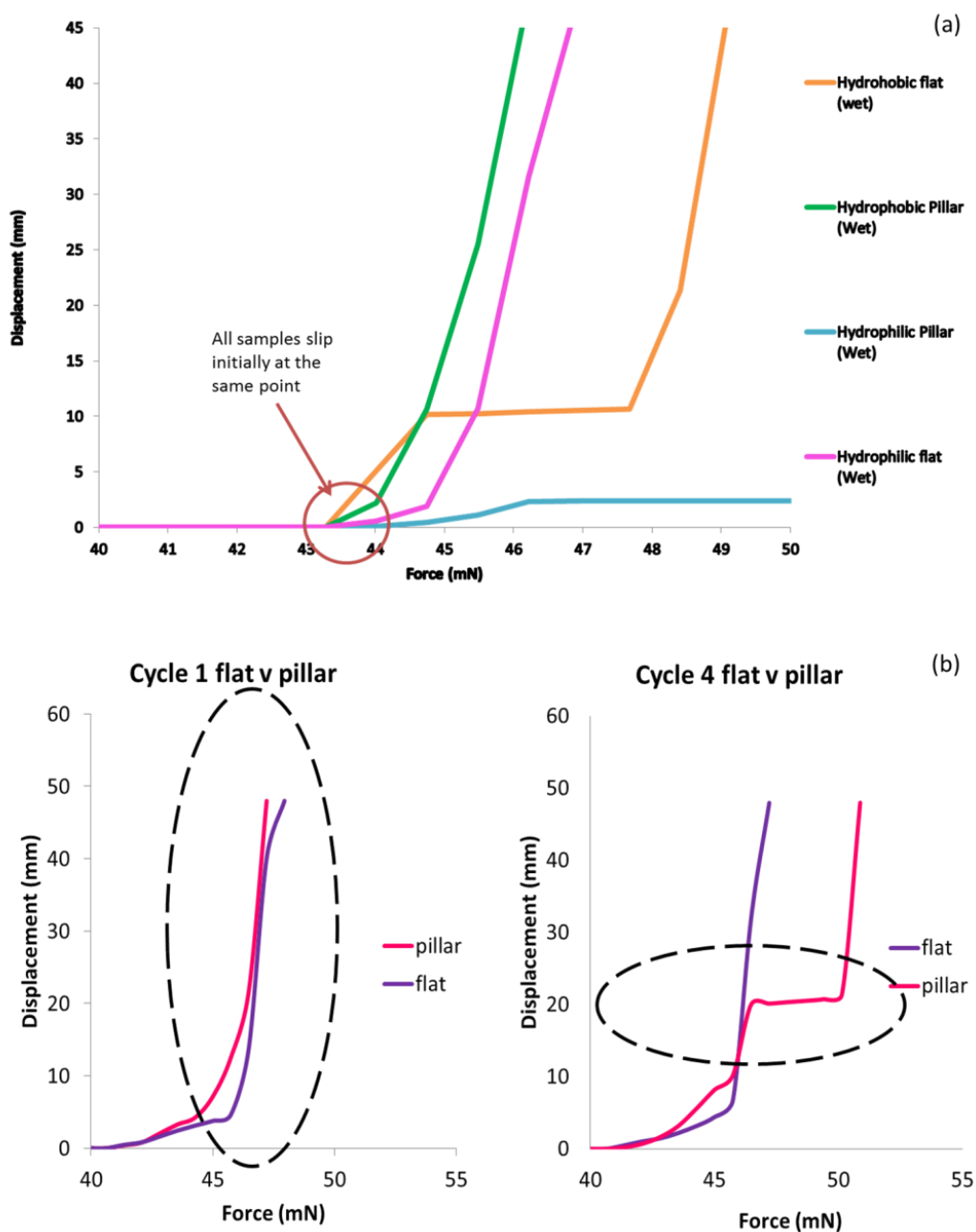


Figure 5.36 - Initial data for work into the viability of micro-structured surfaces in the colon to produce traction on a miniature robotic device.

Initial results are shown in Figure 5.36 (a) & (b), where (a) shows the traction capability of the micro-structured pillars against wet glass. It is shown that all samples slip at an initial point, however, the hydrophilic pillars gain better traction and prevent further slip as the force is ramped. The hydrophobic flat sample does

regain traction. But it then slips again and continues to do so along with the hydrophobic pillars and hydrophilic flat samples until a maximum is reached. (b) Shows that as the tissue dries and the fluid viscosity increases (cycle 4) the pillars can gain traction, where during the initial cycle there is no distinction between a flat surface and a pillar surface.

5.5 Summary

This chapter has incorporated aspects of sample preparation and results from a parametric study of the adhesion measurements. Initially, this has involved adhesion tests against glass which has been coated in either water or a glycerol-water mix, for varying surface wettability's and geometries. Following this, the adhesion results of the pillared surfaces against *ex-vivo* peritoneal tissue were presented. The ultra-soft nature of the tissue has added a new complexity to the interface. The key findings of this chapter are highlighted below:

- The original Autotex[®] samples provide greater adhesive forces than equivalent PDMS surfaces in the same geometry.
- The effect of the fluid surface tension dominates over the effect of the fluid viscosity.
- Against glass which is coated in either fluid, hydrophobic surfaces provide greater adhesion than equivalent hydrophilic surfaces. It is suggested that this is due to the surfaces with the lowest contact angle acting super hydrophilic and flooding. This would result in the formation of no liquid bridges and have a detrimental effect on the adhesion force.
- The theoretical model predicts adhesive forces up to 1000 times greater than that of the experimental adhesive forces.

- Adhesion tests against tissue have shown there is no dependence on surface geometry or wettability.
- It is apparent that in most instances tissue provides greater adhesion, than both glass systems.

These findings are discussed further in Chapter 7.

Chapter 6. Results - Mathematical Wet Adhesion Model

6.1 Introduction

Wet adhesion mechanisms are very well illustrated via everyday occurrences such as a wet glass sticking to a glass table top, to the way a tree frog adheres to naturally occurring wet surfaces. However, what is in its infancy is the understanding of the interaction that occurs at the surface formed by a patterned polymer substrate and an extremely flexible, soft, viscoelastic material such as biological tissue. Table 6.1 compares the elastic modulus values of a range of materials for comparison. Biological tissue has many small scale imperfections and variations across its surface, for example the Young's modulus of the peritoneum can vary from 1-100 kPa [154, 155]; this will affect the adhesion mechanism in play, in particular at the tissue-device interface during laparoscopic surgery. As well as variations in the mechanical properties, the viscosity of the fluid on the surface of the peritoneum is also variable across the tissue surface. This fluid also varies during surgical procedures when exposed to CO₂ during insufflation of the abdomen as investigated by Ott *et al.* [148]. Understanding the mechanisms involved in producing reliable, reversible adhesion at the surface such as a tissue interface is a key aspect of the work reported in this thesis.

Table 6.1 - Comparison of elastic modulus of common materials [148, 156, 157]

Material	Elastic Modulus (GPa)
Peritoneum	$1 \times 10^{-6} - 1 \times 10^{-4}$
Rubber	0.01-0.1
Skin	0.03
Muscle	0.48
Tendon	0.56
Oak Wood	11
Aluminium	69
Steel	200
Diamond	1220

This chapter explores the wet adhesion mechanism, which is comprised of both capillary forces and Stefan adhesion. A model is provided to determine the capillary forces present at the tip of a single pillar and the Stefan adhesion. These are summed to provide the total adhesion force on the tip of such a pillar, allowing the total surface adhesion to be calculated by multiplying this by the number of pillars present on the surface. The total number of pillars on the surface is determined using an empirical relationship between the pillar radius, the pillar separation and the total sample size. A similar adhesion model has been performed by Cheung *et al.* [95], where mushroom shaped micro-fibres have been modelled against an oil coated surface. In this work they calculate the pull-

off force of the total array by calculating the combined contributions of each individual fibre in contact with the surface.

Initially it had been thought, that due to the low modulus of the PDMS surface, the adhesion may have been reduced when in contact with a rigid glass surface despite the fluid being present. This would be due to the pillars deforming as a result of the preload force, leading to an effectively flat surface if the pillars are deformed by more than their height. However, this would not be the case when the surfaces are in contact with tissue as tissue is more compliant than the PDMS and will therefore deform around the pillars. By investigating Hooks law (3.1); where the force is equal to the pre-load applied, 10 mN, and the spring constant is the elastic modulus of the PMDS, 3 MPa; it was found that the deformation which would occur on a pillar tip is 3.3×10^{-9} m. This equates to a new pillar height 99.89% of that of the original. This however does not account for any deformation in the supporting base, but as the deformation is so small any effects of the base would remain negligible.

6.2 Capillarity

Capillarity occurs between two incompatible fluids, usually a liquid and a gas, where the separating interface deforms in order to minimize their surface energy [60]. As a liquid flows, it can adopt a stable shape, which is smooth on an atomic scale and barely deformable due to the cohesion attraction between molecules.

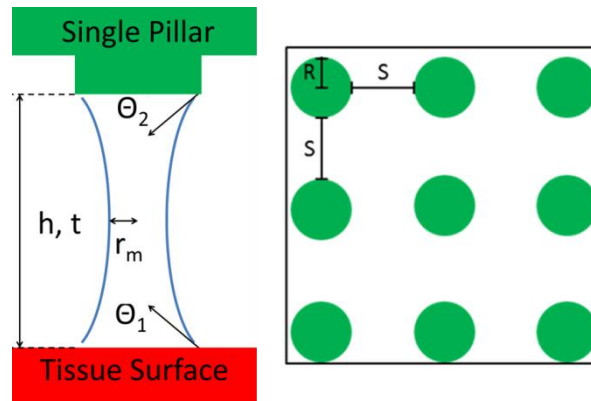


Figure 6.1 - Variables involved in wet adhesion mathematical model.

Where: θ_1 = contact angle at the tissue surface, θ_2 = the contact angle at the pillar, r_m = radius of the meniscus and h = separation of the two surfaces over the given time, t . R = pillar radius and s = spacing between pillars.

Capillarity is dependent on the pressure difference across a fluid-air interface, known as the Laplace pressure see (6.1), which in turn is dependent on the surface tension, γ , and the meniscus radius, r_m (6.2). The latter is dependent on the contact angle, θ , (6.3) of the surfaces in contact [158-160]. Assuming that this contact angle is constant at the contact line formed at a solid boundary, the Laplace pressure should also remain constant. However the surface area involved will have an effect on the capillarity, as shown below.

$$\Delta P = \gamma \left(\frac{1}{R_1} + \frac{1}{R_2} \right) \quad (6.1)$$

Where: P = Pressure, γ = Surface tension, R_1 and R_2 = The radii of curvature

The surface area of an ideal liquid bridge at a separation, h , and radius r_m , is given as:

$$\text{Surface Area} = 2\pi r_m h \quad (6.2)$$

Where: r_m = Radius of the meniscus, h = separation of the two surfaces

Assuming that the surface is hydrophilic, θ_1 and θ_2 will be small. Therefore the separation of the two surfaces, h , can be given as:

$$h = R_1 \cos\theta_1 + R_2 \cos\theta_2 \quad (6.3)$$

Where: θ_1 and θ_2 = contact angle on each surface

Therefore the capillary force, F_{cap} , is given by, the product of the surface area and pressure:

$$F_{\text{cap}} = 2\pi r_m \gamma (\cos\theta_1 + \cos\theta_2) \quad (6.4)$$

However, this model describes the effect of two rigid surfaces; therefore we will face issues, such as elastic modulus variation across the surface.

Persson *et al.* [13] have shown that a soft elastic solid can be pulled closer into contact, with another surface, at interfaces where capillary forces are acting; this requires liquid bridges. For elastic solids there will be an immediate reaction in the opposite direction, to that of the approach surfaces. Tissue is viscoelastic; therefore an elastic response is delayed and so can be pulled into contact, making it more likely to form capillary bridges as the structured polymer is wetted. Menisci are formed, from the fluid on the surface, around the pillars, holding them in place by capillary adhesive forces through lateral propagation of the contact and the stable capillary action across the interface. The mechanism occurs through three stages, snap on, contact propagation and a variable point (Figure 6.2).

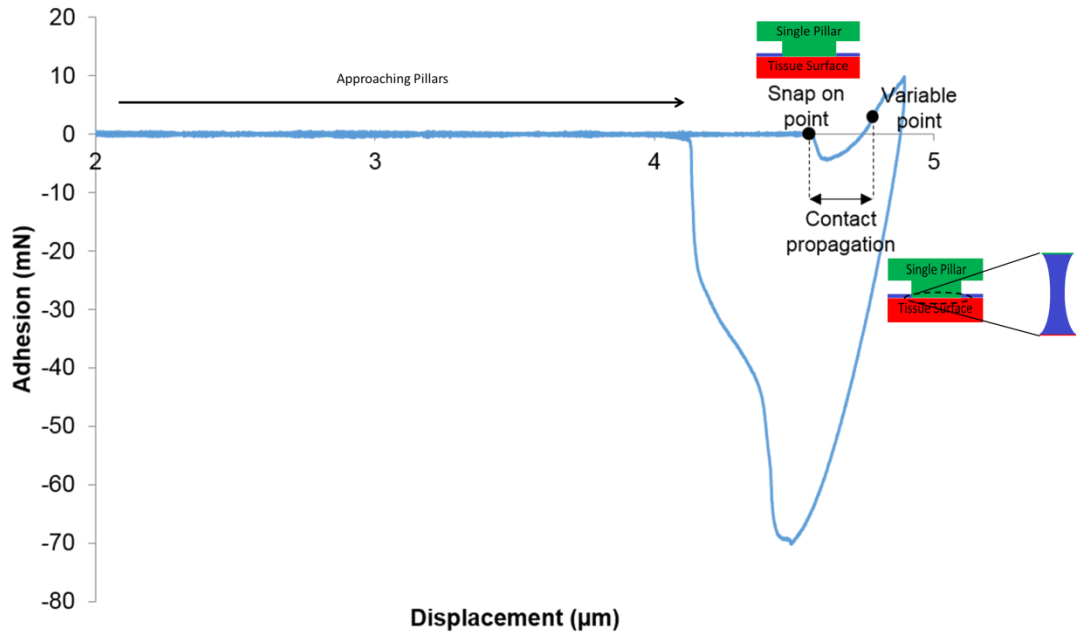


Figure 6.2 - Example of a force-displacement curve highlighting the contact mechanism - snap on point, contact propagation and the variable point.

The snap on mechanism is the point at which the attractive forces pull the surfaces together; this is mediated by the capillary bridges. The contact propagation occurs through three interactions, firstly capillary bridges, then capillary rise followed by cohesive forces keeping the surfaces in contact. At the variable point, no further contact is made; the pillars are pushed into the surface where the contact in the previous two steps has been formed.

6.3 Tissue Characterisation

It is vital when considering an adhesion mechanism to evaluate the materials involved, as the chemistry, mechanical properties and surface roughness will all affect adhesion. The polymers employed to provide a suitable contact surface have been evaluated in the previous chapter: Chapter 4. Here, the focus is the characterisation of the tissue itself, centred on the topographical characteristics

and mechanical properties of the peritoneum. This facilitates a clearer understanding of the mechanisms involved at the tissue device interface.

The peritoneum is a thin layer of tissue which provides protection to abdominal organs, the diaphragm and the abdominal wall. Its basic structure is composed of an outer layer of mesothelial cells (1-2 μm thick) [161] covering a sheet of connective tissue, consisting mainly of collagen fibres, to provide support, elastin fibres, to provide elasticity, as well as blood vessels, lymphatic channels and immune system cells [17]. The mesothelial layer contains a number of folds in the cell membrane, microvilli [162, 163], which are approximately 1.5 - 2 μm long and 90-110 nm in diameter [163], and able to act dynamically, expanding and contracting depending on their local conditions [15, 164]. The cell membrane is formed of a phospholipid bilayer, see Figure 6.3, 2-4 nm thick [16, 165], surrounding the cell cytoplasm. The cytoplasm is viscoelastic, and is sensitive to external stimuli [166]. The mesothelial layer secretes a fluid containing phospholipids similar to those which make up the phospholipid bilayer. They contain a hydrophilic head group, and a hydrophobic tail, allowing them to be easily absorbed onto the surface of the membrane, aiding lubrication due to cohesion between the molecules. This cohesion forms multiple layers on the surface and increases the lubrication due to the low shear planes.

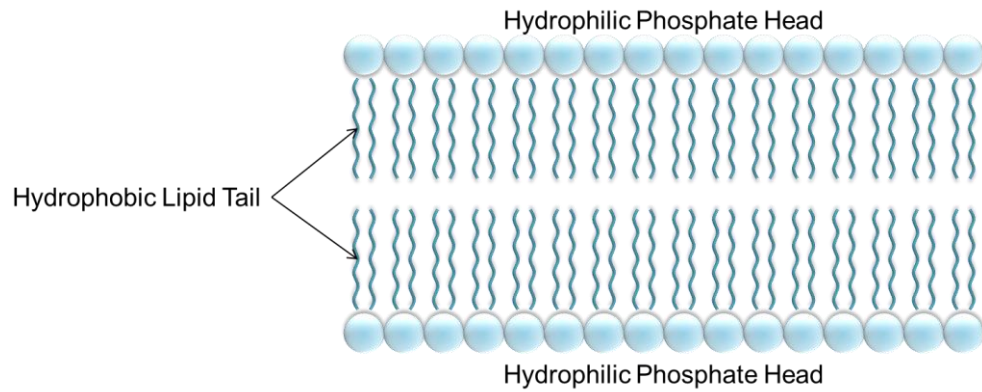


Figure 6.3 - Schematic of a phospholipid bilayer, consisting of a hydrophilic head group and hydrophobic tail, allowing phospholipids to be easily absorbed onto the outer surface of the cell membrane.

It is not sufficient to rely on mechanical property measurements of cells alone as these exhibit large variations with very small changes in samples [17]. It is also difficult to image the peritoneum accurately due to rapid drying of the surface causing changes in the surface structure. This is an important consideration, as in the present work it is necessary to ensure the surface remains hydrated to prevent this occurring. It was found by Taylor *et al* [17] that the peritoneum is a relatively flat surface at the micron scale, although height variations in the range of 50-100 μm exist, which increases with an increasing scan area. As it is required to enable advantageous capillary adhesion to occur, there must be close contact over the contact area, particularly at the micro-scale. This can be achieved through the use of a flexible polymer substrate. Taylor *et al.* [17] showed also that the lipid rich fluid layer covering the mesothelial cells is a heterogeneous arrangement, which will affect the hydrophobicity in certain areas; the contact angle can vary across the peritoneal surface from 38° to 61° . The effect of varying wettability over a single surface occurs widely in nature to optimise adhesion via the formation of liquid bridges at key points where the hydrophilic phases are located. This is a promising feature in relation to the present work since, despite

the variation in contact angle; it is still a viable option to rely on liquid bridge formation and capillary adhesion.

In vivo, the peritoneum is covered with a fluid layer and therefore the surface appears to be fully wetted, which appears as a thin fluid film covering the surface [167]. The fluid present on the peritoneal surface provides lubrication, to enable mobile abdominal organs to slide over one another and the abdominal wall. This fluid is rich in phosphates which act as surfactants allowing them to be readily adsorbed and become a continuation of the surface. This mechanism lowers the surface tension as the hydrophobic tail groups face out into the abdominal cavity. With this in mind, it initially appears that this will be unfavourable to the formation of liquid bridges. However, the excess free phospholipids direct their tail groups away from the water and thereby form another bilayer by joining the adsorbed molecules on the membrane. This again forms multiple layers on the surface enhancing the lubrication and covering the initially hydrophobic layer. It has been reported that the peritoneal fluid has a contact angle of 43° by Hills *et al.* [150] and 38° by Gomez-Suarez *et al.* [151]. Proving that the fluid is not as hydrophobic as first thought, therefore, assuming the capillary bridge formed is convex until the contact angle rises to allow the combination of contact angles to add up to 180° [82], it can be expected that any contact angle less than 115° will still result in a concave meniscus, and consequently the peritoneum would need to be very hydrophilic to prevent the formation of attractive liquid bridges [17].

De Souza *et al.* [81] show that an array of multiple capillary bridges imparts the greatest adhesive forces, not in strongly hydrophilic conditions but in those with a contact angle of around 70° .

6.4 Proposed Mechanism

Inspired by the tree frog's ability to adhere to naturally occurring wet surfaces repeatedly and reliably, micro-structured surfaces have been investigated. These will utilise the liquid present on tissue surfaces providing the adhesive forces necessary to allow a device to dock, against gravity, whilst providing minimal tissue damage.

As discussed in section 2.3.6, it is shown that although the micro-structured surfaces fabricated in this thesis are modelled on the footpads of the tree frog however, there are differences in the adhesion mechanism. The tree frogs pads are permanently wetted by mucous glands which open onto the surface, allowing the mucus to spread over the pad through hexagonal channels [64]. However, experimental studies have shown that the tree frog is able to stick to a surface by using the combined forces of surface tension and viscosity, generated by a fluid filled joint between the pad and the substrate [62, 65-69]. This is shown by a visible meniscus around the area of contact between the substrate and toe pad [62] as well as the sticking ability becoming reduced when the toe pads are fully immersed in water [62, 70]. Therefore the adhesion mechanism proposed is similar, in that a fluid filled joint will form between the wet surface and the structured polymer providing the adhesive forces necessary. It should also be noted that the toe pads of the tree frog are detached from surfaces through peeling, minimising the forces required to overcome adhesion [65]. This differs in this work where the detachment mechanism relies on a direct pull-off force.

Micro-structured pillars have been fabricated, the method of which is described in Chapter 4 to allow the formation of discrete capillary bridges at their tips. It is the sum of these, which gives rise to the total adhesive force (Figure 6.4).

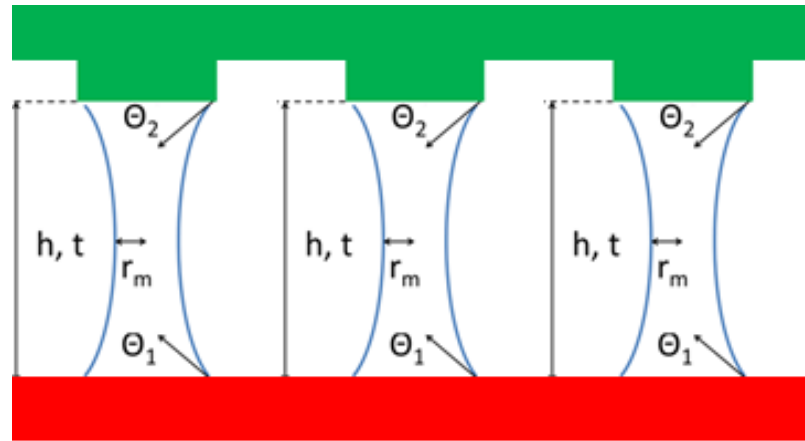


Figure 6.4 - Schematic to show the formation of discrete liquid bridges on the tip of each individual pillar when in contact with a wet interface. It is the sum of these which give rise to the total adhesive force.

The shape and size of the meniscus forming a capillary bridge is dependent on a number of variables: surface wettability, fluid surface tension, the pillar radius, the height of the fluid film and the separation between the pillar tip and the wet surface.

Stefan adhesion also plays a part in the total adhesive force, being the main component at short separations before the capillary force takes over. Stefan adhesion is a stress which occurs when two flat surfaces are placed in contact and pulled apart with a fluid film which is forced into the expanding gap. The force which is required to push the fluid into the gap, translates into a force which resists the separation of the surfaces - promoting adhesion [168]. The Stefan force however is a simplification, in that it assumes un-deformable surfaces and a uniform flow of the fluid into the gap [169, 170]. These assumptions are likely to be breached in the present work where very compliant tissue and micro-

structured surfaces are investigated [169, 171, 172], and therefore it may be apparent that there are other forces in play. Similar to the capillary force there is a range of variables to be investigated in order to optimise this adhesion: fluid viscosity, pillar radius and separation of the two surfaces.

$$F_{\text{Per Pillar}} = F_{\text{cap}} + F_{\text{stef}} \quad (6.5)$$

$$F_{\text{cap}} = 2\pi r_m \gamma (\cos\theta_1 + \cos\theta_2) \quad (6.6)$$

$$F_{\text{stef}} = \frac{3\pi R^4 \eta}{2h^2 t} \quad (6.7)$$

$$N_{\text{Pillars}} = \frac{A_{\text{surface}}}{2(R + S)^2} \quad (6.8)$$

$$F_{\text{Total Surface}} = F_{\text{Per Pillar}} * N_{\text{Pillars}} \quad (6.9)$$

This model assumes a discrete liquid bridge forming on the tip of every pillar on the surface. However, due to the fabrication technique taking place outside a cleanroom, as shown in section 4.3.3.1 there may be pillars missing, deformities and a roughness to the substrate base. These would all result in fewer contacts and therefore fewer liquid bridges forming, as shown in Figure 6.5, and as a consequence, lower adhesion than predicted in this wet adhesion model. As with the experimental testing, throughout this model the surface area has been kept constant.

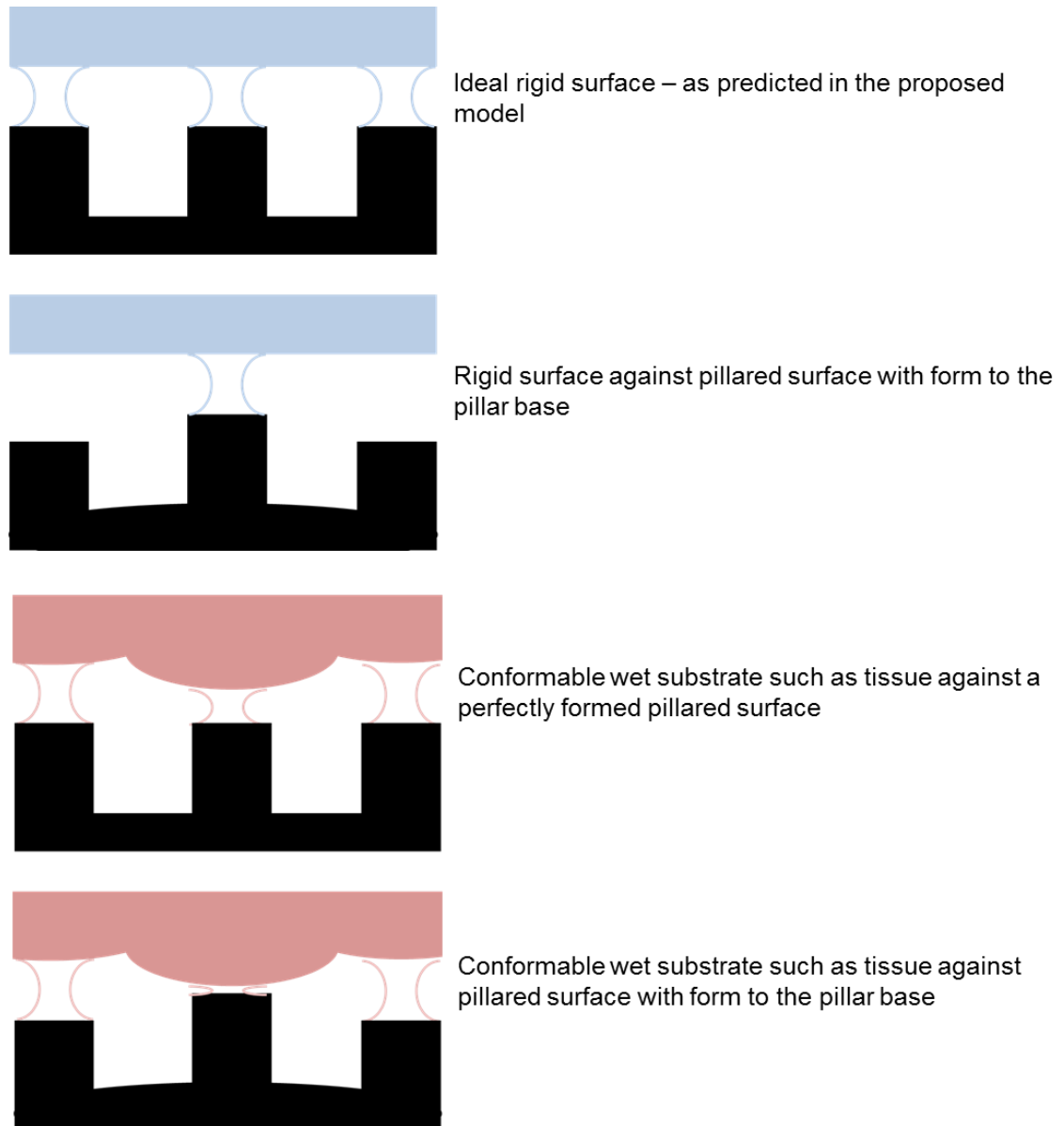


Figure 6.5 - The effect on the formation of liquid bridges, due to surface roughness at the base of the pillars and contact with a conformable surface.

By systematically investigating each variable independently, it is possible to identify the adhesion mechanism which is taking place in this unique system. This has been carried out theoretically in this chapter; the following chapter will discuss the experimental aspects. During these studies, the pillar radius, bridge height, surface tension, and time will remain fixed for the same test area (113 mm²). All tests will be simulated for water, ex-vivo tissue and in-vivo tissue, where the fluid

viscosity and wet interface contact angle vary accordingly. These constants were given in Table 5.3, where the values have been obtained from the literature. Roshan *et al* [21] obtained force-displacement curves for a range of fluids. This model incorporates their experimental values for water specifically referring to their findings for bridge height, H , and the time, t . Both of these values are inversely proportional to the adhesion force, however, as the time is only present in the Stefan component of adhesion, the effects of this are negligible on the total adhesion force. Ott *et al.* [148] observed changes in the viscosity of peritoneal fluid during exposure to CO_2 , during laparoscopic surgery, their values, before the addition of CO_2 , have been used for the *ex-Vivo* model, and their values for the change in viscosity once CO_2 had been added, have been averaged and used for the *in-vivo* model.

As mentioned earlier, peritoneal fluid has been found to have a contact angle in the region of 43° and 38° [150, 151]. Therefore an average of these values has been taken and used as the contact angle for both tissue systems (40.5°).

6.5 Theoretical Results

As previously mentioned, the closer the separation between the wet surface and the pillar tip, the higher the Stefan forces. However as the separation of the two surfaces increases, this force begins to diminish and the Capillary forces become dominant. At larger separations [21], capillary forces make up over 99% of the total adhesion. This will be key when working with an ultra-soft substrate such as tissue, as this separation distance will remain lower for longer resulting in an increased importance of the Stefan component. However, when working with a rigid surface, such as glass, the importance is diminished. This phenomenon is investigated first, followed by the effect of the wettability of the pillared polymer

surface and the effect of pillar spacing. These are explored for the three geometries proposed as well as for all three fluid systems: water, *ex-vivo* peritoneal fluid and *in-vivo* peritoneal fluid. As tissue is viscoelastic, it is possible that the surface itself may have a fluid like property, increasing the viscosity. However, this is not assumed within this work.

6.5.1 Effect of Separation on the Adhesion Mechanism Occurring

This study looks at the separation of one pillar in the micro-pillared array from the wet surfaces; values from Table 5.3 have been used for a separation range of 0 - 0.1 μm . As this work is focused on the effect of a single pillar, only the values for wafer 1 are displayed as there will be no variation in each wafer. The graphs in Figure 6.6 have been focused on the region of small separation. It is unlikely that experimentally it is possible to obtain adhesion forces dominated by Stefan adhesion, due to the small separation distances over which it occurs.

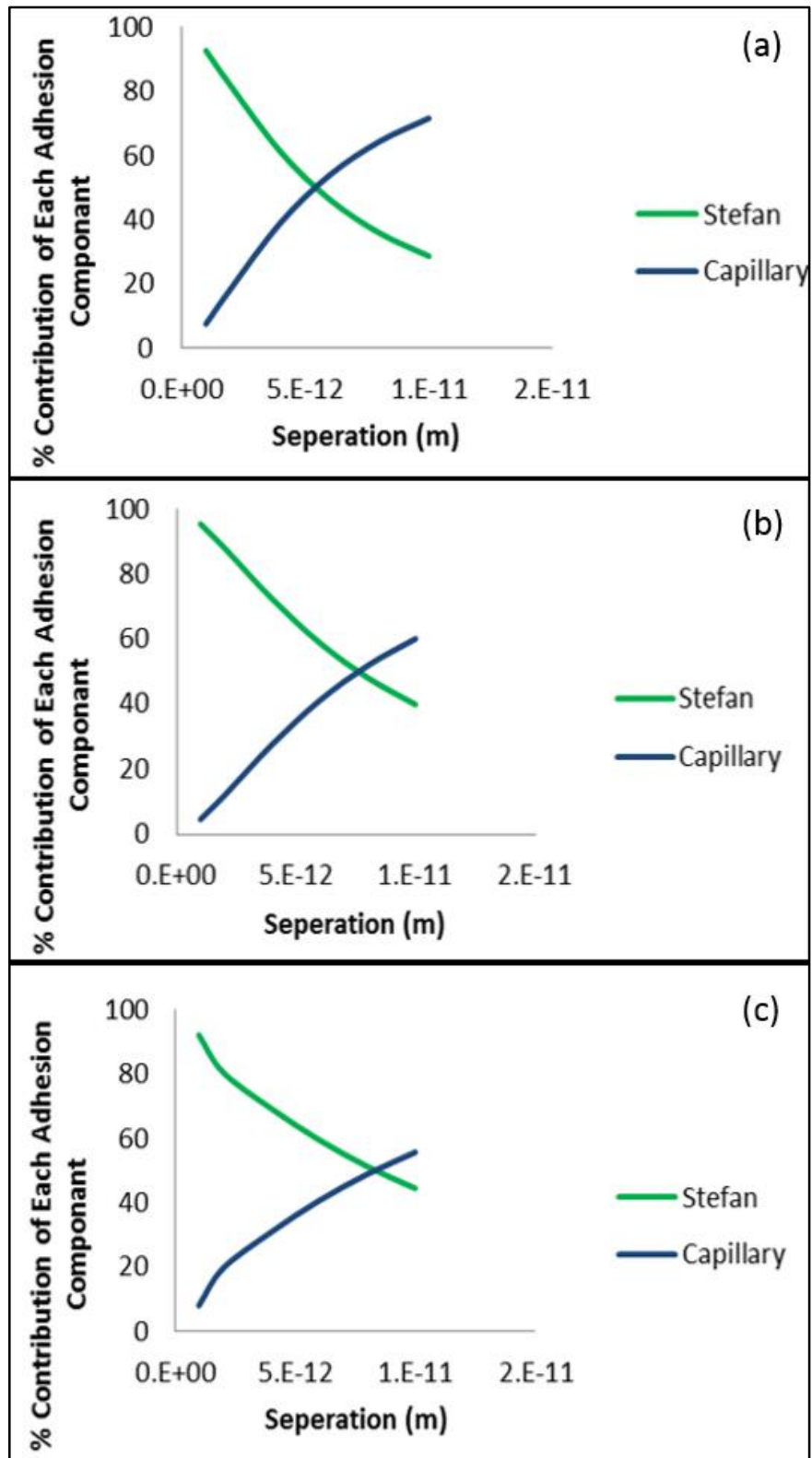


Figure 6.6 - The effect of separation on the percentage contribution of each adhesion component for varying viscosity fluids: (a) water, (b) ex-vivo and (c) in-vivo.

From Figure 6.6, it can be seen that the switch from Stefan adhesion to Capillary is at close separations, in the order of 1×10^{-12} m. However, as shown in Figure 6.7, the separation point at which the contribution of adhesion switches from Stefan dominating to capillary is directly proportional to the fluid viscosity. This is expected due to the viscosity component of Stefan Adhesion, this is key to this work as the Stefan force is a stronger force than the capillary. Therefore the longer we remain in this adhesion mechanism range the higher the overall adhesion. In summary, the higher the fluid viscosity, the larger the component of Stefan adhesion and therefore the higher the overall adhesion force. Therefore it can be assumed that in order to optimise the wet adhesion the viscosity is required to be maximised. However, as discussed in section 5.3.3 the surface tension of the fluid has a higher impact on the total adhesion force. Therefore in order to harness the potential adhesive force it is necessary to consider both properties in conjunction with each other.

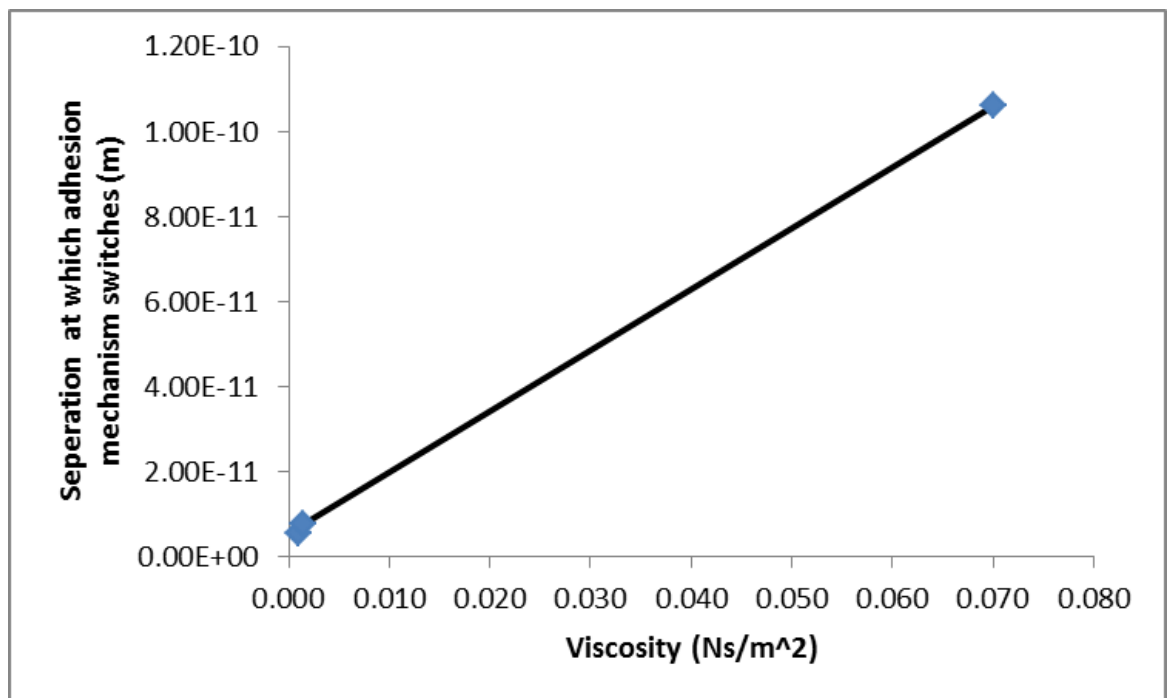


Figure 6.7 - Effect of fluid viscosity on the separation point at which capillary action dominates rather than Stefan forces.

6.5.2 Effect of Surface Wettability (Pillared Polymer Surface)

Next, the effect of surface wettability has been investigated. As previously mentioned in section 6.3, it was found by De Souza *et al.* that there is an optimal adhesion of a micro-pillared array at 70° [81] and therefore not too hydrophilic.

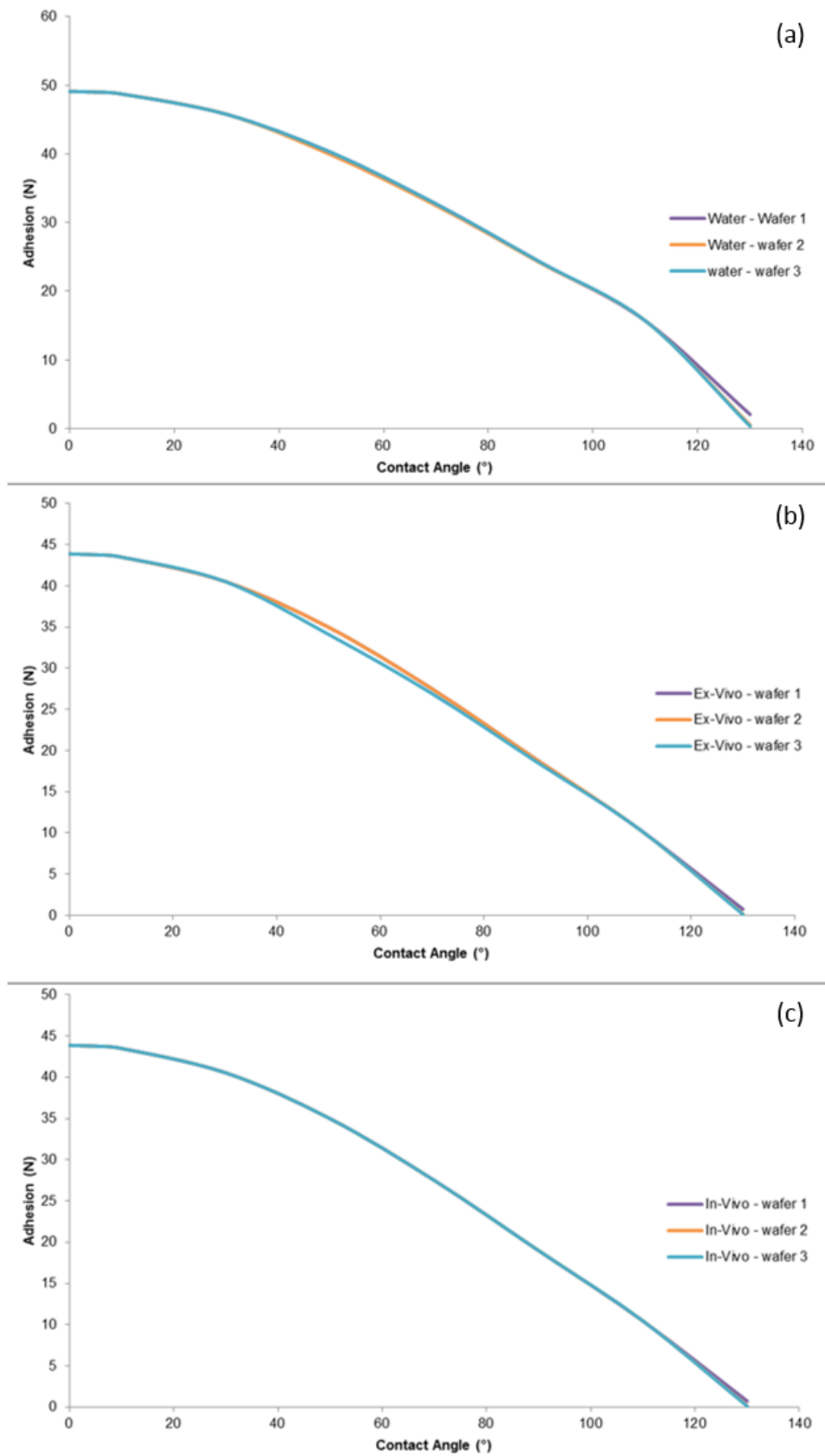


Figure 6.8 - The effect of surface wettability in different environments, (a) wet glass, (b) ex-vivo tissue and (c) in-vivo for the three geometries.

It can be seen that there is very little distinction between the effects of each wafer. Therefore, the spacing in this model has no effect on the wettability. This is due to the effects being over discrete pillars rather than the surface being considered as a whole.

When this data is compared for each wet surface alone (Figure 6.9), it can be seen that the adhesion is predicted to be higher for wet glass than that of tissue. This could be due to the fact that capillary forces are dominating the adhesion as shown previously, and there is no component of viscosity in capillary action, just Stefan. However, capillary action does have a component of surface tension, this is similar to that of water for both *ex-vivo* and *in-vivo* peritoneal fluid.

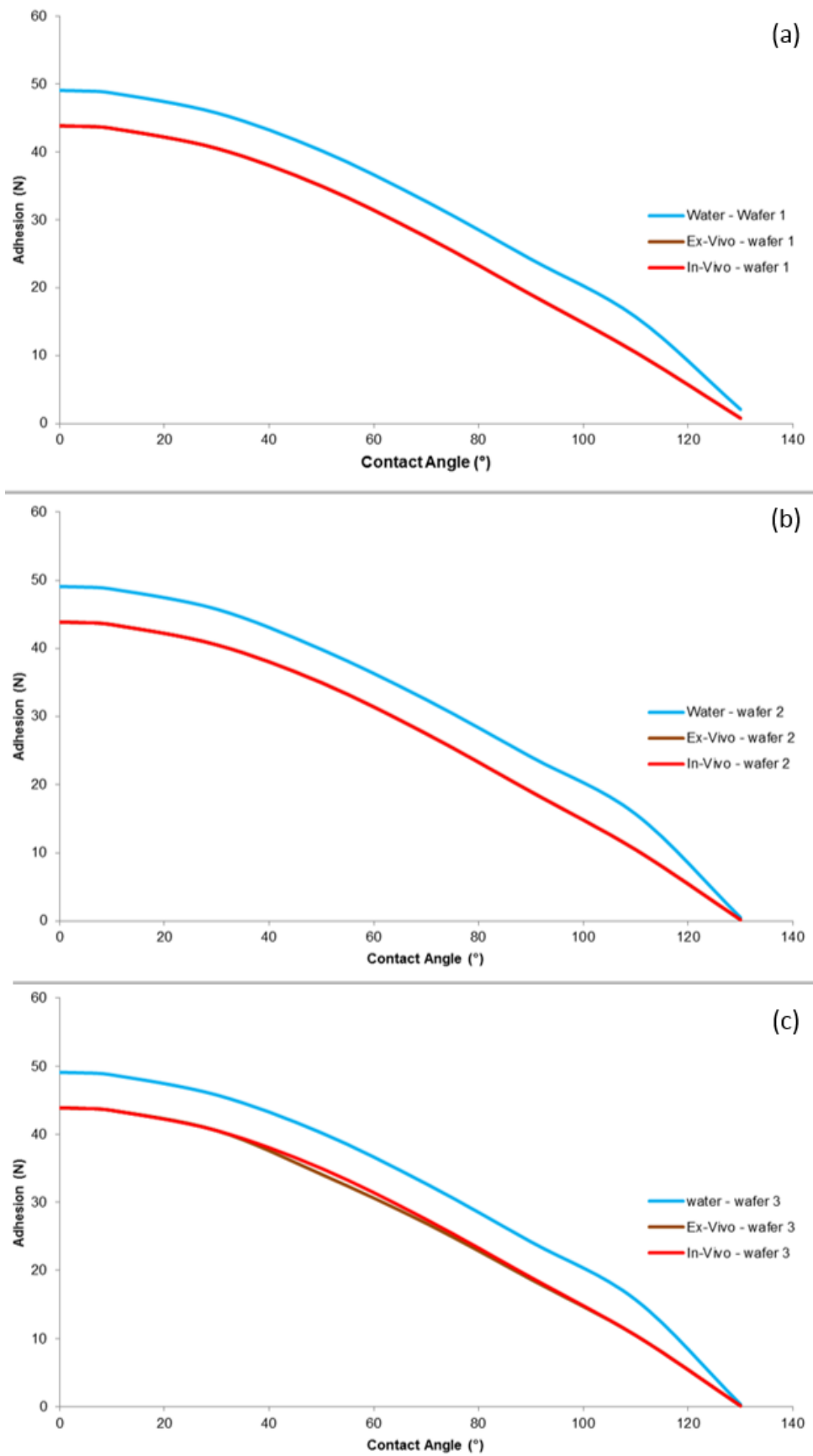


Figure 6.9 - The effect of wettability on the adhesion. (a) wafer 1, (b) wafer 2 and (c) wafer 3.

6.5.3 Effect of Micro-Pillared Geometry (Spacing)

Finally, the effect of pillar spacing has been investigated. Initially this has looked at the total adhesion at the separation point which Roshan *et al.* used during their experimental testing [21] - the optimal adhesion at a range where capillary action is dominating. Following this, the effects were explored at a closer separation in which the adhesion mechanism is working in the Stefan regime, as found earlier.

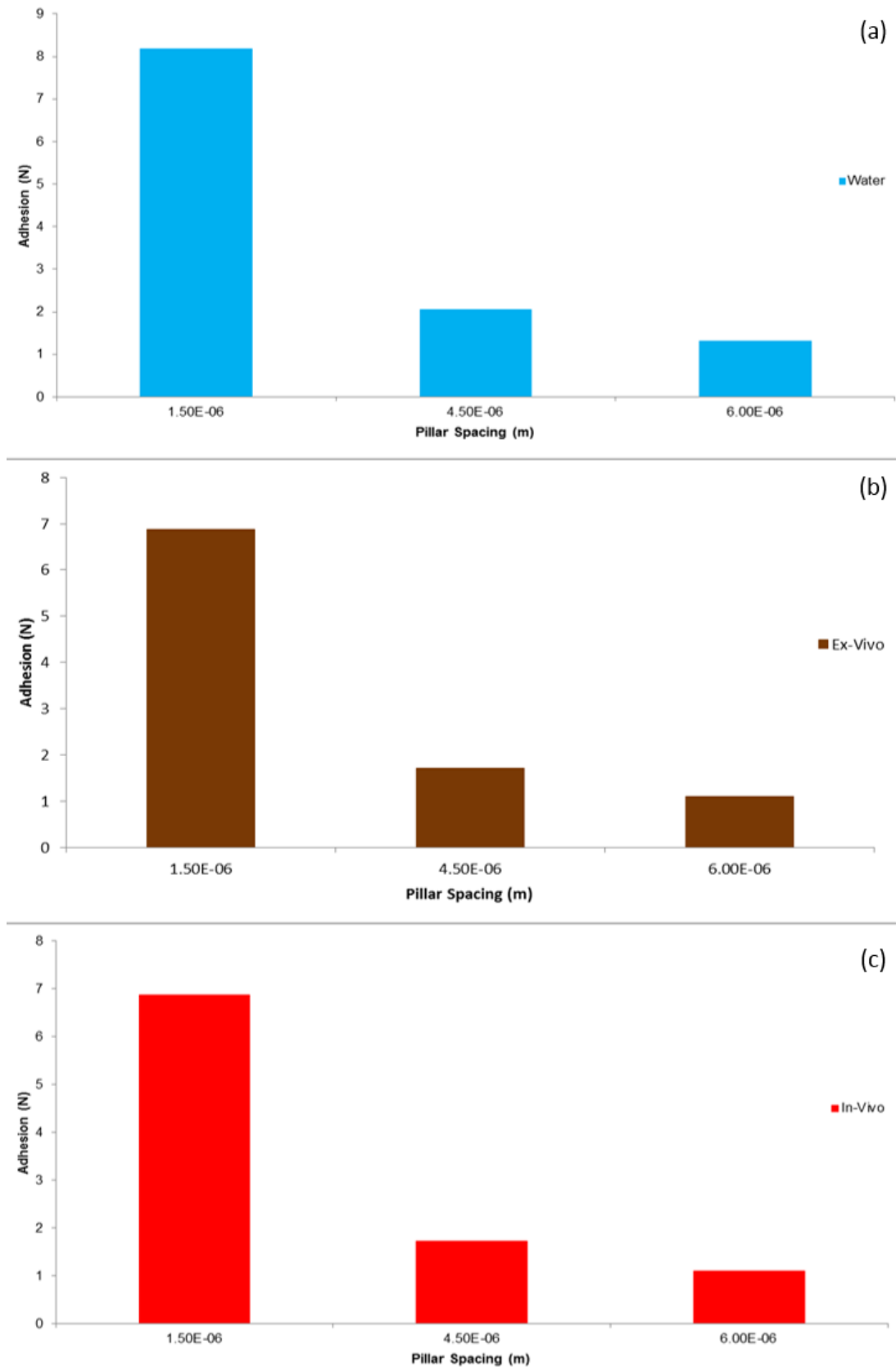


Figure 6.10 - The effect of pillar spacing in each environment, (a) water, (b) *ex-vivo* and (c) *in-vivo* - whilst adhesion is due to capillary forces.

Figure 6.10, shows as expected that the smaller the pillar spacing, the higher the adhesion force, due to an increased number of pillars on the surface and therefore an increased number of liquid bridges contributing to the total adhesion force.

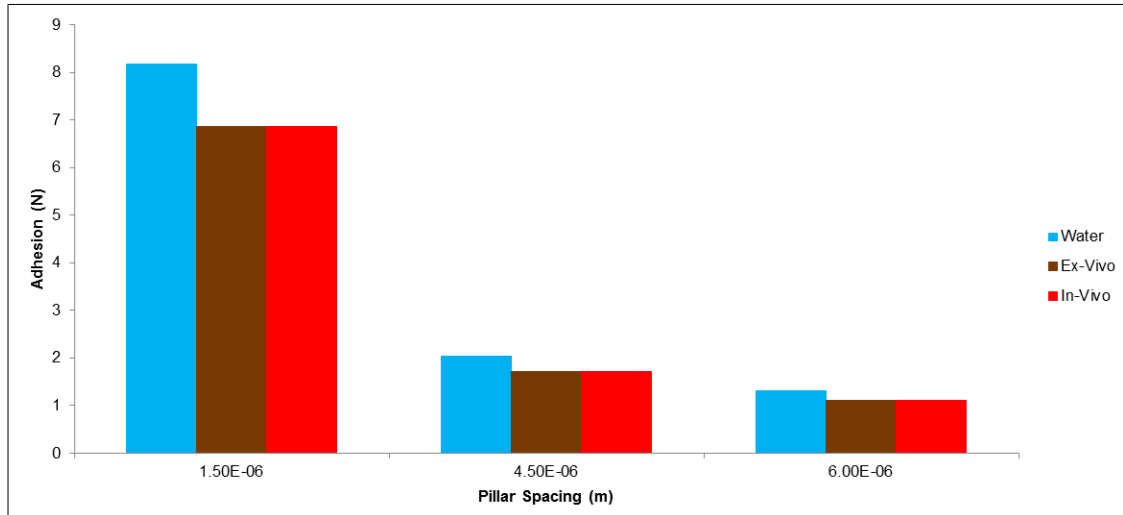


Figure 6.11 - Summary - The effect of pillar spacing in each environment.

Here, where the capillary action is dominating - it can be seen that the adhesion is optimal in a water/glass environment and there is no change between *ex-vivo* and *in-vivo*. This is again due to the lack of dependence on viscosity in this regime.

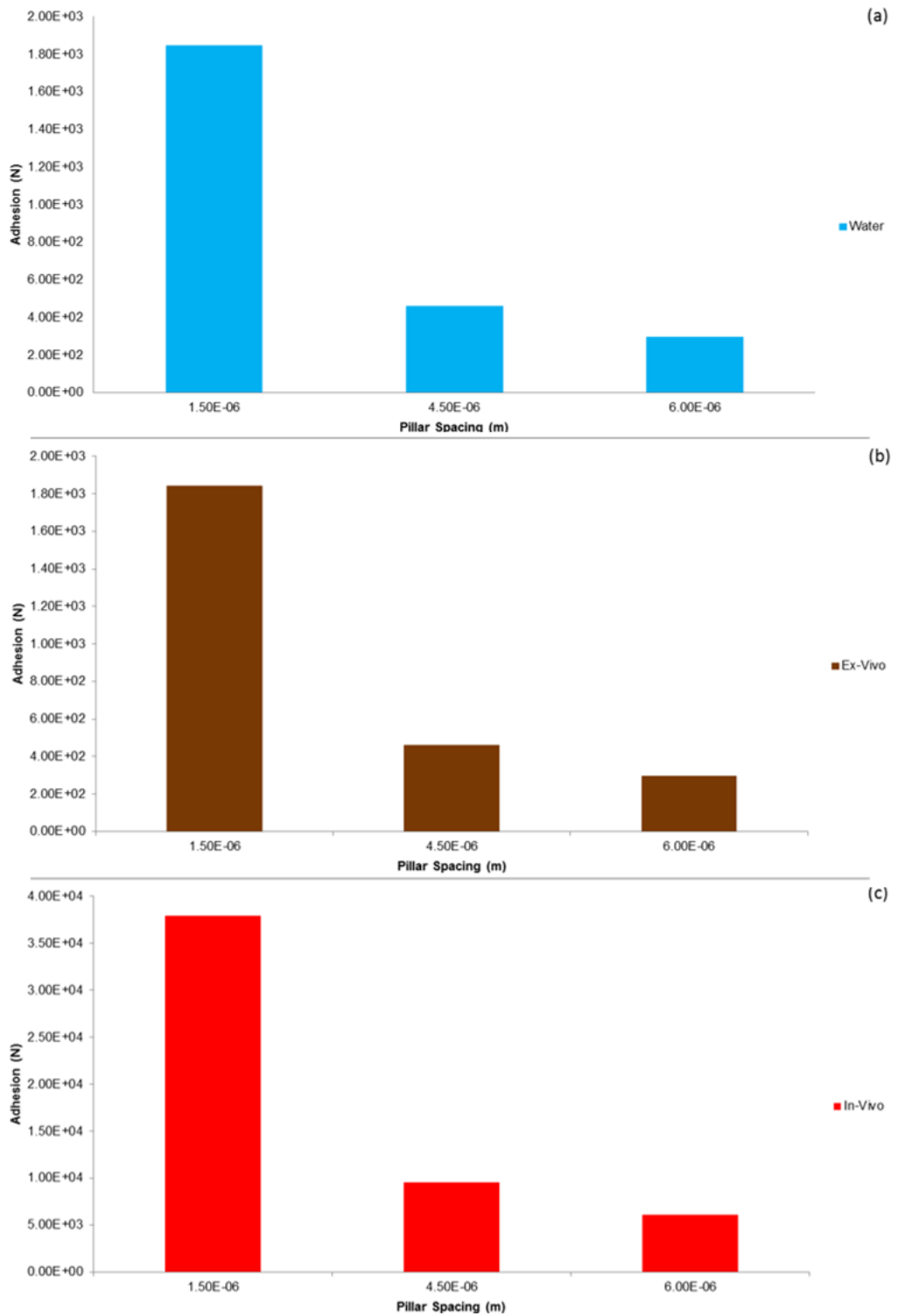


Figure 6.12 - The effect of pillar spacing in each environment, (a) water, (b) *ex-vivo* and (c) *in-vivo* - whilst adhesion is due to stefan forces.

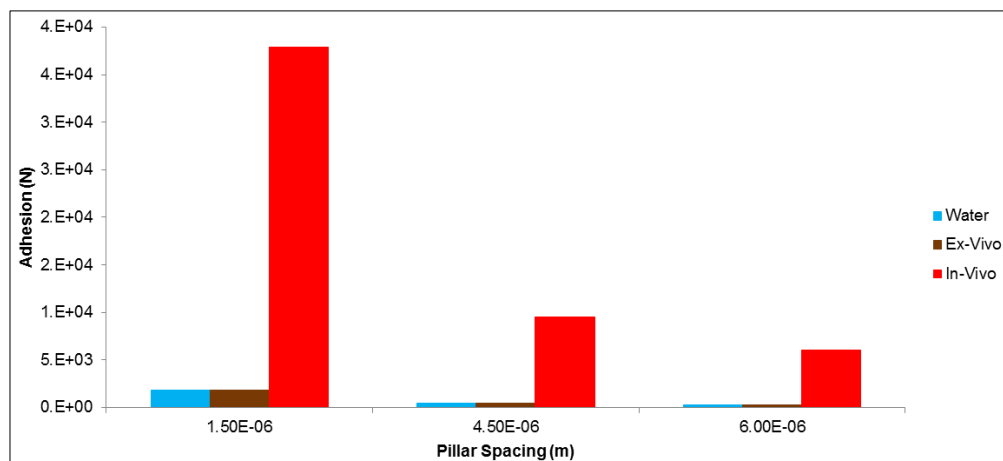


Figure 6.13 - Summary of the effect of pillar spacing in each environment.

Figure 6.12 shows the effect of pillar spacing on adhesion, when the separation is at a minimum and the adhesion is occurring due to mainly Stefan forces. Here, when viscosity is a major factor in the adhesion mechanism, there is a large difference in the adhesion forces available - the lower the fluids viscosity, the smaller the adhesion forces. It is also worth noting that the adhesive forces available theoretically are 1×10^7 times larger when working in this regime. Unfortunately, this model does not take account for the conformable surface, and instead assumes two rigid surface, therefore it is unable to describe the exact effect which will occur between two conformable surfaces, but, it might be postulated that due to the conformable nature of the surfaces the adhesion will remain in the Stefan regime for longer and therefore aid the adhesion. This model also assumes that there is perfect contact, resulting in all of the pillars being in contact at the same time and removed at once. However, this again may not be the case due to the conformity of both of the surfaces; and as expressed earlier, there is a large variation of the peritoneum and the peritoneal fluid in a small sample. This model does however give an indication into the trends we can expect to see during experimental testing. The key findings of this chapter are discussed further in the following discussion chapter.

6.6 Summary

This chapter has highlighted an understanding of the interaction which occurs at a patterned polymer substrate and a viscoelastic material. The mechanism proposed in this chapter encompasses both capillary and Stefan adhesive forces, and has been utilised to determine the adhesive forces present on the tip of a single pillar, and as a result the total surface adhesion.

As a result of this investigation it has been found that:

- It is unlikely for the total adhesion force to have a regime dominated by Stefan forces.
- The distances over which the capillary forces dominate the adhesion mechanism is directly proportional to the fluid viscosity.
- The pillar spacing has a direct effect on adhesion due to the variation in the number of pillars on the surface, and therefore the number of liquid bridges.

The proposed model in this chapter presumes two rigid surfaces coming into contact and separating perfectly, however in the case of this work there will be an issue of conformity. Therefore, this model has been found to not be a true representation of the adhesion mechanism taking place. However, it does give an indication to the trends which can be expected during experimental testing.

Chapter 7. Discussion

7.1 Introduction

This thesis has explored the viability of using micro-pillars to utilise the fluid present on a surface, in order to provide adhesive forces through the formation of discrete liquid bridges. Micro-structures have been successfully fabricated in polymer substrates, using a nano-imprint lithography and a range of polymers have been selected to allow the fabrication of structures in the selected geometries. This incorporates inspiration from the sub-micron structures on the tree frogs toe pad, and also the work of Roshan *et al.* [21] and Taylor [17]. However, the polymers have also been selected to allow the effect of wettability on adhesion to be investigated. A parametric study could then be performed, investigating the effects of pillar spacing and wettability on the adhesion forces produced.

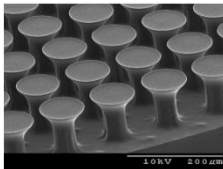
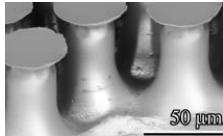
Wet adhesion is something which has been explored by a number of research groups; however, the system considered here is different to previous systems due a number of reasons. Firstly due to the fact that it is concerned with two deformable surfaces as opposed to rigid ones. The low elastic modulus of the materials investigated, the irregularity of the tissue surface and fluid properties suggests that the proposed simple model is deficient in this respect. Aspects of the adhesion system are understood as a result of this thesis which helps to improve the clarity to more accurately model the adhesion process.

This thesis has shown that the use of micro-pillars is a feasible method of providing adhesion to tissue. However, future work would focus upon the effects of the pillared surface contact angle, considering a wider range and investigating their effects on adhesion.

7.2 Uniqueness of This System

The issue of wet adhesion is one which has been widely addressed in the literature. However, as shown in Table 7.1, there are many differences between previous conventional wet adhesion investigations and the work presented in this thesis. Specifically in terms of surface geometry, when comparing the experimental work in this thesis against a glass surface coated with a liquid film. This highlights an area of novelty, perhaps due to fabrication difficulties, the scales on which the micro-structured surfaces have been fabricated, are at least a tenth of those used in wet adhesion investigations reported in literature. Such small features were chosen in this work in order to allow firstly, many individual discrete contact points with the wet surface. This also relates back to the inspiration of this work, where sub-micron features on the toe pad of the tree frog are utilised. However, due to the differences in the adhesion mechanism as discussed in section 6.4, the features need to be larger in adhesion mechanism proposed in this work in order to prevent the collapsing of capillary bridges. It has been proposed by Qian and Gao [79] that the minimal pillar radius is around 0.8 μm .

Table 7.1 - Table of literature comparisons of wet adhesion mechanisms with various micro-structured surfaces.

Author	Shape of the structures	Structure Geometry	Adhesion Result
Cheung et al. [95]	Polyurethane mushroom, against a glass hemisphere coated in oil	Mushroom tip = 100 μm , Height = 100 μm , Separation = 120 μm  SEM image of polyurethane fibres with mushroom tips [95]	115 mN/cm ²
He et al. [173]	PDMS Square pillars, against glass coated in water.	Length = 100 μm Width = 100 μm Spacing = 15 μm Height = 10 μm Surface Area = 240 mm ² [173]	100 mN
Kovalev et al. [174]	Poly-(vinylsiloxane) mushrooms against glass coated in oil.	Mushroom tip = 50 μm , Height = 65 μm , Separation = 60 μm Surface Area = 7.1 mm ²  Surface profile of micro-structured surface [174]	6 mN

These results have been compared to the greatest adhesion force produced in this thesis (hydrophobic, wafer 3, against a glycerol-water mix). The results are shown in Figure 7.1.

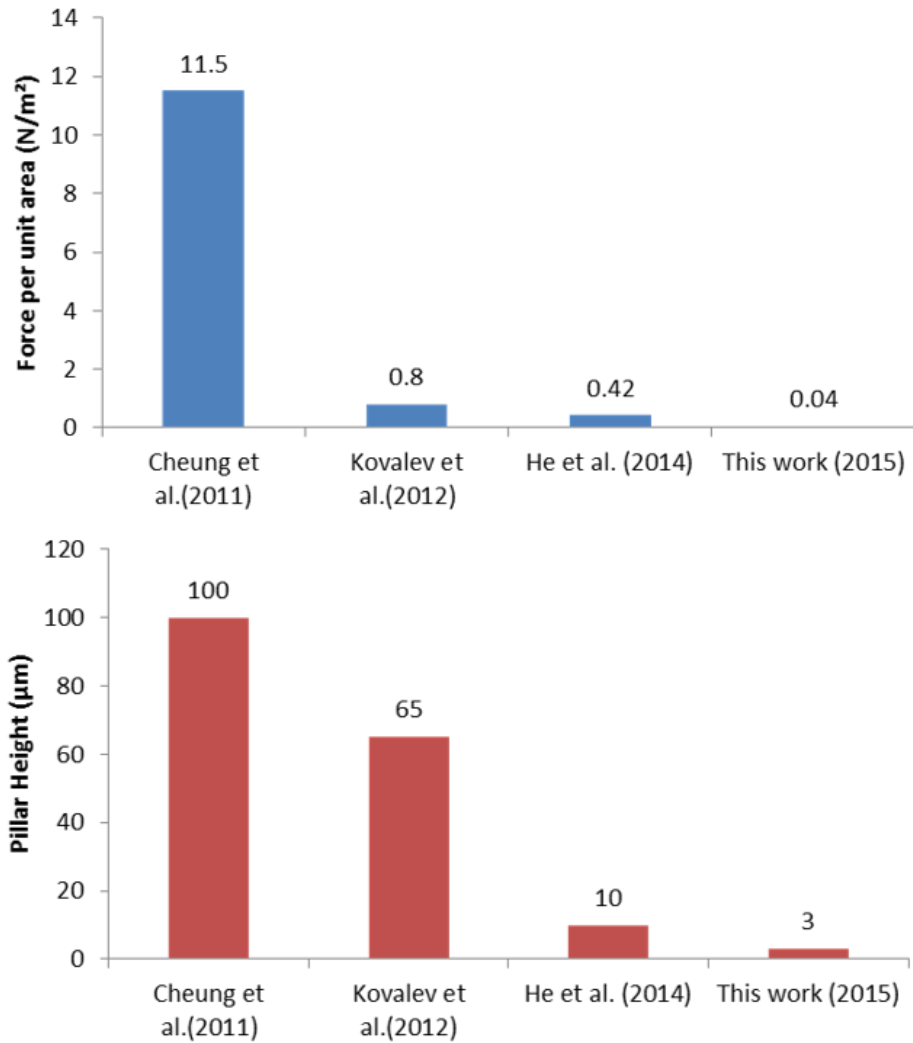


Figure 7.1 - Adhesion results from literature compared to the maximum adhesion force acquired with PDMS and Autotex[®] through this thesis.

Results are also related to pillar height.

It can also be shown by Figure 7.1, that the adhesion trend is proportional to the pillar height – the larger the pillar height the higher adhesion. Where Cheung *et al.* [95] have a pillar height 33.3 times higher than those in this thesis, resulting in a 287 times higher adhesion force. This shows another dependence of a wet adhesion system which is not accounted for in the proposed model. However, this does not take into account the wettability of each surface.

Another area of novelty which is apparent as a result of this review is the testing against biological tissue, specifically the peritoneum. Working with biological tissue presents a number of issues when looking at wet adhesion. In particular the soft nature of the tissue, the irregularity of the tissue, both in terms of the varying fluid properties from one small area to another and also the roughness which varies across the surface. Another issue which arises when working with biological tissue is the movement of proteins. This mechanism is dependent on a liquid interface between the tissue surface and a polymer. However, it has been found that there is a strong adsorption of proteins, which will bind onto the PDMS surface due to its porosity [175, 176]. This has only been investigated in a limited fashion, but what has been investigated has shown that it is possible for proteins to form a film on the surface of PDMS [177], which as a result can alter the surface properties. This has not been investigated as part of this thesis. However, if this work were to be continued, it would be necessary to look into this further in order to optimise the system.

7.3 Discussion of Experimental Results

Chapter 6 showed the potential adhesion forces capable of being produced by micro-structured surfaces. However, experimentally the surfaces did not behave as expected according to the model discussed. This could be due to a number of reasons, firstly, surface form. If there is any form to the base on which the pillars are fabricated this could result in not all of the pillars coming into contact and forming liquid bridges at once. This would result in a reduced number of capillary bridges and therefore a lower force of adhesion, this would be a consequence of the fabrication technique used. PDMS is fabricated without the use of an electro-spinner, which was used for the production of the Autotex[®] samples, resulting in

a flatter base for the Autotex[®] pillars than the PDMS ones and therefore higher adhesion forces would be expected from the Autotex[®] samples than the PDMS this is shown in the schematic diagram shown in Figure 7.2.

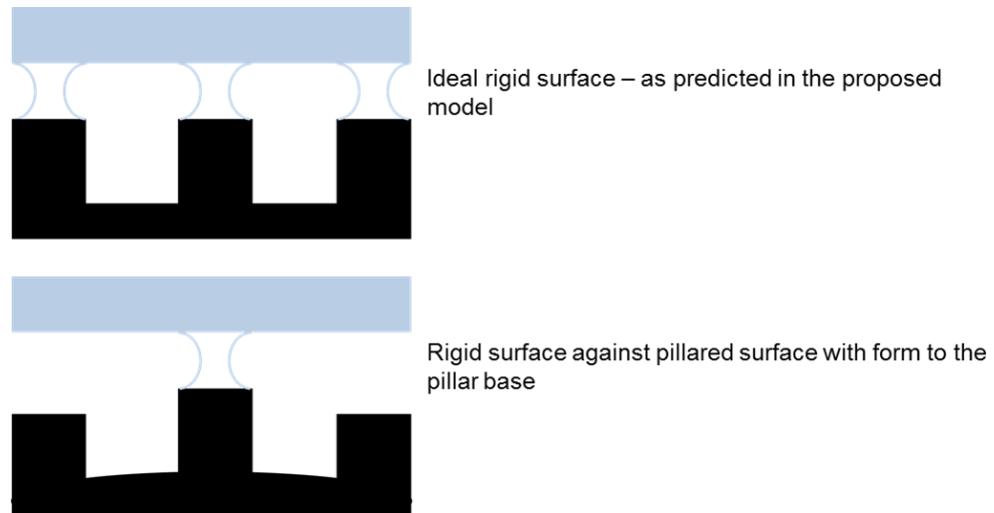


Figure 7.2 - The effect of having any form to the base on which the pillars have been fabricated, where the maximum separation at which bridges can form is dependent on the fluid film thickness.

Secondly, as discussed previously the adhesion mechanism considered in this thesis relies on capillary and Stefan forces which are present when separating two surfaces with liquid mediating contacts. Cai *et al* , showed that hydrophilic surfaces produce concave menisci on a pillar tip producing attractive forces; whereas a hydrophobic surface will produce convex menisci and therefore repulsive forces [61].

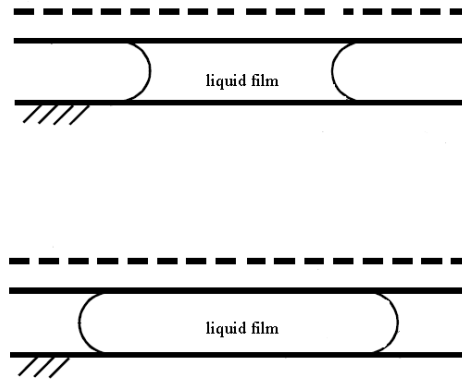


Figure 7.3 - Modified schematic diagram from Cai *et al.* showing the separation of two smooth surfaces – hydrophilic forming concave menisci and hydrophobic forming convex [61].

They also showed that an increase in contact angle will result in a decrease in attractive meniscus forces and an increase repulsive meniscus forces. However, they found that a slight attractive force is observed for a hydrophobic surface during the end stage of separation, although the magnitude is small.

It is shown in Quéré *et al.* that if the pillar height of a hydrophilic surface is much smaller than the capillary length of the fluid the surface will act super-hydrophilic [178], therefore wetting the surfaces and preventing the formation of any menisci and again resulting in poor adhesion. Where the capillary length is defined as:

$$\lambda_c = \sqrt{\frac{\gamma}{\rho g}} \quad (7.1)$$

Where: γ = surface tension of the fluid, ρ = fluid density and g = gravitational acceleration.

For the system described in this thesis the pillar height is 3 μm , compared to a capillary length of water of water, which from equation (7.1), is 2.7 mm. Therefore

it can be said that for this system the pillar height is much smaller than the capillary length of water.

This means for the system discussed in this thesis there may be an optimum contact angle between 90 and 50 degrees which will allow the formation of attractive concave menisci on the pillar tip, this is shown in Figure 7.4. This effect would be observed regardless of the pillar spacing as it is only the pillar height which determines the formation of such menisci. Such an effect would explain why the adhesion forces, when PDMS is explored, is greater for a hydrophobic surface, as the small attractive forces present at the end stage of separation, despite being small, are still greater than the effect of a super-hydrophilic surface. This can be explained by investigating the work of adhesion.

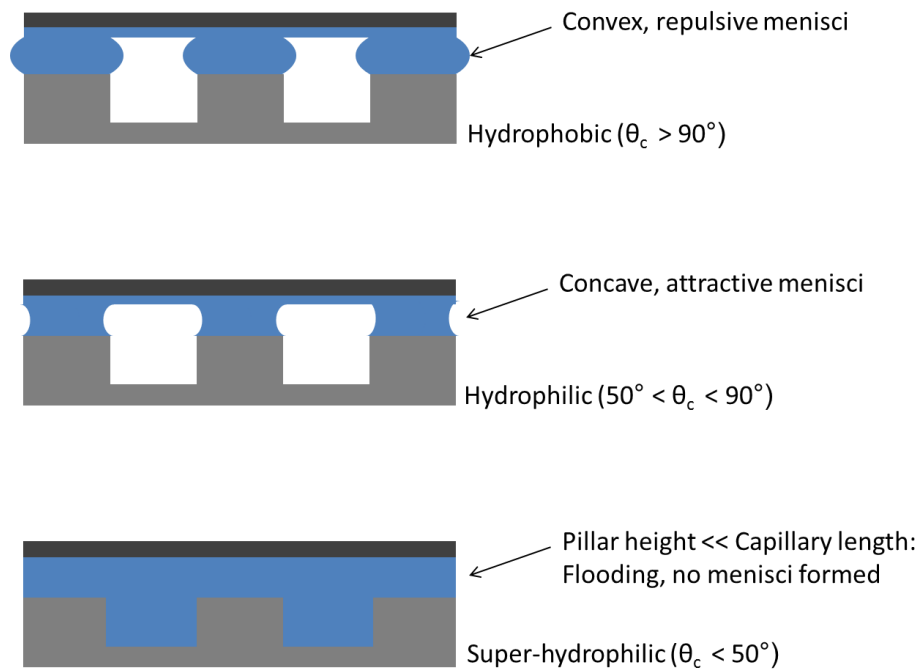


Figure 7.4 - The effect of contact angle, pillar height on meniscus formation. If the contact angle is less than 50° it is proposed that the surface will act super hydrophilic, and the surface will completely flood, resulting in no liquid bridge formation and therefore minimal adhesion forces.

To investigate this effect further, the adhesion properties of flat PDMS structures were investigated, hydrophobic, with a contact angle of 105.8° , and hydrophilic, with a contact angle of 40.3° . The results are shown in Figure 7.5, where it can be seen, that for the hydrophilic sample there is no clear dependence on the presence of pillars on the wet adhesion forces. This confirms the hypothesis of a super-hydrophilic surface which is completely flooding; as if it was totally flooding there will be no liquid bridges regardless of the presence of pillars. It is also shown that for a hydrophobic surface the adhesion is greater for a flat surface than one which contains pillars. Therefore, this suggests that the adhesion mechanism taking place would favour one large convex meniscus, pinned at the circumference of the sample, over a number of discrete convex menisci on each pillar tip (Figure 7.6).

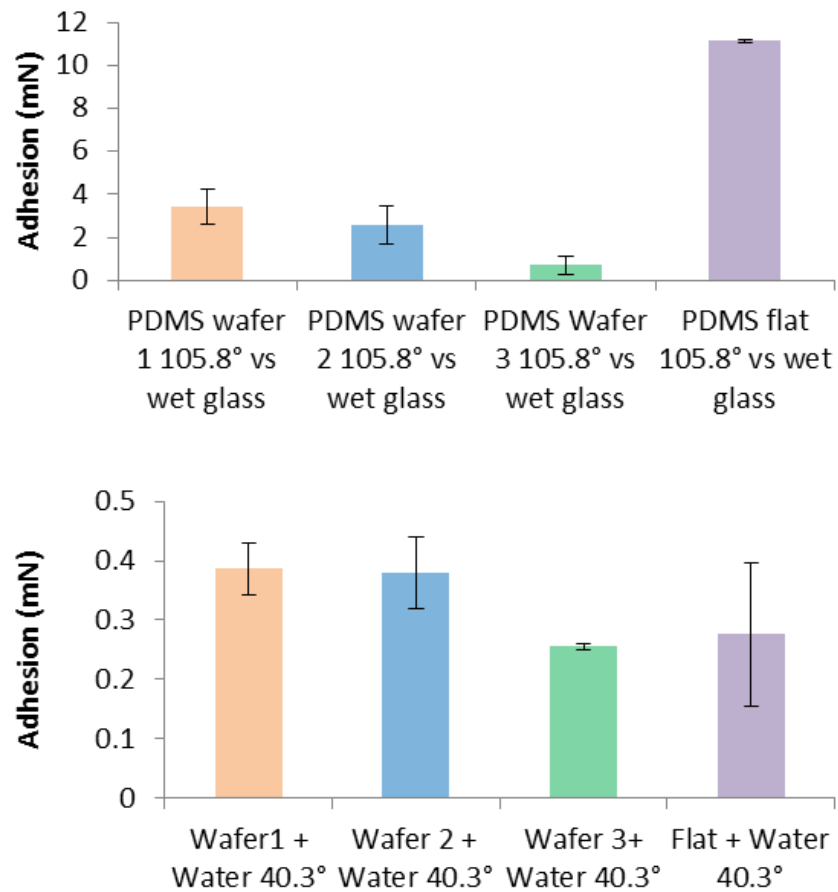


Figure 7.5 - The effect of pillars on the adhesion forces provided, for hydrophobic and a hydrophilic PDMS samples.

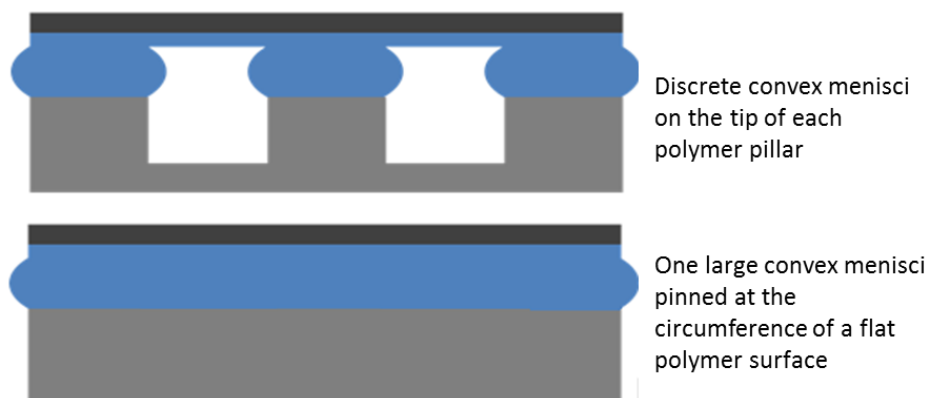


Figure 7.6 - Liquid bridge formation on individual hydrophobic pillar tips and a flat hydrophobic surface.

7.4 Work of Adhesion

The work of adhesion is calculated from the force-displacement curves. It is the area between the force and the horizontal axis – the distance travelled during retraction, as shown in Figure 7.7. The area has been calculated using Matlab²⁰.

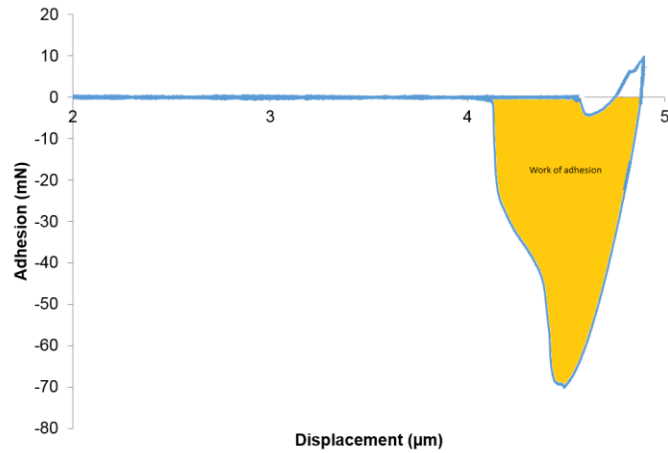


Figure 7.7 - Image to show the work of adhesion from a force-displacement curve.

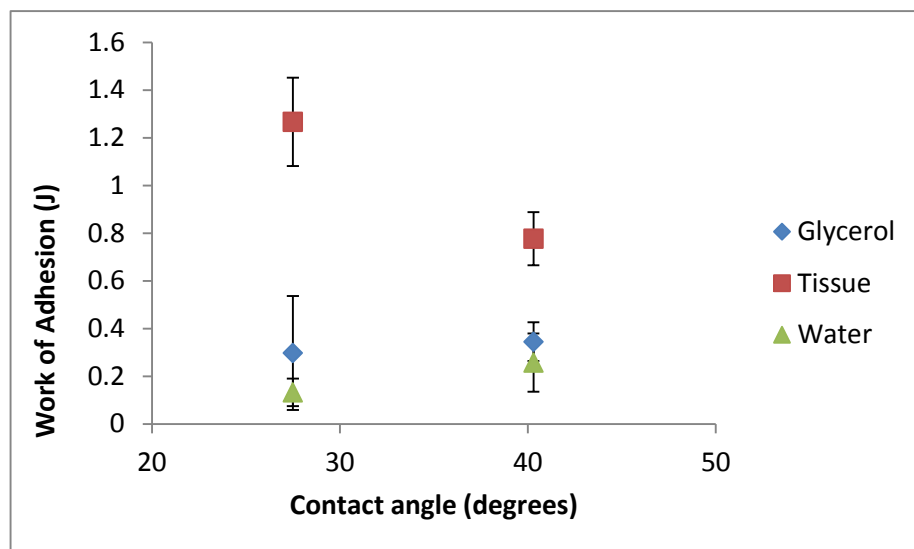


Figure 7.8 - Work of adhesion as a function of contact angle. All three wafers are averaged to remove the effect of surface geometry.

²⁰ Code constructed by Mr Nicholas Delbosc, University of Leeds, UK

The work of adhesion is an indicator to the adhesion mechanism taking place. If the work of adhesion is negative, there are repulsive forces acting within the meniscus; whereas if the work of adhesion is positive, there are attractive forces within the meniscus - indicating the formation of convex and concave menisci respectively. As the work of adhesion tends to zero, this indicates fewer liquid bridges are forming on the pillar tips. From Figure 7.8, it can be seen that on average, when in contact with glass coated with a mediating fluid, the work of adhesion is 0.2 J - indicating that there are no/very few liquid bridges forming on the surface, and instead the surface is fully wetting. This could be due to a number of reasons as previously discussed. However, when the surface is in contact with tissue, all wafers provide on average a work of adhesion of 0.97 J. These show there are more liquid bridges forming due to the conformability of the tissue, and the adhesion mechanism remaining in the Stefan force regime for longer. However, comparing this data to results obtained by Taylor [17], for the same contact surface area, it is evident that the work of adhesion is much higher – 16 J. Indicating that more attractive, concave liquid bridges are forming. This again confirms the earlier hypothesis that as the contact angle decreases below a certain value the surface begins to act super-hydrophilic, as this work has the same pillar height, but a higher contact angle – 67.5° .

7.5 Mathematical Model Discussion

The wet adhesion model used in this thesis has been inspired by the tree frog's ability to adhere to naturally occurring wet surfaces repeatedly and reliably.

Although the micro-structured surfaces fabricated in this thesis are modelled on the footpads of the tree frog, they have some major differences. Specifically those in order to provide adhesion to a wet surface, the tree frogs pads are permanently

wetted by mucous glands which open onto the surface allowing the mucus to spread over the pad through the hexagonal channels, rather than being a passive system dependant on the formation of liquid bridges on each discrete structure. However, experimental studies have shown that the tree frog is able to stick to a surface by using the combined forces of surface tension and viscosity generated by a fluid filled joint between the pad and the substrate [62, 65-70]. Therefore, it can be assumed that in terms of the forces in play the adhesion mechanisms are similar, however the effect of a viscous mucus film and the ability to deform at the micro-scale enabling a larger surface area of contact, may result in the adhesion mechanism relying heavier on the viscous force. Another difference between these two mechanisms is that of scale; specifically where sub-micron features are utilised on the toe pad of the tree frog. Whereas, due to the differences in the adhesion mechanism the features need to be larger in adhesion mechanism proposed in this work in order to prevent the collapsing of capillary bridges. It has been proposed by Qian and Gao [79] that the minimal pillar radius is around $0.8 \mu\text{m}$.

This mechanism is reliant on the formation of discrete capillary bridges at the tip of micro-pillars and it is the sum of these which gives rise to the total adhesive force. The shape and size of the meniscus forming a capillary bridge is dependent on a number of variables: surface wettability, fluid surface tension, the pillar radius, the height of the fluid film and the separation between the pillar tip and the wet surface.

Stefan adhesion also plays a part in the total adhesive force, being the main component at short separations before the capillary force takes over. It can however be seen in section 6.5.1, the effect of Stefan adhesion is negligible in this system as the separations over which the viscous Stefan force is dominant

are far too small, to effect the overall adhesion mechanism. Therefore it is only the capillary forces which are taking effect, specifically the surface tension and surface wettability, as shown in equation (7.2).

$$F_{\text{cap}} = 2\pi r_m \gamma (\cos\theta_1 + \cos\theta_2) \quad (7.2)$$

However, what has not been investigated in this thesis is the effect of pillar radius, which will not only affect the number of pillars on the surface but also the radius of the menisci (r_m). Also, this model assumes complete contact with each individual pillar on the surface; however, as this system is dealing with two conformable surfaces rather than rigid surfaces, it is likely that there will be some pillars which are not in complete contact as shown in Figure 7.2.

Another factor which will affect this is due to any deformities on fabrication. The number of pillars which should theoretically be on the contact polymer surface is shown in Table 7.2.

Table 7.2 - Theoretical number of pillars on the surface of each wafer

Geometry	Number of Pillars per 113 mm²
Wafer 1	6280000
Wafer 2	1570000
Wafer 3	1004800

The experimental adhesion results are shown to be 100 times smaller than the predicted model for hydrophobic surfaces and 1000 times larger for the hydrophilic. Therefore, the model can be adjusted to account for 100 and 1000 fewer pillars on the surface for hydrophobic and hydrophilic surfaces respectively. With this modification the theoretical results are now a more accurate

representation of the adhesion forces, suggesting that there are approximately 1000 times fewer pillars in contact with the surface at the point at which the adhesion is being measured, and therefore resulting in 1000 fewer capillary bridges forming. There is however, still low adhesion forces predicted for the model used. Again indicating that there may be an issue with the wettability as described in Figure 7.4. Another area which could impact this is the coalescing of the micro-pillars. It has been discussed by Chandra [179], that when a liquid is removed from a micro-pillared array, the pillars bend and cluster together. This is due to a small capillary interaction, whilst surrounded by a continuous film of liquid. In this case, the pillars are brought together and can form complex patterns. As the work in this thesis is concerned with an array of micro-pillars, this interaction would not only occur with the nearest neighbouring pillars [180]. However, such an effect would be unlikely in this system due to the low aspect ratio of the pillars (aspect ratio of 1) compared to literature where this effect has been investigated with high aspect ratio structures by Chandra (aspect ratio of 9 and 12) [179] and Wei (aspect ratio of 30) [180].

As a result of this mathematical model and experimental adhesion results it can be seen that there are a number of ways in which adhesion can be optimised for a wet system. Firstly, pillar height, as shown in section 7.2, where there is a dependence of pillar height on adhesion which is not addressed in the model. This is also important in terms of the wetting regime in which the surfaces are acting. If the pillar height is much smaller than the capillary length, the surface will act super-hydrophilic and flood, preventing the formation of discrete liquid bridges. Secondly, when working in a complex system, such as that with an ultra-soft material such as tissue compliance would need to be addressed. As the more the surface deforms, the higher the percentage of pillars which will be available

to form liquid bridges, resulting in a higher adhesion force. Therefore, if a term for pillar height, the form of the counter surface and compliance were to be included into the model; it would be possible to better predict the number of liquid bridges forming on the surface and as a result the adhesive force to be produced. Plotting the results from Table 7.1 in section 7.2, it can be seen that there is an exponential dependence of pillar height on the adhesion forces as shown in Figure 7.9. However, these values are independent of the wettability; therefore this is not an accurate representation. It has also been assumed that having a form to the counter surface will decrease the adhesion by around 1000 times. However, when there is also a factor of compliance it can be assumed that this number will decrease due to the increased contact from the softer surface, which in this case would be the tissue sample as shown in the earlier Figure 6.5.

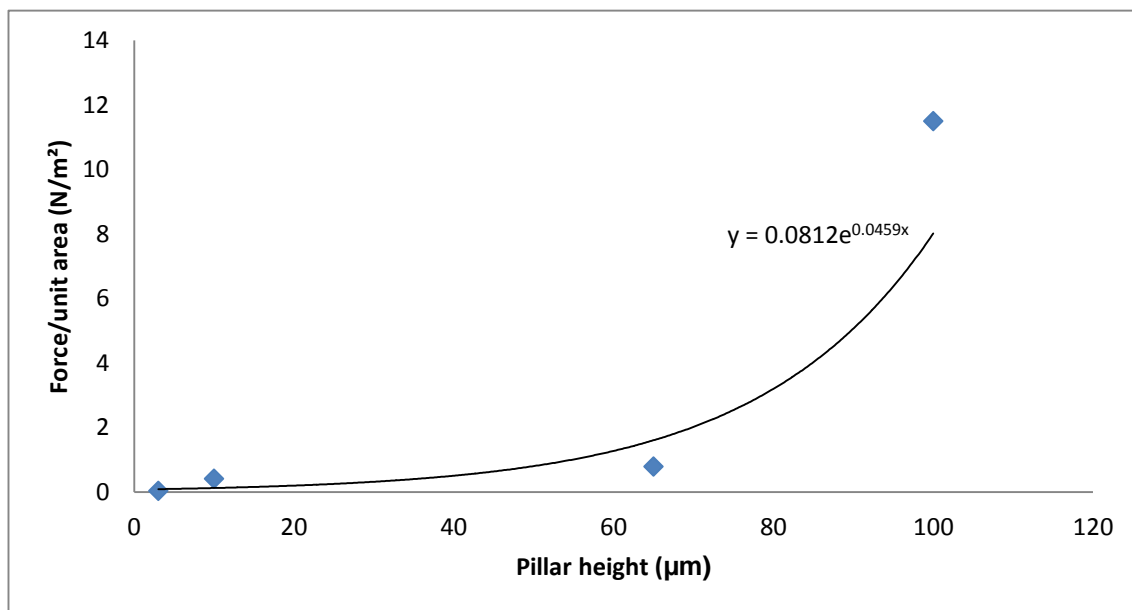


Figure 7.9 - The effect of pillar height on the adhesive forces produced.

This data incorporates wet adhesion results from Cheung et al. [95] He et al. [173] Kovalev et al. [174].

7.6 Summary

In summary, this chapter has highlighted the areas of novelty in this work:

Micro-structure geometry

Micro-scale pillars are a viable option for the proposed wet adhesion model, however when comparing the adhesion mechanism in this thesis to that in literature, it can be seen that the scale of the micro-structures investigated is as low as one tenth of that in literature. Small components such as these were chosen as this enabled there to be many individual contact points with the wet surface. This ties in closely with the original inspiration of this thesis; that of the tree frog and the features found upon its toe pads. As previously discussed in section 6.4 however, these sub-micron features that can be found on the tree frog's toe pad are not necessarily repeatable in larger adhesion mechanisms. This is to prevent the collapsing of the capillary bridges. It has been proposed by Qian and Gao [79] that the minimal pillar radius is around $0.8 \mu\text{m}$. This not only will affect the adhesion regime, specifically in terms of reaching a point of super-hydrophilicity. Where, the closer the pillar height is to the capillary length of the fluid, for a hydrophilic surface, the more capillary bridges will be able to form. This will result in a higher adhesion force.

Biological tissue

The main aim of this work was to produce a micro-structured surface capable of providing adhesion forces large enough to hold a device to the peritoneum. This raised many uncertainties in this work, specifically, due to compliance and varying fluid properties. As well as the potential that the

PDMS polymer surface may be adsorbing proteins - the effect of which is unknown.

This chapter has highlighted a potential issue with the mathematical model when working with a compliant material such as PDMS on such small scales. The proposed wet adhesion model assumes that discrete liquid bridges would be formed on each pillar tip resulting in a total adhesion force. It also proposed that the lower the contact angle on the surface, the higher the adhesion. Both of these proposals have shown to be incorrect for the geometries specified in this thesis. Firstly it has been shown that it appears that there are actually around 1000 times less bridges forming in the actual experimental set up, than expected from the theoretical value. Secondly this work suggests that as the contact angle decreases below 50° , it is possible that the surface acts super-hydrophilic, and totally wets the surface, due to the relationship between the pillar height and the capillary length of the fluid on the surface. In this case the adhesion mechanism would appear to favour a hydrophobic surface. Therefore it can be speculated that in order to have optimal adhesion on a surface of micro-structures, of pillar heights as low as those in this thesis, there may be an optimal contact angle between 50° and 90° . Where 50° is suggested as the lowest contact angle from previous adhesion results by Taylor *et al.* [17] and the highest being 90° , beyond which the surface will act hydrophobic.

7.7 Practical Applications

There are many cases during minimally invasive surgery when it would be beneficial to be able to control adhesion and traction at a tissue device interface.

This thesis has shown that a maximum weight of 83 mg²¹ can be held against tissue using the discussed PDMS surfaces. This is not a sufficient weight to be able to dock a light device such as the PillCam [33] which weighs a maximum of 4 g over its surface (11 mm x 32 mm) . However, the initial discussed Autotex[®] surfaces, have been shown to be capable of holding 6.7 g [17] over a surface area of 113 mm². This would be more than adequate to hold a lightweight device such as PillCam [33]. As previously discussed the Autotex[®] surfaces have a higher contact angle than its PDMS equivalents in this thesis, where due to their low contact angle the PDMS surfaces act super-hydrophilic and flood. Therefore it can be assumed that by exploring a wider range of contact angles over these surfaces, the adhesion forces will be capable of holding the weight of such surgical devices. This can be achieved by ensuring they are acting in an optimal hydrophilic range as shown in Figure 7.4.

Whilst the main focus of this work has been to optimise adhesion, in order to allow an intra-abdominal device to adhere and traverse the peritoneum, against gravity, there are other surgical devices which would benefit from having such a method of adhesion. By utilising the tissue fluid reversible, repeatable and reliable adhesion and traction can be provided. The main focus of this section however will be a discussion of the use of such surfaces on a miniature robotic system, providing traction through an inflated colon, as well as mention of their use on surgical graspers.

A traction rig has been designed and developed in order to test the viability of the surfaces inside the colon; this will be discussed along with some preliminary testing.

²¹ Wafer 2 with a contact angle of 40.3°

7.7.1 Colon Tissue as a Comparison to Peritoneal Tissue

The body of this thesis has looked at the peritoneum, a relatively thin tissue with a thin fluid film on its surface. However, as the suggested applications would involve traversing or manipulating the colon, it is necessary to categorise the tissue, in order to provide the adhesion forces necessary. The colon is a thick, rough surface increasing the contact whilst reducing the separation distances between itself and the pillared surface, hence aiding adhesion as previously discussed. However, the layer of mucosa gel on the colon surface can be as thick as 800 μm [181, 182] compared to the phospholipid bilayer on the peritoneum which is only 2 - 4 nm thick. This change in thickness of the fluid on the surface may result in poor adhesion as the surfaces may just flood. It is not only adhesion that would be beneficial it would also be useful to be able to control traction at the tissue-device interface for a number of surgical robotic devices. For instance the aforementioned PillCam [33] and a miniature robotic device being explored as part of the CoDir project.

7.7.2 CoDir Applications

Collaborative work between the University of Leeds²² and the University of Dundee²³ has looked at the viability of using a miniature robotic device to perform a hydro colonoscopy. Studies were carried out looking at the viability of filling the colon with a fluid, rather than the conventional method of filling the colon with CO₂ which is known to cause major discomfort to the patient.

²² School of Mechanical Engineering

²³ Institute of Medical Sciences and Technology

7.7.3 Surgical Graspers

Surgical graspers would also benefit from such an adhesion mechanism. Current graspers rely on small metal fenestrations across the grasper jaw to hold and manipulate tissue, in particular the colon. The forces which are applied by the surgeon to allow the movement of tissue are known to cause unnecessary tissue damage along with the fenestrations [2-6]. Therefore if it were possible to utilise the fluid film lining the colon and provide high enough adhesion forces whilst still maintaining the functionality of the graspers it would be possible to produce an atraumatic system. It is proposed that the grasper jaws could be lined with a pillared polymer surface. In this case the system would need to overcome a varied fluid property and a very conformable rough wet surface.

Chapter 8. Conclusions and Recommendations for Future Work

This thesis aimed to provide an understanding of a reversible, reliable and repeatable wet adhesion mechanism. It has been shown that pillars are a good way to approach such a wet adhesion mechanism. Specifically, in terms of how variation in the surface geometry and surface chemistry of bio-inspired structured polymers affect adhesive forces. The effect of the interacting fluid properties on adhesion is also investigated. The combination allows the optimisation of the adhesion system for surgical devices at a tissue device interface, whilst providing minimal trauma.

The objectives of this thesis were:

- To investigate the use of existing lithography methods for the fabrication of micro-structured polymer surfaces with varying surface geometry
- To investigate an optimal wettability of polymer surfaces, specifically how exposure to a plasma treatment affects adhesion without altering the surface geometry.
- To investigate the applicability of a wet adhesion mathematical model, encompassing both capillary and Stefan adhesive forces
- To investigate the viability of such surfaces in a surgical environment, in the simplest case docking a camera, and in the most complex case surgical tools.

The research motivation and need for a micro-structured polymer surface in a surgical environment, has been outlined and a detailed literature review has been conducted. The literature review (Chapter 2) covered the fields of minimally invasive surgery, mechanisms of adhesion and fabrication techniques available to repeatedly and reliably produce a micro-structured polymer surface, this

process highlighted a number of limitations and knowledge within the current methodology. As a result the focus of this thesis was to fabricate a bio-inspired micro-structured surface which will provide repeatable and reliable atraumatic adhesion to tissue. This mechanism would utilise the fluid available on the tissue surface in the form of Stefan adhesion and Capillary forces. As the liquid wets the surface, this model predicted that a meniscus will form around the micro-pillars which are in contact with the wet surface.

Specialist test equipment required to successfully fabricate and analyse micro-structured surfaces has been described. This included a range of sample preparation equipment, post-fabrication equipment - encompassing visual analysis, mechanical property analysis and surface chemistry analysis. Adhesion test rigs were also detailed.

The methodology required to create a micro-scale pillared polymer surface to create adhesive forces between the polymer surface and biological tissue has been outlined in chapter 4. This chapter explored the polymer options available; initially focusing on the use of Autotex[®] - a commercial ethyl acrylate polymer. Despite producing a repeatable micro-structured surface for a specific geometry, due to limitations associated with working with a bespoke industrial product, other polymers were investigated. Firstly, SU8 was explored due to its wide use in micro fabrication in the clean room facility; however this procedure was not suitable to produce a micro-pillared array on a flexible substrate, due to shrinkages in the cross-linking process as a result of the varying glass transition temperatures of the polymers - delamination of the pillars from the PET sheet therefore occurred. SU8 was also explored for viability as a mask/mould for other polymer candidates; however, this was also ineffective due to the developer

becoming exhausted when fabricating holes and as a result failing to produce straight walled columns and instead producing shallow dimples. Finally, PDMS was investigated, resulting in successfully fabricated repeatable micro-structured surfaces for varying geometries. This chapter showed that using an imprint-lithography technique is a viable option to create micro-structured surfaces.

The adhesion forces capable of being produced by these micro-structured surfaces have been shown in chapter 5. Experimentally the surfaces did not behave as expected according to the model discussed in chapter 6. This could be due to a number of reasons, firstly, surface form. If there is any form to the base on which the pillars are fabricated this could result in not all of the pillars coming into contact and forming liquid bridges at once. This would result in a reduced number of capillary bridges and therefore a lower force of adhesion, a consequence of the fabrication technique used. Secondly, as the adhesion mechanism discussed in this thesis relies on the capillary and Stefan forces present, when separating two surfaces with liquid mediating contacts; it is assumed that hydrophilic surfaces will produce concave menisci on a pillar tip. This will result in attractive forces. On the other hand, a hydrophobic surface will produce convex menisci and therefore repulsive forces. It has been shown however, that a slight attractive force is observed for a hydrophobic surface during the end stage of separation, although the magnitude is small.

However, if the pillar height of a hydrophilic surface is much smaller than the capillary length of the fluid the surface will act super-hydrophilic, therefore wetting the surfaces and preventing the formation of any menisci and again result in poor adhesion. This means for the system discussed in this thesis there may be an optimum contact angle between 90 and 50 degrees which will allow the formation of attractive concave menisci on the pillar tip. This effect would be observed

regardless of the pillar spacing as it is only the pillar height which determines the formation of such menisci. Such an effect would explain why the adhesion forces when PDMS is explored is greater for a hydrophobic surface, as the small attractive forces present at the end stage of separation, despite being small, are still greater than the effect of a super-hydrophilic surface.

Chapter 6 explored the proposed wet adhesion mechanism, which comprised of both capillary forces and Stefan adhesion. The model was provided to determine the forces present at the interface between a wet surface and the micro-structured polymer. The effects of pillar spacing, wettability and fluid viscosity on adhesion were explored, along with how the effect of separation between the two surfaces affected the dominant adhesion regime; Stefan forces or capillary action. It could be seen that, the separation distances at which Stefan forces break down and capillary action takes over is proportional to the viscosity of the fluid on the surface; however there was no significance between the pillar spacing. It was also found that there was very little distinction between the effects of pillar spacing when the wettability of the surface was altered. However, the adhesion was predicted to be higher for water on glass, than that of tissue. Finally, the effect of pillar spacing was investigated. It was shown that when capillary action is dominating the adhesion is optimal in the system involving water on a glass surface. However, when the separation is at a minimum and the adhesion is occurring mainly due to the Stefan forces, and there is a high dependency on viscosity, there is a large difference in the adhesion forces produced, where the lower the fluid viscosity, the smaller the adhesion forces. Unfortunately, the model does not take account for a conformable surface, and instead assumes two rigid surfaces in contact. It could therefore be speculated that when working with a conformable surface such as tissue, the adhesion

regime will remain with Stefan forces dominating for longer, and therefore aiding the adhesion. This model also assumed there will be a perfect contact, between all of the pillars and the counter face. This would result in all of the pillars gaining contact with the surface, and then being removed in unison. However, when working with a conformable and varied surface, such as the peritoneum, this model proved an inaccurate representation of the forces produced experimentally.

Chapter 7 highlighted the novelty in this work:

- Micro-structure geometry

When comparing the adhesion mechanism in this thesis to that in literature, it can be seen that the scale of the micro-structures investigated is as low as one tenth of that in literature. This not only will affect the adhesion regime, specifically in terms of reaching a point of super-hydrophilicity, but also highlights issues with fabrication.

- Biological tissue

The main aim of this work was to produce a micro-structured surface capable of providing adhesion forces large enough to hold a device to the peritoneum. This raised many uncertainties in this work, specifically due to compliance, varying fluid properties and compliance, as well as the potential that the PDMS polymer surface may be adsorbing proteins - the effect of which is unknown.

Potential applications have also been highlighted, specifically other surgical devices which would benefit from having a method of reversible, repeatable and reliable adhesion and traction. The main focus being the use of such surfaces on a miniature robotic system, to provide traction through an inflated colon; as well as mention of their use on surgical graspers. A traction rig was designed and

developed in order to test the viability of the surfaces inside the colon; this will be discussed along with some preliminary testing.

Whilst the body of this thesis looked at the peritoneum - a relative thin tissue with a thin fluid film on its surface, this chapter explored the colon. The colon is a thicker rough surface increasing the contact whilst reducing the separation distances between the pillared surface and the substrate therefore aiding adhesion as previously discussed. However, the layer of the mucosa gel on the surface was found to be as thick as 800 μm this thickness of the fluid on the surface may result in poor adhesion as the surfaces may just flood.

Studies have been performed looking at the viability of using a miniature robotic device in the colon - such a device could benefit from having controllable adhesion and traction. Therefore to test this, a bespoke rig was designed and built. Initial tests showed the traction capability of the micro-structured pillars against wet glass. It is shown that all samples slip at an initial point, however, the hydrophilic pillars gain better traction and prevent further slip as the force is ramped. The hydrophobic flat sample does regain traction. But it then slips again and continues to do so along with the hydrophobic pillars and hydrophilic flat samples until a maximum is reached. As the tissue dried and the fluid viscosity increases the pillars can gain traction, where during the initial cycle there is no distinction between a flat surface and a pillar surface.

8.1 Recommendations for Future Work

There is potential to extend this study and build upon the knowledge in this area. Specifically there are two main aspects of this micro-scale bio-inspired structured polymer surface which could be built upon and improved in the future. The first of which is regarding the surfaces wettability and the ability to tune it further in order

to optimise the wet adhesive forces. The second aspect is related to further surgical applications, specifically in terms of surgical tools such as graspers and miniature robotic exploration devices. It is apparent that improving the control of wettability will be essential to allow these further surgical applications to be explored. A final area would be to develop an improved model which could be used as predictive adhesion tools. The details of these are described below.

Accurate tuning of wettability to enhance adhesion

As discussed in Chapter 7, the adhesion mechanism discussed in this thesis relies on capillary and Stefan forces which are present when separating two surfaces with liquid mediating contacts, the dominant of the two being the contact angle driven capillary force. It has been shown as a result of this work that with small features, in the order of 3 microns, a hydrophilic surface will act super-hydrophilic, therefore wetting the surfaces and preventing the formation of any menisci and ultimately resulting in poor adhesion. This means for the system discussed in this thesis there may be an optimum contact angle between 90 and 50 degrees which will allow the formation of attractive concave menisci on the pillar tip. Consequently it can be seen that there is a necessity for accurate tuneable wettability in order to optimise adhesion on this scale, through the production of the liquid bridge formation required, it would be beneficial for any future work to investigate this further. This could be achieved through coatings, self-assembled monolayers and altering the polymer chemistry. As it has been previously described, if the pillar height of a hydrophilic surface is much smaller than the capillary length of the fluid, the surface will act super-hydrophilic. It therefore may also be the case that higher aspect ratio structures (achieved by increasing the pillar height) may also further benefit the adhesion mechanism and diminish this flooding effect.

Surgical Applications

A polymer micro-structured adhesive surface as that described in this thesis could benefit many surgical devices, not only in terms of adhesion but also traction, reducing tissue trauma compared to current methods. It has been discussed that one ideal case is that of surgical graspers. Current graspers rely on small metal fenestrations across the grasper jaw to hold and manoeuvre tissue during abdominal surgery, in particular the colon. However, the forces which are applied by the surgeon to allow the manipulation of tissue are known to cause unnecessary and in some cases irreversible tissue damage to the patient. Therefore if it were possible to utilise the fluid film lining on the tissue, through the adhesion mechanism discussed, it may be possible to provide high enough adhesion and traction forces whilst still maintaining the functionality of the graspers; ultimately producing an atraumatic system. It is proposed that this could be achieved by lining the surgical grasper jaws with a pillared polymer surface. This work would also need to take advantage of the wettability investigations described above, as well as dealing with a much more conformable and varied surface than the peritoneum. As mentioned earlier, initial work has investigated the effects of micro-structured surfaces on traction. This initial work seemed promising, preventing slip and recovering from slip, when in contact with colon tissue. This work could be continued further for specific devices.

References

1. Sauerland, S., R. Lefering, and E.A. Neugebauer, *Laparoscopic versus open surgery for suspected appendicitis*. Cochrane Database Syst Rev, 2004(4): p. CD001546.
2. Russell, L., *The Design and Development of an Intelligent Atraumatic Laparoscopic Grasper*, in *School of Mechanical Engineering 2015*, University of Leeds.
3. Van der Voort, M., E. Heijnsdijk, and D. Gouma, *Bowel injury as a complication of laparoscopy*. British Journal of Surgery, 2004. **91**(10): p. 1253-1258.
4. Puntambekar, S.P., et al., *Laparoscopic Gynae-oncological Procedures: Lessons Learnt After a Single Institution Audit of Complications and Their Management in 567 Consecutive Patients*. The Journal of Obstetrics and Gynecology of India, 2014. **64**(1): p. 36-40.
5. Chung, B.I., M.M. Desai, and I.S. Gill, *Management of intraoperative splenic injury during laparoscopic urological surgery*. BJU international, 2011. **108**(4): p. 572-576.
6. Levy, B., et al., *Bladder injuries in emergency/expedited laparoscopic surgery in the absence of previous surgery: a case series*. Annals of the Royal College of Surgeons of England, 2012. **94**(3): p. e118-20.
7. Montellano López, A., *A miniature bio-inspired locomotion mechanism for an intra-abdominal adhesion-reliant robot*, in *School of Mechanical Engineering 2013*, University of Leeds.
8. Patronik, N., M. Zenati, and C. Riviere, *Crawling on the Heart: A Mobile Robotic Device for Minimally Invasive Cardiac Interventions Medical Image Computing and Computer-Assisted Intervention – MICCAI 2004*, C. Barillot, D. Haynor, and P. Hellier, Editors. 2004, Springer Berlin / Heidelberg. p. 9-16.
9. Menciassi, A. and P. Dario, *Bio-inspired solutions for locomotion in the gastrointestinal tract: background and perspectives*. Philosophical Transactions of the Royal Society of London A: Mathematical, Physical and Engineering Sciences, 2003. **361**(1811): p. 2287-2298.
10. Menciassi, A., et al., *Shape memory alloy clamping devices of a capsule for monitoring tasks in the gastrointestinal tract*. Journal of Micromechanics and Microengineering, 2005. **15**(11): p. 2045-2055.
11. La Spina, G., et al., *A novel technological process for fabricating micro-tips for biomimetic adhesion*. Journal of Micromechanics and Microengineering, 2005. **15**(8): p. 1576.
12. Ota, T., et al., *Minimally invasive epicardial injections using a novel semiautonomous robotic device*. Circulation, 2008. **118**(14 suppl 1): p. S115-S120.
13. Persson, B., *Capillary adhesion between elastic solids with randomly rough surfaces*. Journal of Physics: Condensed Matter, 2008. **20**(31): p. 315007.

14. Becker, H. and U. Heim, *Hot embossing as a method for the fabrication of polymer high aspect ratio structures*. Sensors and Actuators A: Physical, 2000. **83**(1): p. 130-135.
15. Gorelik, J., et al., *Dynamic assembly of surface structures in living cells*. Proceedings of the National Academy of Sciences, 2003. **100**(10): p. 5819-5822.
16. Lis, L.J., et al., *Interactions between neutral phospholipid bilayer membranes*. Biophysical Journal, 1982. **37**(3): p. 657-665.
17. Taylor, G.W., *Biomimetic adhesion strategies for an intra-peritoneal surgical device*, in *School of Mechanical Engineering 2011*, University of Leeds.
18. Clinic, M. *Laparoscopic oophorectomy*. 1998-2015; Available from: <http://www.mayoclinic.org/tests-procedures/oophorectomy/multimedia/laparoscopic-oophorectomy/img-20007474>.
19. Medicine, A.S.f.R., *Patient Fact Sheet-Minimally Invasive Surgery*, A.S.f.R. Medicine, Editor 2008. p. 1.
20. Klein, A. *Bioplastics and the artificial heart*. in *ANTEC*. 1987.
21. Roshan, R., et al., *Effect of tribological factors on wet adhesion of a microstructured surface to peritoneal tissue*. Acta Biomater, 2011.
22. Aggarwal. R, D.A., Yang. G-Z, *Robotics in Surgery-past, present and future*. Medical sciences. **II**.
23. G.W Taylor, A.N., D. G. Jayne, R. Roshan, T. Liskiewicz, P. H. Gaskell *Wet adhesion for a miniature mobile intra-abdominal device based on biomimetic principles*. Proceedings of the Institution of Mechanical Engineers Part C Journal of Mechanical Engineering Science, 2010. **224**(7): p. 1473.
24. Zdrahala, R.J. and I.J. Zdrahala, *Biomedical Applications of Polyurethanes: A Review of Past Promises, Present Realities, and a Vibrant Future*. Journal of Biomaterials Applications, 1999. **14**(1): p. 67-90.
25. Rattner, D. and A. Kalloo, *ASGE/SAGES Working Group on Natural Orifice Transluminal Endoscopic Surgery*. Surgical Endoscopy And Other Interventional Techniques, 2006. **20**(2): p. 329-333.
26. Harrell, A.G. and B.T. Heniford, *Minimally invasive abdominal surgery: lux et veritas past, present, and future*. The American Journal of Surgery, 2005. **190**(2): p. 239-243.
27. Zdrahala, R.J., et al., *Thermoplastic polyurethanes. Materials for vascular catheters*. Polyurethanes in Biomedical Engineering II. Amsterdam: Elsevier Science Publishers, 1987: p. 1-18.
28. Taylor, R.H. and D. Stoianovici, *Medical robotics in computer-integrated surgery*. Robotics and Automation, IEEE Transactions on, 2003. **19**(5): p. 765-781.

29. Li, J., et al., *Optimization of a novel mechanism for a minimally invasive surgery robot*. The International Journal of Medical Robotics and Computer Assisted Surgery, 2010. **6**(1): p. 83-90.
30. Mathur, A., et al., *Characterisation of PMMA microfluidic channels and devices fabricated by hot embossing and sealed by direct bonding*. Current Applied Physics, 2009. **9**(6): p. 1199-1202.
31. Mukhopadhyay, S., et al., *Experimental study on capillary flow through polymer microchannel bends for microfluidic applications*. Journal of Micromechanics and Microengineering, 2010. **20**(5): p. 055018.
32. Li, J., et al., *PMMA microfluidic devices with three-dimensional features for blood cell filtration*. Journal of Micromechanics and Microengineering, 2008. **18**(9): p. 095021.
33. Imaging, G. *PillCam*. 2001-2012; Available from: <http://www.givenimaging.com>.
34. Mathur, A., S.S. Roy, and J.A. McLaughlin, *Transferring vertically aligned carbon nanotubes onto a polymeric substrate using a hot embossing technique for microfluidic applications*. J R Soc Interface, 2010. **7**(48): p. 1129-33.
35. Datta, P. and J. Goettert, *Method for polymer hot embossing process development*. Microsystem technologies, 2007. **13**(3-4): p. 265-270.
36. Mukhopadhyay, S., et al., *Nanoscale surface modifications to control capillary flow characteristics in PMMA microfluidic devices*. Nanoscale Research Letters, 2011. **6**(1): p. 1-12.
37. Kolff, W., et al., *Artificial heart in the chest and use of polyurethane for making hearts, valves and aortas*. ASAIO Journal, 1959. **5**(1): p. 298-303.
38. Stone, A., *The theory of intermolecular forces*. 2013: Oxford University Press.
39. Chao, H.-H. and D.F. Torchiana, *BioGlue: Albumin/Glutaraldehyde Sealant in Cardiac Surgery*. Journal of Cardiac Surgery, 2003. **18**(6): p. 500-503.
40. Tissuemed, S.f. *TissuePatch, Surgical Sealent Film*. 2015; Available from: <http://www.tissuepatch.com/>.
41. Pugno, N.M., *Velcro® nonlinear mechanics*. Applied Physics Letters, 2007. **90**(12): p. 121918.
42. Menzies, D. and H. Ellis, *Intestinal obstruction from adhesions--how big is the problem?* Annals of the Royal College of Surgeons of England, 1990. **72**(1): p. 60.
43. Ellis, H., et al., *Adhesion-related hospital readmissions after abdominal and pelvic surgery: a retrospective cohort study*. The Lancet, 1999. **353**(9163): p. 1476-1480.
44. Wilson, M.S., et al., *Demonstrating the clinical and cost effectiveness of adhesion reduction strategies*. Colorectal Disease, 2002. **4**(5): p. 355-360.
45. Zhigang, W., et al., *Ferromagnetization of Target Tissues by Interstitial Injection of Ferrofluid: Formulation and Evidence of Efficacy for Magnetic*

- Retraction*. Biomedical Engineering, IEEE Transactions on, 2009. **56**(9): p. 2244-2252.
46. Lin, Y.-S., *Tissue manipulation using nano-particles ferrofluids for minimal access surgical applications*, 2014, University of Leeds.
 47. Scott, D., et al., *Completely transvaginal NOTES cholecystectomy using magnetically anchored instruments*. Surgical Endoscopy, 2007. **21**(12): p. 2308-2316.
 48. Aksak, B., M.P. Murphy, and M. Sitti, *Gecko inspired micro-fibrillar adhesives for wall climbing robots on micro/nanoscale rough surfaces*. 2008 IEEE International Conference on Robotics and Automation, Vols 1-9, 2008: p. 3058-3063.
 49. Autumn, K. and A.M. Peattie, *Mechanisms of Adhesion in Geckos*. Integrative and Comparative Biology, 2002. **42**(6): p. 1081-1090.
 50. Greiner, C., E. Arzt, and A. del Campo, *Hierarchical Gecko-Like Adhesives*. Advanced Materials, 2009. **21**(4): p. 479-482.
 51. Gao, H., et al., *Mechanics of hierarchical adhesion structures of geckos*. Mechanics of Materials, 2005. **37**(2): p. 275-285.
 52. Menon, C., M. Murphy, and M. Sitti, *Gecko inspired surface climbing robots*. IEEE ROBOTICS 2004: Proceedings of the IEEE International Conference on Robotics and Biomimetics, 2004: p. 431-436.
 53. Unver, O., et al., *Geckobot: A gecko inspired climbing robot using elastomer adhesives*. 2006 IEEE International Conference on Robotics and Automation (Icra), Vols 1-10, 2006: p. 2329-2335.
 54. Sitti, M. and R.S. Fearing, *Nanomolding based fabrication of synthetic gecko foot-hairs*. Proceedings of the 2002 2nd IEEE Conference on Nanotechnology, 2002: p. 137-140.
 55. Sitti, M., M.P. Murphy, and B. Aksak, *Gecko-inspired Directional and Controllable Adhesion*. Small, 2009. **5**(2): p. 170-175.
 56. Yanik, M.F., *Towards gecko-feet-inspired bandages*. Trends in Biotechnology, 2009. **27**(1): p. 1-2.
 57. Autumn, K., P.H. Niewiarowski, and J.B. Puthoff, *Gecko adhesion as a model system for integrative biology, interdisciplinary science, and bioinspired engineering*. Annual Review of Ecology, Evolution, and Systematics, 2014. **45**(1): p. 445.
 58. Arenas, I., et al., *Bio-inspired Gecko Micro-surface for Drag Reduction in Turbulent Flows*. Bulletin of the American Physical Society, 2014. **59**.
 59. Cutkosky, M.R., *Climbing with adhesion: from bioinspiration to biounderstanding*. Interface Focus, 2015. **5**(4): p. 20150015.
 60. Quere, D., *Capillarity and wetting phenomena: drops, bubbles, pearls and waves*. 2004: Françoise Broochard-Wyart.
 61. Cai, S. and B. Bhushan, *Meniscus and viscous forces during separation of hydrophilic and hydrophobic surfaces with liquid-mediated contacts*. Materials Science and Engineering: R: Reports, 2008. **61**(1): p. 78-106.

62. Federle, W., et al., *Wet but not slippery: boundary friction in tree frog adhesive toe pads*. Journal of The Royal Society Interface, 2006. **3**(10): p. 689-697.
63. Persson, B.N.J., *Wet adhesion with application to tree frog adhesive toe pads and tires*. Journal of Physics-Condensed Matter, 2007. **19**(37).
64. Barnes, W., *Dynamic adhesion in animals: mechanisms and biomimetic implications*. Journal of Comparative Physiology A: Neuroethology, Sensory, Neural, and Behavioral Physiology, 2006. **192**(11): p. 1165-1168.
65. HANNA, G., W. Jon, and W.J. BARNES, *Adhesion and detachment of the toe pads of tree frogs*. Journal of Experimental Biology, 1991. **155**(1): p. 103-125.
66. Green, D.M., *Treefrog toe pads: comparative surface morphology using scanning electron microscopy*. Canadian Journal of Zoology, 1979. **57**(10): p. 2033-2046.
67. EMERSON, S.B. and D. DIEHL, *Toe pad morphology and mechanisms of sticking in frogs*. Biological Journal of the Linnean Society, 1980. **13**(3): p. 199-216.
68. Nachtigall, W., *Biological mechanisms of attachment*. 1974.
69. Endlein, T., et al., *Sticking under Wet Conditions: The Remarkable Attachment Abilities of the Torrent Frog, <italic>Staurois guttatus</italic>*. PLoS ONE, 2013. **8**(9): p. e73810.
70. Emerson, S.B. and D. Diehl, Biol. J. Linn. Soc., 1980. **13**: p. 199-216.
71. Federle, W., et al., *An Integrative Study of Insect Adhesion: Mechanics and Wet Adhesion of Pretarsal Pads in Ants*. Integrative and Comparative Biology, 2002. **42**(6): p. 1100-1106.
72. Barnes, G.H.a.J.P., *Adhesion and detachment of the toe pads of tree frogs*. J. exp. Biol, 1990. **155**: p. 103-125.
73. Green, D.M., *Adhesion and the Toe-Pads of Treefrogs*. Copeia, 1981. **1981**(4): p. 790-796.
74. Ruibal, R. and V. Ernst, *The structure of the digital setae of lizards*. Journal of Morphology, 1965. **117**(3): p. 271-293.
75. Autumn, K., et al., *Evidence for van der Waals adhesion in gecko setae*. Proceedings of the National Academy of Sciences of the United States of America, 2002. **99**(19): p. 12252-12256.
76. Autumn, K., et al., *Evidence for van der Waals adhesion in gecko setae*. Proceedings of the National Academy of Sciences, 2002. **99**(19): p. 12252-12256.
77. Israelachvili, J., *Intermolecular and surface forces*. 1992, Academic Press: London.
78. Liu, K., X. Yao, and L. Jiang, *Recent developments in bio-inspired special wettability*. Chemical Society Reviews, 2010. **39**(8): p. 3240-3255.
79. Qian, J. and H. Gao, *Scaling effects of wet adhesion in biological attachment systems*. Acta Biomaterialia, 2006. **2**(1): p. 51-58.

80. Arzt, E., S. Gorb, and R. Spolenak, *From micro to nano contacts in biological attachment devices*. Proceedings of the National Academy of Sciences, 2003. **100**(19): p. 10603-10606.
81. De Souza, E., et al., *Enhancement of capillary forces by multiple liquid bridges*. Langmuir, 2008. **24**(16): p. 8813-8820.
82. De Souza, E.J., et al., *Capillary Forces between Chemically Different Substrates*. Langmuir, 2008. **24**(18): p. 10161-10168.
83. J. A. Burdick, R.L.M., *Biomaterials for tissue engineering applications - A review of the past and future trends*. 2011, Philadelphia: Springer-Verlag/Wien.
84. DeFranco, J.A., et al., *Photolithographic patterning of organic electronic materials*. Organic Electronics, 2006. **7**(1): p. 22-28.
85. Deval, J. and et al., *Reconfigurable hydrophobic/hydrophilic surfaces in microelectromechanical systems (MEMS)*. Journal of Micromechanics and Microengineering, 2004. **14**(1): p. 91.
86. Jaeger, R.C., *Introduction to Microelectronic Fabrication*. 2002: Prentice Hall.
87. Spohr, R., *Ion Tracks and Microtechnology - Principles and applications*, ed. K. Bethge. 1990, Darmstadt: Bertelsmann Publishing group International 269.
88. Research, G.M. *Basic Techniques in Lithography*. [cited 2015 May 2015]; Available from: <http://ion-tracks.de/iontracktechnology/10/1/1.html>.
89. Qin, D., Y. Xia, and G.M. Whitesides, *Soft lithography for micro- and nanoscale patterning*. Nat. Protocols, 2010. **5**(3): p. 491-502.
90. Shahsavan, H., D. Arunbabu, and B. Zhao, *Biomimetic Modification of Polymeric Surfaces: A Promising Pathway for Tuning of Wetting and Adhesion*. Macromolecular Materials and Engineering, 2012: p. n/a-n/a.
91. Ghodssi, R., *MEMS materials and processes*. 2011, Maryland: Springer New York Dordrecht Heidelberg London.
92. Dey, P.K., *Microstructuring of SU-8 resist for mems and bio-applications*. International Journal on smart sensing and intelligent systems, 2010. **3**(1).
93. Cheung, E., *Biologically inspired polymer micro-patterned adhesives*. US Army research and development and engineering command, 2008(ECBC-CR-097).
94. G. Hubbard, S.J.A., Q. Chen, *Wafer-Scale Transfer of Nanoimprinted patterns into silicon substrates*. 2008.
95. Cheung, E. and M. Sitti, *Enhancing Adhesion of Biologically Inspired Polymer Microfibers with a Viscous Oil Coating*. The Journal of Adhesion, 2011. **87**(6): p. 547-557.
96. Glass, P., et al., *Enhanced Wet Adhesion and Shear of Elastomeric Micro-Fiber Arrays with Mushroom Tip Geometry and a Photopolymerized p(DMA-co-MEA) Tip Coating*. Langmuir, 2010. **26**(22): p. 17357-17362.
97. Kim, S., B. Aksak, and M. Sitti, *Enhanced friction of elastomer microfiber adhesives with spatulate tips*. Applied Physics Letters, 2007. **91**(22).

98. Kim, S. and M. Sitti, *Biologically inspired polymer microfibers with spatulate tips as repeatable fibrillar adhesives*. Applied Physics Letters, 2006. **89**(26).
99. Murphy, M.P., B. Aksak, and M. Sitti, *Adhesion and anisotropic friction enhancements of angled heterogeneous micro-fiber arrays with spherical and spatula tips*. Journal of Adhesion Science and Technology, 2007. **21**(12-13): p. 1281-1296.
100. Sitti, M., B. Aksak, and M.P. Murphy, *Adhesion of biologically inspired vertical and angled polymer microfiber arrays*. Langmuir, 2007. **23**(6): p. 3322-3332.
101. Sitti, M. and E. Cheung, *Enhancing Adhesion of Biologically Inspired Polymer Microfibers with a Viscous Oil Coating*. Journal of Adhesion, 2011. **87**(6): p. 547-557.
102. Sitti, M., S. Kim, and E. Cheung, *Wet Self-Cleaning of Biologically Inspired Elastomer Mushroom Shaped Microfibrillar Adhesives*. Langmuir, 2009. **25**(13): p. 7196-7199.
103. Zhang, Y., et al., *Replica Molding of High-Aspect-Ratio Polymeric Nanopillar Arrays with High Fidelity*. Langmuir, 2006. **22**(20): p. 8595-8601.
104. Verpoorte, E. and N.F. de Rooij, *Microfluidics meets MEMS*. Proceedings of the IEEE, 2003. **91**(6): p. 930-953.
105. optics, E. *Intraocular lenses*. Available from: <http://www.eagleopticsindia.com/intraocular-lens.html>.
106. Webb, J.C.J. and R.F. Spencer, *The role of polymethylmethacrylate bone cement in modern orthopaedic surgery*. Journal of Bone & Joint Surgery, British Volume, 2007. **89-B**(7): p. 851-857.
107. Elveflow. *Microfluidics and microfluidic devices: A review*. 2015; Available from: <http://www.elveflow.com/microfluidic-tutorials/microfluidic-reviews-and-tutorials/microfluidics-and-microfluidic-device-a-review/>.
108. Abidin, U., B.Y. Majlis, and J. Yunas. *Polydimethylsiloxane (PDMS) microchannel with trapping chamber for BioMEMS applications*. in *Semiconductor Electronics (ICSE), 2014 IEEE International Conference on*. 2014.
109. Mata, A., A. Fleischman, and S. Roy, *Characterization of Polydimethylsiloxane (PDMS) Properties for Biomedical Micro/Nanosystems*. Biomedical Microdevices, 2005. **7**(4): p. 281-293.
110. Boland, J.J., *Flexible electronics: Within touch of artificial skin*. Nat Mater, 2010. **9**(10): p. 790-792.
111. Solutions, L.M.-M. *Precision Dicing Saws - MicroAce 66*. 2015; Available from: <http://www.loadpoint.co.uk/systems/microace-66/>.
112. Instruments, O. *Reactive Ion Etching (RIE)*. 2015 [cited 2015 02/2015]; Available from: <http://www.oxford-instruments.com/products/etching-deposition-and-growth/plasma-etch-deposition/rie>.
113. GmbH, G.L.I., *Instruction Manual Plasma Prep 2*.

114. Materials, M. *Nanoindentation*. Available from: <http://www.micromaterials.co.uk/the-nano-test/nanoindentation/>.
115. Pharr, G.M., *Measurement of mechanical properties by ultra-low load indentation*. Materials Science and Engineering: A, 1998. **253**(1–2): p. 151-159.
116. D. Campbell, R.A.P., J. R. White, *Polymer Characterization - Physical Techniques*. 2000, UK: Chapman and Hall.
117. Leeds, U.o. *Scanning Electron Microscopy, Facilities, LEMAS*. 2010-2014; Available from: <http://www.engineering.leeds.ac.uk/imr/lemas/scanning-electron-microscopy.shtml>.
118. Bruker. *NPFLEX-Overview*. 2015 [cited 2015 02/2015]; Available from: <http://www.bruker.com/products/surface-analysis/3d-industrial-optical-microscopy/npflex/overview.html>.
119. Angstroms, F.T. *FTA4000*. 2015 [cited 2015 02/2015]; Available from: <http://www.firsttenangstroms.com/products/fta4000/fta4000.html>.
120. Devices, S.M. *S100 - Thin Film Load Cells*. 2015 [cited 2015 June]; Available from: <http://www.smdsensors.com/Products/S100-Thin-Film-Load-Cell/>.
121. Campo, A.d. and C. Greiner, *SU-8: a photoresist for high-aspect-ratio and 3D submicron lithography*. Journal of Micromechanics and Microengineering, 2007. **17**(6): p. R81.
122. Zhang, J., et al., *Polymerization optimization of SU-8 photoresist and its applications in microfluidic systems and MEMS*. Journal of Micromechanics and Microengineering, 2001. **11**(1): p. 20.
123. Nagstrup, J., et al., *3D microstructuring of biodegradable polymers*. Microelectronic Engineering, 2011. **88**(8): p. 2342-2344.
124. Zhou, J., A.V. Ellis, and N.H. Voelcker, *Recent developments in PDMS surface modification for microfluidic devices*. ELECTROPHORESIS, 2010. **31**(1): p. 2-16.
125. Wu, D., et al., *Facile creation of hierarchical PDMS microstructures with extreme underwater superoleophobicity for anti-oil application in microfluidic channels*. Lab on a Chip, 2011. **11**(22).
126. Shin, J.-H., K.-S. Han, and H. Lee, *Anti-reflection and hydrophobic characteristics of M-PDMS based moth-eye nano-patterns on protection glass of photovoltaic systems*. Progress in Photovoltaics: Research and Applications, 2011. **19**(3): p. 339-344.
127. Grilli, S., V. Vespini, and P. Ferraro, *Surface-Charge Lithography for Direct PDMS Micro-Patterning*. Langmuir, 2008. **24**(23): p. 13262-13265.
128. Carlberg, P., L. Montelius, and J. Tegenfeldt, *Nanoimprint in PDMS on glass with two-level hybrid stamp*. Microelectronic Engineering, 2008. **85**(1): p. 210-213.
129. Burgoyne., F., *Optimal protocol for moulding PDMS with a PDMS master*, 2010, Royal Society of Chemistry.
130. Paek, J. and J. Kim, *Microsphere-assisted fabrication of high aspect-ratio elastomeric micropillars and waveguides*. Nat Commun, 2014. **5**.

131. Deng, Y.-L. and Y.-J. Juang, *Polydimethyl siloxane wet etching for three dimensional fabrication of microneedle array and high-aspect-ratio micropillars*. *Biomicrofluidics*, 2014. **8**(2): p. 026502.
132. Papadopoulos, P., et al., *How superhydrophobicity breaks down*. *Proceedings of the National Academy of Sciences*, 2013. **110**(9): p. 3254-3258.
133. Glass, P., et al., *Enhanced Reversible Adhesion of Dopamine Methacrylamide-Coated Elastomer Microfibrillar Structures under Wet Conditions*. *Langmuir*, 2009. **25**(12): p. 6607-6612.
134. del Campo, A., C. Greiner, and E. Arzt, *Contact Shape Controls Adhesion of Bioinspired Fibrillar Surfaces*. *Langmuir*, 2007. **23**(20): p. 10235-10243.
135. Lee, J.B., et al., *Wetting transition characteristics on microstructured hydrophobic surfaces*. *Materials transactions*, 2010. **51**(9): p. 1709-1711.
136. Kanungo, M., et al., *Effect of Roughness Geometry on Wetting and Dewetting of Rough PDMS Surfaces*. *Langmuir*, 2014. **30**(25): p. 7358-7368.
137. Hegemann, D., H. Brunner, and C. Oehr, *Plasma treatment of polymers for surface and adhesion improvement*. *Nuclear Instruments and Methods in Physics Research Section B: Beam Interactions with Materials and Atoms*, 2003. **208**: p. 281-286.
138. Wu, W.-I., et al., *Polyurethane-based microfluidic devices for blood contacting applications*. *Lab on a Chip*, 2012. **12**(5): p. 960-970.
139. Wang, P., et al., *Ultrasensitive quartz crystal microbalance enabled by micropillar structure*. *Applied Physics Letters*, 2014. **104**(4): p. 043504.
140. Neil, J.S., et al., *The use of high aspect ratio photoresist (SU-8) for superhydrophobic pattern prototyping*. *Journal of Micromechanics and Microengineering*, 2004. **14**(10): p. 1384.
141. Du, P., et al., *Investigation of cellular contraction forces in the frequency domain using a PDMS micropillar-based force transducer*. *Microelectromechanical Systems, Journal of*, 2013. **22**(1): p. 44-53.
142. Jiang, X., et al., *Polymer-on-polymer stamping: universal approaches to chemically patterned surfaces*. *Langmuir*, 2002. **18**(7): p. 2607-2615.
143. Plasma, H. *Micro-fluidic Devices*. 2014 [cited 2015 August]; Available from: <http://harrickplasma.com/applications/microfluidic-devices>.
144. Guo, L.J., *Nanoimprint Lithography: Methods and Material Requirements*. *Advanced Materials*, 2007. **19**(4): p. 495-513.
145. Holmes, M., et al., *Optimized piranha etching process for SU8-based MEMS and MOEMS construction*. *Journal of Micromechanics and Microengineering*, 2010. **20**(11): p. 115008.
146. Swallowe, G.M., *Mechanical Properties and Testing of Polymers: an A-Z reference*. Vol. 3. 2013: Springer Science & Business Media.
147. Marmur, A., *Wetting on Hydrophobic Rough Surfaces: To Be Heterogeneous or Not To Be?* *Langmuir*, 2003. **19**(20): p. 8343-8348.

148. Ott, D.E., *Laparoscopy and tribology: the effect of laparoscopic gas on peritoneal fluid*. J Am Assoc Gynecol Laparosc, 2001. **8**(1): p. 117-23.
149. Trudnowski, R.J. and R.C. Rico, *Specific gravity of blood and plasma at 4 and 37 C*. Clinical chemistry, 1974. **20**(5): p. 615-616.
150. Hills, B. and K. Thomas, *Surfactant barrier lining peritoneal mesothelium: lubricant and release agent*. Peritoneal dialysis international, 1998. **18**(2): p. 157-165.
151. Gómez-Suárez, C., et al., *Hydrophobicity of peritoneal tissues in the rat*. Journal of colloid and interface science, 2002. **253**(2): p. 470-471.
152. Hrnčir, E. and J. Rosina, *Surface tension of blood*. Physiol Res, 1997. **46**(4): p. 319-21.
153. Mills, C.O., et al., *Surface tension properties of human urine: relationship with bile salt concentration*. J Clin Chem Clin Biochem, 1988. **26**(4): p. 187-94.
154. Weisenhorn, A.L., et al., *Deformation and height anomaly of soft surfaces studied with an AFM*. Nanotechnology, 1993. **4**(2): p. 106.
155. Radmacher, M., et al., *Measuring the viscoelastic properties of human platelets with the atomic force microscope*. Biophysical journal, 1996. **70**(1): p. 556-567.
156. toolbox, T.e. *Tensile Modulus - Modulus of Elasticity or Young's Modulus - for some common Materials*. [cited 2015; Available from: http://www.engineeringtoolbox.com/young-modulus-d_417.html].
157. McKee, C.T., et al., *Indentation versus tensile measurements of Young's modulus for soft biological tissues*. Tissue Engineering Part B: Reviews, 2011. **17**(3): p. 155-164.
158. De Boer, M. and P. De Boer, *Thermodynamics of capillary adhesion between rough surfaces*. Journal of colloid and interface science, 2007. **311**(1): p. 171-185.
159. Wang, J., J. Qian, and H. Gao, *Effects of capillary condensation in adhesion between rough surfaces*. Langmuir, 2009. **25**(19): p. 11727-11731.
160. Kim, D.-I., et al., *Origin of adhesion in humid air*. Langmuir, 2008. **24**(5): p. 1873-1877.
161. Mutsaers, S.E., *The mesothelial cell*. The International Journal of Biochemistry & Cell Biology, 2004. **36**(1): p. 9-16.
162. Michailova, K., W. Wassilev, and T. Wedel, *Scanning and transmission electron microscopic study of visceral and parietal peritoneal regions in the rat*. Annals of Anatomy-Anatomischer Anzeiger, 1999. **181**(3): p. 253-260.
163. Gaudio, E., et al., *A scanning electron microscopy morphometric study of the rabbit peritoneal surface*. The Anatomical Record, 1990. **228**(2): p. 145-150.
164. Madison, L.D., et al., *Regulation of surface topography of mouse peritoneal cells. Formation of microvilli and vesiculated pits on omental mesothelial cells by serum and other proteins*. The Journal of cell biology, 1979. **82**(3): p. 783-797.

165. Lewis, B.A. and D.M. Engelman, *Lipid bilayer thickness varies linearly with acyl chain length in fluid phosphatidylcholine vesicles*. Journal of molecular biology, 1983. **166**(2): p. 211-217.
166. Hoffman, B.D., et al., *The consensus mechanics of cultured mammalian cells*. Proceedings of the National Academy of Sciences, 2006. **103**(27): p. 10259-10264.
167. Hills, B.A., *Graphite-like lubrication of mesothelium by oligolamellar pleural surfactant*. Journal of Applied Physiology, 1992. **73**(3): p. 1034-1039.
168. Washington, U.o. *Adhesion - Biomechanics*. 2013; Available from: <http://courses.washington.edu/biomechs/lectures/lecture15.pdf>.
169. Dirks, J.-H., *Physical principles of fluid-mediated insect attachment - Shouldn't insects slip?* Beilstein Journal of Nanotechnology, 2014. **5**: p. 1160-1166.
170. Smith, A.M., *Integr. Comp. Biol.*, 2002. **42**: p. 1164-1171.
171. Dirks, J.H., et al., *Acta Biomater.*, 2012. **8**: p. 2730-2736.
172. Gorb, S., *Attachment devices of insect cuticle*. 2001, Dordrecht, Boston: Kluwer Academic Publishers.
173. He, B., et al., *Wet adhesion inspired bionic climbing robot*. Mechatronics, IEEE/ASME Transactions on, 2014. **19**(1): p. 312-320.
174. Kovalev, A.E., M. Varenberg, and S.N. Gorb, *Wet versus dry adhesion of biomimetic mushroom-shaped microstructures*. Soft Matter, 2012. **8**(29): p. 7560-7566.
175. Huang, B., et al., *Coating of poly (dimethylsiloxane) with n-dodecyl- β -D-maltoside to minimize nonspecific protein adsorption*. Lab on a Chip, 2005. **5**(10): p. 1005-1007.
176. Chumbimuni-Torres, K.Y., et al., *Adsorption of Proteins to Thin-Films of PDMS and Its Effect on the Adhesion of Human Endothelial Cells*. RSC advances, 2011. **1**(4): p. 706-714.
177. Yu, L., et al., *AFM study of adsorption of protein A on a poly(dimethylsiloxane) surface*. Nanotechnology, 2009. **20**(28): p. 285101.
178. Quéré, D., *Wetting and roughness*. Annu. Rev. Mater. Res., 2008. **38**: p. 71-99.
179. Chandra, D. and S. Yang, *Stability of High-Aspect-Ratio Micropillar Arrays against Adhesive and Capillary Forces*. Accounts of Chemical Research, 2010. **43**(8): p. 1080-1091.
180. Wei, Z., et al., *Elastocapillary coalescence of plates and pillars*. Vol. 471. 2015.
181. Atuma, C., et al., *The adherent gastrointestinal mucus gel layer: thickness and physical state in vivo*. American Journal of Physiology-Gastrointestinal and Liver Physiology, 2001. **280**(5): p. G922-G929.
182. Johansson, M.E., J.M.H. Larsson, and G.C. Hansson, *The two mucus layers of colon are organized by the MUC2 mucin, whereas the outer layer is a legislator of host-microbial interactions*. Proceedings of the national academy of sciences, 2011. **108**(Supplement 1): p. 4659-4665.

